Fault Detection
In the Electrohydraulic Actuator
Using Extended Kalman Filter

A Thesis Submitted to
the College of Graduate Studies and Research
in Partial Fulfillment of the Requirements
for the Degree of Doctor of Philosophy
in the Department of Mechanical Engineering
University of Saskatchewan, Saskatoon
Canada

By
Yuvin Adnarain Chinniah

Permission to Use

In presenting this thesis in partial fulfillment of the requirements for a Postgraduate degree from the University of Saskatchewan, I agree that the Libraries of this University may make it freely available for inspection. I further agree that the permission for copying this thesis in any manner, in whole or in part for scholarly purposes, may be granted by the professors who supervised my thesis work or, in their absence, by the Head of the Department or Dean of the College in which my thesis work was conducted. It is understood that any copying or publication or use of this thesis or parts thereof for financial gain shall not be allowed without my written permission. It is also understood that due recognition shall be given to me and to the University of Saskatchewan in any scholarly use which may be made of any material in my thesis.

Requests for permission to copy or to make other use of material in this thesis, in whole or part, should be addressed to:

Head of the Department Mechanical Engineering
University of Saskatchewan
College of Engineering
57 Campus Drive
Saskatoon, Saskatchewan S7N 5A9
Canada

Abstract

In this thesis a fault detection technique for a high performance hydrostatic actuation system was developed and evaluated. The Extended Kalman Filter (EKF) was used for parameter identification and was applied to an Electrohydraulic Actuator (EHA) and the performance of the technique is discussed. The EHA is a high performance, closed loop actuation system consisting of an AC variable speed electric motor, a bi-directional gear pump, an accumulator, check valves, a cross-over relief valve, connecting tubes and a custom made symmetrical actuator. The EHA has potential applications in the aerospace industry for flight surface actuation and in robotics. Failures in the EHA can pose a safety hazard and unscheduled maintenance can result in costly downtime. Fault detection in the EHA will increase its safety and efficiency.

The proposed preventive maintenance approach involves monitoring the EHA by estimating two parameters of interest, namely the effective bulk modulus and the viscous damping coefficient. Lowering of the effective bulk modulus, as a result of air entrapment, will affect the response of the EHA and may cause stability issues, by lowering the bandwidth of the system. Changes in the damping coefficient for the actuator can indicate deterioration of the oil, wear in the seals or changes in external friction characteristics. The two parameters were estimated using the EKF and changes in the estimated values were related to faults in the system.

Prior to applying the EKF to the EHA prototype, an extensive simulation study was carried out to investigate the feasibility of the approach as well as the level of accuracy to be expected with the experimental system. The simulation study was used to verify that changes in the two parameters were detected and accurately estimated.

In this study, an attempt was also made to visit some of the problems reported with the use of the EKF for fault detection purposes, namely the difficulty in setting the correct values in the matrices to initialize the EKF algorithm and the presence of biases in the estimates. The problem was believed to be linked to system observability which

was investigated in this research. It was found that using observable state space models for the EKF improved the ability of the EKF to estimate parameters, both in terms of accuracy of the estimations and repeatability of experimental results. System observability was investigated in this work by first using simple mechanical systems and then using the more complex EHA system. An iterative approach was presented whereby parameters were not estimated at the same time but iteratively and using different models. System observability was maintained by reducing the number of states and by using the correct type and number of system measurements. Also, the use of observable systems eliminated the need to choose parameter values, in the initial state vector of the EKF, close to the desired parameter values, as was very often done in previous research. No a-priori knowledge about the parameters was assumed in this research. Biases in the estimates (this has been reported in previous studies) are believed to be due to the filter facing a local minima problem. This problem is linked to the error covariance matrix not converging to a global minimum. In the Kalman Filter, the main objective of the error covariance matrix is to compute the Kalman gain, which is in turn used to correct an estimate with the latest sensor measurement. Errors in the Kalman gain may lead to biases in the estimates. In this study, it was also found that although the system is not observable, it can be detectable, although the converse is not true, and as such, changes in parameters can be detected but not necessarily accurately estimated. Observability ensures uniqueness of the estimate.

The effective bulk modulus and viscous damping coefficient were estimated successfully, both in simulations and using experimental data. Faults were introduced in the EHA prototype and changes in the parameters were detected and estimated.

The friction characteristic of the actuator for the EHA was also investigated. A novel empirical friction model was proposed. The EKF was used to estimate iteratively (to maintain system observability), the coefficients of that friction function which was believed to be a realistic representation of friction effect in the prototype. Simulation and experimental results were presented. In summary, the application of the EKF technique to the EHA has produced very promising results.

Acknowledgements

The author expresses his gratitude to his supervisors, Dr. R.T. Burton and Dr. S. Habibi for their guidance and advice during the course of this research and the writing of this thesis. The technical assistance of Mr. D.V. Bitner is also gratefully acknowledged.

Financial support in the form of graduate student monthly stipend, University of Saskatchewan Graduate Student Scholarship and Canadian Commonwealth Scholarship is also acknowledged.

Special gratitude must be conveyed to my wife, Priscilla, whose patience and support have been invaluable during my studies.

I also wish to express my gratitude to my family, especially to my parents and brothers for their encouragement and support.

Table of Contents

List of Tables

List of Figures

Nomenclature

Q_a	Flow delivered by the pump (m^3/s)
Q_b	Flow entering the pump (m^3/s)
ξ	Pump cross-port leakage coefficient (m^3/sPa)
D_p	Pump volumetric displacement (m^3/rad)
P_a	Pump pressure at its outlet port (Pa)
P_b	Pump pressure at its inlet port (Pa)
V_a	Pump section volume associated with its outlet port (m^3)
β_e	Effective bulk modulus of hydraulic oil (Pa)
V_b	Pump section volume associated with its inlet port (m^3)
ω_p	Pump angular velocity (rad/s)
C_{ep}	Pump external leakage coefficient (m^3/sPa)
P_r	Accumulator pressure (Pa)
A	Symmetrical actuator working area (m^2)
Q_1	Flow in the actuator (m^3/s)
Q_2	Flow out of the actuator (m^3/s)
x	Piston/load displacement from mean position (m)
$\dot{x}$	Piston/load velocity (m/s)
V_{0ac}	Pipe volume plus actuator chamber volume at zero position (m^3)
P_1	Pressure in chamber C1 of the actuator (Pa)
P_2	Pressure in chamber C2 of the actuator (Pa)
L	Actuator external leakage coefficient (m^3/sPa)
I_c	Control input current (A)
V_c	Control input voltage (V)

R_c Electric motor line-to-line resistance (Ω)

L_c Electric motor line-to-line inductance (H)

τ_e Electric motor electrical circuit time constant (s)

T_m Electric motor torque (Nm)

K_c Electric motor gain (Nm/A)

θ Electric motor angular position (rad)

J_{pm} Electric motor/pump inertia (Nms^2/rad)

T_{DB} Nonlinear friction (including static and coulomb) at pump/motor interface

$K_{P_{cs}}$ Proportional gain

$K_{I_{cs}}$ Integral gain

V_o Total mean volume (m^3)

F Force acting on mass (N)

M Load mass (Kg)

B Viscous damping coefficient (Ns/m)

C_T Total leakage coefficient of the system (m^3/sPa)

Chapter 1

Introduction

1.1 Preliminary Remarks

Hydraulic systems are found in a wide range of airborne, mobile and stationary applications, such as in the aerospace industry (e.g. flight surface actuation), off highway equipment (e.g. backhoes and loaders), agricultural machinery, the manufacturing industry (e.g. hydraulic presses) and robotics. Some of the unique features of hydraulic systems include a wide operating range (in terms of force/torque, speed and direction), high force to mass ratio (actuators/motors develop relatively large force/torque for comparatively small devices) and the fluid itself acts as a lubricant [Merrit, 1967].

In this study, fault detection in a high performance hydrostatic system, referred to as an Electrohydraulic Actuator (EHA) is investigated. The EHA is a closed-loop, hydrostatic system consisting of an AC variable speed electric motor, a fixed displacement bi-directional gear pump (only in this particular application), an accumulator, connecting tubes, a custom made symmetrical actuator and sensors. Potential applications of the EHA are in the fields of robotics and aerospace industry mainly [Habibi, 2000]. The EHA has advantages such as high energy efficiency, high positional accuracy and compactness. In the EHA, the pump only delivers sufficient flow to move the actuator piston, as compared to a conventional hydrostatic system with a variable displacement pump running at constant speed, where the pump runs irrespective of the motion of the piston. For a conventional system, by changing the swash plate angle, the flow is changed and when the actuator piston is not required to move, the swash plate may be adjusted so that the pump does not deliver any flow. This strategy is not particularly energy efficient since the electric motor still drives the pump in spite of the pump not delivering any flow.

The EHA has demonstrated a high level of performance, with high positional accuracy (1 micron) [Habibi, 2000] mainly due to the control strategy and

instrumentation used. Another distinct advantage of the EHA lies in its custom made symmetrical actuator which is as compact as a single rod actuator and has equal flows in and out of the actuator, very similar to a conventional double rod, symmetrical piston. In robotics and aerospace applications in particular, these advantages are appealing [Habibi, 1998]. Having the electric motor and the actuator close to each other, i.e. having the supply and actuation module in a lumped unit configuration, results in greater hydraulic stiffness (fast response), a reduction in the volume of oil required (reducing the fire hazard risks) and a reduction in the length of tubes or hoses (thereby reducing risks of leakages). This configuration is appealing for flight surface actuation in aircrafts, where the EHA can be positioned at the wing itself instead of centralized fluid power systems with long hoses and tubes. " *The new Lockheed Martin F-35 Joint Strike Fighter's flight controls will use electrohydrostatic actuation (EHA) technology for the first time in a production aircraft. This technology provides several benefits. The actuators are smaller and weigh less; performance is more efficient and the F-35 is less vulnerable to enemy fire.*" [Heney, 2002, pp. 16].

In robotic applications, the supply module (consisting of the electric motor, controller, gear pump, accumulator and crossover relief valve) and the actuation module (consisting of the custom made actuator) can be used separately if needed. In such applications, the force to mass ratio of the actuation system plays a very significant role in the bulk and overall mass of a manipulator (heavy actuation units would require heavier links). Therefore, in robots with high degrees of freedom, the EHA can be used as a single lumped unit (supply and actuation module forming an integral part, resulting in a stiff system) near the base of the robot and a different configuration where the supply module, still being near the base of the robot, is connected to the actuation module further away from the base. This separate configuration of the EHA can be used to manipulate links found further away from the base of the robot (in order to minimize weight at the actuation point), although the hydraulic stiffness will be reduced by the use of longer flexible hoses to connect the supply module to the actuation module [Habibi, 2000]. Other advantages of the EHA for robotics application are high

positional accuracy, efficiency and a relatively smaller actuator than the conventional symmetrical double-rod actuator.

An effective fault detection strategy is important for the EHA because certain failures in the system can result in system breakdown and as such, can be costly. Failures of the EHA in safety critical applications such as in flight surface actuation in aircraft can be catastrophic, resulting in loss of lives. Early fault detection based on detecting a gradual degradation of the performance of the system is therefore useful in allowing preventive maintenance, thus increasing safety and reducing downtime.

1.2 Techniques Used in Health Monitoring of Hydraulic Systems

Health monitoring in hydraulic systems is mostly done by monitoring pressure, flow rate and temperature of the fluid, as well as visual inspection for leakage, fluid aeration, water contamination and presence of solid contaminants [Hunt, 1986]. Fluid condition monitoring is important since failures in hydraulic systems can be directly related to the fluid condition [Coreless et al, 1984]. Other techniques also include power consumption and vibration analysis [Hunt, 1986]. Nowadays, in addition to these techniques, progress in sensor technology and computers have paved the way for relatively new monitoring techniques such as neural networks [Atkinson, 1996], [Crowther et al, 1996], [Rosa, 2001], [Hindman, 2002] and expert systems [Guo et al, 1989], [Hogan, 1996] and these methods have been applied to off highway equipment, mining equipment, power generating plants and machine tools [Stecki, 2000]. A more comprehensive description of the mentioned monitoring techniques is given in Chapter 2.

1.3 The Extended Kalman Filter (EKF) in Condition Monitoring

"*Condition monitoring consists of constantly processing measurable data or input-output signals from the plant until useful quantities that best describe the current health condition of the system are extracted. The processed information is then compared against some known or pre-determined normal quantities*", [Zavarehi, 1997, pp. 5].

Zavarehi has used the Kalman Filter to "extract" information about the particular hydraulic system which was under investigation. The Kalman Filter is a well-known state estimator, which uses measurements linearly related to the states. The Extended Kalman Filter (EKF) is basically the Kalman Filter applied to a nonlinear system using a linearization procedure. Using the measurements, Zavarehi, as well as other authors such as [Cao, 2001] and [Wright, 2001], have applied the EKF to different hydraulic systems and have used the EKF to estimate some critical parameters for their systems. The parameters so estimated, were directly related to the health of the hydraulic systems. The estimations were compared to the "normal" parameter values (for a healthy system) and deviations from the normal values were interpreted as faults.

When the EKF is used to estimate critical parameters in a system, faults in that system are detected at an early stage (when the faults first appear), and corrective actions can be taken to remedy the situation. The advantage is increased reliability and safety in systems. Faults will not propagate to other system components, which could potentially cause catastrophic failures. Also, appropriate decisions regarding the severity of the situation can be made and the problem fixed in a more cost-effective and risk-reducing manner.

Previous research involving the EKF for condition monitoring of hydraulic systems has reported some unexplained difficulties or phenomena (such as biases) in estimating some parameters. The EKF has been used to estimate viscous friction and Coulomb friction at the actuator with some success in [Zavarehi, 1997], although the author reported some difficulties believed to be linked to "*the lack of observability.*" Initialization of the EKF algorithm was found to affect the ability of the EKF to estimate the parameters successfully. It was found that Cao and Wright often used initial parameter values very close to the desired ones in the EKF code for the estimation to be successful. Zavarehi stated that "*All the initial states/parameters in the enhanced state vector were set to small random numbers.*" [Zavarehi, 1997, pp. 168]. Also, the research done by these authors focused mainly on using the filter as a tool for parameter estimation. A better understanding of the filter is believed to be essential to define its limitations in terms of parameter estimation in hydraulic systems.

1.4 Parameters of Interest in the Hydrostatic Actuation System

In this study, two important parameters, namely the effective bulk modulus and the equivalent viscous damping coefficient are considered. The bulk modulus is the most important fluid property in determining the dynamic performance of hydraulic systems because it relates to the stiffness of the liquid. It is a measure of fluid resistance to compression and it is defined as the change in pressure divided by the fractional change in volume at constant temperature [Merrit, 1967]. Bulk modulus is a function of the pressure, the temperature and the entrained gas content in the fluid. It increases with increasing pressure and decreases with increasing temperature. "*In a pressure range of 0 to 20,000 psi, bulk modulus increases linearly with pressure at a constant temperature. For pressures above 20,000 psi, bulk modulus was found to exhibit a nonlinear relationship with pressure due to relations between the free space and the intermolecular forces. With regard to temperature, bulk modulus decreases logarithmically with increasing temperature. The effect of temperature on liquid bulk modulus is greater than that of pressure due to the logarithmic nature. These relationships and approximations apply to degassed fluids*" [Burton, 1971, pp. 13].

In all hydraulic fluids, air is present which causes the fluid to become compressible. This results in a slower response time as the liquid bulk modulus decreases and causes a general loss of horsepower in the system since work is spent on air compression. In addition, a reduction in the bulk modulus will lower the natural frequency of the hydraulic system and can cause stability problems [Merrit, 1967]. Air can exist in a fluid in three forms: free air, entrained air and dissolved air. Free air is that which is not entirely in contact with the fluid and exists in the form of pockets within the system; it can be eliminated to a certain degree by proper flushing of the system. Entrained air is that which is in suspension in the fluid. It is usually found suspended in the form of small air bubbles. Dissolved air is that which is in solution. Bulk modulus decreases in the presence of free air and entrained air, but dissolved air has been found to have no significant effect on liquid bulk modulus while in solution [Merrit, 1967]. Fluids which contain dissolved air can be considered incompressible, as the air is essentially part of the molecular structure of the fluid.

With a sudden drop of static pressure, a substantial increase in fluid temperature or an acceleration of fluid through an orifice, the dissolved air can be made to come out of the solution in the form of entrained air [Burton, 1971]. It can be re-dissolved into the fluid by increasing the pressure if the entrained air bubbles are not too large or if the fluid is not already saturated with entrained air. As the pressure increases, the fluid can hold more dissolved air. Unfortunately, in practical hydraulic systems, there is no way of knowing the amount of air which is in the free, entrained or the dissolved form in a fluid under normal operating conditions.

Conventional techniques for measuring bulk modulus usually involve pressurizing a sample of oil and measuring either volumetric changes or changes in some property. However, the conditions of pressurizing the oil are not necessarily those experienced by the actual system. Furthermore, the composition of the oil sample may not be representative of the oil in the system. Therefore, indirect methods of measuring bulk modulus using "on-line estimation" techniques may be a better option to determine the bulk modulus of the oil. Burton simulated the dynamics of a transmission line and estimated an effective bulk modulus of the fluid using a manual optimization technique [Burton, 1971]. The technique was able to estimate a value in a repeatable fashion.

In this study (using the EHA), an effective bulk modulus for the EHA is to be estimated. The effective bulk modulus is defined as the overall average bulk modulus exhibited by the fluid when air is present or there is elasticity in the fluid containment [Merrit, 1967]. Estimating this parameter is important in the EHA as it relates to the system response, the stability and the efficiency, and forms an important part of health monitoring in this high performance hydrostatic device. In the EHA, air can get trapped in the system when maintenance actions are being undertaken and components are being replaced. Caution has to be exercised to prevent air entrapment when refilling oil in the system. If the EHA is being used to actuate flight surfaces in an aircraft and if air is trapped into it, the response time as well as the natural frequency of the EHA will be reduced. This may result in system instability and have catastrophic consequences. Therefore, finding the effective bulk modulus value of the EHA before the aircraft takes off is important.

The second parameter of interest in this research is the viscous damping coefficient for the actuator. In hydraulic systems, close fitting surfaces are in relative motion and a low viscosity will increase leakage in the system as compared to a large viscosity value which will decrease efficiency. Viscosity is an important property of the fluid and is essential for lubrication purposes. Viscous friction at the actuator arises because a force is needed to shear the fluid. This force, termed as viscous friction, is proportional to the area in contact, to the velocity of the piston and inversely proportional to the film thickness [Merrit, 1967]. Therefore, changes in this important parameter, when temperature is constant, are a good indication that the seal in the actuator may be experiencing wear, or that the oil is deteriorating, resulting in reduced lubricating properties. The viscous friction coefficient or viscous damping coefficient is a lumped parameter. When the EHA is used for flight surface actuation, friction will not be limited to the actuator viscous friction, but load friction (external friction) may actually dominate. Therefore, quantifying the "total" friction force is important because in addition to giving information about the seal in the actuator and oil condition, it can also reveal potential problems in the movable flight surfaces (sticking). Such problems will be reflected in the load pressure measurements of the EHA and if an unusual damping coefficient is measured (or estimated using load pressure measurements), it may indicate problems with the movable joints of the flight surfaces.

1.5 Research Objectives

The proposed preventive maintenance approach for the EHA involves monitoring the system by estimating parameters of interest. System measurements for the EHA are actuator piston position, piston velocity, load pressure and pump/electric motor angular velocity. The main objectives of this study were:

- To produce an accurate and simplified model for the EHA to be used for simulation studies and for implementing the parameter estimation technique. It must be pointed out that a mathematical model for the EHA in earlier studies has been proposed but revealed some inaccuracies in terms of the values of the parameters used. As such, updating the existing model with some measured parameters was desirable.

- To carry out a simulation study to verify the feasibility of using the Extended Kalman Filter (EKF) to estimate the effective bulk modulus and the viscous damping coefficient in the electrohydraulic actuator (EHA). The simulation involving the EHA, as well as the EKF algorithm were implemented using Matlab/Simulink®.
- To use the simulation study to establish the level of accuracy in the estimations of the parameters, as well as to verify that changes in the parameters can be detected and accurately estimated.
- To better predict the performance of the kalman filter and the Extended Kalman Filter for state/parameter estimations, using concepts such as system observability and sensitivity studies. This was done to understand the filter better, in an attempt to explain some unexplained phenomena reported by authors who have applied the EKF to hydraulic systems.
- To initialize the EKF state matrix without a-priori knowledge rather than using some initial parameter values close to the known values.
- To experimentally determine values for some parameters and to set up the EHA system in order to acquire experimental data. It must be pointed out that the EHA was not in working condition at the beginning of the research.
- To investigate the friction characteristics of the actuator in the EHA and propose a better model for friction in the actuator.
- To use the EKF to characterize the new friction model and estimate changes in the friction model as a result of faults.

1.6 Thesis Outline

The thesis is generally organized in the same sequence as the research was conducted. Chapter 2 provides a literature review of the field of condition monitoring as applied to fluid power systems. This chapter provides an insight into some of the most commonly occurring faults in hydraulic systems. It also includes a brief description of some of the most commonly used monitoring strategies; monitoring fluid

contamination, vibration analysis, temperature, pressure and flow monitoring, along with the use of expert systems, neural networks and parameter estimation techniques.

A description of the Electrohydraulic Actuator (EHA) system, followed by a simplified mathematical model for the EHA is presented in Chapter 3. A faults and effects analysis of the EHA is also included in Chapter 3.

Parameters such as the pump and actuator leakage coefficients of the EHA, are measured in this study and the results given in Chapter 4. The experimental procedures and set up are described. The values for the parameters of a "healthy" EHA are also given and are used to simulate a mathematical EHA model in "Matlab/Simulink®". The simulated responses for a linearized EHA model are compared to their corresponding measured system responses in Chapter 4. Also included in this chapter is a brief description of the instrumentation for the EHA system.

The Kalman Filter followed by the Extended Kalman Filter (EKF) are introduced in Chapter 5. The Kalman filter equations are derived and this chapter serves to better explain the parameter estimation technique used in this study. In this chapter, as mentioned earlier, a deeper understanding of the Kalman Filter and of the Extended Kalman Filter is attempted, especially in terms of system's observability and uniqueness of predictions.

Chapter 6 explains the importance of system observability when applying the Kalman Filter and the Extended Kalman Filter to a system by using three examples, namely a mass-damper system, a mass spring damper system and the EHA. An extensive simulation study using the simple mechanical systems and the more complex electrohydraulic actuator model is presented. The foundations of applying the EKF to the EHA are laid and the general methodology used is explained. The inclusion of parameters as states and reformulation of the resulting discrete state space model is also explained. The unique iterative approach used in this study to estimate parameters using an observable system is explained. A sensitivity study of the parameters of interest for the EHA is also presented in this chapter. Next, the parameters are changed in simulation and the EKF is used to detect and estimate the new parameters.

The methodology explained in Chapter 6 is used to estimate the parameters in the EHA prototype and experimental results are presented in Chapter 7, using the EKF code developed for the simulation study. The estimated effective bulk modulus and equivalent viscous damping coefficient in the actual system are shown. Faults are then introduced in the prototype and the EKF is used to detect and estimate the new parameters successfully.

Experiments conducted on the EHA to measure the viscous friction coefficient are described in Chapter 8. Using a novel "quadratic friction" model to represent the friction characteristics in the prototype, simulation studies are conducted. The EKF is subsequently used to estimate the coefficients of the quadratic model, in simulation and in the actual prototype.

A summary of the thesis is given in Chapter 9 followed by a list of contributions. Some conclusions and recommendations for future research are also presented in this chapter. The novelties of this research were essentially;

1. Estimation of the effective bulk modulus, an extremely difficult parameter to measure, using the EKF,
2. Use of system observability to enhance the performance of the EKF, illustrated by first using simple mechanical examples and then using the more complex system,
3. Use of an iterative approach, whereby parameters were not estimated simultaneously but one at a time using different models, to ensure system observability,
4. Use of sensitivity function to identify an appropriate input signal to the filter,
5. Use of no a-priori knowledge about estimated parameters to initialize the EKF,
6. Showing that changes in parameters in the hydrostatic system were detected but not necessarily accurately estimated when the model was not observable,
7. Modeling of the nonlinear friction characteristics at the hydraulic actuator in a unique way, and
8. Use of the EKF to successfully estimate the coefficients of the proposed nonlinear model for the actuator in simulation and using experimental data.

Chapter 2

Condition Monitoring Strategies in Fluid Power

This chapter serves to summarize some of the most commonly used condition monitoring strategies for fluid power applications. Also, previous research done on the use of the Extended Kalman Filter (EKF) for parameter estimation is reported. Finally, the choice of using the EKF for condition monitoring purposes in the electrohydraulic actuator (EHA) is explained.

2.1 Introduction

In the early years of fluid power (pre 1960's), maintenance was mostly done when systems broke down and hydraulic machines were usually operated until they wore out or broke down, resulting in costly repairs. Furthermore, a fault originating in one single component (considerable wearing for example) usually propagated through the system (e.g. through metal particles in the oil), causing more damage. In some instances, time based monitoring techniques have been implemented, where faults in a system were detected only when measured values exceeded their normal limits [Isermann, 1984]. Non-measurable, yet critical quantities such as the viscous damping coefficient, the spring constant and the Coulomb friction could not be monitored.

In the last two decades, condition monitoring techniques have been used to increase reliability and safety of hydraulic machines. The main reason for this increased interest in this form of preventive fault detection was the increased complexity of fluid power systems and advances in real time monitoring and fault diagnosis tools and strategies [Hindman, 2002]. In particular, increasingly powerful computers have opened the possibility of applying new numerical methods for condition monitoring. The emphasis nowadays is, therefore, on early fault detection in fluid power systems. Deterioration in the performance of some critical pieces of equipment can be detected at an early stage and corrective measures taken to prevent failures. This preventive maintenance approach is becoming increasingly popular in hydraulic systems that are

continuously operated. As such, preventive maintenance is cost effective, when considering financial losses that can result from downtime of equipment (for example in the aerospace industry where unscheduled maintenance can have high financial implications, and in factories where unexpected shut down of a production line can result in very substantial losses). This strategy increases safety, and reduces risks of accidents due to catastrophic failure of hydraulic components [Zavarehi, 1997]. Monitoring the health of hydraulic equipment can also extend a machine operating life cycle and increase its energy efficiency.

Fluid power involves the use of pressurized fluid, which can be dangerous, if proper maintenance of the system is not ensured [Esposito, 2000]. Some of the most common causes of hydraulic failures are given in Table 2.1 which has been reproduced from [Hunt, 1986] and provides a good illustration of sources, conditions and characteristics of failures in fluid power systems. Most of these problems can be avoided if proper condition monitoring is undertaken.

Health monitoring in hydraulic systems is usually done by monitoring pressure, flow rate, and temperature of the fluid, as well as by visual inspection for leakage, fluid aeration, water contamination, and presence of solid contaminants [Hunt, 1986]. Other techniques also include power consumption and vibration analysis.

In general, the behavior of any hydraulic system such as erratic action of the actuator and loss of motor speed can be used to detect faults. Although these techniques are valid, the development of new sensors, the emergence of powerful computing tools and simulation packages to capture the dynamic behavior of hydraulic components and the appearance of neural networks and of expert systems, have improved fault detection and diagnosis of fluid power systems. These methods have been applied to off highway equipment, mining equipment, power generating plants and machine tools [Stecki, 2000]. In the following sections, a brief overview of established methods of condition monitoring in fluid power systems is presented.

2.2 Monitoring Fluid Condition

About 70% of all hydraulic system failures are related directly to the fluid condition [Hindman, 2002]. Hence, sampling and testing the fluid is an effective method to test the condition of the system. The vast majority of hydraulic system failures are due to the presence of foreign materials (contaminants) in the working fluid.

Table 2.1: Commonly Encountered Problems in Fluid Power Systems [Hunt, 1986, pp.290]

Feature of fluid power	**Condition for failure**	**Failure Characteristics**
Fluid pressure	• Excessively high • Excessively low	• Hose/ Tubing/Pipes burst • Wear in components such as pumps • Cavitation and erosion • Leaking seals
Fluid level	Low	Overheating and cessation of operation
Flow forces in valves	High/Concentrated	Jet erosion of spools and valves
Flow and Pressure Pulses	Resonant	Fatigue
Filtration	Clogged or blocked with contaminants	• Cavitation, erosion • Filter bursts, hose burst, back pressure
Fluid /Containment material	Incompatible	Swelling of seals and corrosion of surfaces
Fluid borne contamination	• High particulate concentration in fluid • Chemicals	• Wear in sliding parts • Blockage of ports • Corrosion
Circuit design	Loads excessive	Cracks and breakage

Fluid contamination occurs either due to "*external ingression*" or "*internal generation*" of solid debris or changes in the oil properties as described in [Hunt, 1986]. Since fluid power systems generally work under high pressures, (implying fine clearances, close tolerances and a high standard of surface finish during manufacture), high standards of cleanliness are vital for their operation. Since machining and assembling processes for fluid power components have tremendously improved, their sensitivity to contamination has increased as well.

Furthermore, as reported in [Coreless et al, 1984, pp. 3], "*in a clean environment, the contamination level in the fluid is most likely due to faults in the system and thus monitoring the contamination level is monitoring the system itself*". Solid contaminant monitoring is most prevalent. Solid contaminants cause scoring and wear to all types of components resulting in catastrophic failures when components cease to operate, break up and thereafter cause further contamination of the system.

Figure 2.1 [Stecki, 2000], illustrates the location of some of the wear, leakage and contamination points in a typical hydraulic circuit. It can be seen that contaminants can enter into the system at locations such as at the actuator and at the reservoir. Leakage can occur at the actuator, pump and at connections. Wear in a hydraulic system can occur at the actuator seal and at different valves.

" *Intermittent failure*" [Coreless et al, 1984] occurs when the solid particles prevent a valve from seating correctly but eventually get washed away when the valve reopens. Intermittent failures render the diagnosis operation more difficult and reduce system reliability. "*Degradation failures*" [Coreless et al, 1984] involve wearing, corrosion, and cause internal leakage in components. Very often, degradation failures degenerate into catastrophic failures. In servovalves, solid contaminants cause friction between the spool and the sleeve, thus eroding the metering edges. This in turn increases center flow, silting, sticking of the spool and in some cases complete failure due to clogging of internal orifices [Merrit, 1967]. Small particles such as metallic parts and oil residues can combine to form silts that clog the fine passages in control valves. These particles can also act as an abrasive paste that erodes the sharp control edges of the spool valve. This produces more contamination and opens up the diametrical

clearances permitting even larger particles to enter and consequently lead to component break down [Sasaki et al 1984]. Solid contaminants such as metallic particles from the normal wear of components such as pumps, motors, seals and shedding of hoses, filter material and rust, are self generated within the system [Sasaki et al, 1984].

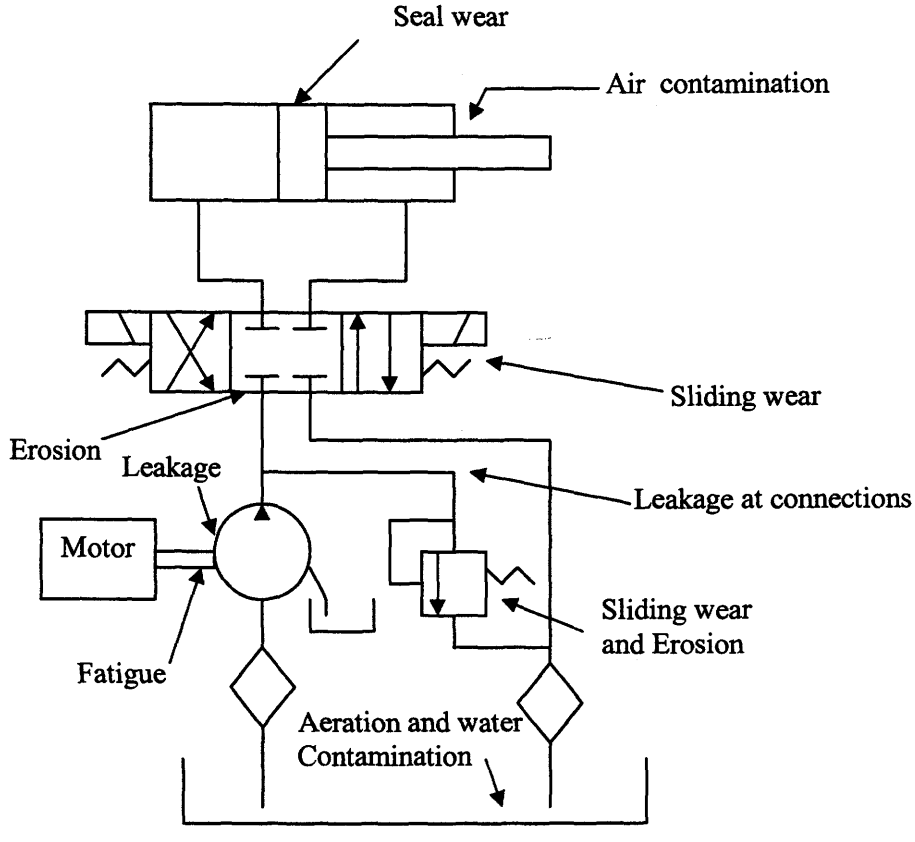

Figure 2.1 Wear, Leakage and Contamination Entry Points in a Typical Hydraulic System, reproduced from [Stecki, 2000, pp.15]

Built-in contamination occurs during manufacture, installation and repair of components. This type of contamination results in cloth fiber grits and chips from grinding and machining to appear in the working fluid. Airborne particles can also enter the system as contaminants. Cylinder seals are fitted with wiper rings to remove fine contaminants from the piston rod which is exposed to the atmosphere. These wiper rings tend to wipe the rod dry, subsequently causing wear of the seal itself and enabling foreign matter to enter the system [Sasaki et al, 1984].

In order to determine the contamination level in the hydraulic system, techniques such as "*visual inspection, gravimetric analysis and particle counts*" [Sasaki et al, 1984] are used. "*A dirty fluid to the human visibility implies the presence of particles of size greater than 40 microns*" [Merrit, 1967]. This test is sufficient for non-critical applications where servovalves are not being used. In gravimetric analysis, a certain volume of contaminated fluid is passed through a dry, preweighed filter paper which retains the contaminant. The next steps are to remove the retained oil by using a solvent and to dry and weigh the filter in order to determine the weight of the contaminant (usually expressed in milligrams per litre). Electronic particle counts involve passing the contaminated fluid through a transparent tube and then projecting a light beam through the tube. A photocell senses the light intensity and electronic counters record the number of light interruptions, which is a measure of the number of particles [Merrit, 1967]. Other methods used to analyze the contamination level and nature of contaminants involve the use of microscopes and determination of the ferromagnetic content. Chemical changes of the fluid such as its acidity, additive losses and physical changes such as viscosity can also be used to condition monitor the hydraulic system. It is worth noting that most of these methods are essentially "off line" since the tests involve collecting a sample of the fluid for analysis, away from the system itself.

Contaminants can be removed by flushing the system thoroughly. The velocity of the flushing oil needs to be sufficiently high to maintain turbulent flow inside the hoses and pipes to ensure that all of the solid contaminants are removed [Coreless et al 1984]. Also the use of a filter can ensure that particle size in the fluid is restricted to a satisfactory maximum size for the operation.

Contamination of the hydraulic fluid (petroleum based oil) also occurs through fluid oxidation, caused by the chemical reaction of air with oil particles [Esposito, 2000]. The products of oxidation which include "*sludge, varnish and insoluble gums*" increase the viscosity of the oil [Esposito, 2000]. To make matters worse, they are also acidic in nature, causing a chemical reaction between the metal and the acid. This is

usually referred to as corrosion of components. Oxidation is accelerated under high temperatures. Usually additives are used in the oil to inhibit oxidation.

Figure 2.2, [Sasaki et al, 1984, pp. 116], shows oil contamination and machine properties in hydraulic equipment. The figure illustrates the correlation of oil contamination and hydraulic problems as a result of a degradation of the physical and chemical properties of the fluid.

There have been studies made in order to simulate the contamination within fluid power systems. Dynamic Contamination Control techniques [Stecki 2000, Lui et al 1990] categorize the fluid power components into filters, cylinder seals and reservoirs which are components that remove, allow entry of, and store contaminants respectively. "*The contamination control system, is represented by a block diagram in which each block represents a linear function of a single hydraulic component. The contamination control system is solved using digital simulation and the results provide information about contamination levels at various locations in the circuit in response to varying sizes and distribution of ingressed or generated contaminant.*" [Stecki and Schoenau, 2000, pp. 337].

2.3 Vibration Analysis

Vibration analysis is a popular monitoring technique that is either categorized as airborne (acoustic) or structure borne (feeling) [Hunt, 1986]. Vibration analysis is a powerful tool for fault detection and diagnosis in mechanical systems (gearboxes in particular).

In fluid power applications, vibration analysis has been used to diagnose faulty pumps and motors by monitoring their pressure pulses or ripples caused by the movement of gears and pistons [Hunt, 1986]. Accelerometers are placed on the casing of the components and pressure transducers can be used to obtain signatures for the system. In general, "*signals often consist of low frequency components with large amplitudes which mainly determine the nominal values of the signal and higher frequency components with small amplitudes which give additional information on the inner state of the process*" [Isermann, 1984, pp. 388].

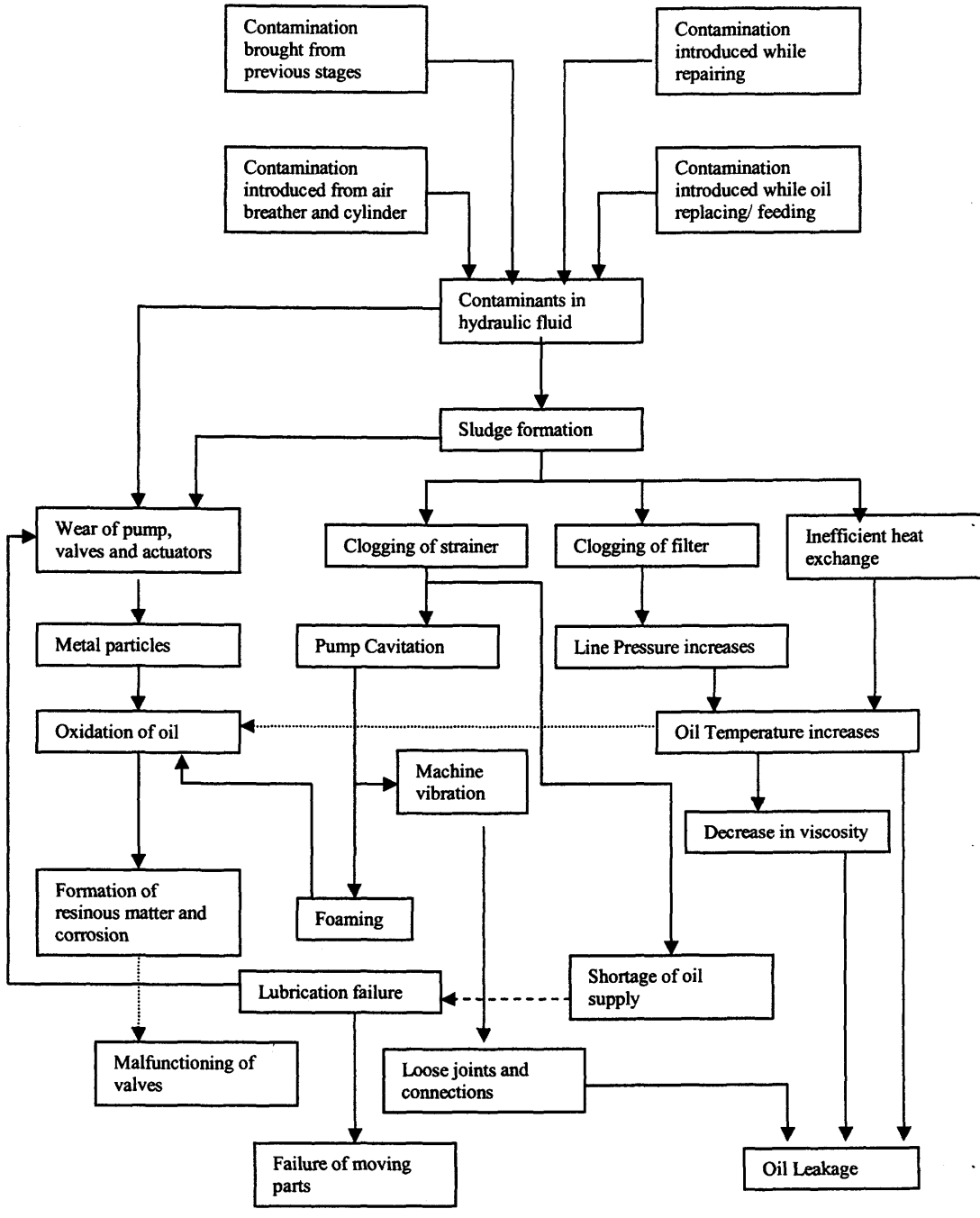

Figure 2.2: Correlation of Oil Contamination and Hydraulic Problems, reproduced from [Sasaki et al, 1984, pp. 116]

In gear pumps for example, a small amplitude high frequency ripple component is usually superimposed on the mean flow rate due to meshing and unmeshing action of the teeth [Zavarehi, 1997]. Spectral analysis of the pressure ripple data is an insight into the health of the pump. The pressure ripple's fundamental frequency depends on the number of teeth, and on the pump speed. Its frequency and shape can change with wear for example. Through the ripple characteristics, effective monitoring of the pump condition can be achieved.

An extensive review of condition monitoring strategies in fluid power is given in [Hunt, 1984] and [Hindman et al, 2002]. Hunt reveals that both time based and frequency based analyses have been used to indicate wear or faults. As the signal in a rotating machine repeats itself in a cyclic manner, time domain analysis is an easy method of interpreting a vibration signal. However, as reported in [Zavarehi, 1997, pp.11], "*one of the limitations of vibration analysis for condition monitoring in fluid power is that although spectral analysis (frequency based analysis) is a powerful tool for condition monitoring of high frequency systems such as rotating pumps and motors, they fail to provide adequate information when used to detect faults affecting low frequency responses such as in linear actuators and valves*".

2.4 Temperature Monitoring

Temperature monitoring is measuring the temperature rise of the hydraulic fluid as it passes through a component such as a pump [Hunt, 1986]. In general, excessive temperature hastens oxidation of the oil, reduces oil viscosity, promotes wear in pumps, valves and actuators as well as accelerates seal deterioration. Monitoring this parameter is therefore important. The change in temperature occurs due to the horsepower loss (product of pressure drop and flow) as the fluid passes through hydraulic resistances such as orifices, valves, pipes and leakage paths [Merrit, 1967]. Certain temperature rises are normal due to pressure changes but if a change in flow characteristics occurs, the temperature change is going to be modified. In pumps for instance, a temperature rise in the fluid can be interpreted as a drop in efficiency of the pump as slippage increases due to wear. However, care should be exercised when using this technique

since changes in room temperature or of the hydraulic system environment need to be taken into consideration for reliable diagnosis to be made. Similar approaches can be made in regards to condition monitoring of valves and filters. In addition, the use of thermographs using infra-red cameras can indicate hot spots in a hydraulic system due to inefficiencies of components as a result of wear or temperature rise at points of leakage [Hunt, 1986]. Monitoring the oil temperature in the reservoir will also give valuable information about the health of the hydraulic system.

2.5 Pressure and Flow Monitoring

Pressure measurements can provide a good indication of leakage problems and faulty components such as pumps, flow control valves, pressure relief valves and actuators. Excessive pressure drops in hoses or pipelines can also be detected by pressure measurements. Pressure monitoring in pumps and at different locations in the system by the use of pressure transducers, is a valid fault-detection scheme [Hunt, 1986]. Loss of pressure may indicate a faulty pump, load failure or bursting of hoses for instance. This technique is not specific to a particular component but rather a monitoring scheme for the complete system. Pressure pulsation monitoring is, in fact, used in conjunction with vibration analysis to diagnose faults.

Flow monitoring involves the use of flow meters [Hunt, 1986]. A reduction in the normal flow can be due to leakage in the system, pump fault, or component wear and deterioration. Monitoring the case drain flow in a pump for instance can give valuable information about the condition of the pump. Flow meters can indicate whether or not the actuator is receiving the expected flow rate. In addition to flow and pressure measurements, checking the level of fluid in the reservoir is another easy method to determine leakage in the system.

A flow measurement strategy will work more easily in the open loop configuration to detect leakage than in the closed loop systems. An example is when a closed loop position system is operating, excessive pump slippage, which could be detected by monitoring pump flow in the open loop form, is compensated for by an increase in the speed of the motor driving the pump. Therefore, this fault cannot be

detected by monitoring the pump flow alone but if the speed of the motor is monitored as well, an increase in speed without a corresponding increasing in flow indicates a pump fault. Another drawback of using flow measurements or pressure measurements to monitor the health of the system is that "*noise associated with these measurements, can be misinterpreted as faults*" [Zavarehi,1997]. In addition, it is not always feasible to have these sensors on the hydraulic machines, especially off-highway equipment, because the sensors can be damaged when the machines operate in harsh environments [Hindman, 2002]. Also accurate and robust flow meters are very expensive.

2.6 Expert Systems for Condition Monitoring in Fluid Power

Much research has been conducted in the area of automatic fault detection and diagnosis using expert systems-also referred to as knowledge-based systems. "*Expert systems are computer programs in which the special problem solving skills of an expert in a particular area have been transferred to a computer. The expert system codifies and stores in a computer the knowledge and experience of an expert*"[Guo et al, 1989, pp.310]. This approach for fault diagnosis has been motivated primarily by the emergence of increasingly complex hydraulic systems, with a large number of components and the requirement for rapid and reliable fault diagnosis. For instance, if by the use of two flowmeters, flow upstream and downstream of a directional control valve, are monitored, leakage in the component can be detected by a difference in the flow measurement. This example is taken from [Burton et al, 1990]. A simple set of rules to implement this procedure is as follows:

IF Flow upstream [entering the control valve] is monitored;
AND Flow downstream [leaving the valve] is monitored;
AND Flow upstream is not equal to Flow downstream;
AND control valve is not in the closed center position;
THEN Leakage is occurring at the control directional valve;
AND THEN Operator is informed.

This example illustrates a simple application of an expert system in condition monitoring. This technique of using conditional statements, "*IF-THEN*" rules, is

commonly referred to as the production rules where the IF's are called the antecedents and the THEN's consequents [Burton et al 1990]. Furthermore, as the hydraulic machine increases in size and complexity, the number of rules needed to fully diagnose faults becomes enormous. Fault Tree Analysis is usually used to analyze the system and identify all of the possible component fault combinations which could be responsible for particular failures [Hogan et al, 1996]. However, the fault detection and diagnosis time increases enormously with the increasing set of rules for complex systems [Zavarehi, 1997].

Moreover, another drawback of this technique, as reported in [Burton et al 1990, pp. 539], is that "*there is no guarantee that the knowledge acquisition process, or the set of rules, will be sufficient to correctly diagnose a fault because of incorrect or incomplete a priori information*". Also, expert systems tend to be specified for a certain plant only and knowledge is not easily generalized to other plants. Noisy measurements can severely affect the results of fault diagnosis since expert systems have little capability for robust handling of noisy data [Zavarehi, 1997].

2.7 Neural Networks for Condition Monitoring in Fluid Power

The fundamental principle in neural computing is that a complex function can be processed by a large number of simple, interconnected elements in a network. The neural network thus consists of multiple layers of neurons connected in series and parallel and this interconnection of neurons allows the network to learn complex non-linear functions. The neural network is basically trained, rather than programmed, by making use of a set of input and output data. Mathematically, the influence of one neuron on another is described by the weight associated with the interconnections and the training process consists of modifying the weights in the network [Atkinson et al, 1996]. Figure 2.3 (a), reproduced from [Gupta, 2001], is a schematic of a single neuron. It has an array of sampled inputs which are multiplied by weights, followed by an addition operation of all the weighed inputs to generate a single value which in turn, goes through a nonlinear, mapping operation to generate an output. This output can be an input to another neuron. Figure 2.3(b), also reproduced from [Gupta, 2001],

illustrates the training of a neural network, where the training algorithm modifies the weights in the neural network by making use of the error between the actual system output and the network output. The network is trained when it is able to mimic the actual system.

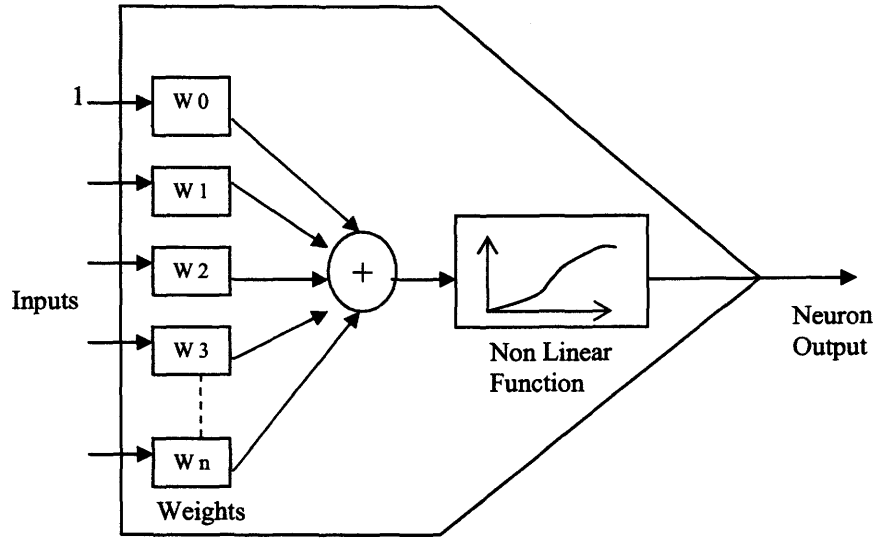

Figure 2.3 (a) Schematic of a Neuron [Gupta, 2001]

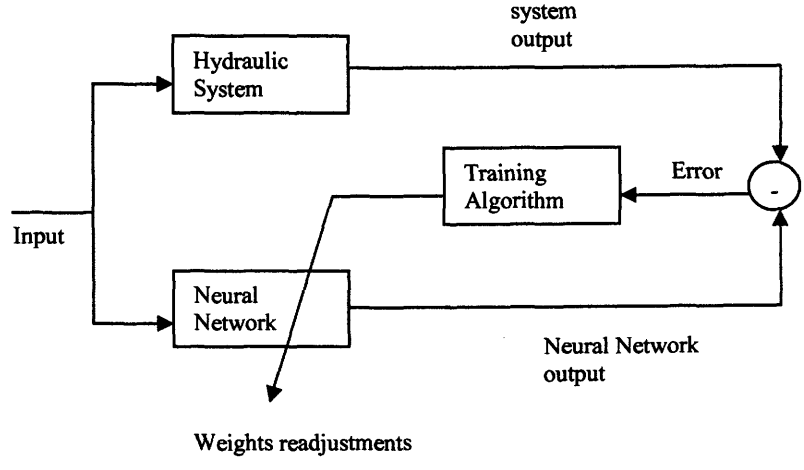

Figure 2.3 (b) Training Process of a Neural Network [Gupta, 2001]

In fault diagnosis using neural networks, the fact that a neural network, with at least one hidden layer containing non-linear functions, can learn any continuous, bounded, nonlinear functions is of interest [Atkinson et al, 1996]. One approach is to make the network learn the mapping between the state space behavior of the hydraulic system (velocity, pressure, displacement, and flow) and the values of parameters (viscous damping coefficient, leakage coefficient) that need to be monitored. Thus the input to the neural network is the system measurements while the outputs of the network are parameters of interest [Crowther et al, 1996]. A slight variation of this approach is to use the weights of the networks as parameters of interest [Rosa, 2001].

Rosa used a neural network to estimate the parameters of a proportional solenoid valve and monitoring these parameters indicated the presence of faults in the component. The parameters of interest were the main spool viscous friction constant, the main spool Coulomb friction constant, the main spool orifice area gradient, main spool spring constant and the main spool spring pre-compression. The spool displacement and velocity were used as inputs to a single neuron. The weights of the trained neuron were the parameters of interest.

Neural networks are able to establish heuristic, unstructured relationships between inputs and outputs of non-linear systems. The major disadvantage of this method is that the data used for training has to represent a broad range of operating conditions for the systems and such richness and availability of data are not always easy to obtain. Also, another issue becomes the selection of measurements or inputs which are the most appropriate for the neural networks. Furthermore, the training process can be quite tedious, especially when the number of faults increases [Zavarehi, 1997]. Neural networks also tend to identify steady state faults more easily than dynamic faults, occurring during transient periods [Crowther et al, 1996].

In addition to approximating nonlinear functions, neural networks have been used for condition monitoring purposes as pattern classifiers, where fault classes are produced corresponding to the different fault situations. In this approach, the neural networks assign input patterns, which consist of a vector of system features selected for distinguishing between the fault classes, to a finite number of classes [Zavarehi, 1997].

The classifier partitions the input feature measurements into decision regions that indicate to which class any of the input patterns belong. Neural network pattern classifiers form nonlinear discriminant functions using single or multilayer neural networks. However, a steady state needs to be reached for reliable classification.

In [Hindman, 2002], a method for evaluating the condition of a valve and of the actuator in a mobile hydraulic system was developed. In his study, an artificial neural network was used to map pressure and temperature changes to actuator and valve faults. The inputs of the neural network were pressure and temperature measurements and its outputs indicated and detected the actuator failure and the valve failure; the artificial neural network mapped the network input to an actuator and valve fault condition (increase in internal leakage). Data obtained, using a pre-specified procedure, was used to train the neural network, and the output of the network assigned a numerical value indicating the severity of the fault (the pressure profile was used to quantify the fault condition).

2.8 Fault Detection Using Mathematical Models of the Systems

A brief review of condition monitoring strategies involving direct measurements, fluid analysis, expert systems and neural networks has been presented in the previous sections. In this research, the approach used for fault detection differs from the techniques mentioned previously: although measurements (sensor data) are needed, a mathematical model of the system is also required. These methods can be used for predicting signals and estimating non-measurable state variables and process parameters. Therefore, the strategy is essentially a parameter estimation method; an approach which has become popular with the emergence of powerful digital computers. The process model parameters are constant coefficients, which appear in the mathematical description of the relationship between the input and the output signals [Isermann, 1984]. In this health monitoring approach, system measurements, which are normally corrupted by noise, are taken and fed to the parameter estimation algorithm, which has a mathematical model of the system embedded in it. This condition

monitoring approach is illustrated in Figure 2.4, reproduced from [Isermann, 1984, pp. 390].

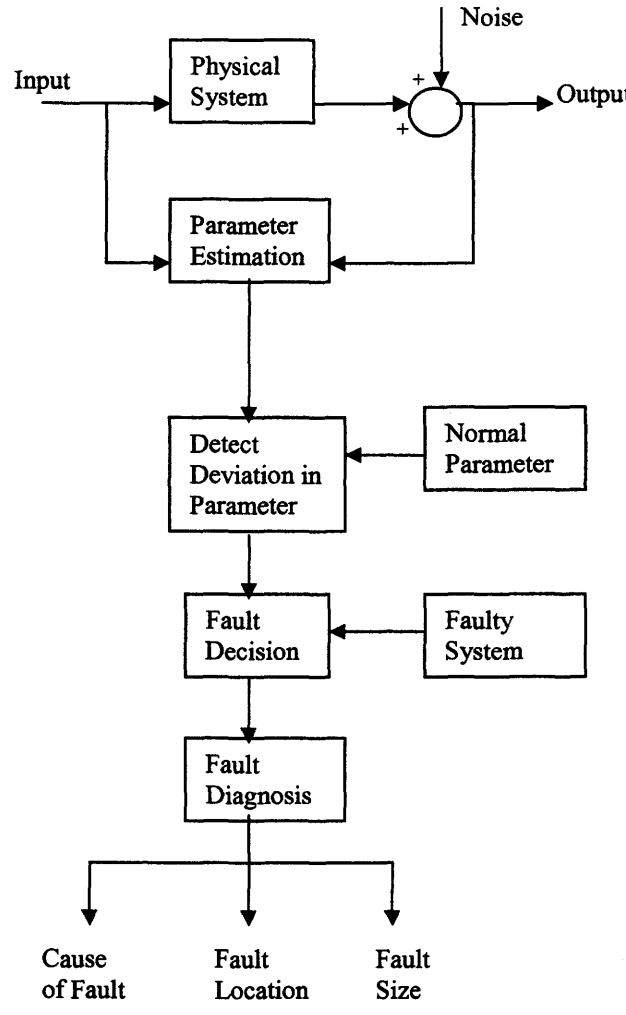

Figure 2.4 Fault Detection Based on Parameter Estimation

Thus, for a hydraulic system, estimating critical parameters, (such as the viscous damping coefficient, the leakage coefficient, etc.) can be used to monitor the health of the system. Any deviation of these parameters from their normal values can be interpreted as faults. This is shown in Figure 2.4 where the non-measurable estimated parameter value is compared to its normal value and a "fault decision" is subsequently

made. These non-measurable states and parameters of interest are estimated based on physical laws and are obtained by applying recursive parameter estimation techniques such as the Extended Kalman Filter [Zavarehi, 1997,Cao, 2001,Wright, 2001] and least squares method [Ansarian, 2001] to the system. The final step in this generalized structure of fault detection method is based on process models and non-measurable quantities is fault diagnosis, which implies fault location, cause and magnitude.

Ansarian, used two techniques, namely the ordinary least square and the maximum likelihood methods to estimate parameters in a hydraulic valve [Ansarian, 2001]. The experiments consisted of closed outlet port tests to estimate spring constant and precompression (flow forces on the spool are eliminated) and open port tests where valve orifice area gradient and deadband were estimated. The ordinary least square method consists of "*minimizing a sum of squares based on the difference between the measured values and the predicted values*" [Ansarian et al, 2002]. The other parameter estimation method is the maximum likelihood method and it makes use of the "*statistical information available regarding the distribution of the observations*" [Ansarian et al , 2002].

2.9 Condition Monitoring Using the Extended Kalman Filter

In this study, the Extended Kalman Filter (EKF) is used to estimate some critical parameters in a hydrostatic system, referred to as the Electrohydraulic Actuator (EHA). The Extended Kalman Filter has been used previously with success for condition monitoring of hydraulic systems. The Extended Kalman Filter is a state and parameter estimation technique which makes use of the model of the system embedded in it to estimate current states and predict future states and parameters in the presence of noisy measurements. The Kalman Filter estimates the states of a linear stochastic system but parameter estimation (as explained in more detail in Chapter 6) involves a nonlinear function and the Extended Kalman Filter (EKF) is used instead.

Cao [2001] used the Extended Kalman Filter to estimate parameters for a swash plate assembly and control piston in a load sensing pump [Cao, 2001]. These pumps compensate for variations in the load conditions, and this is achieved by a piston which

controls the swash plate movement of the pump. Parameters such as the viscous damping coefficient and spring constant coefficient as well as the spring pretension coefficient in the swash plate were estimated using the EKF. Simulation results showed that accurate prediction of the parameters could be achieved. Experimental results showed that parameters estimated were reasonably repeatable for similar operating conditions.

Wright made use of the EKF to estimate some critical parameters of a proportional solenoid valve [Wright, 2001]. The study showed the application of the EKF technique to the main stage of a two-stage solenoid proportional valve. The experimental procedures, which were similar to the one used by [Ansarian 2001], consisted of two distinct operating conditions, namely the closed and the open port scenarios. During the closed port tests (no flow through the valve), the EKF technique was used to estimate parameters such as the valve spring coefficients, spring precompression, viscous friction and Coulomb friction. It was found that the estimated values of the spring constant and the spring precompression coefficient were repeatable but estimates of the valve spool viscous damping coefficient were not. Furthermore, the EKF was not able to detect Coulomb friction effects. The open port tests (shorting the valve flow) were used to predict the deadzone (spool overlap) and the flow force spring coefficient (used to find the orifice area gradient). The EKF was successful in estimating the valve deadzone and the flow force spring coefficient.

Zavarehi used the EKF technique to monitor the condition of a hydraulic system consisting of a solenoid proportional valve and of an actuator [Zavarehi, 1997]. The EKF was used to estimate states and parameters which could not be measured directly and included the solenoid magnetic force and coil resistance, the pilot valve flow rate and the orifice area.

2.10 Condition Monitoring for the EHA System Using the EKF

In this study, the EKF technique is applied to a hydrostatic system referred to as the Electrohydraulic Actuator (EHA) rather than using some of the other mentioned

techniques. The EKF is chosen as the condition monitoring scheme for the EHA, at the expense of other condition monitoring strategies for the following reasons:

1. The EHA is a hydrostatic system and as such there is no oil reservoir. Contamination monitoring is not practical since an oil sample is not readily obtained. Investigating the contaminants in the oil can be done as part of a scheduled maintenance program where the aircraft for example is grounded for some time, but it will still imply opening up the lines and refilling the system with oil, thereby increasing the risk of having air being trapped in the system.
2. The EKF has been applied successfully to hydraulic systems in the past and using it in this particular application seems logical.
3. The EKF can work in the presence of noise in the data. The algorithm has some terms that quantify the level of noise to be expected in the data. Position measurement in the EHA is currently being made using an optical encoder which produces a "clean" signal. But earlier feasibility studies involving the EKF made use of noisier sensor data and the EKF was able to estimate the parameters successfully. Therefore, it can be expected that the EKF will predict parameters without major difficulties using clean signals.
4. The EKF is known to detect changes in parameters as well as to predict the new parameters accurately. Therefore, its use for condition monitoring purposes in the EHA is justified in the sense that it both diagnoses the fault (since the parameters can be related to typical faults) as well as quantifies the fault (the level of parameter deviation from the normal value).
5. The EKF requires a fairly accurate model for the system under investigation. A mathematical model for the EHA was already available at the beginning of the research.
6. The parameters of interest for this study are the effective bulk modulus and the viscous damping coefficient. The effective bulk modulus is mostly dominant in the transient region and as such the use of neural network or expert systems to estimate this parameter or to detect a fault due to this parameter is believed to be challenging. The EKF is well suited since fast convergence to the desired parameter can be

achieved by using the proper initial conditions for the filter (using a large initial error covariance for the states). Techniques such as limit checking for pressures and flow rates are valid condition monitoring strategies, but cannot be used in this particular application since the parameters of interest are not readily measured.

7. The EKF, in addition to estimating parameters, estimates states as well. This has its own advantages since the more information one has about a system, the better equipped one is to detect faults and even diagnose them.
8. As mentioned in earlier sections vibration/spectral analysis is mostly applied to rotary systems (high frequencies) and since the EHA has a linear actuator, this technique is not believed to be the best approach. Nevertheless, this does not exclude its use to detect faults in the bi-directional gear pump (wearing of gears is reflected in the pressure ripples).
9. Expert systems and neural networks show challenges of their own, in terms of difficulties in codifying the set of rules for fault detection and training of the neurons. The EKF can be tedious to "tune" but as seen earlier, one of the objectives of this research is to make this process a little less tedious by making the filter work without assuming any priori information to initialize the state matrix.

2.11 Conclusions

In this chapter some of the most commonly encountered condition monitoring schemes in the fluid power area have been presented. Previous research involving the use of the Extended Kalman Filter for parameter estimation is reported. The reasons for choosing the strategy used for condition monitoring of the Electrohydraulic Actuator are explained. In Chapter 3, the Electrohydraulic Actuator (EHA) is presented. A mathematical model for the EHA is described. Furthermore, a faults and effects analysis for the EHA is proposed.

Chapter 3
Electrohydraulic Actuator (EHA)

This chapter serves as an introduction to the Electrohydraulic Actuator (EHA). The different components of the EHA are briefly described. A linearized mathematical model of the EHA is also presented. A faults and effects analysis of the EHA concludes this chapter.

3.1 Introduction

Two types of hydraulic transmission systems are commonly used in industry, namely valve controlled and pump controlled hydraulic systems. A typical valve controlled hydraulic system is shown in Figure 3.1, [Habibi, 2000]. The valve acts as the control element, regulating the flow to and from the supply system. The electric motor drives the hydraulic pump, which delivers oil to the circuit. The pump runs at a constant speed, giving a constant flow rate. Depending on the magnitude of the force acting on the actuator, flow entering into (from) the actuator chambers results in a pressure build up (drop) in the fluid. When the pressure differential exceeds the opposing forces on the actuator (friction), the piston will move. This circuit configuration is commonly found in industry.

Higher performance can be achieved by using a servovalve as the control element. A servovalve is a directional control valve that has infinite variable positioning capability (the valve has variable orifice area) and has precise metering properties. Usually, servovalves are coupled with feedback sensing devices which allow for very accurate control of position, velocity and acceleration of the actuator. It is also worth noting that the use of double rod cylinders (symmetrical actuator), with equal working areas ensures equal flows going to and from the actuator and consequently avoids problems resulting with speed and force asymmetry. However, in industry, asymmetric actuators are commonly used because they require less space, especially in applications where the effective length of the cylinder is limited by fixtures surrounding the piston.

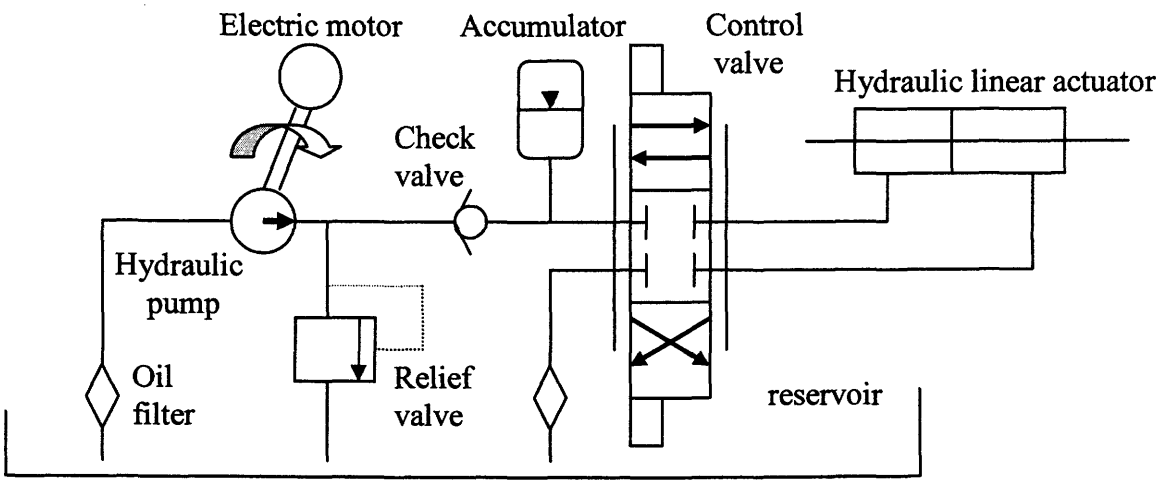

Figure 3.1 Valve Controlled Hydraulic Actuation System.

The major drawbacks of conventional hydraulic systems are an oil reservoir, low efficiency (when a fixed speed electric motor is used to drive a variable displacement pump) and losses at the valves and high costs if servovalves are being used.

A potential alternative to a valve controlled hydraulic actuation system, for niche applications, is hydrostatic transmission, which consists of a hydraulic pump supplying fluid to a hydraulic actuator. In a "closed" form, the pump and the actuator are "connected" directly as shown in Figure 3.2. As such, the pump is the element that controls the flow to the actuator and no valves are required to change the flow.

A typical closed hydrostatic circuit is shown in Figure 3.2. The pump supplies oil to the circuit and controls movement of the actuator. Fluid on the downstream side of the actuator is ported directly to the inlet of the pump. Hydrostatic transmissions have been used as an alternative to servovalve controlled conventional actuation systems when the requirement for positional accuracy is not very stringent. Most hydrostatic circuits, as illustrated in Figure 3.2, use a constant speed motor, with a variable displacement pump. In these circuits, moving a swash plate in the pump changes the volumetric displacement of the pump and therefore regulates the oil flow and movement of the hydraulic actuator.

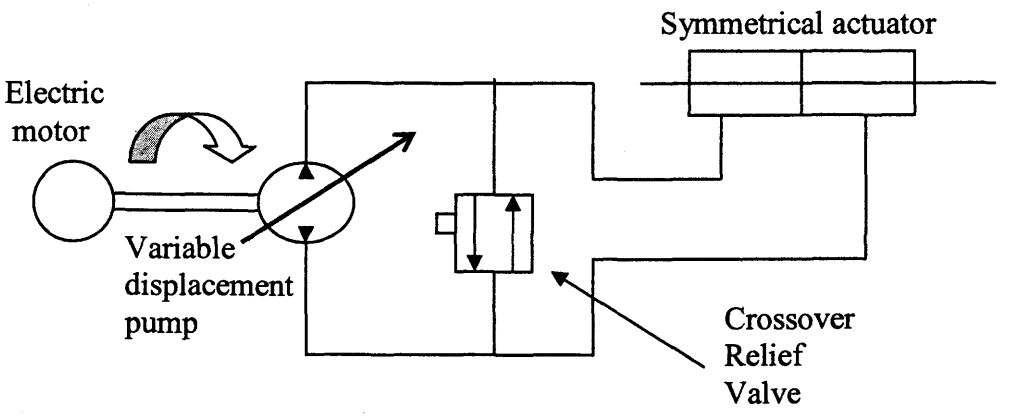

Figure 3.2 Closed Hydrostatic Circuit.

The configuration shown in Figure 3.2 is widely used in industry and contains a variable displacement pump coupled to an actuator or more commonly, a motor. Additional circuitry for swash plate angle control is usually needed. In industry, single rod actuators are commonly used but their application in hydrostatic transmission requires modified and complex circuitry to compensate for the different flow rates at the actuator.

Furthermore, as illustrated in Figure 3.3, a plot of input motor current and motor speed for an electric motor or hydraulic pump (assuming stiff coupling) reveals the presence of a dead-band in hydrostatic actuation [Habibi, 2000]. This dead-band at the pump/motor interface is largely due to a nonlinear friction effect, including static and Coulomb friction and limits positional accuracy and stability of such a system.

3.2 Description of the Electrohydraulic Actuator

The operation of the Electrohydraulic Actuator, in this study referred to as the EHA, is based on the principle of closed-circuit hydrostatic transmission. As mentioned in the previous section, in hydrostatic transmission, the exhaust oil from the cylinder (or motor) is returned directly to the pump inlet. The pump is connected directly to the actuator. The EHA was designed for high positioning accuracy, able to compete with conventional closed loop hydraulic systems, [Habibi, 1999]. As with all conventional hydraulic actuation systems, the EHA has a high torque to mass ratio; however the EHA system offers advantages such as a negligible deadband, high positioning accuracy

(1 micron) in the closed loop form, high efficiency due to the absence of control valves and linearity. The main constituent of the EHA is a bi-directional fixed displacement gear pump which rotates with variable speed in the direction of actuator movement. In the EHA, the effect of the dead-band (Figure 3.3) is resolved by using a high gain inner-loop control strategy.

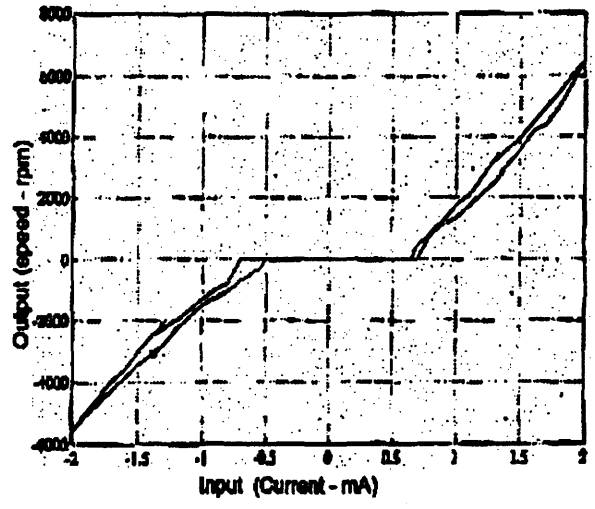

Figure 3.3 Dead-band in a Hydrostatic Actuation System [Habibi et al., 2000, pp. 11].

The components of the EHA are:

- an electric motor,
- a variable speed, fixed displacement, bi-directional gear pump,
- a symmetrical linear actuator (which is designed specifically for the EHA),
- pressure and position sensors,
- an accumulator,
- a cross over relief valve,
- an inertial load, and
- a filtering sub-circuit (which is not present in this study).

A schematic of the EHA is depicted in Figure 3.4.

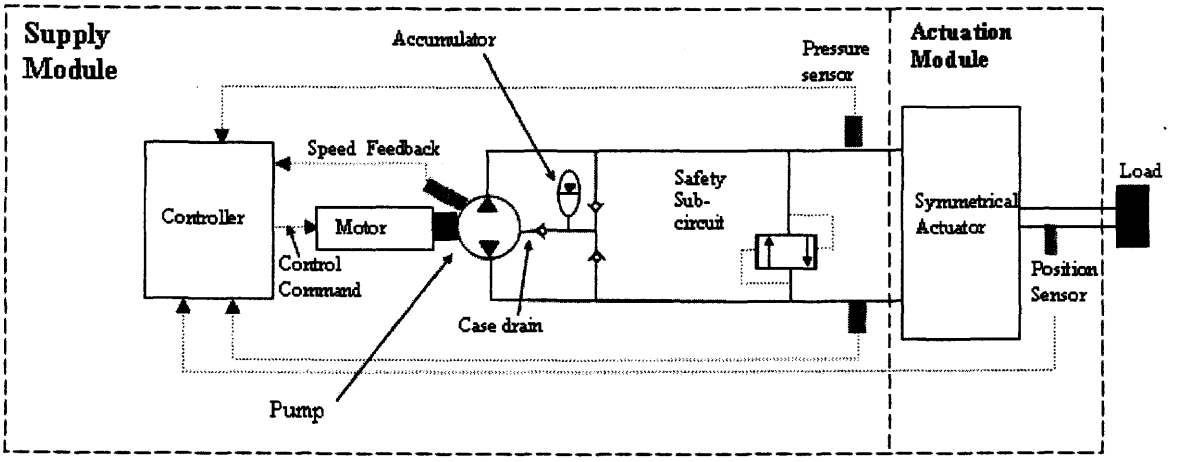

Figure 3.4 Schematic of the Electrohydraulic Actuator (EHA)

The EHA uses a bi-directional, fixed displacement gear pump to supply oil to the actuator. Unlike conventional hydrostatic systems, where the motor speed is kept constant and where there is need for additional circuitry for actuation of the swash plate angle of the variable displacement pump, flow rate control is achieved in the EHA by simply varying the speed of the electric motor. When the flow encounters a resistance such as an actuator, its fluid pressure increases. The pressure difference in the actuator chambers results in exertion of a force on the external load, (in this study, a horizontal sliding mass). A symmetrical actuator has been specially designed for the EHA and is used in its experimental prototype, details of which can be found in [Habibi, 1999].

In the following sections, the different components of the prototype (pump, actuator, accumulator and electric motor) are described briefly, and the relevant equations, which are needed to develop a mathematical model for the system, presented. In addition, the ratings of these components are given in order to have a better understanding of the system. These rating are used to calculate the maximum velocity of the piston and for power calculations, as well as to understand the criteria which were used when these components were selected.

3.2.1 Hydraulic Pump

A bi-directional hydraulic gear pump is used in the EHA. The pump has three ports, with two large diameter ports as input/output ports and a case drain port for pump

external leakage. The input/output ports are connected to the actuator ports via steel tubing and the case drain line is connected to the inner accumulator circuit via check valve (Figure 3.4) in order to minimize oil losses since the oil leaking is returned back to the circuit. It is worth noting that the piston position accuracy is dependent on the pump volumetric displacement. A small displacement per revolution implies finer movement of the cylinder rod, and higher control resolution. But this will be at the expense of rod speed which is proportional to pump displacement. A trade-off between maximum rod speed and positioning accuracy is required.

In the EHA, a fixed displacement gear pump (John S.Barnes G.C series No.04) is used, with a volumetric displacement D_p of 0.065 cu.in/rev (1.065cc. /rev) and a maximum speed of 4000 rpm. The nominal output pressure P_n is 207 bars (3000 psi) and maximum intermittent output pressure is 276 bars (4000 psi). At maximum angular speed $\omega_{\max}$ of 4000 rpm, the flow Q_{pump} delivered by the pump is given by, $Q_{pump} = D_p \omega_{\max}$ and is calculated as being 7.1×10^{-5} m^3/s (4.26 l/min). The nominal output power from the pump, given by, $Q_{pump} P_n$, is 1.5 kW. It should be noted that calculations are for an ideal system with negligible leakage and pressure drops.
The pump flow is modeled as, [Habibi, 2000]:

$$Q_a = D_p \omega_p - \xi(P_a - P_b) - \frac{V_a}{\beta_e}\frac{dP_a}{dt} - C_{ep}(P_a - P_r) \tag{3.1}$$

$$Q_b = D_p \omega_p - \xi(P_a - P_b) + \frac{V_b}{\beta_e}\frac{dP_b}{dt} + C_{ep}(P_b - P_r) \tag{3.2}$$

where Q_a is the flow delivered by the pump (m^3/s), Q_b is the flow entering the pump (m^3/s), ξ is the pump cross-port leakage coefficient (m^3/sPa), D_p is the pump volumetric displacement (m^3/rad), P_a represents pump pressure at its outlet port (Pa), P_b is pump pressure at its inlet port (Pa), V_a is the pump section volume associated with its outlet port (m^3), β_e is the effective bulk modulus of hydraulic oil, (Pa), V_b is the pump section volume associated with its inlet port (m^3), ω_p is the pump angular velocity (rad/s), C_{ep} is the pump external leakage coefficient (m^3/sPa) and P_r is the accumulator pressure (Pa).

3.2.2 New Symmetrical Linear Actuator for the EHA

As mentioned earlier, a symmetrical linear actuator has been specifically designed for the EHA, [Habibi et. al, 1999]. A symmetrical actuator is needed in order to keep the "in going" and "out coming" flows from the actuator the same. Symmetrical actuators are very convenient in robotics, in aircraft (space critical applications) and in industry in general. In this design, there are two working chambers, C1 and C2, as illustrated in Figure 3.5, [Habibi et. al, 1999]. A hollow cylinder, which is closed at one end and which has a circular disc around the opening at the other end, replaces the solid rod of the conventional piston. The surface area of the closed end of the cylinder, A1, is made equal to the area A2 of the disc. A1 and A2 are the active areas of the two pressure chambers and are made equal for symmetry.

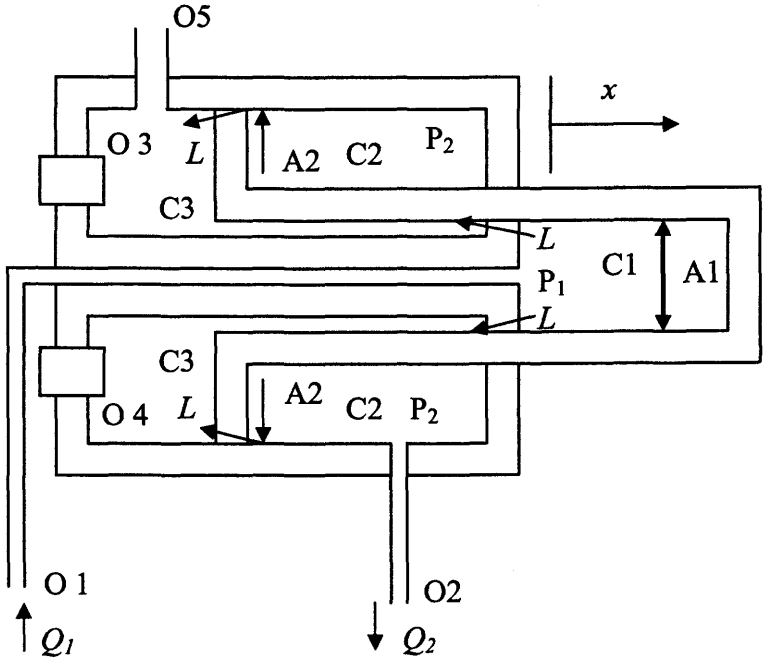

Figure 3.5 Symmetrical Actuator for the EHA

Chamber C3 can be opened to the atmosphere or can be filled with pressurized gas or fluid in applications where a bias is required to counter balance dead weight acting under gravity. The contact between the cylinder and the fixed body of the

actuator is through low friction seals. Hydraulic fluid enters the two chambers of the actuator through openings O1 and O2. There can be some external leakage across the seal into chamber C3. The openings O3 and O4 allow draining of fluid from this chamber. Opening O5 is provided to allow pressurization of chamber C3 for specialized applications. The actuator is made of stainless steel and all dynamic, low friction Teflon seals are of a lip pre-energized type.

The disadvantage of this design is the complicated fabrication procedure compared to conventional single rod cylinder. The piston area $A = A_1 = A_2$ is 5.051×10^{-4} m^2 (0.783 in^2). Thus the theoretical maximum piston velocity, given the maximum flow, is $v_{max} = \frac{Q_{pump}}{A}$ =0.14 m/s. The maximum output force is 10.5 kN and the piston stroke is 12.65 cm.

The mathematical model of this actuator is described by the following equations, [Habibi et al 2000]:

$$Q_1 = A\dot{x} + \left(\frac{V_{0ac} + Ax}{\beta_e}\right)\frac{dP_1}{dt} + LP_1 \tag{3.3}$$

$$Q_2 = A\dot{x} - \left(\frac{V_{0ac} - Ax}{\beta_e}\right)\frac{dP_2}{dt} - LP_2 \tag{3.4}$$

where $A = A_1 = A_2$ and Q_1 represents flow in the actuator (m^3/s), Q_2 is the flow out of the actuator (m^3/s), A is the pressure area in the symmetrical actuator (m^2), x is the displacement from mean position (m), V_{0ac} is the pipe volume plus actuator chamber volume at zero position (m^3), P_1 is the pressure in chamber C1 of actuator (Pa), P_2 is the pressure in chamber C2 of actuator (Pa) and L is the actuator external leakage coefficient (m^3/sPa).

3.2.3 Accumulator

The accumulator is a device that stores the potential energy of an incompressible fluid held under pressure. A bladder type accumulator is used in the EHA. It contains an elastic barrier between the oil and the gas. The accumulator is used to prevent oil cavitation, by pressurizing the forward and return lines to its preset pressure, and to prevent introduction of air in the system [Habibi, 2000]. It also serves as a source of oil for the system, replacing external leakage losses from the actuator, pump or connections. It maintains a minimal system pressure of 2.76 – 6.9 bars (40-100 psi). A pressure higher than 6.9 bars (100 psi) will damage the pump seals (case drain). The accumulator is present in the prototype but it is not included in the mathematical model for the EHA. The reason is that from [Habibi et al, 2000], it is assumed that for control applications, the accumulator dynamics are insignificant and can be neglected in deriving a simplified mathematical model for the EHA.

3.2.4 Control Strategy in the EHA

The EHA system can be divided into two hydraulic sub-circuits, namely a high-pressure outer-circuit connected to the symmetrical actuator and an inner-circuit with the low-pressure accumulator. The inner circuit prevents cavitation and replaces leakage losses. The control strategy used in the EHA is critical for its performance. Two control loops are used, as shown in Figure 3.6.

Loop 1 is a high-gain inner loop controller used to regulate the motor speed and hence provide an accurate control over the pump flow. This flow control strategy desensitizes the system to dead-band occurring due to friction at the pump-motor interface.

Loop 2 is an outer-loop controller, which allows precise control of the output variable (position).

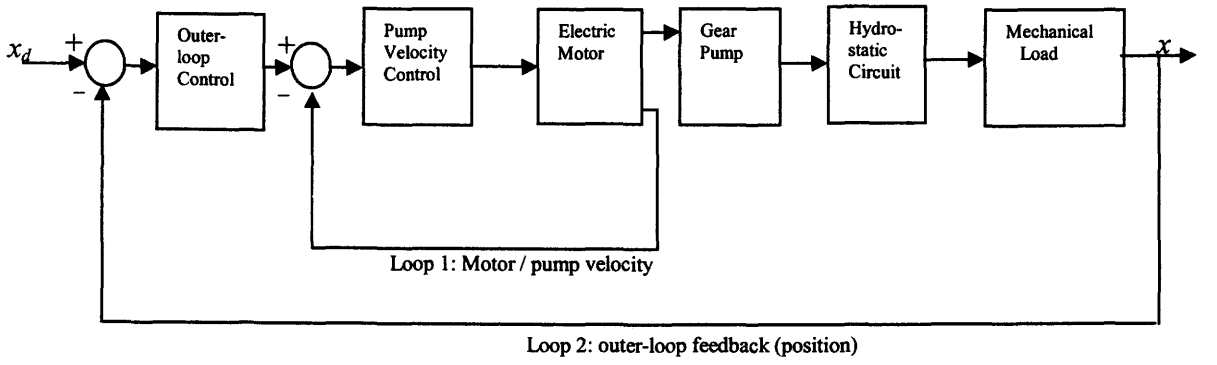

Figure 3.6 Control Block Diagram for the EHA

3.2.5 Electric Motor /Pump Subsystem Model

This section describes the reason for selecting the specific electric motor for the EHA and this is included here for completeness. The electrical motor used for driving the EHA pump is the Infranor Mavilor MA 30 motor. The power requirement of the electric motor, (assuming 80% pump efficiency and using the pump output power) is about 2.5 kW. Based on this requirement and desired characteristics for output torque, maximum speed, mechanical and electrical time constants, the Mavilor MA 30 has been used in this prototype. The motor output power is 3.2 kW and is a high performance three-phase AC brushless electrical motor, with a pancake construction. The motor also includes an integrated resolver which is used to provide motor velocity feedback. The controller (Infranor SMTBD1 digital controller) controls the speed and also monitors motor overheating as well as current overload. The motor speed input command is an analog signal within the range of −10V to +10V. "*Careful selection of the motor in conjunction with a high gain inner loop proportional integral motor speed control strategy can substantially reduce the dead-band*" shown in Figure 3.3 as explained below, [Habibi, 2000, pp. 15].

The relationship between the field current and the input voltage of the three-phase motor can be modeled as a first order transfer function as shown below:

$$G_1 = \frac{I_c}{V_c} \tag{3.5}$$

where $G_1 = \frac{1/R_c}{(L_c/R_c)s+1} = \frac{K_e}{\tau_e s+1}$ with I_c being the control input current (A), V_c is the control input voltage (V), R_c represents motor line-to-line resistance (Ω), L_c is motor line-to-line inductance (H), K_e being motor electrical circuit gain(Ω^{-1}) and τ_e being the motor electrical circuit time constant (s).

The torque generated by the motor is characterized by

$$T_m = K_c I_c - K_\omega \dot{\theta} \tag{3.6}$$

where T_m is the motor torque (Nm), K_c being motor gain (Nm/A), K_ω being motor equivalent viscous-friction constant (Nms/rad), and θ representing motor angular position (rad). Given that the motor is connected directly to the pump, the torque exerted on the pump driving shaft is given by

$$T_m = J_{pm}\dot{\omega}_p + K_{P_{visc}}\omega_p + T_{DB} + D_p(P_a - P_b) \tag{3.7}$$

where J_{pm} is the motor/pump inertia (Nms^2/rad), $K_{P_{visc}}$ coefficient due to oil viscosity (Nms/rad), T_{DB} is the nonlinear friction (including static and coulomb) at pump motor interface which is considered for this analysis as an external disturbance.

Equating (3.6) to (3.7) and taking the Laplace transform gives the pump speed as follows:

$$\omega_p(J_{pm}s + K_{Pvisc} + K_\omega) = K_c I_c - D_p(P_a - P_b) - T_{DB}$$

$$\omega_p = G_2 K_c I_c - G_2 D_p(P_a - P_b) - T_{DB} G_2 \tag{3.8}$$

where

$$G_2 = \frac{1}{J_{pm}s + K_{Pvisc} + K_\omega} = \frac{1/(K_{Pvisc} + K_\omega)}{(J_{pm}/(K_{Pvisc} + K_\omega))s+1} = \frac{K_m}{\tau_m s+1} \tag{3.9}$$

where K_m is the gain of the motor/pump transfer function and is equal to $\frac{1}{K_{Pvisc} + K_\omega}$

and $\tau_m = \frac{J_{pm}}{K_{Pvisc} + K_\omega}$ is the time constant.

A block diagram relating the pump angular velocity to the input motor voltage is illustrated in Figure 3.7.

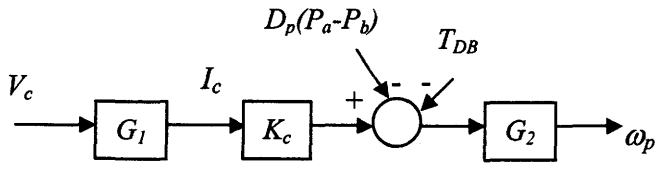

Figure 3.7 Block Representation of Equation (3.8)

When the specially designed inner loop controller is integrated into the system, the block diagram of Figure 3.7 becomes that shown in Figure 3.8.

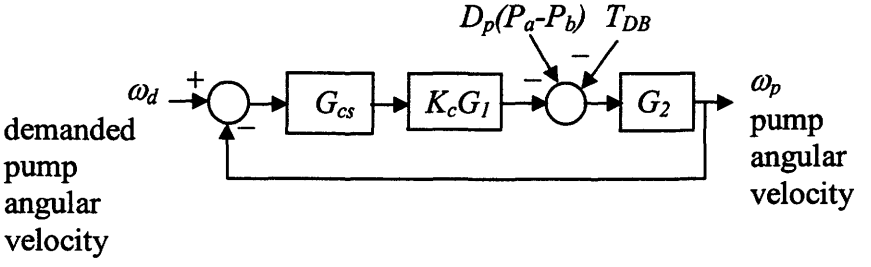

Figure 3.8 Inner-loop Controller Block Diagram

The inner loop high gain controller, G_{cs}, which is a PI type controller, becomes:

$$G_{cs} = K_{P_{cs}} + \frac{K_{I_{cs}}}{s} \tag{3.10}$$

where $K_{P_{cs}}$ and $K_{I_{cs}}$ are the proportional and integral gains respectively.

Furthermore, the relationship between the motor input and the inner controller can be characterized as $V_c = (\omega_d - \omega_p)G_{cs}$ as shown in Figure 3.8.

The overall closed loop function for the motor/pump subsystem can be expressed as:

$$\omega_p = \frac{G_{cs}K_cG_1G_2}{1+G_{cs}K_cG_1G_2}\omega_d - \frac{G_2}{1+G_{cs}K_cG_1G_2}T_{DB} - \frac{G_2}{1+G_{cs}K_cG_1G_2}D_p(P_a - P_b) \tag{3.11}$$

This equation reveals that the effect of T_{DB} and $D_p(P_a - P_b)$ which are undesirable can be minimized by using a high gain inner loop velocity controller, which

makes $G_{cs}K_cG_1G_2 >> 1$ [Habibi, 2000]. Thus it is seen from Equation (3.11) that a high gain inner loop control strategy can reduce the effect of deadband in the system.

Experimental determination of the prototype's motor/pump model has enabled the identification of the following transfer function, which relates the system input voltage to the motor velocity, as explained and reported in [Habibi, 2000].

$$\frac{\omega_p(s)}{V(s)} = \frac{2.779\times10^{-1}s + 40.55}{1 + 1.0162\times10^{-2}s + 5.7803\times10^{-5}s^2} \tag{3.12}$$

3.2.6 Linearized Model of the EHA

In this section the assumptions needed to derive the mathematical model for the EHA are presented. It is assumed that the accumulator dynamics are insignificant, i.e. the discharge flow from the accumulator is instantaneous and transients associated with the accumulator discharge are neglected. These assumptions imply that the inner circuit is at a constant pressure and that the check valves do not leak and their dynamics are insignificant.

Furthermore, it is assumed that leakage flows in the actuator and pump are laminar, i.e., leakage is proportional to pressure difference. Another assumption is that the coupling between the electric motor shaft and the pump shaft is very stiff and therefore, the angular motor speed and angular pump speed are the same. It is also assumed that there are negligible coulomb and static friction at the load linear bearings and low friction, teflon dynamic seals in the actuator. Only viscous friction is considered in the model. However, as seen later in this study, this assumption is not valid since the actuator friction characteristic is nonlinear. The other assumptions have been shown to be reasonable.

Moreover, since steel tubes are used as connecting lines, their expansion is negligible and consequently dynamic effects resulting from pipe elasticity is neglected. Also, the initial piston position is assumed such that there are equal volumes in the lines and the changes in piston position from initial position are small. This is a "weak" assumption but is required for a linearized analysis.

Consequently, the derivation for the linearized model for the EHA begins with considering the flow from the pump being equal to the flow to the actuator and this can be expressed as $Q_a = Q_1$ and $Q_b = Q_2$. The load flow Q_l can be written as:

$$Q_l = \frac{Q_1 + Q_2}{2} = \frac{Q_a + Q_b}{2} = D_p \omega_p \tag{3.13}$$

The pump/actuator pipe connection is modeled as a pressure drop, P_{pipe}. Using Darcy's pipe flow equation as

$$P_{pipe} \approx K_{pipe} Q_l^2 \approx K_{pipe} D_p^2 \omega_p^2 \tag{3.14}$$

where

K_{pipe} is the pipe coefficient relating pressure drop to flow (Pa s^2/m^6)

In a linearized form

$$\Delta P_{pipe} \approx 2K_{pipe} D_p^2 \omega_{p0} \Delta\omega_p \tag{3.15}$$

The relationship between the pump port pressures and the actuator chamber pressures can be approximated to:

$$P_a = P_1 + P_{pipe}$$

$$P_b = P_2 - P_{pipe} \tag{3.16}$$

Substituting Equations (3.1), (3.2), (3.3) and (3.4) into (3.13) yield:

$$A\dot{x} + \left(\frac{V_{0ac} + Ax}{\beta_e}\right)\frac{dP_1}{dt} + LP_1 + A\dot{x} - \left(\frac{V_{0ac} - Ax}{\beta_e}\right)\frac{dP_2}{dt} - LP_2$$

$$= D_p\omega_p - \xi(P_a - P_b) - \frac{V_a}{\beta_e}\frac{dP_a}{dt} - C_{ep}P_a + D_p\omega_p - \xi(P_a - P_b) + \frac{V_b}{\beta_e}\frac{dP_b}{dt} + C_{ep}P_b \tag{3.17}$$

Assuming that due to symmetry of the EHA, $V_a \approx V_b$, Equation (3.17) becomes:

$$2A\dot{x} + \frac{V_{0ac}}{\beta_e}\left(\frac{dP_1}{dt} - \frac{dP_2}{dt}\right) + \frac{Ax}{\beta_e}\left(\frac{dP_1}{dt} + \frac{dP_2}{dt}\right) + L(P_1 - P_2)$$

$$= 2D_p\omega_p - \frac{V_a}{\beta_e}\left(\frac{dP_a}{dt} - \frac{dP_b}{dt}\right) - 2\xi(P_a - P_b) - C_{ep}(P_a - P_b) \tag{3.18}$$

Rearranging Equation (3.18) gives:

$$D_p\omega_p - \frac{V_a}{2\beta_e}\left(\frac{dP_a}{dt} - \frac{dP_b}{dt}\right) - \xi(P_a - P_b) - \frac{C_{ep}}{2}(P_a - P_b)$$

$$= A\dot{x} + \frac{V_{0ac}}{2\beta_e}\left(\frac{dP_1}{dt} - \frac{dP_2}{dt}\right) + \frac{Ax}{2\beta_e}\left(\frac{dP_1}{dt} + \frac{dP_2}{dt}\right) + \frac{L}{2}(P_1 - P_2) \tag{3.19}$$

Since $\frac{dP_a}{dt} \approx \frac{dP_1}{dt}$ and $\frac{dP_b}{dt} \approx \frac{dP_2}{dt}$ and due to symmetry of the actuator, $\frac{dP_1}{dt} \approx \frac{-dP_2}{dt}$ for $V_o = V_{0ac} + V_a$, with V_o being the total mean volume, a simplified pump/actuator model is obtained as:

$$D_p\omega_p = A\dot{x} + \frac{V_o}{2\beta_e}\left(\frac{dP_1}{dt} - \frac{dP_2}{dt}\right) + (\xi + \frac{C_{ep}}{2})(P_1 + P_{pipe} - P_2 + P_{pipe}) + \frac{L}{2}(P_1 - P_2) \tag{3.20}$$

Further rearrangement of Equation (3.20) gives:

$$D_p\omega_p = A\dot{x} + \frac{V_o}{2\beta_e}\left(\frac{dP_1}{dt} - \frac{dP_2}{dt}\right) + (\xi + \frac{C_{ep}}{2})(P_1 - P_2) + (2\xi + C_{ep})P_{pipe} + \frac{L}{2}(P_1 - P_2) \tag{3.21}$$

In this study, the EHA is connected to a horizontal sliding mass. The displacement of the mass can be related to the output force by the Equation (3.22), assuming negligible coulomb and static friction and assuming only viscous friction,

$$F = (P_1 - P_2)A = M\ddot{x} + B\dot{x} \tag{3.22}$$

where F is the output force acting on mass (N), x is displacement of load from mean position (m), M is load mass (kg),and B is viscous damping coefficient (Ns/m). Rearranging Equation (3.22) as:

$$(P_1 - P_2) = \frac{M\ddot{x} + B\dot{x}}{A} \tag{3.23}$$

Substituting Equations (3.23), (3.15) and (3.16) into (3.21) gives

$$D_p\omega_p(1 - 4K_{pipe}(\xi + C_{ep}/2)D_p\omega_{p0}) \tag{3.24}$$

$$= A\dot{x} + \frac{V_o}{2\beta_e}\left(\frac{M\ddot{x} + B\ddot{x}}{A}\right) + (\xi + \frac{C_{ep}}{2})\left(\frac{M\ddot{x} + B\dot{x}}{A}\right) + \frac{L}{2}\left(\frac{M\ddot{x} + B\dot{x}}{A}\right)$$

Rewriting Equation (3.24) gives:

$$\ddot{x}\left(\frac{MV_o}{2\beta_e A}\right)+\dot{x}\left(\frac{BV_o}{2\beta_e A}+\frac{\xi M}{A}+\frac{LM}{2A}+\frac{C_{ep}M}{2A}\right)+\dot{x}\left(\frac{A^2+B\xi+LB/2+C_{ep}B/2}{A}\right)$$

$$=\omega_p\left(D_p-4K_{pipe}(\xi+C_{ep}/2)D_p^2\omega_{p0}\right) \tag{3.25}$$

The transfer function $G_h(s)=\dfrac{x(s)}{\omega_p(s)}$ can be obtained as:

$$\frac{x(s)}{\omega_p(s)}=\frac{D_p\left(1-4K_{pipe}(\xi+C_{ep}/2)D_p\omega_{p0}\right)}{s^3\left(\dfrac{MV_o}{2\beta_e A}\right)+s^2\left(\dfrac{LM/2+(\xi+C_{ep}/2)M+BV_o/2\beta_e}{A}\right)+s\left(\dfrac{A^2+B(\xi+C_{ep}/2)+LB/2}{A}\right)} \tag{3.26}$$

Rearranging Equation (3.26) gives:

$$\frac{x(s)}{\omega_p(s)}=\frac{D_p\left(1-4K_{pipe}(\xi+C_{ep}/2)D_p\omega_{p0}\right)\dfrac{2\beta_e A}{MV_o}}{s^3+s^2\left(\dfrac{B}{M}+(\dfrac{2\xi+C_{ep}+L}{V_0})\beta_e\right)+s\left(A^2+B(\xi+C_{ep}/2)+LB/2\right)\dfrac{2\beta_e}{MV_o}} \tag{3.27}$$

The transfer function given in Equation (3.27) describes the hydraulic system and it can be represented in a general form as:

$$\frac{x(s)}{\omega_p(s)}=\frac{\kappa_h\omega_{nh}^2}{s\left(s^2+2\zeta_h\omega_{nh}s+\omega_{nh}^2\right)} \tag{3.28}$$

Since in practice, $4K_{pipe}D_p(\xi+C_{ep}/2)\omega_{p0}<<1$, the following approximations can be made:

$$\omega_{nh}=\sqrt{\left(\frac{A^2 2\beta_e}{MV_o}+\frac{B\beta_e}{MV_0}\left(2\xi+L+C_{ep}\right)\right)}\approx\sqrt{\frac{2A^2\beta_e}{MV_0}}\ ,$$

$$\zeta_h\approx\left(\frac{B}{M}+\frac{(L+2\xi+C_{ep}/2)\beta_e}{V_o}\right)\left(\frac{1}{2\omega_{nh}}\right),\ \text{and}$$

$$\kappa_h\approx\left(\frac{D_p}{A}\right) \tag{3.29}$$

From Equation (3.29) it is seen that the natural frequency is lowered by increasing the mass and the trapped volume, whereas the effect of effective bulk modulus and piston area is opposite. Therefore, a high bulk modulus and short transmission lines are needed for high natural frequency. Also, it is seen that viscous damping at the actuator and leakage (actuator and pump) affect the overall damping of the system. Furthermore, the gain of the system is a function of pump displacement and piston area.

Using these approximations, the transfer function given in Equation (3.27) can be simplified to

$$\frac{x(s)}{\omega_p(s)} \approx \frac{\frac{2D_p\beta_e A}{MV_o}}{s^3 + s^2\left(\frac{B}{M} + \frac{C_T\beta_e}{V_0}\right) + s\left(\frac{2\beta_e A^2}{MV_o} + \frac{C_T B\beta_e}{MV_0}\right)} = \frac{\kappa_h \omega_{nh}^2}{s\left(s^2 + 2\zeta_h\omega_{nh}s + \omega_{nh}^2\right)}, \quad (3.30)$$

where the total leakage coefficient of the system, consisting of pump cross port leakage, pump external leakage and actuator leakage, is given by $C_T = 2\xi + C_{ep} + L$.

The transfer function given by Equation (3.30) is the general mode of operation and applies for conditions when both pressures P_1 and P_2 vary simultaneously. This occurs when the pump switches the flow direction and the pressure in the return lines starts to increase from the accumulator pressure value, while the pressure in the forward lines start to drop.

Equation (3.30) is different from the model derived in previous studies involving the EHA. Measurements carried out on the EHA prototype (reported in Chapter 4) revealed the importance of the viscous friction coefficient as compared to the leakage coefficients (pump and actuator). Furthermore, the model reported in [Habibi, 2000] had estimated values for leakage coefficients and viscous friction that subsequent measurements proved to be inaccurate. These and minor inaccuracies in the form of a missing factor of "2" and pump displacement were reported and later corrected in a joint publication in [Chinniah et al, 2003].

3.3 Failure Modes and Effects Analysis for the EHA Components

In this section, an attempt is made to consider some of the possible faults that may occur when the EHA is operating. This is crucial when considering implementing a condition monitoring scheme for any machine. Knowing the possible faults and having a better understanding of these faults enable the identification of critical parameters which can be monitored. Furthermore, it can provide some guidance in deciding which type of condition monitoring approach to use.

As described in Chapter 1, the effective bulk modulus is the most important fluid property in determining the dynamic performance of hydraulic systems because it relates to the stiffness of the liquid. A typical value for petroleum products is about 1720 MPa (250,000 psi). However, such a large value is rarely achieved in practice because the bulk modulus decreases sharply with small amounts of entrained air in the liquid, (as explained in Chapter 1). In addition, the bulk modulus can be lowered by mechanical compliance, such as elasticity of structural members (hydraulic motor housings and lines connecting valves and pumps to actuators). However, in the EHA, hydraulic lines are not made of Teflon or hard rubber (no flexible hoses are used). Steel tubes connect the pump to the actuator and therefore possible reduction in bulk modulus is believed to be mainly influenced by air in the fluid.

In any practical situation, it is extremely difficult to determine the effective bulk modulus other than by direct measurement since it is impossible to know the amount of entrapped air in the system. A lowered bulk modulus value can cause system instability. Also system performance can be affected (lowered gains and bandwidths). Thus, monitoring this parameter is very useful and it gives a good indication of the health of the actuation system.

Leakage flows and friction are the sources of losses in hydraulic machines. Because all clearances are intentionally made small to reduce losses, these leakage flows are laminar and therefore are proportional to pressure. The leakage coefficients associated with leakage in the actuator and pump in the EHA are other useful parameters in considering condition monitoring of the EHA. Excessive leakage flow is undesirable. Subsequently, the pump volumetric efficiency decreases. This means that,

more power will be required to drive the pump for the same performance level (i.e. to overcome the leakage losses).

Hydraulic systems generate heat as a result of internal losses. Usually, in hydraulic systems, the major heat generators are the orifices and valves used to control the flow. The hydraulic power consumed by these devices is dissipated in heating the fluid. In the EHA, which is a pump controlled hydraulic circuit, heat is generated by leakage flow losses in the pump and actuator. Another source of potential heat generation is the resistive pressure drops in hydraulic lines, fittings and filters. The cross over relief valve also generates heat but this only becomes a factor in stall load conditions. Also, seal friction, mechanical friction and viscous drag between surfaces in the pump and actuator, generate heat. The compression of oil, and especially of entrained air to higher pressures in the pump can cause heat generation. Temperature of the hydraulic oil is extremely important when considering system performance.

Viscosity of the oil is an important property when considering lubrication. Close fitting surfaces in relative motion occur in most hydraulic components and if the viscosity is too low, leakage flow increases and if too large, component efficiencies decrease because of the additional power required to shear the fluid. Viscosity decreases rapidly with increased temperature. In addition at high temperatures, fluids can decompose and form solid reaction products which can clog filters, pumps and actuator. A decrease in lubricity of the oil also occurs at higher temperatures. Lubricity refers to the fluid capability to act as a boundary layer lubricant. Lack of lubricating properties promotes wear and shortens component life. Increased clearances between surfaces due to wear results in degraded performance in the form of increased leakage, loss in efficiency and failure to build up pressures.

A fixed displacement, bi-directional gear pump is used in the EHA. A typical fault for gear pumps in general includes excessive pump noise which might be due to a misalignment of pump motor coupling, a low level of oil, excessively high speed, air leak in the suction line, flow restriction in the suction side, broken or worn parts or a wrong choice of fluid. Two other potential faults associated with gear pumps are excessive heat generation due to excessive pump pressure, excessive friction and

leakage as well as oil leakage at pump seals due to abrasive substances on the pump shaft, incorrect seal installation, damaged shaft seal or poor coupling alignment.

The linear symmetrical actuator is another very important component of hydraulic systems. Some of the typical failures in the hydraulic actuator in general include: (1) drift due to leakage in the piston seals and connecting lines, (2) failure to move due to excessive friction load, too low pressure, seal leak, erratic cylinder action due to high viscosity during warm up period and due to air in the system and (3) finally excessive leakage due to excessive pressure or damaged seals due to wear as a result of contaminated fluid.

In hydraulic circuits, pressure relief valves are used to prevent excessive pressure build up in the lines. Some of the typical failures include a low system pressure as a result of dirt or chip holding the valve partially open or as a result of a damaged seat or poppet, a damaged or weak spring. Another fault linked to the relief valve is overheating of the system as a result of continuous operation at relief setting, which causes oil viscosity to fall and leakage in the system to increase.

3.3.1 Faults and Effects Analysis for the EHA

In this section, the potential faults in the EHA and their possible effects are described for each component of the system.

- **Symmetrical Actuator**

Fault	Effect
(a) Seal wear.	(a) Friction characteristics change (coulomb and viscous friction). (b) Actuator leakage coefficient increases.
(b) Oil degradation –Change in its lubricating properties.	(a) Change in viscous friction (when the temperature is unchanged).

- **Gear Pump**

Fault	Effect
(a) Wearing of gears –As a result of contaminants in oil.	(a) Volumetric efficiency reduced and more slippage. (b) Higher levels of noise.
(b) Seal wear.	(a) Leakage along electric motor and gear pump coupling shaft.
(c) Case drain seal failure	(a) Excessive external leakage into accumulator (b) Low efficiency. (c) Increase in accumulator pressure during operation. (d) Oil temperature increases. (e) Decrease in actuator velocity.

- **Connections (Loose Fittings)**

Fault	Effect
External Leakage.	System failure or contamination to environment.

- **Cross-Over Relief Valve**

Fault	Effect
Clogged or stuck because of debris and not fully open or closed.	(a) Actuator velocity is lowered relatively to motor speed, since less flow delivered to actuator as leakage occurs through cross-over relief valve (if not fully closed). (b) Oil Temperature rises.

- **Oil (Changes in physical properties)**

Fault	Effect
Lowering of the effective bulk modulus because of potential air pockets in the system. This may occur for two reasons, namely: (a) When refilling the EHA with oil, dissolved air at atmospheric pressure in the oil may form air bubbles. (b) Complete flushing of ANY hydraulic system is difficult. In this design as the system is fully closed, air flushing can only occur when the EHA is being refilled, thus making removal of trapped air particularly difficult. In this case, the frame of the actuator will need to be rotated for releasing the trapped air.	Lowers the natural frequency of the system and affects system response.

- **Hydraulic Oil – Contaminants in Fluid**

Fault	Effect
Contaminants can get into the system when replenishing with oil or at the actuator, where air borne contaminants get deposited onto the exposed piston and can enter the system (especially if the seal is damaged).	The effect of contaminants can be very harmful because the hydrostatic system makes use of a relatively small volume of oil. Contaminants can damage the pump (wearing) as well as change the physical and chemical properties of the oil.

- **Electric Motor**

Fault	Effect
Overheating of coils- The EHA has a protecting mechanism that limits the maximum current in the motor and frequency of the input signal.	System shuts down. (electric motor switches off)

- **Mechanical Coupling Between Electric Motor and Pump**

Fault	Effect
Fatigue and wear	(a) Break. (b) Increased vibration and noise.

- **Check Valves**

Fault	Effect
Failure to hold pressure	Excessive leakage

3.4 Summary

In this chapter, a brief description of the Electrohydraulic Actuator (EHA) has been provided and a simplified, linearized model for the EHA has been presented. In addition, some of the potential faults that can occur in the EHA have been discussed and a list of faults and effects for the EHA are given. In Chapter 4, numerical values for the parameters appearing in Equation (3.29) are presented. The parameters are obtained either from manufacturers' specification sheets or are determined experimentally. A simulation study is then conducted and the linearized model is validated in the next chapter by comparing time responses of the mathematical model to that of the EHA prototype.

Chapter 4

EHA Instrumentation and Model Validation

In Chapter 3, the EHA was described and a linearized mathematical model developed. Thus a lumped parameter model for the EHA was proposed. In this chapter, the values of the different parameters are determined experimentally. Some parameters are obtained from the literature and others from the specification sheets of the components. The measurements of the pump leakage coefficients (cross port and external) as well as the actuator leakage coefficients have not been done previously for the Electrohydraulic Actuator. The viscous damping coefficient of the EHA is also measured (as explained in detail in Chapter 8) .The sensors used in this particular study of the EHA are new; namely the LVDT (linear variable differential transformer), the differential pressure transducer and the optical encoder (improved resolution compared to the one used previously). The instrumentation is also briefly described in this chapter.

Finally, using the parameter values, obtained from experiments, specification sheets (for pump and actuator) and estimated using the EKF (equivalent viscous damping coefficient and effective bulk modulus), the updated EHA closed loop linearized model is presented and compared to the actual system response.

4.1 Experimental Determination of EHA Parameters

Parameters such as the pump volumetric displacement, actuator area, volume of oil in the lines and actuator and inertial load are obtained from the specification sheets, measurement of the dimensions of piston diameter and dimensions of lines. In the EHA, the pump displacement value stated by the manufacturer is 1.6925×10^{-7} m^3/rad. An experiment was performed where the motor speed was varied and the piston velocity measured. In the absence of leakage and dynamic effects, a simple relationship between the pump displacement and the actuator velocity is illustrated by Equation (4.1),

$$D_p\omega_p \approx A\dot{x} \tag{4.1}$$

where D_p is the pump displacement, ω_p is the pump velocity, A is the piston area and $\dot{x}$ is piston velocity. A graph of piston velocity in m/s against pump speed in rad/s, at a fixed temperature of $24 \pm 1\ ^0$C, is shown in Figure 4.1. As expected, a linear relationship exists and the slope of the graph ideally represents the ratio of $\frac{D_p}{A}$.

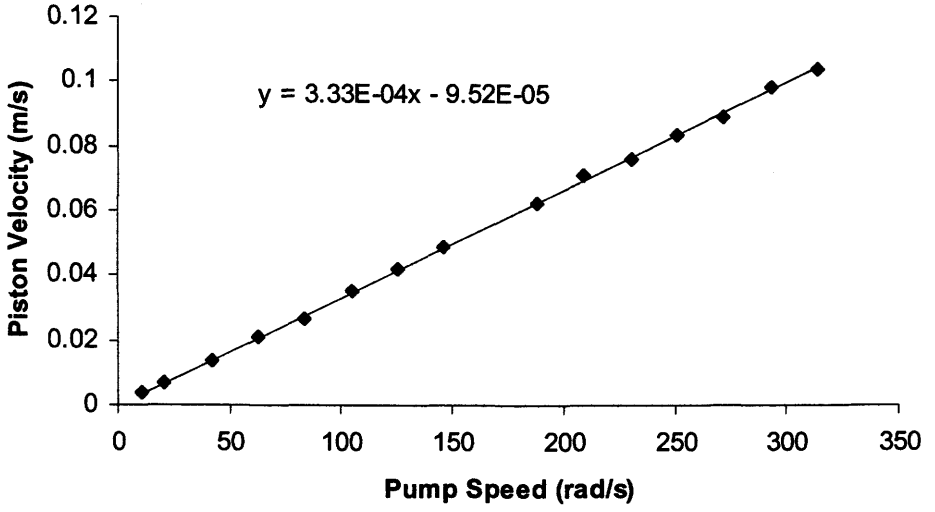

Figure 4.1 Measured Piston Velocity with Increasing Pump Speed at Fixed Temperature

The experimentally measured ratio was 3.33×10^{-4} m/rad (the ideal value being 3.356×10^{-4} m/rad). The experiment was performed only once, at an oil temperature of $24 \pm 1\ ^0$C with the 20 kg inertial load attached to the piston, and it was performed to confirm the values for the piston area and the pump displacement.

4.2 Experimental Determination of the Pump Leakage Coefficient

In previous studies involving the EHA, the pump cross leakage coefficient as well as the actuator external leakage coefficients have been predicted using an optimization technique. The EHA prototype responses were compared to a simulated EHA system and parameters were optimized until the actual and simulated responses matched [Habibi, 2000]. The problem with this approach was the possibility of ending up with a local minima. In this study, the leakage coefficients for the pump and the

actuator were measured. It is to be noted that, the measurement of these coefficients revealed one important property for the EHA system, namely that their contribution to the dynamics of the overall system, (in terms of damping), was smaller than initially believed.

In this section the experimental procedure used to determine the leakage coefficient in the pump is described. Leakage flow was assumed to be laminar and therefore linearly dependent on pressure. As the pump pressure increased, the pump leakage flow increased linearly and a linear decrease in the flow delivered by the pump was observed. The experiment consisted of keeping the speed of the motor constant and varying the pressure by means of a needle valve. The flow delivered by the pump was calculated by using oil volume and time information. This was done at a constant temperature of 24 $\pm 1^0$C. The equation describing the pump flow is given by

$$Q_p = D_p \omega_p - C_p P_p \tag{4.2}$$

The slope of the line for a plot of measured pump flow and pressure measurements, represents the lumped pump leakage coefficient. A schematic of the experimental set up is depicted in Figure 4.2.

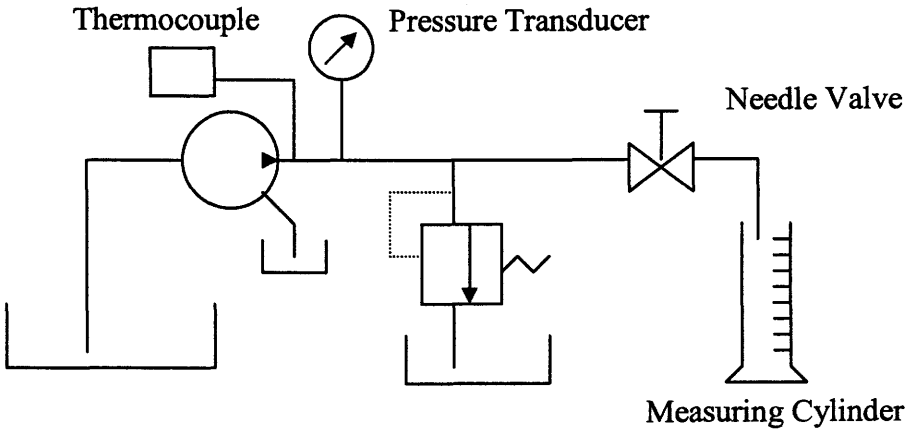

Figure 4.2: Schematic for the Experimental Set Up Used to Measure Pump Leakage.

The needle valve was used to vary the pressure; closing the valve increased pump pressure. The system pressure was always kept below the relief valve pressure in

order to prevent oil passing through the relief valve. Since the leakage flow was laminar, it was by nature very dependent on temperature. An increase in temperature will increase the leakage flow, by decreasing oil viscosity. In the experiment, temperature at the pump outlet port and at the case drain were both monitored carefully using thermocouples and all the tests were done at the same temperature. The use of a large reservoir also helped in keeping the oil temperature constant (24 $\pm$ 1^{0}C).

A measuring cylinder was used to collect the oil and the volume flow rate was determined. This method was used, rather than measuring flow rate with a flowmeter because it was more accurate since the pump flow rate was relatively low. The pump pressure was measured using a pressure transducer that had been calibrated using a "dead weight tester" prior to being used. The pressure-voltage linear relationship is shown in Figure 4.3 (calibration done twice). The dead weight tester consisted of a hand pump static pressure generator and a piston of precisely known area loaded by accurately calibrated weights. The differential pressure transducer was connected to the pressure generator outlet and the same pressure was applied to the weighted piston.

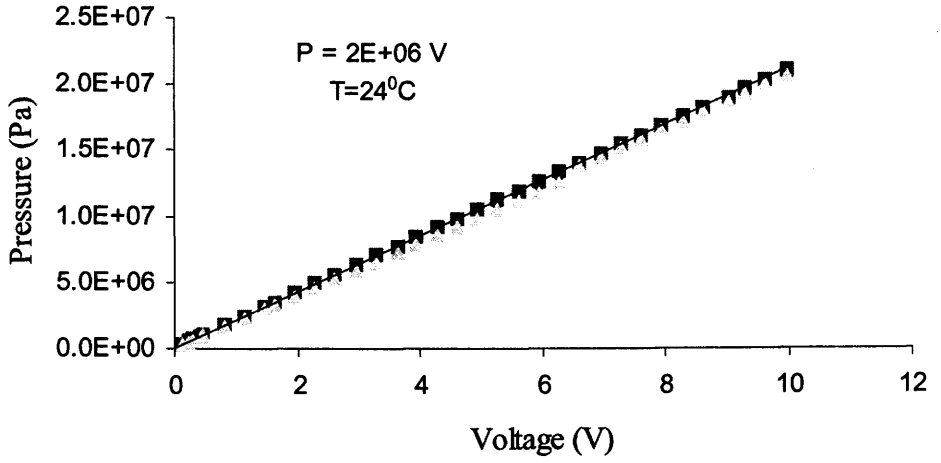

Figure 4.3: Pressure Transducer Pressure/Voltage Relationship

When the pressure generator pump developed a pressure that balanced the force (weight) on the known area, the piston rose. The piston was rotated manually to

eliminate static friction effects. Also, the absence of seals (piston had a close fit to the bore) eliminated seal friction forces.

A plot of flow rate versus pressure at a constant pump speed of 500 rpm is depicted in Figure 4.4. As expected, a linear relationship was obtained, with the slope of the line representing the total pump leakage coefficient. The pump pressure was increased to a maximum of 1.1×10^{7} Pa (1520 psi), at which point the pump flow reached a minimum of 7.4×10^{-6} m^3/s (0.44 l/min).

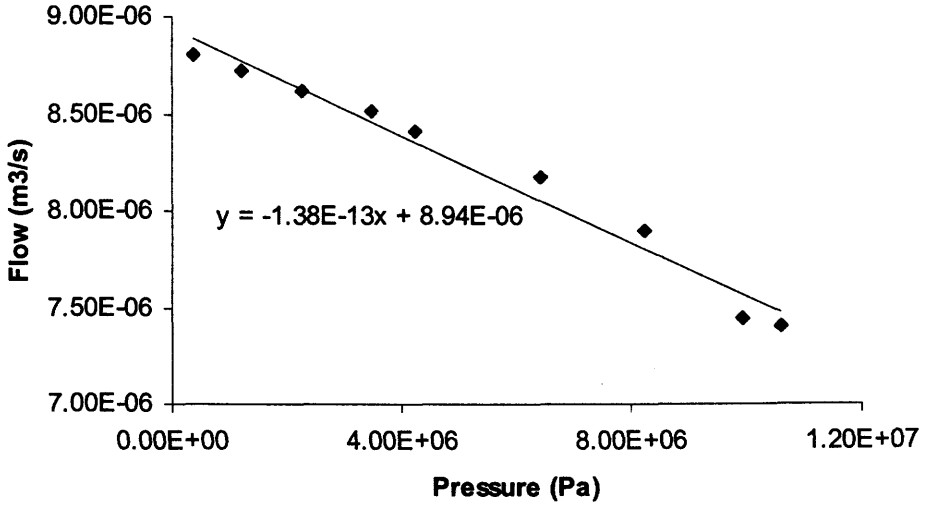

Figure 4.4: Flow Versus Pressure at Pump Speed of 500 rpm

The pump leakage coefficient was found to be 1.38×10^{-13} m^3/sPa. For repeatability purposes, the experiment was done several times (Figure 4.5), at the same pump speed (500 rpm) and temperature (24 $\pm$ 1^0C). An average overall pump leakage coefficient of 1.5×10^{-13} m^3/sPa was used.

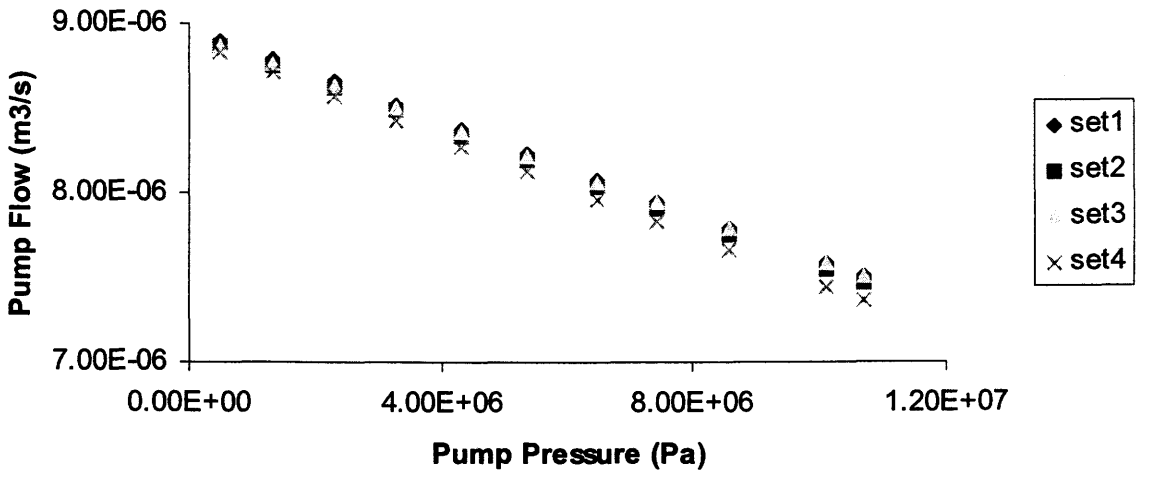

Figure 4.5: Pump Flow and Pressure Relationship at a Pump Speed of 500 Rpm

The pump volumetric efficiency plot (Figure 4.6) was generated by taking the ratio of the measured flow to the theoretical flow (obtained by multiplying the pump volumetric displacement with the pump velocity) as shown by the following equation.

$$\eta_v = \frac{Q_p}{Q_{Theoretical}} = \frac{D_p\omega_p - C_p P_p}{D_p\omega_p} = 1 - \frac{C_p}{D_p\omega_p} P_p \qquad (4.3)$$

From the efficiency plot, it can be seen that as the pump pressure increases, the volumetric efficiency decreases, reaching a low value of 83% at about 1.05×10^7 Pa (1520 psi). The oil temperature was 24 $\pm$ 1^{0}C.

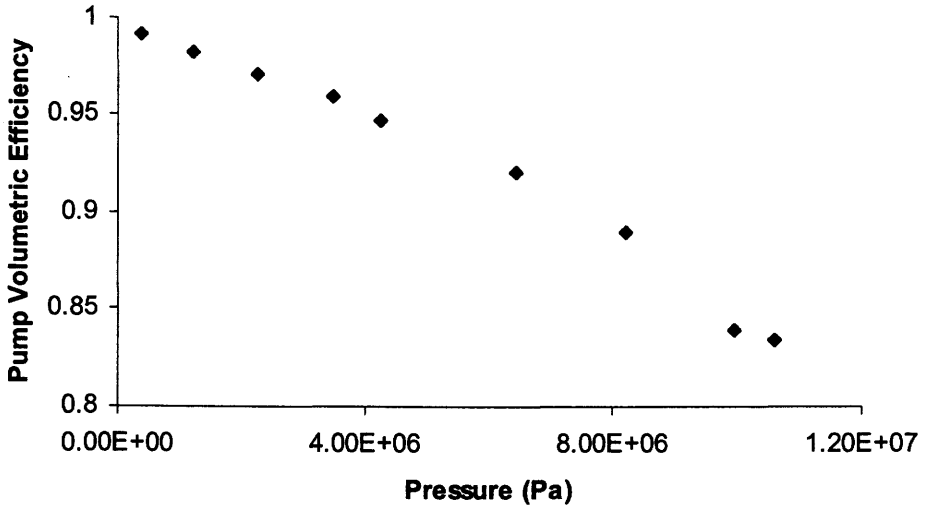

Figure 4.6: Plot of Pump Volumetric Efficiency Against Pump Pressure at 500 Rpm

In addition, experiments were also performed to quantify the external leakage coefficient of the pump, i.e. its case drain flow. These experiments consisted of varying the pump pressure and measuring the case drain flow by connecting a hose to the case drain and collecting the oil in a smaller measuring cylinder. This was used for greater accuracy since the volume of oil collected was smaller than previously. The result for one experiment is shown in Figure 4.7. The oil temperature was once again 24 $\pm$ 1^{0}C.

The case drain flow was expected to be directly proportional to pump pressure, assuming constant temperature. Each time, at a constant pressure, the leakage flow was measured by recording the volume and time information. Moreover, the procedure was repeated for various pump speeds and it was found that if temperature was carefully monitored, repeatability was achieved. An external pump leakage coefficient of 7×10^{-14} m^3/sPa was used. Thus, for the EHA, the pump cross port leakage and the external leakage coefficients were about the same order of magnitude.

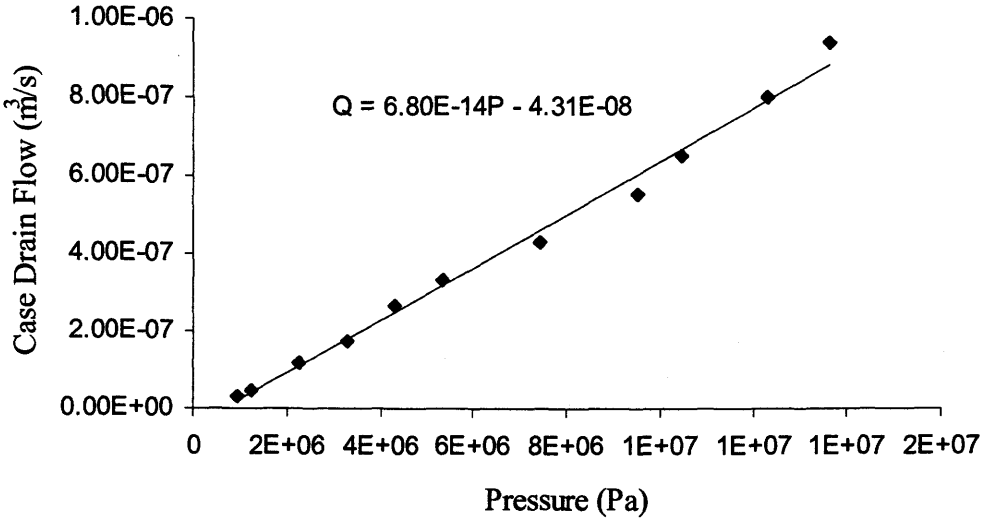

Figure 4.7: Case Drain Flow Versus Pressure at a Speed of 600 rpm.

4.3 Experimental Determination of the Actuator Leakage Coefficient

Having determined the pump leakage parameters, the next step was to determine the leakage coefficients for the actuator. It was assumed that leakage flow consisted primarily of external leakage into chamber 3 (illustrated in Figure 3.5). A clamp was built to hold the actuator while it was tested and to prevent the piston from moving, as shown in Figure 4.8. The first set of experiments consisted of pressurizing the chamber C1, (which would normally result in the piston extending) as shown in Figure 4.8 The leakage path is also illustrated using an arrow in Figure 4.8. The actuator pressure in this test was relief valve pressure. The leakage flow was measured by collecting the fluid in a 10 ml measuring cylinder and timing it. Actuator leakage was assumed to be laminar in nature.

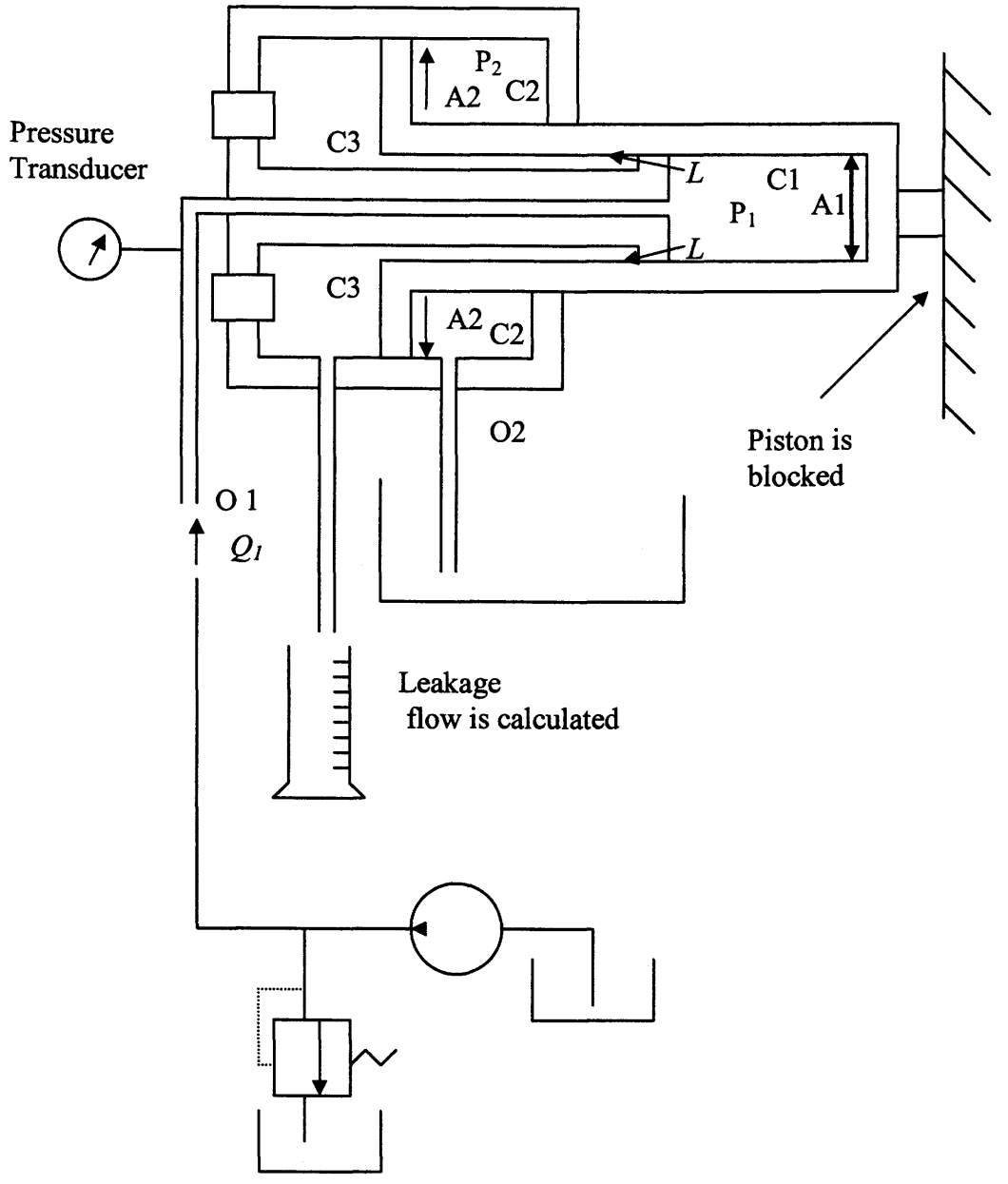

Figure 4.8: Experiment Set Up to Determine Actuator Leakage Coefficient

The experiments were performed at different relief valve settings. The use of a large reservoir maintained the temperature constant. This strategy was applicable in this case since the flow rate through the relief valve was low. A plot of actuator pressure and leakage flow is shown in Figure 4.9.

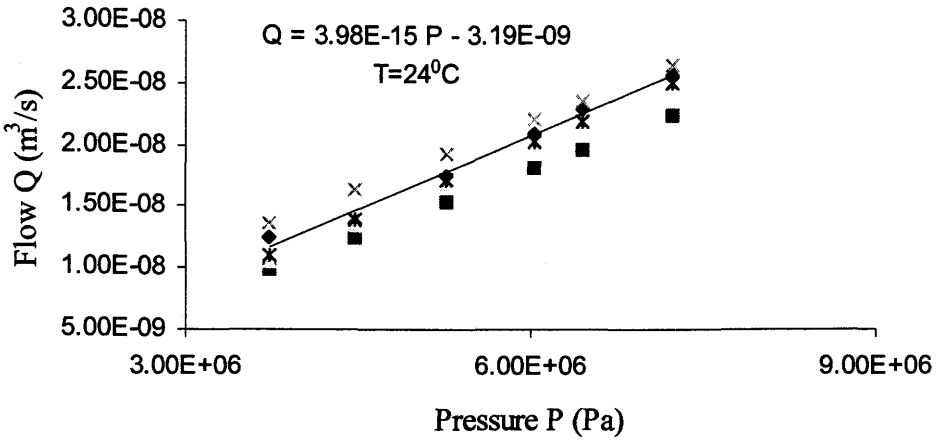

Figure 4.9: Plot of Actuator Leakage Flow Versus Pressure

The slope of the line in Figure 4.9 represents the actuator leakage coefficient, when the actuator is in the extension mode. The results are given in Table 4.1. It can be seen that the actuator leakage coefficient is negligible when compared to the pump lumped leakage coefficient.

The leakage coefficient for the actuator in the retraction mode was also determined experimentally using the same approach but this time pressurizing the other chamber of the actuator, as illustrated in Figure 4.10. However, it was found that negligible leakage (too small to be measured using a 10 ml measuring cylinder), occurred when the actuator was in the retracting mode. The piston was blocked at different positions and the same observation was made even though pressures as high as 8.3 MPa (1200 psi) were being used. From Table 4.1, an average actuator leakage coefficient of 4×10^{-15} m^3/sPa was used for the EHA, when deriving its linearized transfer function model.

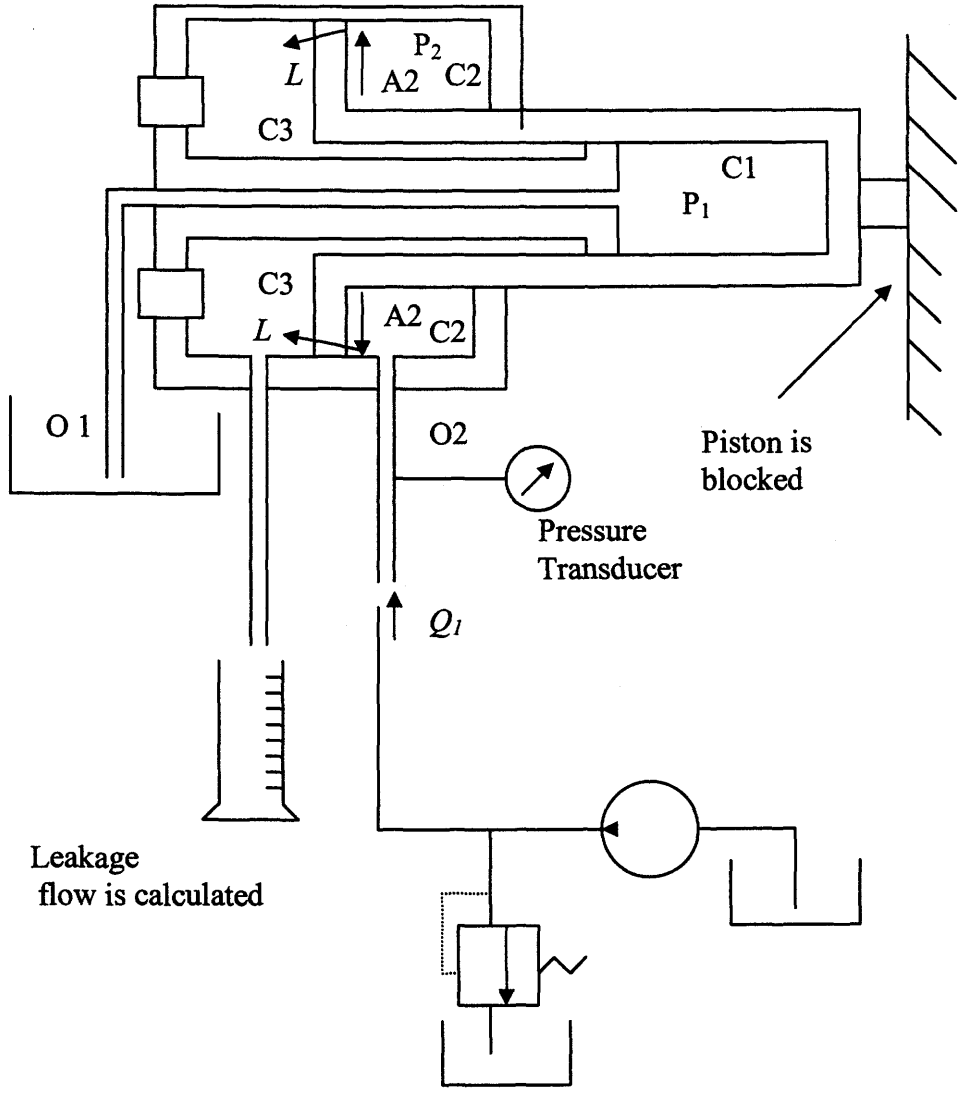

Figure 4.10: Experiment to Measure Actuator Leakage Coefficient in Retraction Mode.

4.4 Simplified Model for the EHA

From Chapter 3, the simplified model for the EHA was derived as:

$$\frac{x(s)}{\omega_p(s)} \approx \frac{\frac{2D_p\beta_e A}{MV_o}}{s^3 + s^2\left(\frac{B}{M} + \frac{C_T\beta_e}{V_0}\right) + s\left(\frac{2\beta_e A^2}{MV_o} + \frac{C_T B\beta_e}{MV_0}\right)} \tag{4.4}$$

Table 4.1: Actuator Leakage Coefficient at Different Piston Positions

Piston displacement (cm)	Actuator Leakage Coefficient (m^3/sPa)	Temperature (^{0}C)
2.5	3.65×10^{-15}	24 ± 1
2.5	3.98×10^{-15}	24 ± 1
5	3.55×10^{-15}	24 ± 1
5	3.7×10^{-15}	24 ± 1
8	4.14×10^{-15}	24 ± 1
8	4.04×10^{-15}	24 ± 1

The parameter values of the EHA are tabulated in Table 4.2. Using these values, the hydraulic transfer function for the EHA, given by Equation (4.4), reduces to:

$$\frac{x(s)}{\omega_p(s)} = \frac{26.21}{s^3 + s^2(39.5) + s(7.8E4)} \tag{4.5}$$

Table 4.2: Parameter Values for the EHA

Symbol	**Definitions**	**Values (Prototype)**
A	Piston area in symmetrical actuator	5.051×10^{-4} m^2
D_p	Pump volumetric displacement.	1.6925×10^{-7} m^3/rad
M	Load mass	20 Kg
β_e	Effective bulk modulus.	2.1×10^{8} Pa
V_0	Oil volume	6.85×10^{-5} m^3
B	Viscous friction coefficient.	760 Ns/m
C_T	Lumped pump and actuator leakage coefficient	5×10^{-13} m^3/sPa

4.5 Linear Variable Differential Transformer (LVDT)

A linear variable differential transformer (LVDT) was used initially to measure the piston displacement. It produced an electrical output proportional to the displacement of a separate movable core. The operation of an LVDT is as follows:

An AC carrier excitation is applied to a primary coil. Two identical secondary coils are symmetrically spaced from the primary and are connected externally in a series-opposing circuit. Motion of the non-contacting magnetic primary coil and core varies the induced voltage in the secondary coils. If the core is centered between the secondary windings, the voltage induced in each secondary is identical and 180^0 out of phase so there is no net output. If the core is moved off center, the mutual inductance of the primary and one secondary is greater than with the other, and a differential voltage appears across the secondaries in series. This voltage is essentially a linear function of displacement.

The DC LVDT maintains all the desired characteristics of the AC LVDT but has the simplicity of DC operation. It is comprised of two integral parts: an AC operated LVDT and a carrier generator/signal condition module. The carrier oscillator produces a constant amplitude sine wave to excite the primary of the LVDT. In the EHA prototype, a DC operated LVDT was used initially (before using the optical encoder) for piston displacement measurement. The LVDT used was a Schaevitz (Durham Instruments) 5000 DC-E model LVDT. The input was 15 V DC and the sensitivity was 80.75 mV/mm (0.8075 V/cm).

The LVDT was calibrated by using a vernier caliper to measure the displacement from the null position, and a digital voltmeter was used to measure the corresponding voltage. The results are shown in Figure 4.11.The measured slope was 0.01257 m/V (0.796 V/cm) which was very close to the value of 0.8075 V/cm given in the LVDT manufacturer's specification sheet.

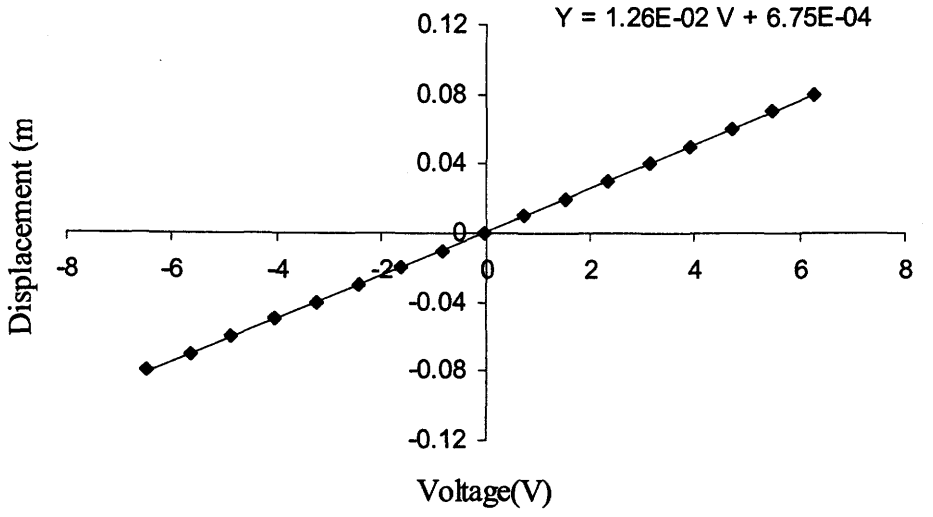

Figure 4.11: Plot of Displacement Versus Measured Voltage for LVDT

4.6 Measured Output of the EHA Prototype Using the LVDT

The EHA hydraulic transfer function was given in Equation (4.5). Using this model and the model given by Equation (3.12), in Chapter 3, representing the electric motor, a simulated response to an input consisting of a sine wave, 0.01 m amplitude and 4 Hz frequency was obtained and compared to the measured response from the EHA prototype, as shown in Figure 4.12. The simulated model was a linearized closed loop model for the EHA, with the sine wave being the desired piston position and the output being the simulated piston position. The measured output was the measured piston response using the LVDT. From Figure 4.12, it can be seen that there is good agreement between the simulated and measured responses.

The procedure was repeated using a higher frequency, lower amplitude sine wave as the desired input to the closed loop simulated and experimental system. The input was a sine wave with a frequency of 25 Hz and amplitude of 0.005 m. The simulated and measured actuator piston as a result of applying this input to the simulated EHA model and the actual EHA prototype response are shown in Figure 4.13. The simulated and measured responses were found to match each other very closely.

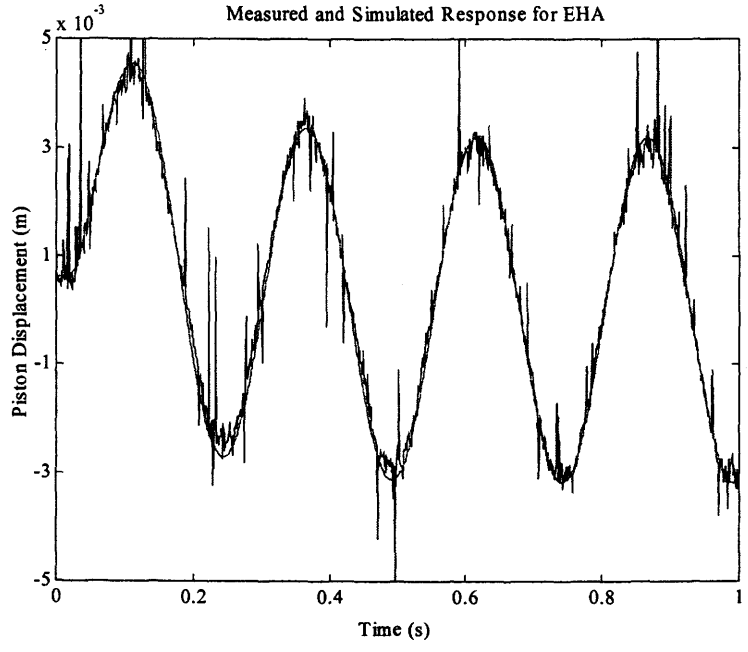

Figure 4.12: Measured and Simulated Responses (4Hz, 0.01m, sinusoid)

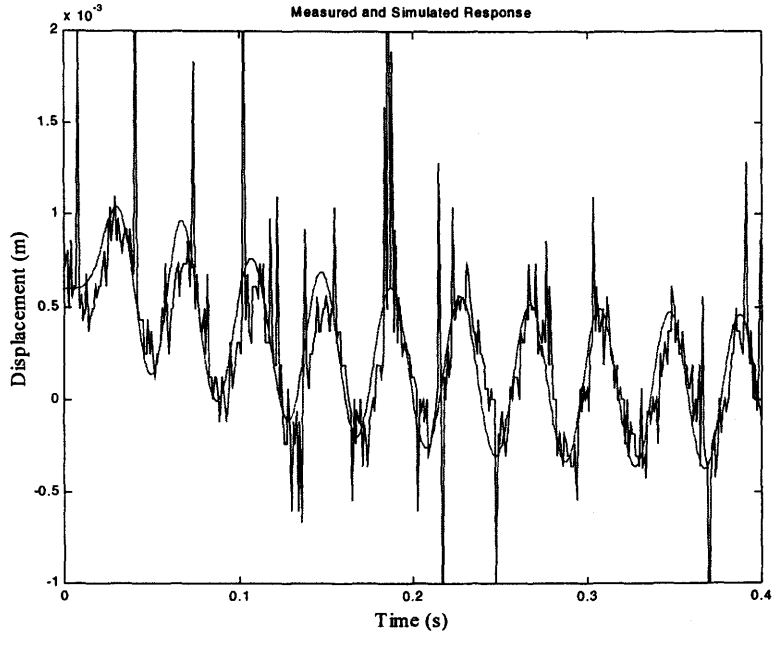

Figure 4.13: Measured and Simulated Responses (25 Hz, 0.005m, sinusoid)

From the plots, the simulated and measured responses showed reasonable correlation and therefore, it was concluded that the simulated model was a good representation of the actual prototype. The purpose was not to get an accurate model but a representative model from which simulation studies could be based. From these plots it could also be seen that the measured displacement was very noisy. The LVDT used to measure piston displacement was picking up noise from the electric motor.

4.7 Differential Pressure Transducer

A differential pressure transducer was used in the prototype to measure the pressure difference across the piston. The load pressure measurement was needed for estimating the equivalent viscous friction using the Extended Kalman Filter, as explained in Chapter 6. Prior to connecting the pressure sensor to the Electrohydraulic Actuator, it was calibrated using a dead weight tester and the results for the calibration of the differential pressure transducer is shown in Figure 4.14.

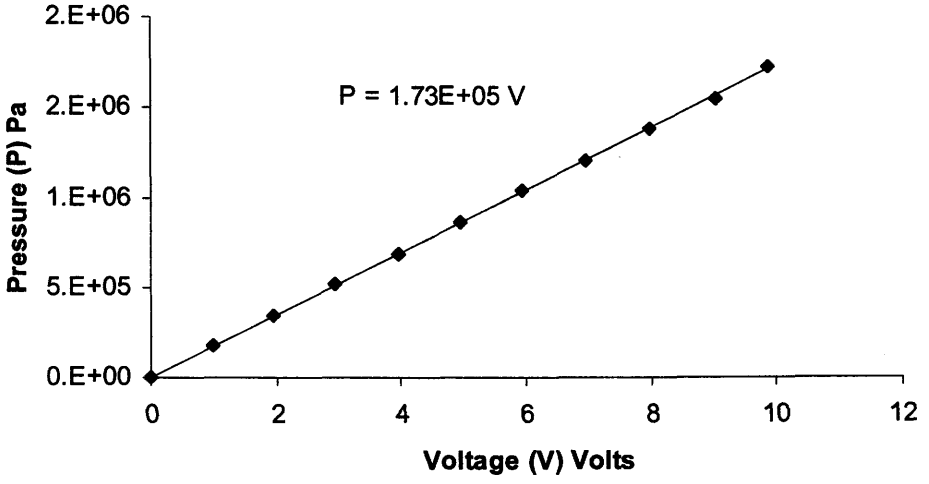

Figure 4.14: Calibration of Differential Pressure Transducer

As illustrated in Figure 4.14, the output of the pressure sensor was 1 V for a measured pressure difference of 0.17 MPa (25 psi) approximately.

4.8 Linear Optical Encoder

At a later stage in the study, a high precision optical encoder was used to measure piston displacement. The LE18 optical incremental linear encoder, manufactured by Gurley Precision Instruments was used in the EHA. An encoder is a device that converts linear displacement into digital or pulse signals. The most popular type of encoder is an optical encoder which consists of a moving pattern of opaque and transparent sectors and as the pattern moves, they interrupt the light emitted onto a photodetector, generating a digital or pulse signal output. The incremental encoder generates a pulse (as opposed to an entire digital word for an absolute encoder) for each incremental step. The incremental encoder uses two output channels to sense position. Using two code tracks with sectors positioned 90^0 out of phase, the two output channels indicate both position and direction of motion. Therefore by monitoring both the number of pulses and the relative phase of the two signals, both position and direction of motion can be tracked. The LE 18 model used in the EHA provides a resolution of 1 micron.

Using the optical encoder, the measured responses for different inputs were compared to the simulated responses using similar inputs and the results are shown in Figures 4.15 to 4.18. The inputs used were a 4Hz sine wave (0.01 m amplitude), a 25 Hz sine wave (amplitude of 0.005 m), a step response (0.01 m amplitude) and a square wave (0.005 m amplitude and 0.5 Hz frequency). The measured responses, as illustrated in Figures 4.15 to 4.18 are "cleaner" and show good agreement with simulated responses.

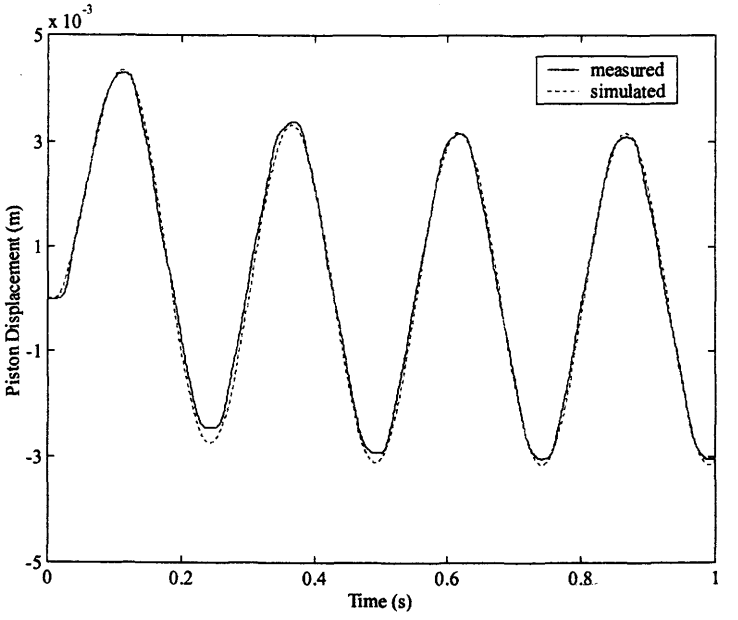

Figure 4.15: Measured and Simulated Responses for the EHA (4Hz sine input)

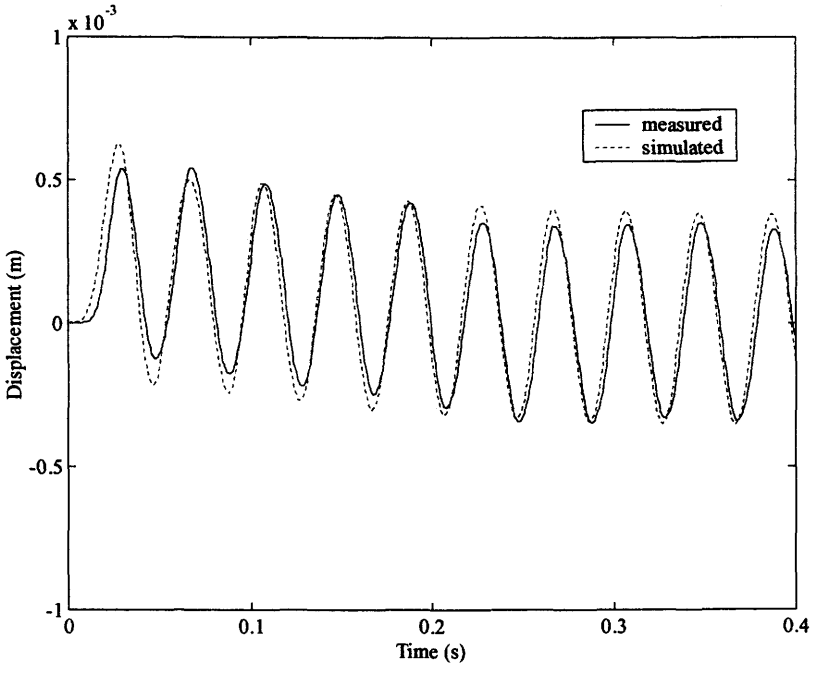

Figure 4.16: Measured and Simulated Responses for the EHA (25 Hz sine wave)

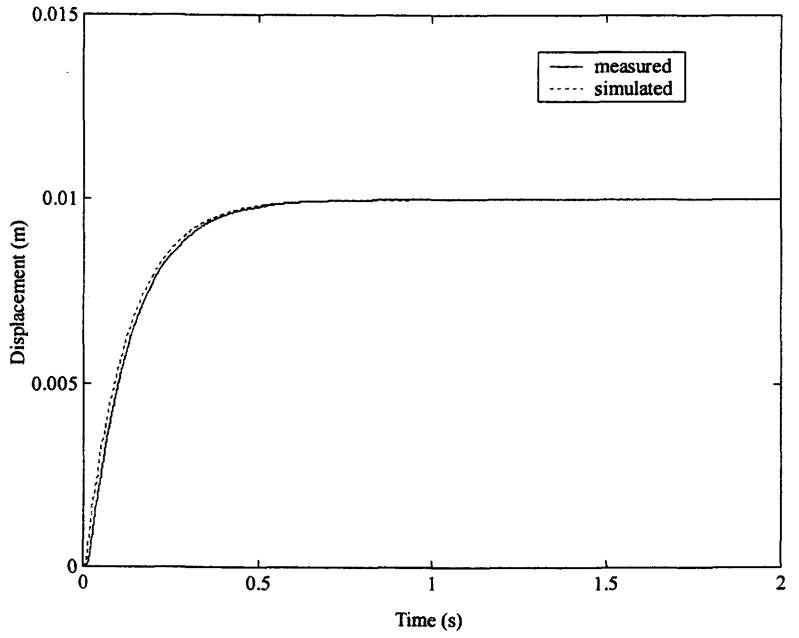

Figure 4.17: Measured and Simulated Step responses (0.01 m)

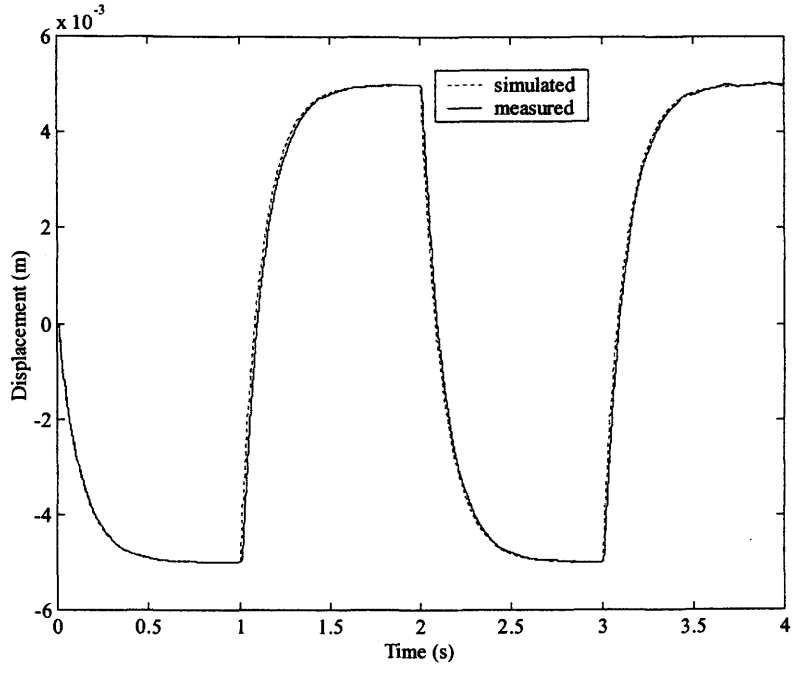

Figure 4.18: Measured and Simulated Square Wave Responses

4.9 Concluding Remarks

In Chapter 4, the experimental set up to measure two important parameters for the EHA namely the pump leakage coefficient and the actuator leakage coefficient is described. In previous studies, these two parameters were obtained using an optimization technique which compared simulated and measured responses and varied the values for the parameters until the two responses showed good agreement. Measurements carried out in this study revealed that the previous values corresponded to local minima conditions and were inaccurate. Also, in this chapter, the values of all the parameters required to simulate the linearized model of the EHA using Matlab/Simulink® is presented. Simulated responses are compared to experimental results. The instrumentation used in the EHA is also briefly described. The model presented in this chapter is used as described in Chapter 6, to generate simulated data required to apply the Kalman and the Extended Kalman Filter to the EHA.

Chapter 5 serves as an introduction to the Kalman and the Extended Kalman Filter. The equations for the Kalman and the Extended Kalman Filters are derived and explained. Chapter 5 can be regarded as a good literature review of the Kalman Filter and is necessary in order to understand how the filter estimates states. This is important since one of the objectives of this study is to further understand the Kalman Filter and the EKF in order to address some of the issues in previous research involving condition monitoring of hydraulic systems using the EKF.

Chapter 5
Introduction to the Kalman Filter

This chapter serves as an introduction to the Kalman filter and provides insight on the parameter estimation technique used in this study. Although the development of the Kalman and the Extended Kalman Filters equations are well known, for completeness and continuity, the development of the appropriate equations and the underlying assumptions are presented in this chapter. The adaptation of the Kalman filtering concept for its application to nonlinear systems is referred to as the Extended Kalman Filter and is explained. Issues pertaining to the divergence of the filter are discussed. Chapter 6 explains both the state formulations required when applying the Kalman filter and the Extended Kalman Filter to the Electrohydraulic Actuator (EHA).

5.1 Introduction

In this study the Extended Kalman Filter, a modified form of the Kalman filter, is used for parameter and state estimation. The Kalman filter is an optimal state estimation process applied to a dynamic system with random perturbations. More precisely, as defined by Chen, " *the Kalman filter gives a linear, unbiased and minimum mean error variance recursive algorithm to optimally estimate the unknown state of a dynamic system from noisy data taken at discrete real time intervals*,"[Chen, 1987, pp.36]. The Kalman filter has produced a virtual revolution in the field of systems engineering. Kalman filters are used in such diverse areas as navigation, guidance [Bryson et al.1971], oil drilling, geodetic surveys, video and laser tracking systems, ballistic missile trajectory estimation [Zarchan, 1997], radar and power systems [Brown, 1997].

Basically, the Kalman filter is a set of mathematical equations that provides an efficient computational (recursive) solution of the least square method [Brown, 1997]. With the recent development of high-speed computers, the Kalman filter has become more useful even for very complicated real time applications. In fact, the recursive

property of the Kalman filter makes it possible to process measurements on line. There is no need for storing measurement data, thus reducing considerably the amount of memory space needed in computers. In the Kalman filter, each new estimate is formed as a "*blend of the old estimate and the current measurement*" [Brown, 1997, pp. 191].

5.2 Statistical Review

When considering Kalman filtering, it is necessary to model the process and the measurement noise as being random signals, having a normal probability distribution, zero mean and known covariance matrices [Brown, 1997]. Furthermore, the criterion used in Kalman filtering is minimum mean square error. A brief review of random (stochastic) signals is provided in Appendix A and some definitions are presented. These definitions are required to develop the mathematical equations describing the Kalman filter.

5.3 Discrete State Space Model of a Linear System

The continuous state space model for a linear system having system and measurement noise matrices as $w(t)$ and $v(t)$ respectively, can be expressed as [Brown,1997]:

$$\dot{X}(t) = AX(t) + BU(t) + w(t) \tag{5.1}$$

$$Z(t) = CX(t) + v(t) \tag{5.2}$$

where $X(t)$ is the state vector, $(n \times 1)$ matrix, A is the system, $(n \times n)$ matrix, B is the input matrix, $(n \times p)$, C represents the output matrix, $(m \times n)$, $U(t)$ is the input vector, $(p \times 1)$, $Z(t)$ is the output vector, $(m \times 1)$, $w(t)$ is the system noise, $(p \times 1)$, and $v(t)$ stands for measurement noise, $(m \times 1)$.

The Kalman filter requires a discrete state space model of the system. In this study, a simplified discrete form for the state space model is generated by using the "forward difference" approximation, as shown in Equation (5.3) [Zavarehi, 1997].

$$\dot{X}(t) \approx \frac{X(k+1) - X(k)}{T_s} \tag{5.3}$$

where T_s is the sampling period.

Applying the forward difference approximation to Equations (5.1) and (5.2) yields the following discrete state space model,

$$X(k+1) = \Phi X(k) + GU(k) + W(k) \tag{5.4}$$

$$Z(k) = HX(k) + V(k) \tag{5.5}$$

$$\text{with } \Phi(k) = T_s A + 1 \tag{5.6}$$

$$G(k) = T_s B \tag{5.7}$$

$$W(k) = T_s w(k) \tag{5.8}$$

$$V(k) = v(k) \tag{5.9}$$

and where Φ represents the discrete system matrix, G is the discrete input matrix, H is the discrete output matrix, $W(k)$ represents process noise and $V(k)$ is measurement noise.

Elements of $W(k)$ and $V(k)$ which represent the process noise and measurement noise respectively are assumed to be uncorrelated and white, [Brown, 1997]. Thus,

$$W \approx N(0, Q(k)) \text{ and } V \approx N(0, R(k)) \tag{5.10}$$

where $Q(k)$ and $R(k)$ are known covariance matrices of $W(k)$ and $V(k)$ respectively. The noise covariance matrices are defined as [Brown, 1997]

$$\begin{aligned} E[W_i(k)W_j(k)^T] &= Q(k) \qquad i = j \\ &= 0 \qquad\quad i \neq j \\ E[V_i(k)V_j(k)^T] &= R(k) \qquad i = j \\ &= 0 \qquad\quad i \neq j \end{aligned} \tag{5.11}$$

5.4 The Kalman Filter

The Kalman filter consists of two stages, namely the estimation stage and the prediction stage [Brown, 1997], [Dean, 1986]. The estimation stage is depicted in Figure 5.1. The Kalman filter estimates states by comparing the measurement data $Z(k)$, which are affected by both the system and measurement noise, with the predicted output $\hat{y}^-(k)$. Using this error vector and a Kalman gain, $K(k)$, it improves upon an

initial estimation of the state vector $\hat{X}^-(k)$ to produce a better estimate, $\hat{X}(k)$, in this study, referred to as the "refined state estimate". As such, $\hat{X}^-(k)$ is referred to as the "unrefined estimate".

From Figure 5.1, the estimation equation of the Kalman filter is given by

$$\hat{X}(k) = \hat{X}^-(k) + K(k)[Z(k) - \hat{y}^-(k)]$$
$$= \hat{X}^-(k) + K(k)[Z(k) - H\hat{X}^-(k)] \qquad (5.12)$$

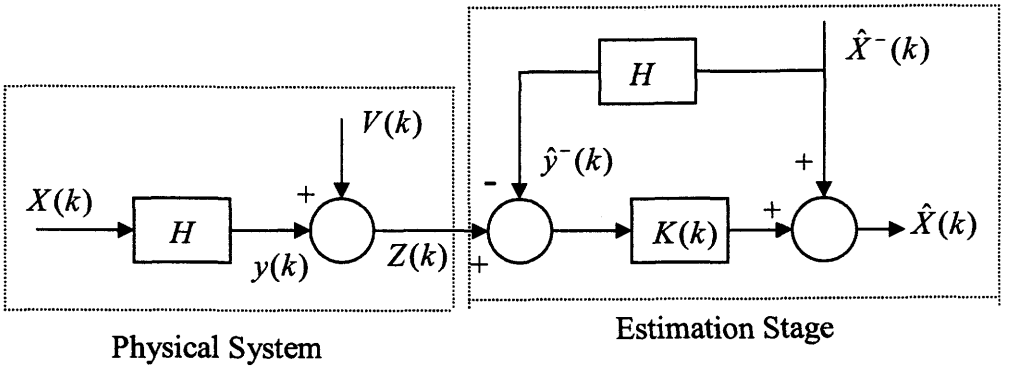

Figure 5.1:The Estimation Stage in the Kalman Filter.

The objective of the Kalman filter is to get an optimal estimate of the states and this is achieved by using the "*minimum mean square error criterion*", [Brown, 1997]. Much of the remaining derivation is based on the approach by [Brown, 1997].

The goal of the "prediction stage", of the Kalman filter is to obtain a new unrefined value for $\hat{X}^-(k)$ for the next step at $k+1$. The prediction stage is shown in Figure 5.2. The prediction equation is described by:

$$\hat{X}^-(k+1) = \Phi\hat{X}(k) + GU(k) \qquad (5.13)$$

In this stage, a refined estimate of $\hat{X}(k)$ at step k is now used to predict what $\hat{X}^-(k+1)$ is at the next step, $k+1$, based on the modeled dynamics of the plant.

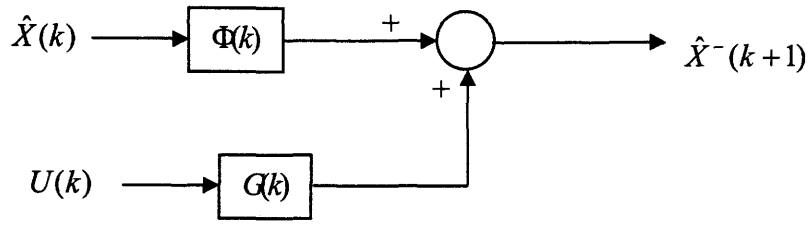

Figure 5.2: The Prediction Stage of the Kalman Filter

5.4.1 Derivation of Kalman Filtering Equations

To start the derivation of the Kalman filter equations, it is necessary to define the error vectors associated with $\hat{X}^-(k)$ and $\hat{X}(k)$. The error vectors are $e^-(k)$ and $e(k)$ respectively and are defined as:

$$e^-(k) = X(k) - \hat{X}^-(k) \tag{5.14}$$

$$e(k) = X(k) - \hat{X}(k) \tag{5.15}$$

The covariance matrices associated with $e^-(k)$ and $e(k)$, which in fact represent the mean square error, are $P^-(k)$ and $P(k)$ respectively. They are defined as:

$$P^-(k) = E[e^-(k)e^-(k)^T] = E\{[X(k) - \hat{X}^-(k)][X(k) - \hat{X}^-(k)]^T\} \tag{5.16}$$

$$P(k) = E[e(k)e(k)^T] = E\{[X(k) - \hat{X}(k)][X(k) - \hat{X}(k)^T\} \tag{5.17}$$

where $P^-(k)$ is the unrefined estimate of the error covariance matrix and $P(k)$ is the refined estimate of the error covariance matrix.

As mentioned previously, the Kalman filter is based on the criterion of minimum mean square error and as such, in the error covariance matrix, $P(k)$, the diagonal represents the mean squared error. Substituting Equation (5.12) into Equation (5.17), $P(k)$ can be expressed as:

$$P(k) = E\{[X(k) - \hat{X}^-(k) - K(k)(Z(k) - H\hat{X}^-(k))]$$
$$[X(k) - \hat{X}^-(k) - K(k)(Z(k) - H\hat{X}^-(k))]^T\} \quad (5.18)$$

Substituting Equations (5.14) and (5.5) into Equation (5.18), $P(k)$ becomes:

$$P(k) = E\{[e^-(k) - K(k)[HX(k) + V(k) - H\hat{X}^-(k)]]$$
$$[e^-(k) - K(k)[HX(k) + V(k) - H\hat{X}^-(k)]]^T\} \quad (5.19)$$

Simplifying $[e^-(k) - K(k)[HX(k) + V(k) - H\hat{X}^-(k)]]$ in Equation (5.19) gives

$$e^-(k) - K(k)HX(k) - K(k)V(k) + K(k)H\hat{X}^-(k)$$
$$= e^-(k) - K(k)H[X(k) - \hat{X}^-(k)] - K(k)V(k)$$
$$= e^-(k) - K(k)He^-(k) - K(k)V(k)$$
$$= [I - K(k)H]e^-(k) - K(k)V(k) \quad (5.20)$$

Simplifying $[e^-(k) - K(k)[HX(k) + V(k) - H\hat{X}^-(k)]]^T$ in Equation (5.19) gives

$$e^-(k)^T - [HX(k) + V(k) - H\hat{X}^-(k)]^T K(k)^T$$
$$= e^-(k)^T - [He^-(k) + V(k)]^T K(k)^T$$
$$= e^-(k)^T - [e^-(k)^T H^T + V(k)^T]K(k)^T$$
$$= e^-(k)^T - e^-(k)^T H^T K(k)^T - V(k)^T K(k)^T$$
$$= [I - H^T K(k)^T]e^-(k)^T - V(k)^T K(k)^T \quad (5.21)$$

Substituting Equations (5.20) and (5.21) into Equation (5.19) gives:

$$P(k) = E\{[[I - K(k)H]e^-(k) - K(k)V(k)][[I - H^T K(k)^T]e^-(k)^T - V(k)^T K(k)^T]\}$$
$$= E\{[I - K(k)H]e^-(k)e^-(k)^T[I - H^T K(k)^T] + K(k)V(k)V(k)^T K(k)^T\}$$
$$= [I - K(k)H]E[e^-(k)e^-(k)^T][I - H^T K(k)^T] + K(k)E[V(k)V(k)^T]K(k)^T \quad (5.22)$$

Now the unrefined estimate of the covariance matrix has been defined as $P^-(k) = E[e^-(k)e^-(k)^T]$. Also, the covariance matrix of the measurement noise is given by $R(k) = E[V(k)V(k)^T]$.

Therefore $P(k)$ can be rewritten as:

$$P(k) = [I - K(k)H]P^{-}(k)[I - H^{T}K(k)^{T}] + K(k)R(k)K(k)^{T} \tag{5.23}$$

Equation (5.23) is a general expression for the error covariance matrix and is valid for any gain, $K(k)$. The Kalman gain is that particular gain, $K(k)$, which minimizes the individual terms along the major diagonal of $P(k)$. This is because these terms represent the estimation error variances.

Equation (5.23) can be expanded and simplified to:

$$P(k) = P^{-}(k) - K(k)HP^{-}(k) - P^{-}(k)H^{T}K(k)^{T} + K(k)[HP^{-}(k)H^{T} + R(k)]K(k)^{T} \tag{5.24}$$

The variances along the diagonal of $P(k)$ are of interest. Since $P^{-}(k)$ equals to $P^{-}(k)^{T}$, the trace of $P^{-}(k)H^{T}K(k)^{T}$ is equal to the trace of its transpose, $K(k)HP^{-}(k)$. Equation (5.24) can be expressed as:

$$P(k) = P^{-}(k) - 2K(k)HP^{-}(k) + K(k)[HP^{-}(k)H^{T} + R(k)]K(k)^{T} \tag{5.25}$$

Differentiating the trace of $P(k)$ with respect to $K(k)$ yields:

$$\frac{d[trace(P(k))]}{dK(k)} = -2[HP^{-}(k)]^{T} + 2K(k)[HP^{-}(k)H^{T} + R(k)] \tag{5.26}$$

In order to obtain the optimal value of $K(k)$ which minimizes the trace of $P(k)$, the derivative is equated to zero, i.e. $\frac{d[trace(P(k)]}{dK(k)} = 0$

The Kalman gain $K(k)$ is therefore obtained as:

$$K(k) = \frac{[HP^{-}(k)]^{T}}{HP^{-}(k)H + R(k)}$$

$$= P^{-}(k)H^{T}[HP^{-}(k)H^{T} + R(k)]^{-1} \tag{5.27}$$

Substituting $K(k)$ into Equation (5.24) yields the optimum $P(k)$ as:

$$P(k) = [I - K(k)H]P^{-}(k) \tag{5.28}$$

The next stage of the Kalman filter algorithm is the prediction stage. From Equation (5.17), the predicted estimate is described by

$$\hat{X}^{-}(k+1) = \Phi\hat{X}(k) + GU(k) \tag{5.29}$$

The estimated error vector associated with $X^-(k+1)$ is given by the following:

$$e^-(k+1) = X(k+1) - \hat{X}^-(k+1) \tag{5.30}$$

Substituting Equation (5.4) and (5.13) into (5.30) yields

$$\begin{aligned} e^-(k+1) &= \Phi X(k) + GU(k) + W(k) - \Phi\hat{X}(k) - GU(k) \\ &= \Phi[X(k) - \hat{X}(k)] + W(k) \\ &= \Phi e(k) + W(k) \end{aligned} \tag{5.31}$$

Now $P^-(k+1) = E[e^-(k+1)e^-(k+1)^T]$ (5.32)

Substituting Equation (5.31) into (5.32) gives

$$\begin{aligned} P^-(k+1) &= E\{[\Phi e(k) + W(k)][\Phi e(k) + W(k)]^T\} \\ &= E\{[\Phi e(k) + W(k)][e(k)^T\Phi^T + W(k)]^T\} \\ &= E[\Phi e(k)e(k)^T\Phi^T + \Phi e(k)W(k)^T + W(k)e(k)^T\Phi^T + W(k)W(k)^T] \end{aligned}$$

Since $Q(k) = E[W(k)W(k)^T]$, $P(k) = E[e(k)e(k)^T]$, $E[W(k)] = 0$ and $E[W(k)^T] = 0$, the above equation can be simplified to

$$P^-(k+1) = \Phi P(k)\Phi^T + Q(k) \tag{5.33}$$

The five Kalman filtering equations have been derived and can be summarized as follows:

Estimation equations:

$$K(k) = P^-(k)H^T[HP^-(k)H^T + R(k)]^{-1} \tag{5.27}$$

$$\hat{X}(k) = \hat{X}^-(k) + K(k)[Z(k) - H\hat{X}^-(k)] \tag{5.12}$$

$$P(k) = [I - K(k)H]P^-(k) \tag{5.28}$$

Prediction equations:

$$\hat{X}^-(k+1) = \Phi\hat{X}(k) + GU(k) \tag{5.13}$$

$$P^-(k+1) = \Phi P(k)\Phi^T + Q(k) \tag{5.33}$$

5.5 Extended Kalman Filter

The Extended Kalman Filter (EKF) is an extension of the linear Kalman filtering theory to nonlinear problems. *"The goal is to minimize the estimation error for the*

states of a nonlinear system along a trajectory by applying a linearization technique." [Brown, 1987]. As seen in the previous sections, the Kalman filter addresses the general problem of estimating the state of a discrete time controlled process that is governed by a linear stochastic difference equation. If the model is nonlinear, the Extended Kalman Filter is used [Horton, 1997]. In this method, the Kalman filter is applied to nonlinear systems by continually updating a linearization around the previous state estimate, starting with an initial guess. The linearization is made around the most recent reference, which is $\hat{X}(k)$ for the system function and $\hat{X}^{-}(k)$ for the measurement function [Brown, 1997].

A Taylor approximation of the system function is made at the refined state estimate $\hat{X}(k)$ and an approximation of the measurement function is made at the unrefined state estimate $\hat{X}^{-}(k)$.

The nonlinear model can be represented by [Ljung 1979]:

$$X(k+1) = f(X(k),U(k)) + W(k) \tag{5.34}$$

$$Z(k) = h(X(k)) + V(k) \tag{5.35}$$

where $f(X(k),U(k))$ and $h(X(k))$ are the nonlinear system and measurement functions respectively.

The linearization is made using the most recent state estimate obtained which is using the unrefined estimate for the system function and the refined estimate for the measurement function, as shown in Figure 5.3.

Therefore, doing a linear Taylor series approximation of $f(X(k),U(k))$ at an operating point $\hat{X}(k)$ and of $h(X(k))$ at the operating point $\hat{X}^{-}(k)$, and ignoring the higher-level terms yields:

$$f(X(k),U(k)) \approx f(\hat{X}(k),U(k)) + \left(\frac{\partial f(X(k),U(k))}{\partial X(k)}\Big|_{\hat{X}(k)}\right)(X(k) - \hat{X}(k)) \tag{5.36}$$

$$h(X(k)) \approx h(\hat{X}^{-}(k)) + \left(\frac{\partial h(X(k))}{\partial X(k)}\Big|_{\hat{X}^{-}(k)}\right)(X(k) - \hat{X}^{-}(k)) \tag{5.37}$$

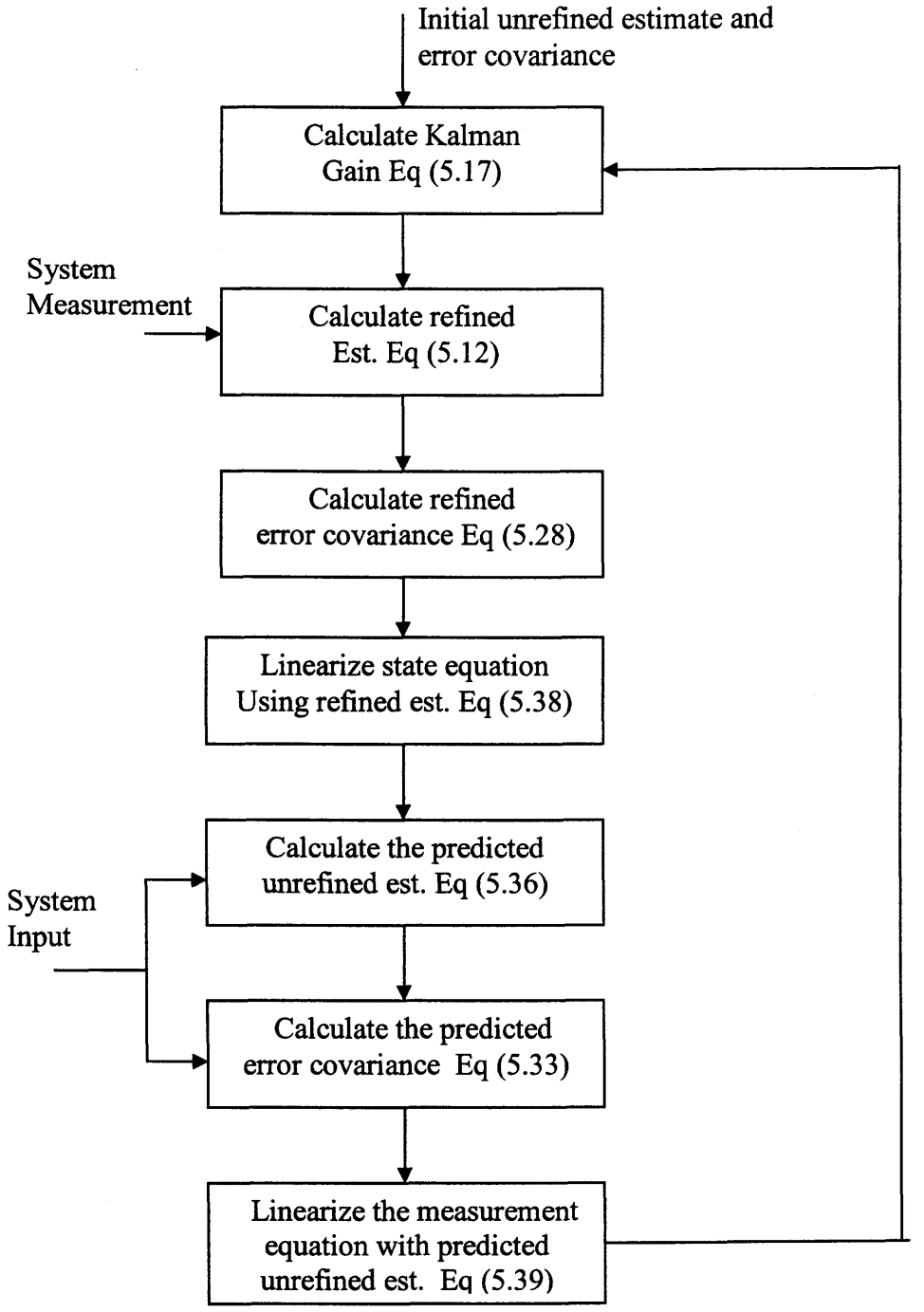

Figure 5.3 The Extended Kalman Filter (EKF) Loop

Substituting Equation (5.36) into (5.35), results in Equation (5.38).

$$X(k+1) = \frac{\partial f(X(k),U(k))}{\partial X(k)}\Big|_{\hat{X}(k)} X(k) + f(\hat{X}(k),U(k)) - \frac{\partial f(X(k),U(k))}{\partial X(k)}\Big|_{\hat{X}(k)} \hat{X}(k) + W(k) \tag{5.38}$$

Substituting Equation (5.37) into (5.35), results in equation (5.39).

$$Z(k) = \frac{\partial h(X(k))}{\partial X(k)}\Big|_{\hat{X}^-(k)} X(k) + h(\hat{X}^-(k)) - \frac{\partial h(X(k))}{\partial X(k)}\Big|_{\hat{X}^-(k)} \hat{X}^-(k) + V(k) \tag{5.39}$$

Rewriting the above equations as follows:

$$X(k+1) = \Phi(k)X(k) + U_1(k) + W(k) \tag{5.40}$$

$$Y(k) = H(k)X(k) + V(k) \tag{5.41}$$

where:

$$\Phi(k) = \frac{\partial f(X(k),U(k))}{\partial X(k)}\Big|_{\hat{X}(k)},$$

$$H(k) = \frac{\partial h(X(k))}{\partial X(k)}\Big|_{\hat{X}^-(k)},$$

$$U_1(k) = f(\hat{X}(k),U(k)) - \Phi(k)\hat{X}(k)$$

$$Y(k) = Z(k) - h(\hat{X}^-(k)) + H(k)\hat{X}^-(k).$$

The linearization procedure is completed and the same Kalman filter equations derived previously are used when estimating states in a nonlinear system. The EKF loop is illustrated in Figure 5.3, with references to the equations used.

5.6 Divergence in the Extended Kalman Filter

In theory, the Kalman Filter is defined in terms of real numbers which have infinite precision. However, when it is implemented on digital computers, it is done in finite precision arithmetic. In binary representation, the rational numbers are transformed into sums of powers of 2 and this representation is limited to 24 bits of mantissa. "*The difference between the true value of the result and the value approximated by the processor is called the roundoff error*" [Brown 1997]. Computer roundoff errors can and do cause the Kalman Filter to diverge [Brown, 1997]. Roundoff

errors can be reduced by using more precision, i.e. more bits in the mantissa of the data format. The EKF can also diverge if the reference about which the linearization takes place is poor. The most common situation of this type occurs at the initial starting point of the recursive process (poor "a priori" information about the true state). This causes a large error in the initial matrix and forces the initial error covariance to be large.

A very large error covariance combined with low-noise measurements at the first step will cause the error covariance matrix to "jump" from a very large value to a small value in one step. This can lead to numerical problems due to roundoff. A non-positive-definite error covariance matrix at any point in the recursive process usually leads to divergence [Brown, 1997].

The initial state matrix is presumably the best estimate prior to receiving any measurement information and thus it is used as the reference for linearization. If the error in the initial state matrix is large, the first-order approximation used in the linearization will be poor, and divergence may occur even with perfect arithmetic [Brown, 1997].

There are several design issues associated with the EKF, such as proper choice of the Q and R matrices to avoid filter divergence. However, when these problems occur, the filter designer must usually apply ad hoc "fixes". As indicated in EKF literature, there is no single cure for all numerical problems. Each case must be considered on its own merits.

Another type of divergence may be caused by inaccurate modeling of the process being estimated. The Kalman Filter has a model embedded in it and if the physical system is behaving differently from the predicted behavior, divergence may occur. As described in [Brown, 1997, pp. 263], the "*obvious remedy for this type of divergence problem is to insert some process noise into each of the state variables, even at the risk of some degree of suboptimality*".

Divergence can also occur when the system is not observable, as reported in [Brown, 1997]. Physically, it means that there are one or more state variables that are hidden from the measurements and "*if the unobserved processes are unstable, the corresponding estimation errors will be unstable*" [Brown, 1997, pp. 264]. The error

covariance matrix will show an increase in the estimation error. The measurements are not providing enough information to estimate all the state variables of the system. Another study carried out by Konrad et al, analyzed the error behavior for a discrete Extended Kalman Filter for a general nonlinear system [Konrad et al, 1998]. It was shown that the "*estimation error remains bounded if the system satisfies the nonlinear observability rank condition and if the initial estimation error as well as the disturbing noise terms are small enough.*"

Another interesting paper, written by Ljung provides a convergence analysis using the Extended Kalman Filter for joint parameter and state estimation problems, [Ljung, 1979]. The study revealed that estimations may be biased or divergent because of "*a lack of coupling between the Kalman gain and the parameter in the algorithm*". The author suggested having "*a coupling term to ensure global convergence*".

5.7 Conclusions

In this chapter, the fundamental equations for the Kalman and the Extended Kalman Filter are described. This chapter serves as an introduction to the parameter estimation technique used in this study, namely the Extended Kalman Filter (EKF) and it also served as a literature review for the Kalman Filter. It is seen that the EKF is based on linearization of the state equations at each time step and of the use of the Kalman Filter (linear estimation theory). EKF in this study is used since the joint state and parameter estimation can be regarded as a state estimation problem for a nonlinear system. Some of the causes associated with divergence of the EKF are also reported in this chapter. The following chapter will further investigate the effect of system observability on the ability of the Kalman filter and of the Extended Kalman Filter to successfully estimate states and parameters. Simple mechanical systems are used at first and the Kalman filter, as well as the EKF will be applied to the systems which will be made observable or unobservable depending on the type of measurements and the number of estimated states (explained in greater detail in the next chapter). The Kalman filter and the Extended Kalman Filter will then be applied to the more complex Electrohydraulic Actuator (EHA) system.

Chapter 6
Parameter Estimation Using Extended Kalman Filter

The overall objective of this research was early fault detection in a high performance hydrostatic system by estimating critical parameters using the Extended Kalman Filter. As seen in Chapter 5, the application of the EKF for a combined parameter and state estimation required a state space formulation of the problem. In order to illustrate the methodology and the degree of accuracy that could be expected using this technique, the EKF was first applied to two simulated, simple mechanical systems (described in Appendix B). The EKF was then applied to a mathematical model of the more complex Electrohydraulic Actuator (EHA), to demonstrate practical difficulties that could be encountered when applying the EKF to a real system. The mathematical model developed for the EHA, described in Chapter 3 was used to estimate two important parameters for the EHA, namely the viscous friction coefficient and the effective bulk modulus. A simulation study was done to show the feasibility of this approach and to determine the level of accuracy in the prediction of the parameters.

It should be pointed out that the application of the EKF in the hydrostatic system is unique. The EKF has never been used to estimate critical parameters in a hydrostatic system, and to detect changes in those parameters. Fault detection in hydraulic components and some very basic circuits using the Extended Kalman Filter have been previously investigated [Zavarehi, 1997, Cao, 2001, Wright, 2001], but, as mentioned, never using a closed complex system such as the EHA. The "effective" bulk modulus is an important parameter dictating the system dynamics, an extremely difficult parameter to measure directly or indirectly; the application of the EKF for the prediction of this parameter was unique.

This chapter also investigates the importance of system observability when using the Kalman filer and the Extended Kalman Filter for state and parameter estimation. This investigation is achieved by first using a simple mechanical system and

then using the more complex EHA model. In this chapter, an attempt is made to further understand the Kalman and the Extended Kalman Filters. Simple examples are used to carry out simulation studies to illustrate state estimations for observable and unobservable systems. The EKF is investigated for parameter estimation for both observable and unobservable systems in simulation. In previous studies involving the EKF and multiple parameter estimation in hydraulic systems, the filters were used as tools for state and parameter estimations. In this study, an in-depth study of the Kalman Filter and of the EKF is used to provide an insight into the limitations of the filters. This is particularly important in this case since difficulties are experienced when the EKF is used for multiple parameter estimation in the EHA.

6.1. Importance of the Observability Condition

By definition, an unobservable state is one which cannot be uniquely obtained through the "observations" and hence the solution provided by the Kalman filter may be a local minima and not necessarily be the correct answer. "*A system is said to be observable at a time step* k_0 *if for a state* $X(k_0)$ *at that time, there is a finite* $k_1 > k_0$ *such that knowledge of the outputs from* k_0 *to* k_1 *are sufficient to determine state* k_0" [Southhall et al, 1998]. In other words, for a system to be observable, the initial states can be uniquely reconstructed using observations or measurements from the system. An illustrative example is provided in Appendix B, where for a mass damper system, using velocity alone as a measurement, the system is unobservable since the initial position cannot be found using velocity measurements. The system thus fails the observability test (explained later in this chapter). However, the use of position makes the mass damper system observable and the initial states can be reconstructed from the position measurements.

Following this definition for observability, an unobservable system is one where the values of some elements in the state vector at time k_0 may not be uniquely determined from examination of the output regardless of the number of observations taken. "*This concept of observability is useful in solving the problem of reconstructing unmeasurable state variables in the minimum possible length of time*" [Ogata, 2002].

Unlike previous studies involving the EKF and parameter estimations in hydraulic systems [Cao, 2001], [Zavarehi, 1997], [Wright, 2001], in this study, no a-priori information was assumed for the estimated parameters or states (that is the initial parameter/state matrix used in the EKF was always zero). The observability test was also carried out whenever the Kalman Filter or the EKF was used to estimate states and parameters. In the case of the EKF, since linearization was involved about an operating point, the observability test was carried out at each iteration, unlike for the Kalman Filter where the state matrix and the measurement matrix do not change. "*A system is known to be completely observable if the rank of the observability is equal to the number of state variables*", [Ogata, 2002]. The observability of the state space model of the system, (when reformulating the model for parameter estimation) has often been overlooked in the previous studies involving the EKF for condition monitoring purposes.

In the research carried out by Zavarehi, it was stated that " *all the initial states/parameters are set to random numbers*" but the author did not provide the actual parameter values used to initialize the EKF algorithm [Zavarehi, 1997]. It was believed that using initial values close to the desired parameter values to initialize the state matrix in the EKF might be an indication of an observability problem. However it should be pointed out that Zavarehi did report that "*the lack of observability of the Coulomb friction and of viscous damping coefficient is responsible for slow convergence rate*" and was used to account for the biases in these two estimated parameters. This bias can also be explained by a local minima resulting from a system where change in the states have an impact on the measured output, but not uniquely attributable to them.

In a different study done by Cao, the EKF was used to estimate three parameters for a swash plate assembly and the control piston, namely the swash plate damping coefficient, swash plate spring constant coefficient and the swash plate pretension coefficient [Cao, 2001]. The only way the author could make the EKF converge to the desired values was by using initial parameter values (used in the EKF algorithm) which were very close to the estimated values. For instance, Cao used an initial value of

5 Nms/rad for the swash plate-damping coefficient in the EKF code when the estimated value was 5.305Nms/rad. The initial values used for the swash plate spring constant coefficient and for the pretension coefficient were also both close to their estimated values. Only the swash plate angular displacement was used as the measurement. However, since the results reported in that study were repeatable and did follow physical changes in system parameters, the actual value was not so much a concern as was the ability of the filter to detect changes.

In the present study, it was believed that the lack of full observability could prevent the EKF from successfully estimating states and parameters. However, initial studies had revealed that extensive tuning (setting the initial noise and error covariance matrices) of the EKF could result in successful parameter estimation in spite of the system being unobservable, as it can be seen in the examples presented in Appendix B. Therefore, a more effective method for estimating several parameters became one of estimating one parameter at a time using different models, and using the known parameter value to estimate the second one from a second model (tackling the problem in an iterative manner). This resulted in reducing the number of states and had a higher probability of making the state space reformulation of the problem observable, as compared to simply including all the parameters to be estimated as states and attempting to estimate them simultaneously.

In order to investigate the importance of observability for the Kalman Filter the following cases were considered.

- Application of the Kalman Filter to an observable system (mass damper system with only position being used as measurement)
- Application of the Kalman Filter to an unobservable system (mass damper system with only velocity being used as measurement).
- Application of the Kalman Filter to an unobservable system made observable by increasing the number of measurements (mass damper system with both position and velocity used as measurements).

- Application of the Extended Kalman Filter to an observable system first (mass damper system; position as measurement) and then to an unobservable system (mass damper system; velocity as measurement) to estimate the damping coefficient.
- The above steps were repeated using a mass spring damper system and using the Kalman filter to estimate the states. Next, the EKF was used to estimate one parameter at a time (viscous damping coefficient and then spring constant coefficient), followed by the two parameters at the same time.

For brevity, only the results, of these scenarios are presented in this chapter and are summarized in Tables 6.1 to 6.5. The actual simulation studies, states space formulations, as well as the augmentation of the state matrices to accommodate parameters are all described in Appendix B. Also included in Appendix B are the different observability matrices.

Table 6.1: Kalman Filter Applied to A Mass-Damper System for State Estimation

Measurements used for State estimation by the Kalman Filter	**Observability Test**	**Agreement between Estimated States and the Simulated States.**
Position	Observable Rank of observability matrix was 2 and length of state vector was 2 (position and velocity being the two states)	Good Agreement (No visible difference) The estimated states converged to the simulated states.
Velocity	Not observable (one unobservable state). Rank of observability matrix was 1.	Poor Agreement between simulated and estimated position. There was a "bias" present between the estimated position and the simulated position, but no divergence of the filter. Convergence of the estimated velocity to the simulated velocity.
Position and Velocity	Observable Rank of observability matrix was 2.	Good Agreement (No visible difference) Estimated position and velocity converged to their simulated values.

Table 6.2: Extended Kalman Filter Applied to the Mass-Damper System (Parameter Estimation)

Measurements used for State/ Parameter Estimation	Observability Test	Agreement between Estimated and the Simulated States
Position	Observable Rank of the observability matrix was 3 and length of the augmented state vector was 3 (2 states and one parameter)	Good agreement for both states (no visible difference) and estimated parameter (viscous damping coefficient) converged to its known value.
Velocity	Not observable. Rank of observability matrix was 2. The length of the augmented state vector was 3. There was 1 unobserved state (position).	Poor agreement between estimated and simulated position (showing the presence of a bias) but good agreement between estimated velocity and simulated velocity. The estimated parameter converged to its known value.
Position and Velocity	Observable Rank of observability matrix was 3 and length of the augmented state vector was 3	Good agreement for both parameter and states. Convergence of the estimated states to their simulated values and of the estimated parameter to its known value.

Table 6.3: Kalman Filter Applied to a Mass-Spring-Damper System (State Estimation)

Measurements used for State Estimation	Observability Test	Agreement between Estimated and the Simulated States
Position	Observable. Rank of the observability matrix was 2 and length of state vector was 2 (position and velocity being the two states).	Good Agreement (No visible difference between estimated and simulated states).
Velocity	Observable. Rank of observability matrix was 2 and length of state vector was 2.	Good Agreement The estimated states converged to the simulated states.
Position and Velocity	Observable Rank of observability matrix and length of state vector were both 2	Good Agreement The estimated states (position and velocity) converged to the simulated states.

It was interesting to note that the Mass-Spring-Damper system remained observable when velocity was used as measurement. As explained in Appendix B, this was due to the displacement term being detectable. The Mass-Spring-Damper system is a Type 0 system but showed similar results as the Mass-Damper system (Type 1 system) in terms of the Kalman Filter estimating states successfully for observable systems.

Next, the EKF was applied to the Mass-Spring-Damper system to estimate the viscous friction and then to estimate the spring constant. The results were similar and only one set of results is presented in Table 6.4.

Table 6.4: Extended Kalman Filter Applied to the Mass-Spring-Damper System for State Estimation and Estimation of 1 Parameter (Damping Coefficient)

Measurements Used For State/ Parameter Estimation	Observability Test	Agreement between Estimated and the Simulated States
Position	Observable. Rank of the observability matrix was 3. Length of the augmented state vector was 3 with 2 states and 1 parameter.	Good agreement for both states and parameter. The estimated states converged to the simulated states. The estimated damping coefficient converged to its known value.
Velocity	Not observable. Rank of observability matrix was 2.	No agreement between the estimated and the simulated position. Estimated velocity converged to the simulated velocity. Estimated parameter (Damping) did not converge to its known value.
Position and Velocity	Observable Rank of observability matrix was 3	Good agreement for both parameter and states. (No visible difference)

Table 6.5: Extended Kalman Filter Applied to the Mass-Spring-Damper System to Estimate Two Parameters (Damping and Spring Constant)

Measurements Used For State/ Parameter Estimation	Observability Test	Agreement between Estimated and the Simulated States
Position	Not Observable (one unobservable state) Rank of the observability matrix was 3 and length of the augmented state vector was 4.	Good agreement for both states (no visible difference) and parameters. The estimated states (position and velocity) converged to the simulated states. The estimated parameters (damping coefficient and spring constant) converged to their known values.
Velocity	Not observable (two unobservable states). Rank of the observability matrix was 2 and length of augmented state vector was 4	The estimated position showed a bias compared to the simulated position. The estimated velocity converged to the simulated velocity. The parameters did not converge to their known values.
Position and Velocity	Not Observable (one unobservable state). Rank of observability matrix was 3 and length of augmented state vector was 4	Good agreement for both parameters and states. (No visible difference)

From the simulation studies carried out on the simple Mass-Damper system and Mass-Spring-Damper, reported in Appendix B, some observations could be made regarding the importance of observability for the Kalman Filter and the Extended Kalman Filter as far as state and parameter estimations are concerned.

Observability was found to be an essential condition for the Kalman Filter to converge (that is for the estimated states to match the simulated ones, without knowledge of initial position) as illustrated by the simple Mass-Damper system and the Mass-Spring-Damper system. In both examples, the use of position as a measurement made the systems observable. The Kalman Filter estimated position and velocity accurately when position was used as the only measurement. However, when the velocity was used as measurement, for the Mass-Damper system that is a Type 1 system, the system was not observable. The observability test revealed the presence of one unobserved state (position). As such, when the velocity was used as the measurement, the estimated position did not show good agreement with the simulated position, revealing the presence of a "bias" when the initial condition was not known. The estimated position was "shifted" by a value equal in magnitude to the initial position condition. This "bias" disappeared when the initial position was known. On the other hand, the estimated velocity converged to the simulated velocity. Therefore, it was confirmed that, as reported in the literature, the Kalman Filter estimated states accurately for observable systems only. In the Mass-Spring-Damper system (a Type 0 system), the use of velocity as the only measurement preserved the observability of the system and the Kalman Filter estimated the two states for the observable system accurately.

When the EKF was applied to the nonlinear systems (using the linearized state matrix and applying the observability condition at each iteration) it was found that the importance of observability was not clear cut but was found to be application-dependent. However, when guaranteeing the observability condition, the EKF always converged to the simulated states and parameters. This was shown by using position as the only measurement for the Mass-Damper system and the Mass-Spring-Damper system. Estimation of one parameter in both examples using position as the only

measurement resulted in the system satisfying the observability condition. The rank of the observability matrix was equal to the length of the augmented state vector in each case. The EKF estimated states (position and velocity) and one parameter (viscous damping or spring constant) successfully.

It also seemed that there were two types of observability conditions; the first one where the measurement itself made the system unobservable (for instance using velocity instead of position) and a second one which resulted from augmenting the state matrix with parameters to be estimated and thereby resulting in an augmented length of the state vector. Using velocity as measurement, the Mass-Damper system was unobservable (1 unobserved state) and the EKF, when used to estimate the position, showed the presence of a "bias" when compared to the simulated position. The estimated velocity converged to the simulated velocity. The estimated damping coefficient converged to its known value, in spite of the system being unobservable as a result of velocity being used as measurement. When position was used to estimate two parameters in the Mass-Spring-Damper system, the rank of the observability matrix was 3 and length of the augmented state vector was 4. As such, the Mass-Spring-Damper system was unobservable. But the states and the two parameters were estimated successfully.

When velocity was used as the only measurement for the Mass-Spring-Damper system, the number of unobserved states in this case was 2 and parameter estimation was not successful. The estimated position showed a "bias" but the estimated velocity converged to the simulated velocity. However, when the initial position was known, both parameter estimation and state estimation were successful. Therefore, it was observed that augmenting the state matrix did not seem to affect state and parameter estimation by the EKF, as illustrated by the Mass-Spring-Damper system which was unobservable when two parameters were included as states but which still demonstrated accurate convergence to the simulated parameters when position was used as measurement. The use of velocity as measurement increased the number of unobserved states to 2 for that same system and when the initial position was not known, parameter estimation was not possible.

In the next section the Kalman Filter and the Extended Kalman Filter are applied to the mathematical model for the Electrohydraulic Actuator. The Kalman Filter was first applied to the EHA to estimate three states, namely piston position, velocity and acceleration. The EHA model used was a Type 1, third order system and as such was expected to demonstrate similar behavior to the Mass-Damper system. This was verified in simulation with the results presented in the next section. Also, the Extended Kalman Filter was later applied to the EHA to estimate the three states as well as two parameters (viscous damping coefficient and effective bulk modulus). System observability was checked in each of the following scenarios presented in the next section.

6.2 Applying the Kalman Filter to the EHA in Simulation

The results obtained when applying the Kalman Filter to a state space model of the Mass-Damper and Mass-Spring-Damper system revealed that the observability condition was necessary to ensure successful state estimation. It was of particular interest in this study to determine if the trends summarized in Section 6.1 would apply to a more complex system such as the EHA.

In Chapter 3, the linearized mathematical model for the EHA was given as:

$$\frac{x(s)}{\omega_p(s)} = \frac{\dfrac{2D_p\beta_e A}{MV_o}}{s^3 + s^2\left(\dfrac{B}{M} + \dfrac{C_T\beta_e}{V_0}\right) + s\left(\dfrac{2\beta_e A^2}{MV_o} + \dfrac{B\beta_e C_T}{MV_0}\right)}$$

Using the third order transfer function above, the following equation can be written as:

$$\dddot{X} + \ddot{X}\left(\frac{B}{M} + \frac{C_T\beta_e}{V_0}\right) + \dot{X}\left(\frac{2\beta_e A^2}{MV_0} + \frac{B\beta_e C_T}{MV_0}\right) = \omega_p\left(\frac{2D_p\beta_e A}{MV_0}\right) \tag{6.1}$$

A state space formulation of the EHA system is expressed as follows:

$$\begin{aligned}
\dot{X}_1 &= X_2 + w_1 \\
\dot{X}_2 &= X_3 + w_2 \\
\dot{X}_3 &= -X_2\left(\frac{2A^2\beta_e}{MV_0} + \frac{BC_T\beta_e}{MV_0}\right) - X_3\left(\frac{B}{M} + \frac{C_T\beta_e}{V_0}\right) + \omega_p\left(\frac{2D_pA\beta_e}{MV_0}\right) + w_3
\end{aligned} \tag{6.2}$$

$$Z = \begin{bmatrix} 1 & 0 & 0 \end{bmatrix} \begin{bmatrix} X_1 \\ X_2 \\ X_3 \end{bmatrix} + v_1$$

where X_1 is the state variable X, X_2 the state variable $\dot{X}$, X_3 the state variable $\ddot{X}$; w_1, w_2, w_3 are the system noise; and v_1 is the measurement noise. In this case, piston position is used as measurement. The electric motor angular velocity ω_p is the Kalman filter input.

Using the forward difference approximation and applying it to the continuous state space model, the discrete state space model of the EHA is:

$$X_1(k+1) = X_1(k) + T_s X_2(k) + T_s w_1(k) \tag{6.3}$$

$$X_2(k+1) = X_2(k) + T_s X_3(k) + T_s w_2(k)$$

$$X_3(k+1) = -X_2(k) T_s \left(\frac{2\beta_e A^2}{MV_0} + \frac{B\beta_e C_T}{MV_0} \right) - X_3 T_s \left(\frac{B}{M} + \frac{C_T \beta_e}{V_0} \right) + X_3(k) + \frac{2D_p A T_s \beta_e}{MV_0} U(k) + T_s w_3(k)$$

The state space model, given by Equation 6.3 was used by the Kalman Filter. A simulation of the EHA linearized model (plant) was done in Simulink/Matlab® to generate simulated data. The input to the closed loop, linearized EHA system (plant) was a sine wave, with a frequency of 4 Hz and amplitude of 0.01 m (desired piston position). The overall transfer function of the EHA consisted of the second order electric motor transfer function in series with the third order hydraulic transfer function and a proportional gain. In the EHA prototype, pump angular velocity measurements were readily available. It should be pointed out that the pump angular velocity was used instead of the desired piston position as the input to the EKF in order to simplify the state estimation problem which would have otherwise involved a fifth order model. The EKF model described by Equation 6.3 was found to be observable, with the rank of the observability matrix being equal to the length of the state matrix, both being equal to 3.

The Kalman Filter was used to estimate the three states, namely piston position, velocity and acceleration in simulation, as shown in Figure 6.1 which depicts the plots

of simulated states superimposed on the estimated states. There is no visible difference between the estimated and simulated states. It is verified that the Kalman Filter estimated successfully the states for the fully observable EHA system.

The observabiliy matrix is, after substituting with the numerical values:

$$Observability\ Matrix = \begin{bmatrix} H \\ HA \\ H(A)^2 \end{bmatrix}, \text{ where } A = \begin{bmatrix} 1 & 0.001 & 0 \\ 0 & 1 & 0.001 \\ 0 & -78.27 & 0.962 \end{bmatrix}$$

$$\text{and } H = \begin{bmatrix} 1 & 0 & 0 \end{bmatrix} \tag{6.4}$$

$$Observability\ Matrix = \begin{bmatrix} 1 & 0 & 0 \\ 1 & 0.001 & 0 \\ 1 & 0.002 & 0.00001 \end{bmatrix}.$$

The rank of the observability matrix and the length of the state vector were both 3.

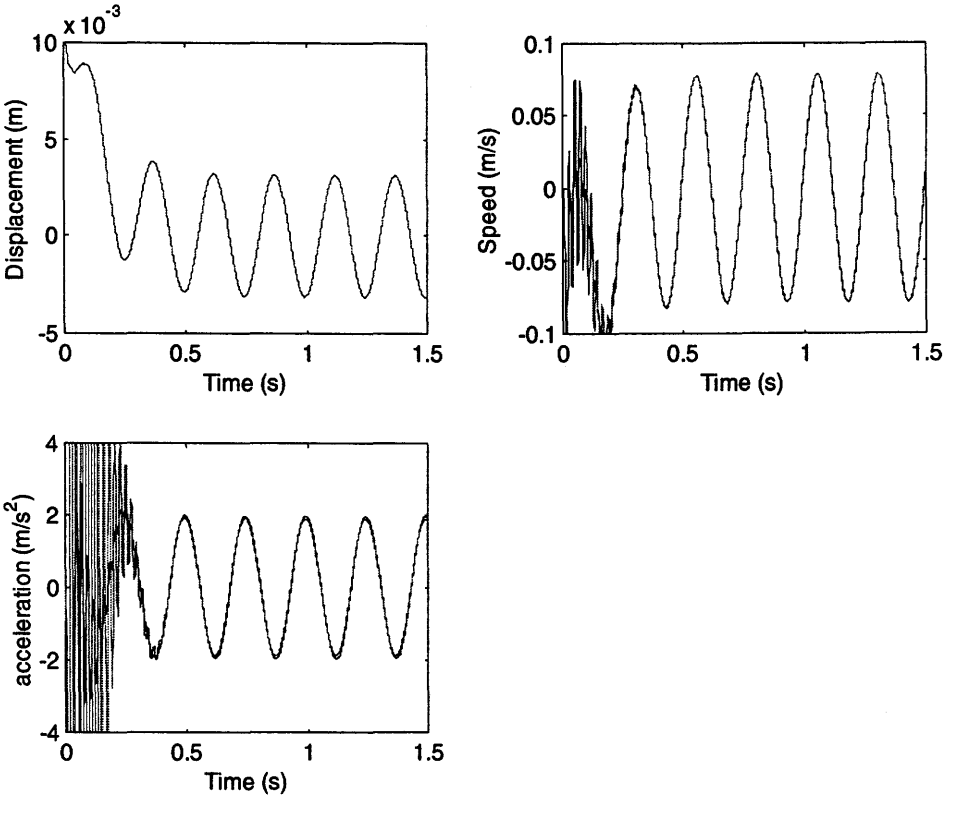

Figure 6.1: Kalman Filter Used to Estimate States in the Simulated Electrohydraulic Actuator Model (Transfer Function Model)

The initial state vector and the initializing matrices for the Kalman Filter were set as:

$$X(0) = [0 \quad 0 \quad 0]^T \qquad R(k) = 1\times10^{-6}$$

$$P(0) = \begin{bmatrix} 1\times10^{1} & 0 & 0 \\ 0 & 1\times10^{1} & 0 \\ 0 & 0 & 1\times10^{4} \end{bmatrix} \qquad Q(k) = \begin{bmatrix} 1\times10^{-5} & 0 & 0 \\ 0 & 1\times10^{-7} & 0 \\ 0 & 0 & 1\times10^{-4} \end{bmatrix} \tag{6.5}$$

Having confirmed that the Kalman Filter worked for an observable system of the EHA, the model was next made unobservable by using simulated velocity as the measurement instead of simulated position (similar to the Mass-Damper example). Thus the observability matrix for this scenario is:

$$\textit{Observability Matrix} = \begin{bmatrix} H \\ HA \\ H(A)^2 \end{bmatrix}, \tag{6.6}$$

$$\text{where } A = \begin{bmatrix} 1 & 0.001 & 0 \\ 0 & 1 & 0.001 \\ 0 & -78.27 & 0.962 \end{bmatrix} \text{ and } H = [0 \quad 1 \quad 0]$$

$$\textit{Observability Matrix} = \begin{bmatrix} 0 & 1 & 0 \\ 0 & 1 & 0.001 \\ 0 & 0.922 & 0.00196 \end{bmatrix}.$$

The rank of the observability matrix was now 2, which was less than the length of the state matrix. Thus it was confirmed that the EKF model was not fully observable. The Kalman Filter was then used to estimate states of the unobservable system as illustrated in Figure 6.2. It is seen that the estimated position does not agree with the simulated position and revealed the presence of a "bias" when the initial position is not known; the results are consistent with those of Section 6.1 (The "bias" in the estimated position disappeared when the initial position was known). The estimated velocity shows good agreement to its simulated state values. The acceleration agreement is acceptable but does show at least a 10% error in magnitude.

The initial state matrix and the initializing matrices for the Kalman Filter were manually set as:

$$X(0) = [0 \quad 0 \quad 0]^T \quad , \; R(k) = 1\times10^{-3}$$

$$P(0) = \begin{bmatrix} 1\times10^{1} & 0 & 0 \\ 0 & 1\times10^{1} & 0 \\ 0 & 0 & 1\times10^{4} \end{bmatrix}, \; Q(k) = \begin{bmatrix} 1\times10^{-5} & 0 & 0 \\ 0 & 1\times10^{-7} & 0 \\ 0 & 0 & 1\times10^{-4} \end{bmatrix} \tag{6.7}$$

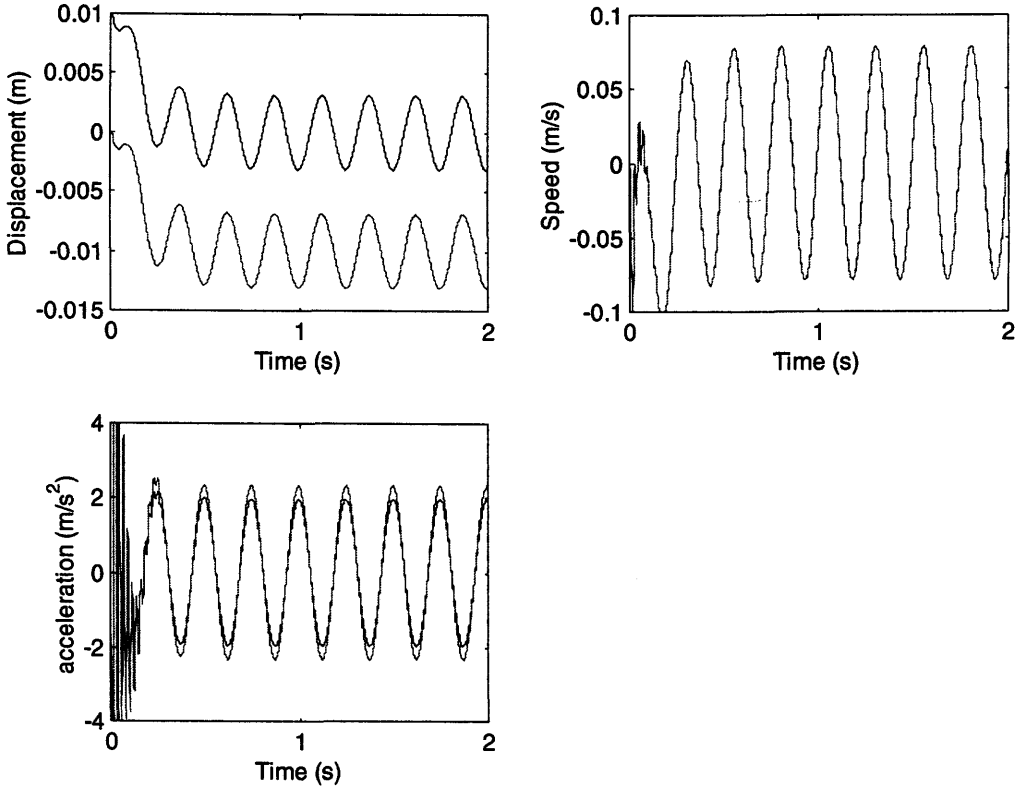

Figure 6.2: Estimating States Using the Kalman Filter for the Unobservable System Set Up of the Electrohydraulic Actuator (EHA)

The Extended Kalman Filter was next applied to the EHA in order to estimate the two key parameters of interest in this study namely, the effective bulk modulus and the viscous damping coefficient. Although inclusion of the two parameters in the augmented state vector made the system unobservable, it was deemed important to

determine if the same trend experienced with the more simple Mass-Spring-Damper system discussed in Appendix B, also applied here.

6.3 Parameter Estimation in the EHA

In Chapter 3, the Electrohydraulic Actuator (EHA) was described and a linearized model describing the hydraulic transfer function for the EHA (the plant) given by Equation 3.33, was derived. In order to apply the EKF to the EHA, a state space model of the hydraulic transfer function was required. The effective bulk modulus of the system, β_e, and the viscous friction coefficient, B, were to be estimated using the EKF. Usually, if two parameters are unknown, they are treated as states and the EKF can be used to estimate them simultaneously as explained in [Wright, 2001], [Cao, 2001] and [Zavarehi, 1997]. In simulation, the same input as in Section 6.1 was applied to the overall closed loop linearized transfer function for the EHA. The piston position was used as measurement for the EKF and the input to the EKF was the electric motor angular velocity (as a result of applying a desired piston position as the input to the overall closed loop EHA system).

A state space formulation resulting from Equation (3.33) for the EHA system is determined to be:

$$\dot{X}_1 = X_2 + w_1 \tag{6.8}$$

$$\dot{X}_2 = X_3 + w_2$$

$$\dot{X}_3 = -X_4 X_2\left(\frac{2A^2}{MV_0} + \frac{X_5 C_T}{MV_0}\right) - X_3\left(\frac{X_5}{M} + \frac{C_T X_4}{V_0}\right) + \omega_p X_4\left(\frac{2D_p A}{MV_0}\right) + w_3$$

$$\dot{X}_4 = w_4$$

$$\dot{X}_5 = w_5$$

$$Z = \begin{bmatrix} 1 & 0 & 0 & 0 & 0 \end{bmatrix} \begin{bmatrix} X_1 \\ X_2 \\ X_3 \\ X_4 \\ X_5 \end{bmatrix} + v_1$$

where X_1 is the state variable X; X_2 is the state variable $\dot{X}$; X_3 is the state variable $\ddot{X}$; X_4 is the effective bulk modulus; X_5 is the viscous friction coefficient; w_1, w_2, w_3, w_4, w_5 are the system noise elements; and v_1 is the measurement noise.

Using the forward difference approximation and applying it to the continuous state space model, the discrete state space model of the EHA is determined to be as follows:

$$X_1(k+1) = X_1(k) + T_s X_2(k) + T_s w_1(k) \tag{6.9}$$

$$X_2(k+1) = X_2(k) + T_s X_3(k) + T_s w_2(k)$$

$$X_3(k+1) = -X_2(k)T_s\left(\frac{2X_4(k)A^2}{MV_0} + \frac{X_5(k)X_4(k)C_T}{MV_0}\right) - X_3 T_s\left(\frac{X_5(k)}{M} + \frac{C_T X_4(k)}{V_0}\right) + X_3(k) + \frac{2D_p A T_s X_4(k)}{MV_0}\omega_p + T_s w_3(k)$$

$$X_4(k+1) = X_4(k) + T_s w_4(k)$$

$$X_5(k+1) = X_5(k) + T_s w_5(k)$$

The linearized system matrix can be written as follows:

$$\Phi(k) = \frac{\partial f(X(k))}{\partial X(k)} = \begin{bmatrix} \Phi_{11}(k) & \Phi_{12}(k) & \Phi_{13}(k) & \Phi_{14}(k) & \Phi_{15}(k) \\ \Phi_{21}(k) & \Phi_{22}(k) & \Phi_{23}(k) & \Phi_{24}(k) & \Phi_{25}(k) \\ \Phi_{31}(k) & \Phi_{32}(k) & \Phi_{33}(k) & \Phi_{34}(k) & \Phi_{35}(k) \\ \Phi_{41}(k) & \Phi_{42}(k) & \Phi_{43}(k) & \Phi_{44}(k) & \Phi_{45}(k) \\ \Phi_{51}(k) & \Phi_{52}(k) & \Phi_{53}(k) & \Phi_{54}(k) & \Phi_{55}(k) \end{bmatrix} \tag{6.10}$$

where

$$\Phi_{11}(k) = 1,\ \Phi_{12}(k) = T_s,\ \Phi_{13}(k) = 0,\ \Phi_{14}(k) = 0, \Phi_{15}(k) = 0$$

$$\Phi_{21}(k) = 0,\ \Phi_{22}(k) = 1,\ \Phi_{23}(k) = T_s,\ \Phi_{24}(k) = 0, \Phi_{25}(k) = 0$$

$$\Phi_{31}(k) = 0,\ \Phi_{32}(k) = \frac{-2A^2 T_s X_4(k)}{MV_0} - \frac{X_5(k)X_4(k)C_T}{MV_0}$$

$$\Phi_{33}(k) = 1 - T_s\left(\frac{X_5(k)}{M} + \frac{C_T X_4(k)}{V_0}\right)$$

$$\Phi_{34}(k) = -\frac{2A^2 T_s X_2(k)}{MV_0} - \frac{X_5(k) C_T X_2(k) T_s}{MV_0} - \frac{X_3(k) T_s C_T}{V_0} + \frac{2D_p A T_s \omega_p}{MV_0}$$

$$\Phi_{35}(k) = \frac{-X_3(k) T_s}{M} - \frac{X_2(k) T_s X_4(k) C_T}{MV_0}$$

$$\Phi_{41}(k) = 0,\ \Phi_{42}(k) = 0,\ \Phi_{43}(k) = 0,\ \Phi_{44}(k) = 1.\ \Phi_{45}(k) = 0$$

$$\Phi_{51}(k) = 0,\ \Phi_{52}(k) = 0,\ \Phi_{53}(k) = 0,\ \Phi_{54}(k) = 0.\ \Phi_{55}(k) = 1.$$

The simulated values for the effective bulk modulus and for the viscous friction coefficient were 2.1×10^8 Pa and 760 Ns/m respectively. The system described by Equation (6.9) was found not to be observable and the observability matrix was calculated at each iteration. The observability matrix using the linearized system matrix given by Equation 6.10 was determined to be:

$$\textit{Observability Matrix} = \begin{bmatrix} H \\ H\Phi \\ H(\Phi)^2 \\ H(\Phi)^3 \\ H(\Phi)^4 \end{bmatrix}, \text{ and } H = \begin{bmatrix} 1 & 0 & 0 & 0 & 0 \end{bmatrix} \tag{6.11}$$

The rank of the observability matrix was found to be 4, compared to the length of the state matrix of 5, and therefore it was confirmed that the system was not observable. The Extended Kalman Filter was applied to this system and two parameters were estimated, as shown in Figure 6.3.

The initial state vector and the initializing matrices for the EKF were set as:

$$X(0) = \begin{bmatrix} 0 & 0 & 0 & 0 & 0 \end{bmatrix} \tag{6.12}$$

$$P(0) = \begin{bmatrix} 1\times10^{1} & 0 & 0 & 0 & 0 \\ 0 & 1\times10^{1} & 0 & 0 & 0 \\ 0 & 0 & 1\times10^{3} & 0 & 0 \\ 0 & 0 & 0 & 1\times10^{20} & 0 \\ 0 & 0 & 0 & 0 & 1\times10^{8} \end{bmatrix}, \quad R(k) = 1\times10^{-9} \tag{6.13}$$

$$Q(k)=\begin{bmatrix} 1\times10^{-12} & 0 & 0 & 0 & 0 \\ 0 & 1\times10^{-6} & 0 & 0 & 0 \\ 0 & 0 & 1\times10^{-5} & 0 & 0 \\ 0 & 0 & 0 & 1\times10^{-8} & 0 \\ 0 & 0 & 0 & 0 & 1\times10^{-9} \end{bmatrix}$$

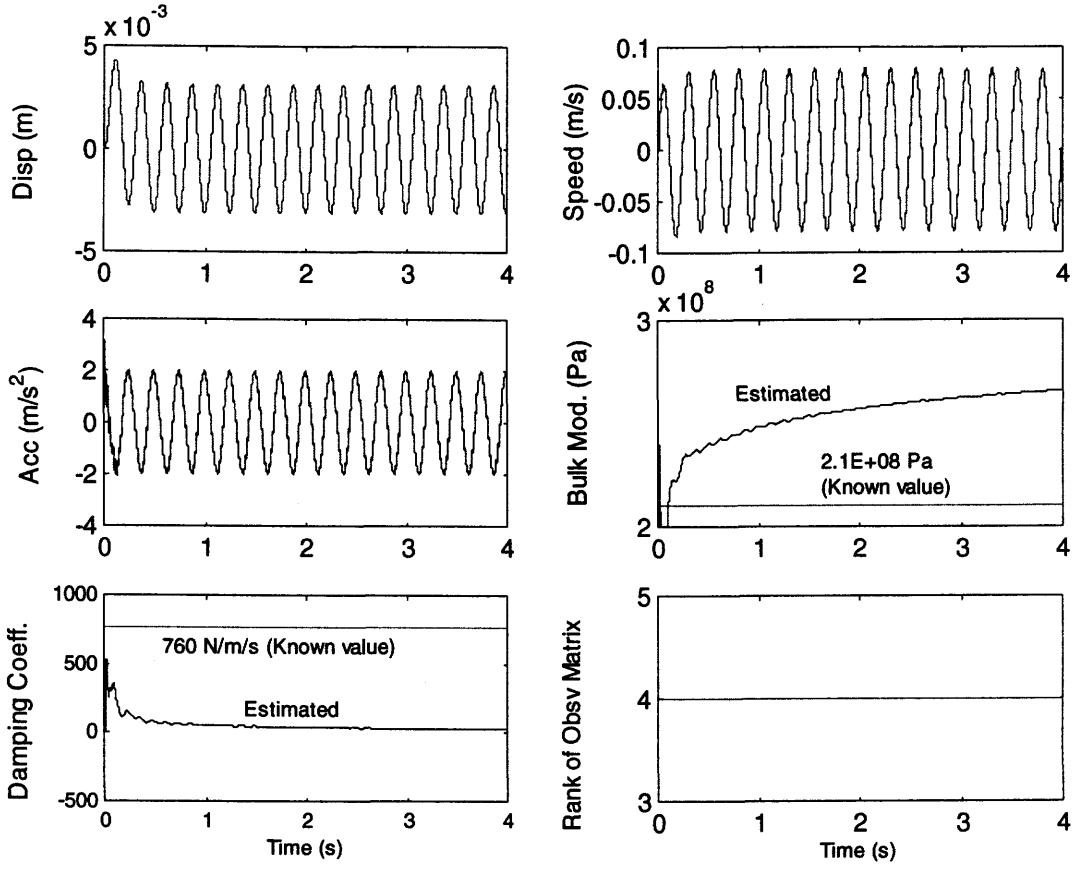

Figure 6.3: Applying the EKF to the EHA Model to Estimate Two Parameters

It can be seen from Figure 6.3 that the parameters do not converge to their known values but do converge to some constant value. The states are estimated accurately, with no visible difference between the estimated and simulated position, velocity and acceleration.

Next, the number of measurements was increased and all the states (position, velocity and acceleration) used as measurements. This was done to try making the system observable and to help the EKF estimate the effective bulk modulus and the

viscous damping coefficient. But the system remained unobservable in spite of increasing the number of measurements. The rank was still 4 and the length of the state vector 5. To demonstrate the effects of the EKF to this particular unobservable configuration, the EKF was applied to the model with increased measured states. The measurement matrix for this case when three states were used as measurements is:

$$Z = \begin{bmatrix} 1 & 0 & 0 & 0 & 0 \\ 0 & 1 & 0 & 0 & 0 \\ 0 & 0 & 1 & 0 & 0 \end{bmatrix} \begin{bmatrix} X_1 \\ X_2 \\ X_3 \\ X_4 \\ X_5 \end{bmatrix} + \begin{bmatrix} v_1 \\ v_2 \\ v_3 \end{bmatrix} \tag{6.14}$$

The measurement noise covariance matrix was set as follows:

$$R(k) = \begin{bmatrix} 1\times10^{-12} & 0 & 0 \\ 0 & 1\times10^{-6} & 0 \\ 0 & 0 & 1\times10^{-5} \end{bmatrix} \tag{6.15}$$

The estimated and simulated states which are piston position, velocity and acceleration are depicted in Figure 6.4. These are superimposed plots and it can be seen that they match very closely. The two parameters of interests, which are the effective bulk modulus and the viscous friction coefficient, are estimated and the results are depicted in Figure 6.4. It can be observed that the estimated parameters do not match the known simulated values but do converge to some steady state values. The simulated values for the effective bulk modulus and for the viscous friction coefficient are known to be 2.1×10^{8} Pa and 760 Ns/m respectively. After 20,000 iterations, the estimated effective bulk modulus is 2.44×10^{8} Pa and the estimated viscous friction coefficient is 871 Ns/m. The estimation errors for the effective bulk modulus are 16.2% and for the viscous damping coefficient, 14.6%. The estimated parameters do not converge to their known values but to some other values, indicating a local minima solution by virtue of the Kalman Filter optimality condition.

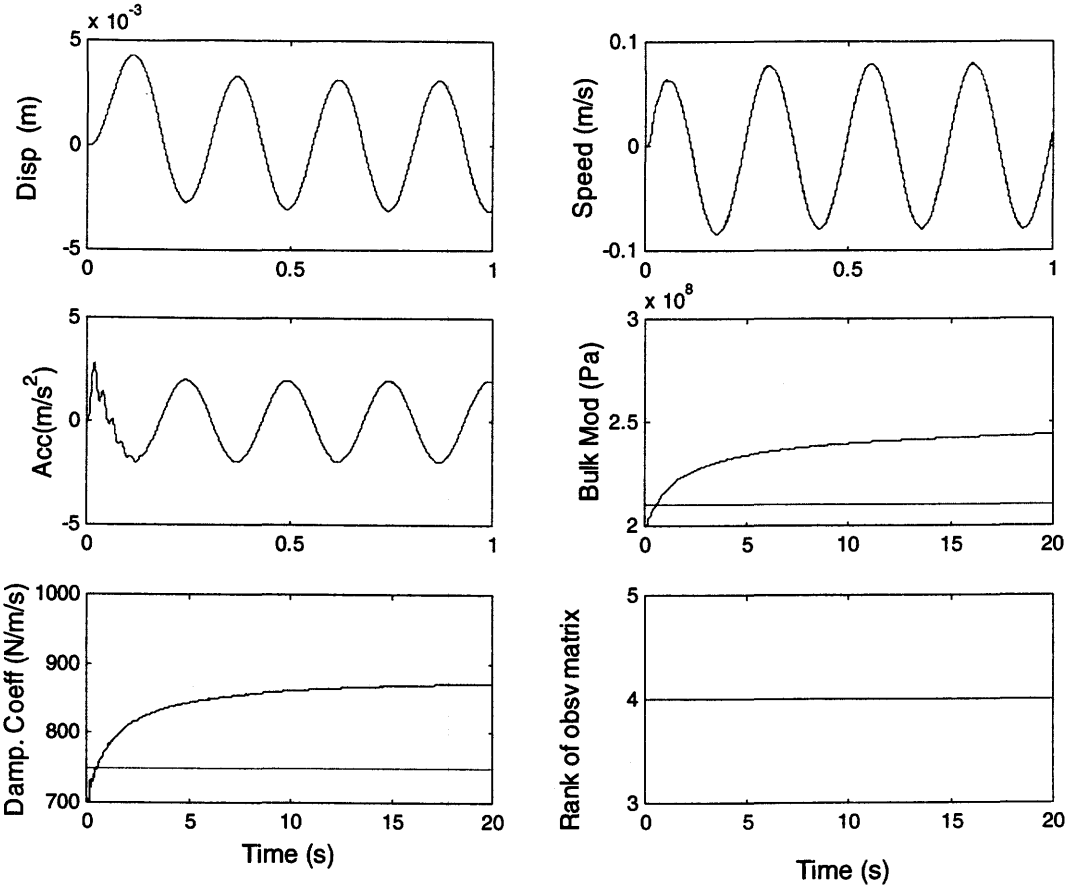

Figure 6.4: Estimated Effective Bulk Modulus and Viscous Damping Coefficient Using Simulated Model of EHA and Position, Velocity and Acceleration as Measurements

Also shown in Figure 6.4 is the rank of the observability matrix at each iteration and it is seen that the system remained unobservable, with the rank of the observability matrix being 4, compared to the state length of 5.

For the above-mentioned case, keeping all conditions the same (initial matrices for the EKF and input signal), the parameters used in the simulated model were changed. This was done in order to investigate whether the EKF could detect the changes and estimate them accurately. For condition monitoring, it is not the absolute value of the parameter that is of concern but the change from some normal value. Thus, even though the estimates are not accurate, the changes in an independent manner are of value. The estimated values for various bulk modulus and damping coefficient values are shown in Table 6.6.

Table 6.6: EKF Predictions when the Parameters were Changed

Simulated Effective Bulk Modulus Pa	Simulated Viscous Damping Coefficient Ns/m	Estimated Effective Bulk Modulus Pa	Estimated Viscous Damping Coefficient Ns/m	Error : Effective Bulk Modulus (%)	Error: Viscous Damping Coefficient (%)
2.1×10^{8}	3800	1.67×10^{8}	3039	20.5	20
2.1×10^{8}	1520	2.152×10^{8}	1554	2.4	2.18
2.1×10^{8}	2280	1.95×10^{8}	2124	7	7
2.1×10^{8}	3040	1.79×10^{8}	2611	14	14
1.05×10^{8}	760	1.11×10^{8}	797	5.43	4.87
2.1×10^{7}	760	2.06×10^{7}	749	1.91	1.45
1.68×10^{8}	760	1.86×10^{8}	835	10.7	9.87
1.47×10^{8}	760	1.6×10^{8}	822	8.98	8.16

From Table 6.6, it is seen that the EKF is able to detect changes in the parameters when other parameters are held constant. But the accuracy of the estimations is poor. Also, changes in one simulated parameter (when the other simulated parameter was kept unchanged) resulted in changes in the estimated value of the other parameter. This is not desirable in a condition monitoring scheme. It appears that the EKF has difficulty in differentiating between the two parameters even when using the three measurements, as confirmed by the lack of observability condition.

Next, the effective bulk modulus and the viscous damping coefficient were once again estimated in simulation but this time a higher frequency input signal was used to excite the system. In Section 6.4.1, a sensitivity study is described and it will be shown that a higher frequency input signal is more suited for estimation of the effective bulk modulus. In this particular scenario, the input signal used to estimate the two parameters was a sinusoid, with a frequency of 25 Hz and amplitude of 0.005 m (as compared to a sinusoid of 4 Hz and amplitude of 0.01 m). The EKF used the simulated pump angular

velocity as its input and the simulated actuator piston position as its measurement. The system remained unobservable, as expected, when the effective bulk modulus and the viscous friction were expressed as states and one measurement (position) being used to estimate them. The EKF was applied to the system and the resulting estimated states and parameters are shown in Figure 6.5. It can be seen that the simulated and estimated states showed good agreement and that the two estimated parameters converge to their known values. The estimated effective bulk modulus is 2.09×10^8 Pa (estimation error of 0.5%) and the estimated viscous damping coefficient is 758 Ns/m (estimation error of 0.26%).

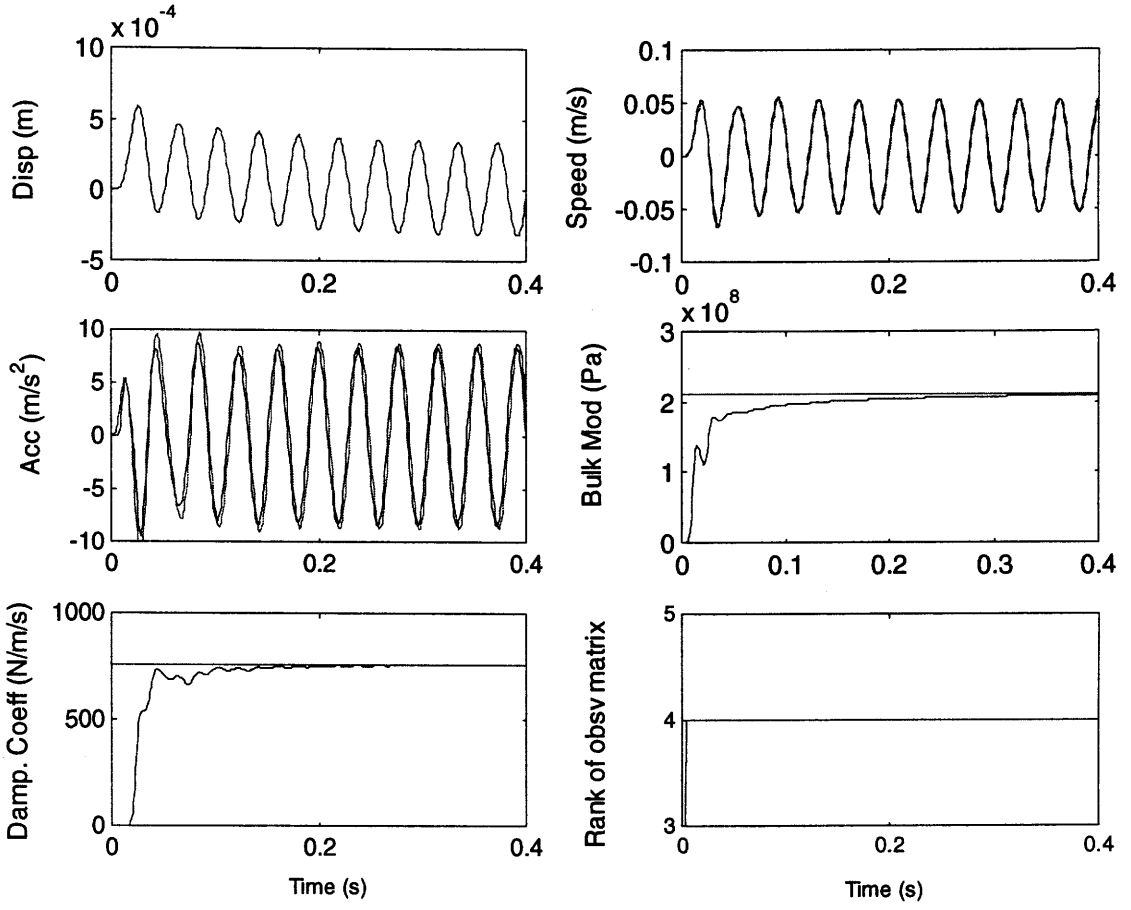

Figure 6.5: Estimated Effective Bulk Modulus and Viscous Damping Coefficient Using Simulated Model of EHA (High Frequency Input) and Position as Measurement

The initial state vector and the initializing matrices for the EKF were set as:

$$X(0)=[0 \quad 0 \quad 0 \quad 0 \quad 0] \tag{6.16}$$

$$P(0)=\begin{bmatrix} 1\times10^{1} & 0 & 0 & 0 & 0 \\ 0 & 1\times10^{1} & 0 & 0 & 0 \\ 0 & 0 & 1\times10^{3} & 0 & 0 \\ 0 & 0 & 0 & 1\times10^{20} & 0 \\ 0 & 0 & 0 & 0 & 1\times10^{9} \end{bmatrix}, \quad R(k)=1\times10^{-12}$$

$$Q(k)=\begin{bmatrix} 1\times10^{-7} & 0 & 0 & 0 & 0 \\ 0 & 1\times10^{-1} & 0 & 0 & 0 \\ 0 & 0 & 1\times10^{-2} & 0 & 0 \\ 0 & 0 & 0 & 0 & 0 \\ 0 & 0 & 0 & 0 & 0 \end{bmatrix}$$

From Figure 6.5 alone, one might conclude that the estimation of the effective bulk modulus and of the viscous friction coefficients are improved when the input signal is of higher frequency and that a more effective indicator for observability condition could be a frequency sensitive function. However, when the parameters were changed and the EKF used to estimate their values, as shown in Table 6.7, the changes in the parameter were detected but the accuracy of the estimations for the other parameter (whose value was kept unchanged) was poor, and in fact changed when they should have remained constant.

From the results of Table 6.6 and 6.7, it appears that if the strategy of estimating both parameters at the same time from one model is used, there will have to be a look up table which shows the changes in one parameter with respect to the other. This approach is not considered to be practical and is believed not to be very reliable. This does not exclude the use of neural networks to train for the various conditions but this is believed to be beyond the scope of this study.

Table 6.7: EKF Predictions when the Parameters were Changed (After 4000 iterations) when Using a Higher Frequency Input Signal (Position as measurement)

Simulated Effective Bulk Modulus Pa	**Simulated Viscous Damping Coefficient Ns/m**	**Estimated Effective Bulk Modulus Pa**	**Estimated Viscous Damping Coefficient Ns/m**	**Error : Effective Bulk Modulus (%)**	**Error: Viscous Damping Coefficient (%)**
2.1×10^{8}	3800	2.08×10^{8}	3963	0.95	4.29
2.1×10^{8}	1520	2.21×10^{8}	1584	5.23	4.21
2.1×10^{8}	2280	2.25×10^{8}	2437	7.14	6.89
2.1×10^{8}	3040	2.19×10^{8}	3255	4.29	7.07
1.05×10^{8}	760	1.09×10^{8}	1186	3.81	56
2.1×10^{7}	760	2.1005×10^{7}	1311	0.024	72.5
1.68×10^{8}	760	1.725×10^{8}	929	2.68	22.2
1.47×10^{8}	760	1.51×10^{8}	1014	2.72	33.4

6.3.1 Discussions

From the simulation study done on the more complex Electrohydraulic System it is seen that the EKF did estimate some values for the two parameters of interest, with substantial errors (14-18%) when the low frequency signal was used. The EKF estimated the two parameters more accurately when a higher frequency signal was used (estimation error less than 1%). This result is similar to the Mass-Spring-Damper example where the EKF was used to estimate two parameters in spite of the system not being observable. In both examples, position was used as the only measurement and the unobservability was due to an augmentation of their state matrices with the parameters to be estimated.

In the Mass-Spring-Damper example, changes in the spring constant and the viscous damping coefficient were accurately estimated by the EKF independent of changes in the other parameter. However for the EHA system, the EKF (although being able to detect changes in the simulated parameters) was not able to estimate their values accurately and the error was not constant when the other parameter was changed. The observability condition did not seem to affect the "detectability" of the EKF when applied to the EHA for multiple parameter estimation, but appeared to affect its "differentiability" between the two parameters. "*Observability implies detectability but the converse is not true and as such the observability condition is a stronger condition*", as reported in [Kamen et al, 1999]. The EKF will be able to differentiate between the two parameters if an observable system was used for parameter estimation.

From the Mass-Spring-Damper system and the EHA examples, it can be concluded that the importance of the observability condition for EKF was dependent on the system. The accuracy "situation" of the estimated parameters (as well as "detectability" and "differentiability") did not surface for the simple Mass-Spring-Damper system example. It is worth mentioning that the EHA system is a Type 1 system, unlike the Mass-Spring-Damper system which is a Type 0 system.

It is also believed that as the complexity of the system increases, this concept of observability will become more important for accurate parameter estimation. In the examples used in this study to illustrate observability, the states are "direct derivatives" i.e position, velocity and acceleration. As such, the use of position as the only measurement makes the system observable in all cases and by inspection of the state space models for each system, it is seen that if position is known (either measured or estimated), velocity or acceleration can be estimated. In more complex hydraulic systems, states are not restricted to direct derivatives but can include pressure, flow or temperature for example. This concept of observability is believed to be even more important for more complex system involving numerous states.

Hence, it is believed that the lack of full observability in the case of the EHA is preventing the EKF from successfully estimating the parameters and changes in them.

A more effective method for estimating both parameters in the EHA needs to be examined and indeed one such approach is presented in the next section: that is, estimating one parameter from one model and using the known parameter value to estimate the second one from a second model. This will reduce the number of states and will result in a higher probability of making the state space reformulation of the problem observable (as compared to including all the parameters to be estimated as states and attempting to estimate them simultaneously).

In summary, from the simple Mass-Spring-Damper system and the more complex EHA system example, it can be observed that parameter estimation is possible when the systems are unobservable but the approach in the case of the EHA, is not reliable and acceptable. Reliable fault detection requires changes in the parameters to be detected and preferably accurately estimated. Thus a different approach is needed for the EHA as described in the following section.

6.4 Estimating the Effective Bulk Modulus in the EHA

It is assumed that the viscous damping coefficient is known, and the effective bulk modulus of the system β_e is to be estimated. Using the hydraulic transfer function of the EHA, the following equation can be written:

$$\dddot{X} + \ddot{X}\left(\frac{B}{M} + \frac{C_T\beta_e}{V_0}\right) + \dot{X}\left(\frac{2\beta_e A^2}{MV_0} + \frac{B\beta_e C_T}{MV_0}\right) = \omega_p\left(\frac{2D_p\beta_e A}{MV_0}\right) \tag{6.17}$$

A state space formulation of the EHA system can be determined as follows:

$$\dot{X}_1 = X_2 + w_1 \tag{6.18}$$

$$\dot{X}_2 = X_3 + w_2$$

$$\dot{X}_3 = -X_4X_2\left(\frac{2A^2}{MV_0} + \frac{BC_T}{MV_0}\right) - X_3\left(\frac{B}{M} + \frac{C_TX_4}{V_0}\right) + \omega_pX_4\left(\frac{2D_pA}{MV_0}\right) + w_3$$

$$\dot{X}_4 = w_4$$

$$Z = \begin{bmatrix} 1 & 0 & 0 & 0 \\ 0 & 1 & 0 & 0 \end{bmatrix}\begin{bmatrix} X_1 \\ X_2 \end{bmatrix} + \begin{bmatrix} v_1 \\ v_2 \end{bmatrix}$$

where X_1 is the state variable X, X_2 the state variable $\dot{X}$, X_3 the state variable $\ddot{X}$, X_4 the effective bulk modulus, w_1, w_2, w_3, w_4 the system noise and v_1, v_2 the measurement noise. The piston position and velocity were used as measurement for the EKF and the input was the electric motor angular velocity.

The discrete state space model of the EHA is determined to be as follows:

$$X_1(k+1) = X_1(k) + T_s X_2(k) + T_s w_1(k) \tag{6.19}$$

$$X_2(k+1) = X_2(k) + T_s X_3(k) + T_s w_2(k)$$

$$X_3(k+1) = -X_2(k)T_s\left(\frac{2X_4(k)A^2}{MV_0} + \frac{BX_4(k)C_T}{MV_0}\right) - X_3 T_s\left(\frac{B}{M} + \frac{C_T X_4(k)}{V_0}\right) + X_3(k) + \frac{2D_p A T_s X_4(k)}{MV_0}\omega_p + T_s w_2(k)$$

$$X_4(k+1) = X_4(k) + T_s w_4(k)$$

The linearized system matrix can be written as:

$$\Phi(k) = \frac{\partial f(X(k))}{\partial X(k)} = \begin{bmatrix} \Phi_{11}(k) & \Phi_{12}(k) & \Phi_{13}(k) & \Phi_{14}(k) \\ \Phi_{21}(k) & \Phi_{22}(k) & \Phi_{23}(k) & \Phi_{24}(k) \\ \Phi_{31}(k) & \Phi_{32}(k) & \Phi_{33}(k) & \Phi_{34}(k) \\ \Phi_{41}(k) & \Phi_{42}(k) & \Phi_{43}(k) & \Phi_{44}(k) \end{bmatrix} \tag{6.20}$$

where

$$\Phi_{11}(k) = 1,\ \Phi_{12}(k) = T_s,\ \Phi_{13}(k) = 0,\ \Phi_{14}(k) = 0.\Phi_{21}(k) = 0,\ \Phi_{22}(k) = 1,\ \Phi_{23}(k) = T_s,$$

$$\Phi_{24}(k) = 0.\Phi_{31}(k) = 0,\ \Phi_{32}(k) = \frac{-2A^2 T_s X_4(k)}{MV_0} - \frac{BX_4(k)C_T}{MV_0}$$

$$\Phi_{33}(k) = 1 - T_s\left(\frac{B}{M} + \frac{C_T X_4(k)}{V_0}\right)$$

$$\Phi_{34}(k) = -\frac{2A^2 T_s X_2(k)}{MV_0} - \frac{BC_T X_2(k)T_s}{MV_0} - \frac{X_3(k)T_s C_T}{V_0} + \frac{2D_p A T_s \omega_p}{MV_0}$$

$$\Phi_{41}(k) = 0,\ \Phi_{42}(k) = 0,\ \Phi_{43}(k) = 0,\ \Phi_{44}(k) = 1.$$

For this case, the length of the state matrix and the rank of the observability matrix were equal to 4; therefore the state space model was observable. The simulated

piston position and velocity were used as measurements in order to make the system observable.

Using the EHA linearized model (the plant), the system was simulated using Simulink/Matlab®. The input to the closed loop system was similar to section 6.2. The state estimations (displacement, velocity and acceleration) and the estimated effective bulk modulus are shown in Figure 6.6, which also shows the rank of the observability matrix at each iteration The measurements for the EKF are simulated piston position and velocity and the input to the EKF is electric motor speed. Three states (displacement, velocity and acceleration) and effective bulk modulus are estimated by the EKF. In simulation, it was found that the EKF estimated the states and parameter accurately when compared to the simulated states and parameter value, as shown in Figure 6.6, which is a plot of the superimposed simulated and estimated states. Also, the estimated effective bulk modulus was 2.106×10^{8} Pa, when a simulated value of 2.1×10^{8} Pa was used (showing 0.29% error).

The initial state vector and the initializing matrices for the EKF were set as follows:

$$X(0)=\begin{bmatrix}0 & 0 & 0 & 0\end{bmatrix}^{T} \qquad R(k)=\begin{bmatrix}1\times10^{-12} & 0\\ 0 & 1\times10^{-6}\end{bmatrix} \tag{6.21}$$

$$P(0)=\begin{bmatrix}1\times10^{19} & 0 & 0 & 0\\ 0 & 1\times10^{19} & 0 & 0\\ 0 & 0 & 1\times10^{19} & 0\\ 0 & 0 & 0 & 1\times10^{19}\end{bmatrix}$$

$$Q(k)=\begin{bmatrix}1\times10^{-12} & 0 & 0 & 0\\ 0 & 1\times10^{-9} & 0 & 0\\ 0 & 0 & 1\times10^{-4} & 0\\ 0 & 0 & 0 & 1\times10^{-8}\end{bmatrix}$$

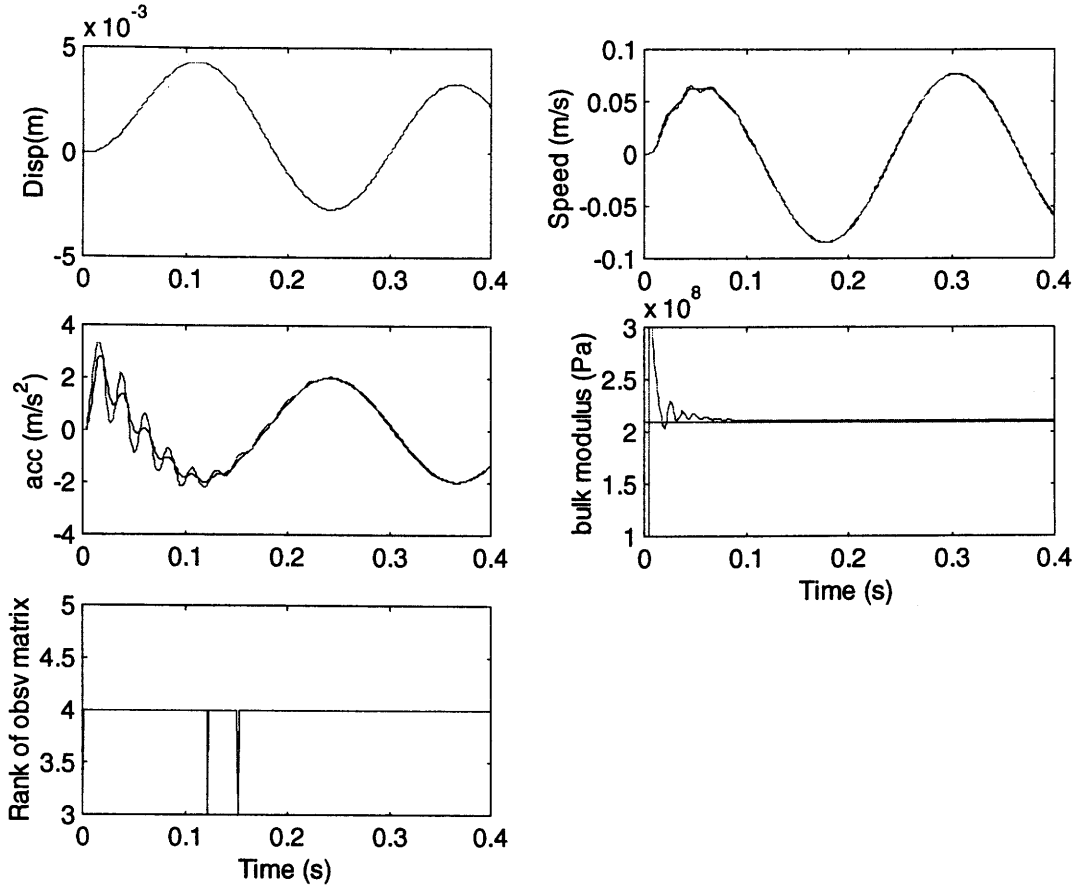

Figure 6.6: Estimation of the Effective Bulk Modulus in the EHA in Simulation Using Piston Position and Velocity as Measurements.

The effective bulk modulus for the EHA model was next changed in simulation and the EKF was used to estimate the new values for this parameter, as given in Table 6.3, which shows the estimated effective bulk modulus, when their values in the EHA "Matlab/Simulink®" model were changed in steps of 10 %.

It is seen that changes are detected but the accuracy of the estimated values for a simulated system with a higher effective bulk modulus value is of concern. When the simulated effective bulk modulus was 4.2×10^{8} Pa, the estimation error was as large as 9.05 %, as shown in Table 6.8.

Table 6.8: Estimated Effective Bulk Modulus Value in Simulation

Simulated β_e (Pa)	Estimated β_e (Pa)	% Error in estimation
2.1×10^8	2.106×10^8	0.29 %
1.89×10^8	1.88×10^8	0.53 %
1.68×10^8	1.67×10^8	0.59 %
1.47×10^8	1.45×10^8	1.36 %
1.26×10^8	1.24×10^8	1.59 %
1.05×10^8	1.04×10^8	0.95 %
8.4×10^7	8.29×10^7	1.31 %
6.3×10^7	6.22×10^7	1.27 %
4.2×10^7	4.14×10^7	1.43 %
2.1×10^7	2.07×10^7	1.43 %
2.31×10^8	2.33×10^8	0.87 %
2.52×10^8	2.57×10^8	1.98 %
2.73×10^8	2.81×10^8	2.93 %
2.94×10^8	3.06×10^8	4.08 %
3.15×10^8	3.32×10^8	5.4 %
3.36×10^8	3.57×10^8	6.25 %
3.57×10^8	3.83×10^8	7.29 %
3.78×10^8	4.08×10^8	7.9 %
3.99×10^8	4.33×10^8	8.52 %
4.2×10^8	4.58×10^8	9.05 %

The effective bulk modulus is known to have most influence on the natural frequency of the system. Thus, it can be expected that the effect of changes in the effective bulk modulus might be expected to be more readily detected by the EKF at higher frequencies, indeed at frequencies approaching the natural frequency of the system (approximately 25 Hz). Thus a more appropriate input signal might be a

sinusoid at a higher frequency (higher than the 4 Hz signal used). This is verified by the sensitivity study described in the next section.

6.4.1 Sensitivity of the Effective Bulk Modulus

Sensitivity is the change in system performance as a result of system parameter variations and it is measured by the ratio of the percentage change in system transfer function to the percentage change in system parameter. Thus for a given parameter, b, in the transfer function, $T(s)$, sensitivity is given by Equation (6.22). Also, since sensitivity is a function of Laplace variable, it varies with frequency and in this study, the sensitivity for the effective bulk modulus is required.

$$S_b^T = \frac{\partial T(s)}{\partial b}\frac{b}{T(s)} \tag{6.22}$$

The hydraulic transfer function was given by Equation (3.33)

$$\frac{x(s)}{\omega_p(s)} = \frac{\dfrac{2D_p\beta_e A}{MV_o}}{s^3 + s^2\left(\dfrac{B}{M} + \dfrac{C_T\beta_e}{V_0}\right) + s\left(\dfrac{2\beta_e A^2}{MV_o} + \dfrac{B\beta_e C_T}{MV_0}\right)} \tag{3.33}$$

Let $X = \dfrac{2D_p A}{MV_0}$, $Y = \dfrac{C_T}{V_0}$, $Z = \dfrac{2A^2}{MV_0}$, $P = \dfrac{B}{M}$ and $Q = \dfrac{BC_T}{MV_0}$, β_e being the parameter of interest.

The transfer function given by Equation (3.33) can be rewritten as:

$$\frac{x(s)}{\omega_p(s)} = T(s) = \frac{X\beta_e}{s^3 + s^2(P + Y\beta_e) + s(Z\beta_e + Q\beta_e)} \tag{6.23}$$

Using equation (6.21), the sensitivity function is:

$$S_{\beta_e}^T = \frac{\partial T(s)}{\partial \beta_e}\frac{\beta_e}{T(s)}$$

where

$$\frac{\partial T(s)}{\partial \beta_e} = \frac{(s^3 + s^2(P + Y\beta_e) + s(Z\beta_e + Q\beta_e))X - X\beta_e(Ys^2 + Zs + Qs)}{(s^3 + s^2(P + Y\beta_e) + s(Z\beta_e + Q\beta_e))^2} \tag{6.24}$$

which can be simplified to:

$$\frac{\partial T(s)}{\partial \beta_e} = \frac{Xs^3 + s^2 PX}{(s^3 + s^2(P + Y\beta_e) + s(Z\beta_e + Q\beta_e))^2} \tag{6.25}$$

$$S_{\beta_e}^T = \frac{Xs^3 + s^2 PX}{(s^3 + s^2(P + Y\beta_e) + s(Z\beta_e + Q\beta_e))^2} \times \frac{\beta_e}{\frac{X\beta_e}{s^3 + s^2(P + Y\beta_e) + s(Z\beta_e + Q\beta_e)}} \tag{6.26}$$

After simplification, the sensitivity function is determined to be:

$$S_{\beta_e}^T = \frac{s^2 + s\ P}{s^2 + s\ (P + Y\beta_e) + (Z\beta_e + Q\beta_e)}, \tag{6.27}$$

or:

$$S_{\beta_e}^T = \frac{s^2 + s\frac{B}{M}}{s^2 + s(\frac{B}{M} + \frac{C_T\beta_e}{V}) + \frac{2A^2\beta_e}{MV} + \frac{BC_T\beta_e}{MV}} \tag{6.28}$$

The Bode plot of the sensitivity function $S_{\beta_e}^T$ given by Equation (6.28) is depicted in Figure 6.7. It is seen that the effect of β_e on the sensitivity function reaches a peak at higher frequencies which implies that changes in β_e has a more profound influence on the output of the transfer function at frequencies approaching the system damped natural frequency. Thus estimation of the effective bulk modulus and subsequent detection of changes in this parameter would be more likely to occur using a higher frequency input than the one used previously. A 25 Hz signal was selected. A higher frequency than 25 Hz was not used because of the over-current protection mechanism in the EHA prototype, which caused the electric motor to shut down.

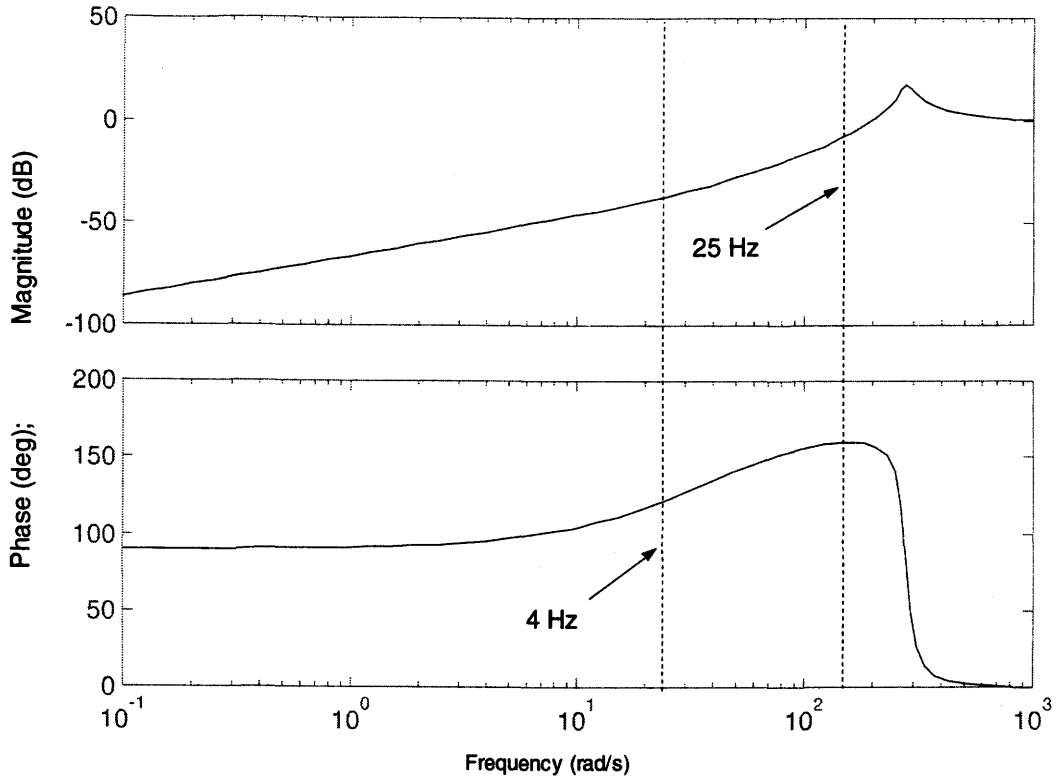

Figure 6.7: Bode Plot of Sensitivity for Effective Bulk Modulus in the EHA.

6.4.2 Estimating the Effective Bulk Modulus (Higher Frequency Input)

From the previous section, it was postulated that a 25 Hz signal would be more appropriate for exciting the system in order to enable the effective bulk modulus prediction from the system measurements. The EKF was used to estimate the effective bulk modulus using a 25 Hz signal input in the simulation. The estimated states (position, velocity and acceleration) and the estimated effective bulk modulus are shown in Figure 6.8.

The input signal was applied to the closed loop EHA linear model (plant) and it had an amplitude of 5 mm and of duration of 0.4 s. The duration for the input signal was short because convergence of this parameter to its desired value was very fast, and occurred within the 0.4 s duration. Also, the amplitude of the input was kept small because the actual EHA prototype had a maximum current protection mechanism

(thermal protection). The value of the estimated bulk modulus was 2.12×10^{8} Pa (known simulated value was 2.1×10^{8} Pa) and the estimation error for the effective bulk modulus was 0.95%.

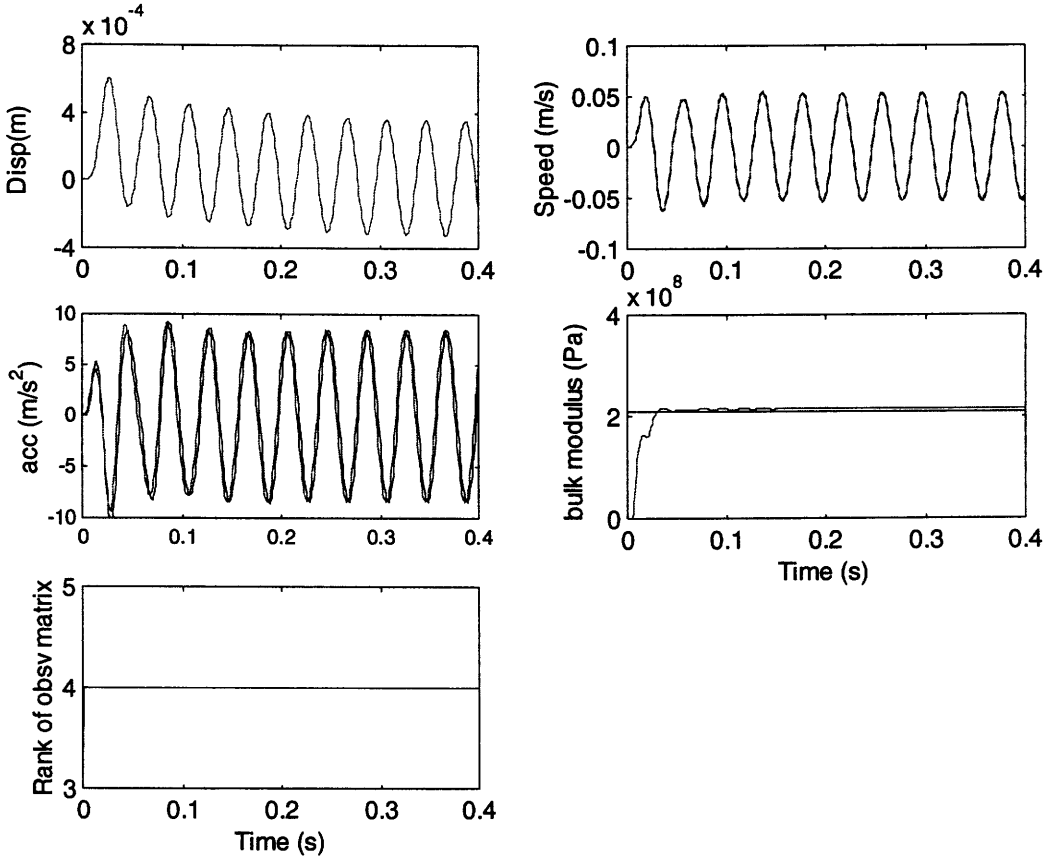

Figure 6.8: Effective Bulk Modulus Estimation Using 25 Hz Input Signal (Position and Velocity as Measurements)

The initial state vector and the initializing matrices for the EKF code when the higher frequency input signal (25 Hz) was used, were set as:

$$X(0) = \begin{bmatrix} 0 & 0 & 0 & 0 \end{bmatrix}^T \tag{6.29}$$

$$R(k) = \begin{bmatrix} 1\times10^{-12} & 0 \\ 0 & 1\times10^{-3} \end{bmatrix}$$

$$P(0) = \begin{bmatrix} 1\times10^{9} & 0 & 0 & 0 \\ 0 & 1\times10^{9} & 0 & 0 \\ 0 & 0 & 1\times10^{19} & 0 \\ 0 & 0 & 0 & 1\times10^{19} \end{bmatrix}$$

$$Q(k) = \begin{bmatrix} 1\times10^{-12} & 0 & 0 & 0 \\ 0 & 1\times10^{-3} & 0 & 0 \\ 0 & 0 & 1\times10^{-9} & 0 \\ 0 & 0 & 0 & 1\times10^{-8} \end{bmatrix}$$

The values of the effective bulk modulus were changed and the EKF was used to detect the changes. The results are presented in Table 6.9. It is seen that compared to the 4 Hz input signal, the accuracy in the prediction the effective bulk modulus is improved for higher bulk modulus values. The maximum error between the estimated and the simulated parameter is less than 5% as compared to a 10% when a 4 Hz signal is used.

The effect (if any) of using different starting values for the initial effective bulk modulus in the EKF code was investigated. Initially, no a priori information about the effective bulk modulus value was assumed. The procedure for estimating the effective bulk modulus in simulation was repeated but this time using a different starting value (for the initial effective bulk modulus) in the EKF algorithm.

The initial values used in the different trials are illustrated in Figure 6.9. It is evident from this figure that the estimated effective bulk modulus always matched the value used in the simulated model, within a small steady state error band. Also, the estimated states matched the simulated ones closely (not shown).

Table 6.9: Estimated Effective Bulk Modulus Value in Simulation Using 25 Hz Input

Simulated β_e (Pa)	Estimated β_e (Pa)	% Error in estimation
2.1×10^8	2.12×10^8	0.95 %
1.89×10^8	1.91×10^8	1.06 %
1.68×10^8	1.7×10^8	1.19 %
1.47×10^8	1.49×10^8	1.36 %
1.26×10^8	1.27×10^8	0.79 %
1.05×10^8	1.055×10^8	0.48%
8.4×10^7	8.37×10^7	0.36 %
6.3×10^7	6.25×10^7	0.79 %
4.2×10^7	4.12×10^7	1.9 %
2.1×10^7	2.06×10^7	1.9 %
2.31×10^8	2.37×10^8	2.6 %
2.52×10^8	2.58×10^8	2.38 %
2.73×10^8	2.79×10^8	2.2 %
2.94×10^8	2.99×10^8	1.7 %
3.15×10^8	3.19×10^8	1.27 %
3.36×10^8	3.38×10^8	0.59 %
3.57×10^8	3.56×10^8	0.28 %
3.78×10^8	3.72×10^8	1.59 %
3.99×10^8	3.88×10^8	2.76 %
4.2×10^8	4.03×10^8	4.05 %

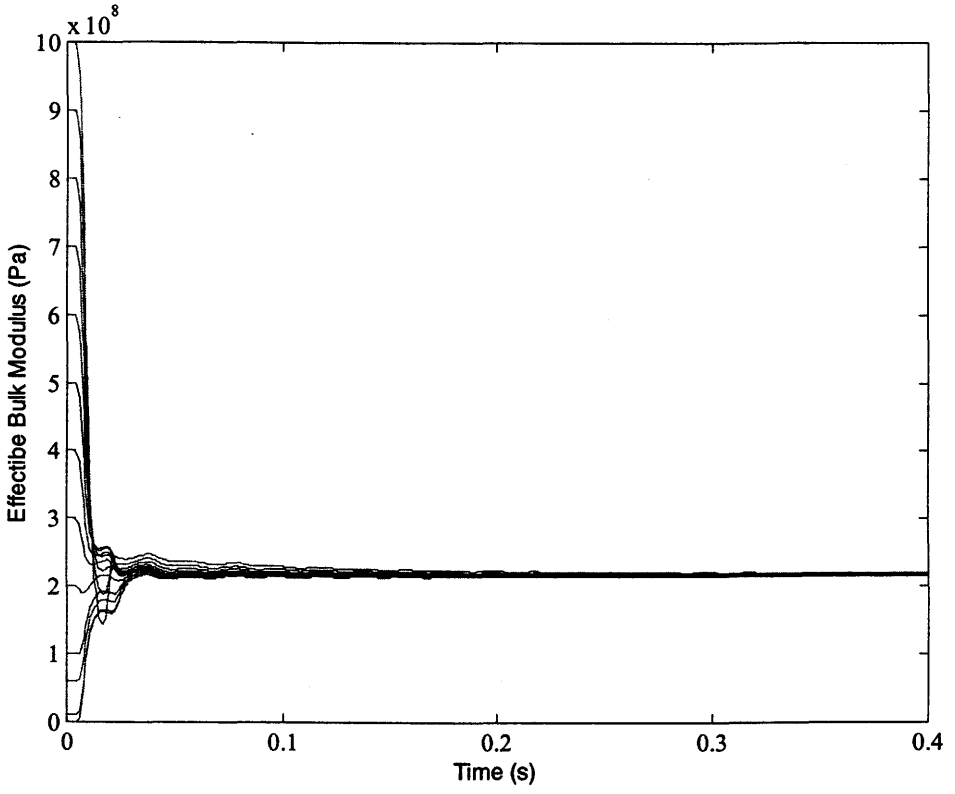

Figure 6.9: Initializing the EKF Code Using Different Effective Bulk Modulus Values.

The "known" value of viscous friction was changed to ensure that the estimation of bulk modulus was independent of the value of the viscous friction. It was found that estimation of effective bulk modulus was relatively independent of viscous friction value at this frequency (25 Hz). A 50 % change in damping coefficient values caused a negligible change (less than 1%) in the effective bulk modulus prediction. This was considered to be a critical observation for condition monitoring applications.

In summary, it was concluded that using an observable system to estimate the effective bulk modulus was an appropriate approach. The viscous damping coefficient was assumed to be known (this parameter appears in the state space formulation of the EHA model required to estimate the effective bulk modulus of the system). Fundamental to this scenario was that the viscous damping coefficient had to be known or would have to be estimated in an independent fashion. Such an approach for the EHA is now considered.

6.5 Estimation of Viscous Damping Coefficient in Simulation

In Section 6.3, the effective bulk modulus and viscous friction coefficient were estimated simultaneously. The system was not observable and the estimates for viscous friction coefficient and bulk modulus were poor. In this section an alternate method for estimating viscous friction coefficient in a linear actuator is presented. The approach is an extension of the work of [Burton, 1974] and [Zavarehi, 1997]. Basically, their method consisted of measuring the pressure difference (from which force could be obtained) across the piston which moved the piston at various constant velocities (zero acceleration). A friction plot consisting of force versus velocity was then used to approximate an average viscous friction value.

In this study, the Extended Kalman Filter is used to estimate an average viscous friction coefficient by using the pressure difference across the actuator as an input and piston position as the measurement. It should be noted that the simulated model assumes a linear viscous friction model. In order to carry out the simulation study using pressure difference as the input to the EKF, the original (plant) model (linearized transfer function model) for the EHA used in earlier sections would not be used. This is because that simplified model relates pump angular velocity to piston displacement and as such does not produce simulated load pressure data. Instead of using a "pure" sine wave to represent load pressure across the lines, a different model for the EHA (described later in this chapter) was developed and simulated in Matlab/Simulink®. The input to that different closed loop EHA model remained desired piston position.

The pressure difference across the chambers of the actuator $(P_1 - P_2)$, as a result of the sine input to the EHA simulated system (physical plant), was a sine "shaped" signal. The simulated load pressure was thus used as the input to the EKF instead of using a "pure" sine wave source to represent the load pressure because the former case was a more accurate representation of the physical system.

The mathematical model used in the EKF described the relationship between the pressure difference $(P_1 - P_2)$ in the actuator chambers and piston displacement and is given as follows:

$$(P_1 - P_2)A = M\ddot{X} + B\dot{X} \tag{6.30}$$

The input to the EKF was the simulated pressure difference and the measurement for the algorithm, the piston displacement. The viscous damping coefficient, $X_3(k)$, is included in the discrete state space model for the actuator, as shown below.

$$X_1(k+1) = X_1(k) + T_s X_2(k) + T_s w_1(k) \tag{6.31}$$

$$X_2(k+1) = \frac{U(k)AT_s}{M} - \frac{X_3(k)T_s X_2(k)}{M} + X_2(k) + T_s w_2(k)$$

$$X_3(k+1) = X_3(k) + T_s w_3(k)$$

$$Z(k) = X_1(k) + v(k)$$

where $X_1(k)$, $X_2(k)$, $X_3(k)$ are the displacement, velocity and viscous friction coefficient respectively, $w(k)$ the system noise, $U(k) = (P_1 - P_2)$ the pressure difference between the actuator chambers, $Z(k)$ measurement vector (piston position) and $v(k)$ the measurement or sensor noise. The system is fully observable, with the rank of the observability matrix being equal to the length of the augmented state matrix (both equals to 3). This was verified in simulation with the observability matrix being calculated at each iteration.

The linearized system matrix is:

$$\Phi(k) = \frac{\partial f(X(k))}{\partial X(k)} = \begin{bmatrix} \Phi_{11}(k) & \Phi_{12}(k) & \Phi_{13}(k) \\ \Phi_{21}(k) & \Phi_{22}(k) & \Phi_{23}(k) \\ \Phi_{31}(k) & \Phi_{32}(k) & \Phi_{33}(k) \end{bmatrix} \tag{6.32}$$

$$\Phi_{11}(k) = 1, \Phi_{12}(k) = T_s, \Phi_{13}(k) = 0, \ \Phi_{21}(k) = 0, \ \Phi_{22}(k) = 1 - \frac{X_3(k)T_s}{M},$$

$$\Phi_{23}(k) = -\frac{X_2(k)T_s}{M}, \Phi_{31}(k) = 0, \ \Phi_{32}(k) = 0, \ \Phi_{33}(k) = 1$$

The first plot in Figure 6.10 shows the pressure difference, as determined from the plant model, across the two chambers of the actuator. The input to the simulated closed loop plant model system was a sine wave (desired piston displacement) of 4 Hz and amplitude of 0.01 m. The damping coefficient used was 760 Ns/m. The "measured" pressure difference from the plant model was the input to the EKF which estimated the piston displacement, velocity and viscous friction coefficient. The simulated piston

displacement, superimposed on the estimated piston displacement, as well as the simulated velocity, superimposed on the estimated piston velocity are depicted in Figure 6.10. No visible difference between the simulated and the estimated responses are observed.

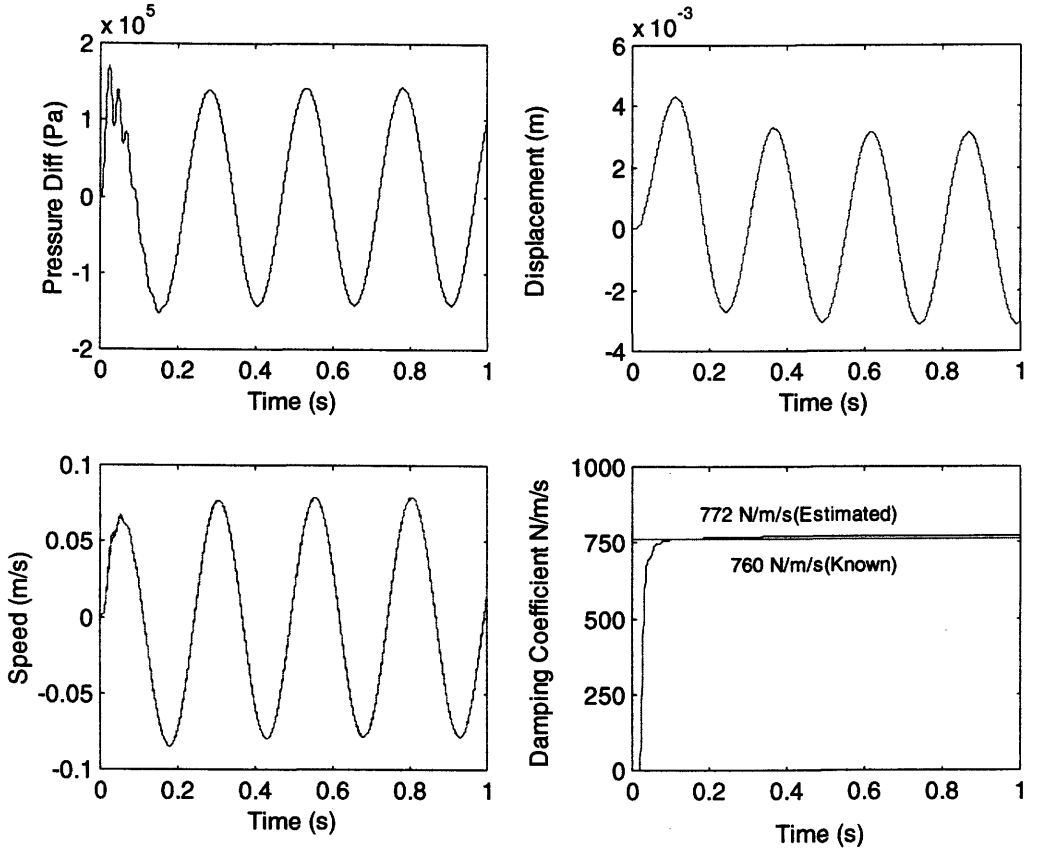

Figure 6.10: Viscous Damping Coefficient Estimation Using the EKF.

It is seen that the estimated and simulated states match closely. The estimated viscous damping coefficient is 772 Ns/m, which is almost the same as the value used in the simulation study (error of 1.6 %).

The initial state vector and the initializing matrices used were set as:

$$X(0)=[0 \quad 0 \quad 0]^T \quad , \; R(k)=1\times10^{-9} \tag{6.33}$$

$$P(0)=\begin{bmatrix} 1\times10^{2} & 0 & 0 \\ 0 & 1\times10^{2} & 0 \\ 0 & 0 & 1\times10^{7} \end{bmatrix} \quad , \; Q(k)=\begin{bmatrix} 1\times10^{-9} & 0 & 0 \\ 0 & 1\times10^{-4} & 0 \\ 0 & 0 & 1\times10^{-4} \end{bmatrix}$$

The viscous damping coefficient value used to initialize the EKF was changed (about the original value) to investigate whether it had any effect on the estimated parameter value. For a fully observable system, the initial matrix will not affect the final value of the estimated parameter. Thus, the initial viscous damping coefficient value used in the EKF algorithm was set to 3000 Ns/m, 2000 Ns/m, 1000 Ns/m and 100 Ns/m. The state/parameter estimations are depicted in Figure 6.11. It is seen that the estimated and simulated states match very closely and the final value of damping coefficient is not affected (estimated parameter is 772Ns/m in each case).

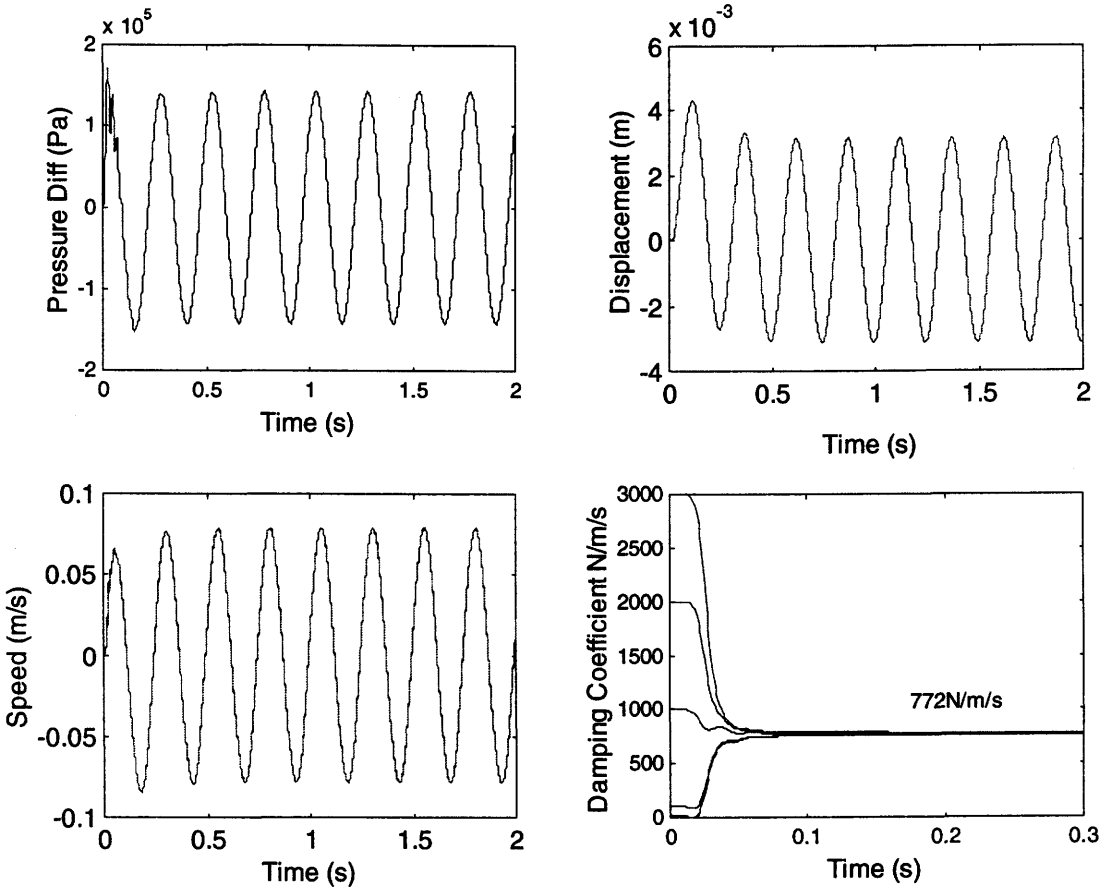

Figure 6.11: Changing the Initial Value for the Estimated Viscous Damping Coefficient in the EKF Code Using Position as Measurement

As a test, the simulated piston velocity was also used in addition to using position as a measurement. The EKF was used to investigate the effect of using two measurements on the accuracy of viscous damping coefficient estimation and it was found that no significant improvement in the estimations were achieved using two measurements as compared to using only one. The reason was believed to be because the system was observable in both cases.

In a physical system, seal wear or oil degradation will tend to affect the viscous damping coefficient and the EKF needs to be able to detect this change. In the simulated model of the EHA, this parameter was changed and the EKF was used to estimate the parameter. Results are given in Table 6.10.

In addition, keeping the viscous friction constant in the EHA simulated model (plant), the values for the effective bulk modulus and lumped leakage coefficient were changed (changes as large as 100%). The EKF was then used to estimate the viscous friction coefficient. It was found that the estimated value for the viscous friction coefficient was unaffected by changes in other parameters (effective bulk modulus and leakage coefficient).

In summary, since the viscous friction estimates converged to the value of the known viscous damping coefficient used in the simulation, it was believed that the Extended Kalman Filter would successfully estimate this coefficient for the EHA prototype using the measured pressure difference across the chambers of the actuator as the input to the EKF algorithm, and the actuator piston displacement as the EKF measurement. Also, since in simulation, changes in the viscous friction coefficient were detected by the EKF and the new values for viscous damping coefficient estimated accurately, it was believed that changes in this important parameter in the actual system would be detected using a similar approach, using a similar input as used for the simulation study and a similar EKF model. Simulation studies also showed that the estimated viscous damping coefficient was independent of changes in the other parameters.

Table 6.10: Changes in the Estimated Viscous Damping Coefficient

Simulated Viscous Damping Coeff. (Ns/m)	**Estimated Damping Coefficient (Ns/m)**	**Estimation Error (%)**
760	772	1.6%
800	813	1.6%
900	912	1.3%
1000	1012	1.2%
2000	2012	0.6%
4000	4007	0.18%
700	712	1.7%
600	612	2%
500	513	2.6 %
400	413	3 %
300	313	4.3 %

In the next section, a different model for the EHA was used to estimate the viscous damping coefficient. This new model was used as the plant in the simulation study. In this approach, to estimate the viscous damping coefficient, the input of the EKF was pump angular velocity and the measurement used was the simulated piston position, velocity and load pressure. The effective bulk modulus, in this method is assumed to be known.

A new state space formulation will be required for the EKF, one which is slightly more complex than used previously to estimate the same parameter. The purpose of the more complex approach is described in the next section for completeness and for an academic purpose only. In a practical situation, it will most probably not be used.

6.6 Using EKF in Estimating the Viscous Damping Coefficient by Using the Known Effective Bulk Modulus Value

From the previous section, it was seen that using a relatively simple model in the EKF, the viscous damping coefficient could be accurately estimated. In this section, an attempt is made to estimate the same parameter but this time using position, velocity and load pressure as measurements and once again making sure that the system remains observable. This implies assuming a known effective bulk modulus value and using a more complex model in the EKF.

The equations describing the pump/actuator flow model of the system have been described in Chapter 3 and will be repeated here to enable the new EKF model to be constructed. Restating Equations (3.1), (3.2), (3.3) and (3.4):

$$Q_a = D_p\omega_p - \xi(P_a - P_b) - \frac{V_a}{\beta_e}\frac{dP_a}{dt} - C_{ep}(P_a - P_r) \tag{3.1}$$

$$Q_b = D_p\omega_p - \xi(P_a - P_b) + \frac{V_b}{\beta_e}\frac{dP_b}{dt} + C_{ep}(P_b - P_r) \tag{3.2}$$

$$Q_1 = A\dot{x} + \left(\frac{V_{0ac} + Ax}{\beta_e}\right)\frac{dP_1}{dt} + LP_1 \tag{3.3}$$

$$Q_2 = A\dot{x} - \left(\frac{V_{0ac} - Ax}{\beta_e}\right)\frac{dP_2}{dt} - LP_2 \tag{3.4}$$

Since $\frac{dP_a}{dt} \approx \frac{dP_1}{dt}$, $\frac{dP_a}{dt} \approx \frac{dP_1}{dt}$ and $V_o = V_{0ac} + V_a$, with V_o being the total mean volume, $Q_a = Q_1$ and $Q_b = Q_2$, the system pressures could be obtained as

$$\frac{dP_1}{dt} = \left[D_p\omega_p - \xi(P_1 - P_2) - LP_1 - C_{ep}(P_1 - P_r) - A\dot{x}\right]\frac{\beta_e}{V_o + Ax} \tag{6.34}$$

$$\frac{dP_2}{dt} = \left[A\dot{x} + \xi(P_1 - P_2) - LP_2 - C_{ep}(P_2 - P_r) - D_p\omega_p\right]\frac{\beta_e}{V_o - Ax} \tag{6.35}$$

From Equations (6.30), (6.34) and (6.35), the load pressure equation becomes

$$\frac{dP_L}{dt} = \left[2D_p\omega_p - 2\xi P_L - LP_L - 2A\dot{x}\right]\frac{\beta_e}{V_t} \tag{6.36}$$

$$P_L A = M\ddot{x} + B\dot{x}$$

where $P_L = P_1 - P_2$ and $V_t = V_0 + Ax = V_0 - Ax = 6.85 \times 10^{-5}\,\mathrm{m}^3$

The state space model can be represented as follows:

$$\dot{X}_1 = X_2 + w_1 \tag{6.37}$$

$$\dot{X}_2 = \frac{X_3 A}{M} - \frac{X_4 X_2}{M} + w_2$$

$$\dot{X}_3 = \left[2D_p \omega_p - 2\xi X_3 - LX_3 - 2AX_2\right]\frac{\beta_e}{V_t} + w_3$$

$$\dot{X}_4 = w_4$$

$$Z = \begin{bmatrix} 1 & 0 & 0 & 0 \\ 0 & 1 & 0 & 0 \\ 0 & 0 & 1 & 0 \end{bmatrix}\begin{bmatrix} X_1 \\ X_2 \\ X_3 \\ X_4 \end{bmatrix} + \begin{bmatrix} v_1 \\ v_2 \\ v_3 \end{bmatrix}$$

where X_1 is the state variable X, X_2 the state variable $\dot{X}$, X_3 the state variable P_L, X_4 the viscous damping coefficient, w_1, w_2, w_3, w_4 the system noise and v_1, v_2, v_3 the measurement noise.

Using the forward difference approximation and applying it to the continuous state space model, the discrete state space model of the EHA is as follows:

$$X_1(k+1) = X_1(k) + T_s X_2(k) + T_s w_1(k)$$

$$X_2(k+1) = X_2(k) + \frac{T_s X_3(k) A}{M} - \frac{X_4(k) X_2(k) T_s}{M} + T_s w_2(k)$$

$$X_3(k+1) = \left[2D_p \omega_p(k) - 2\xi X_3(k) - LX_3(k) - 2AX_2(k)\right]\frac{\beta_e T_s}{V_t} + X_3(k) + T_s w_3(k)$$

$$X_4(k+1) = X_4(k) + T_s w_4(k) \tag{6.38}$$

The linearized system matrix is written as:

$$\Phi(k) = \frac{\partial f(X(k))}{\partial X(k)} = \begin{bmatrix} \Phi_{11}(k) & \Phi_{12}(k) & \Phi_{13}(k) & \Phi_{14}(k) \\ \Phi_{21}(k) & \Phi_{22}(k) & \Phi_{23}(k) & \Phi_{24}(k) \\ \Phi_{31}(k) & \Phi_{32}(k) & \Phi_{33}(k) & \Phi_{34}(k) \\ \Phi_{41}(k) & \Phi_{42}(k) & \Phi_{43}(k) & \Phi_{44}(k) \end{bmatrix} \tag{6.39}$$

where

$$\Phi_{11}(k)=1,\ \Phi_{12}(k)=T_s,\ \Phi_{13}(k)=0,\ \Phi_{14}(k)=0.$$

$$\Phi_{21}(k)=0,\ \Phi_{22}(k)=1-\frac{X_4(k)T_s}{M},\ \Phi_{23}(k)=\frac{T_sA}{M},\ \Phi_{24}(k)=\frac{-T_sX_2(k)}{M}.$$

$$\Phi_{31}(k)=0,\ \Phi_{32}(k)=\frac{-2AT_s\beta_e}{V_t},\ \Phi_{33}(k)=1-\left(\frac{2\xi+L}{V_t}\right)\beta_eT_s,\ \Phi_{34}(k)=0$$

$$\Phi_{41}(k)=0,\ \Phi_{42}(k)=0,\ \Phi_{43}(k)=0,\ \Phi_{44}(k)=1.$$

The observability test done on this particular system showed that the rank of the observablity matrix was the same as the length of the state vector, (both equal to 4). Therefore the system was observable. The estimated states and parameter are shown in Figure 6.12. The viscous damping coefficient was estimated using simulated piston displacement, velocity and load pressure as system measurements. The effective bulk modulus was assumed to be known. The input to the EKF was now the simulated electric motor/pump angular velocity (as compared to load pressure previously) obtained when a 4 Hz sine, 0.01 m was used as the desired input of the simulated closed loop Simulink/Matlab® EHA model. From Figure 6.12, the estimated viscous damping coefficient is 764 Ns/m, showing an estimation error of 0.5 %.

The initial state $X(0)$, error covariance $P(0)$, system noise $Q(k)$ and measurement noise $R(k)$ matrices used were set as:

$$X(0)=\begin{bmatrix}0 & 0 & 0 & 0\end{bmatrix}^T,\quad R(k)=\begin{bmatrix}1\times10^{-10} & 0 & 0\\ 0 & 1\times10^{-9} & 0\\ 0 & 0 & 1\times10^{-2}\end{bmatrix} \tag{6.40}$$

$$P(0)=\begin{bmatrix}1\times10^{1} & 0 & 0 & 0\\ 0 & 1\times10^{2} & 0 & 0\\ 0 & 0 & 1\times10^{5} & 0\\ 0 & 0 & 0 & 1\times10^{3}\end{bmatrix}$$

$$Q(k) = \begin{bmatrix} 1\times10^{-10} & 0 & 0 & 0 \\ 0 & 1\times10^{-7} & 0 & 0 \\ 0 & 0 & 1\times10^{-2} & 0 \\ 0 & 0 & 0 & 1\times10^{-9} \end{bmatrix}$$

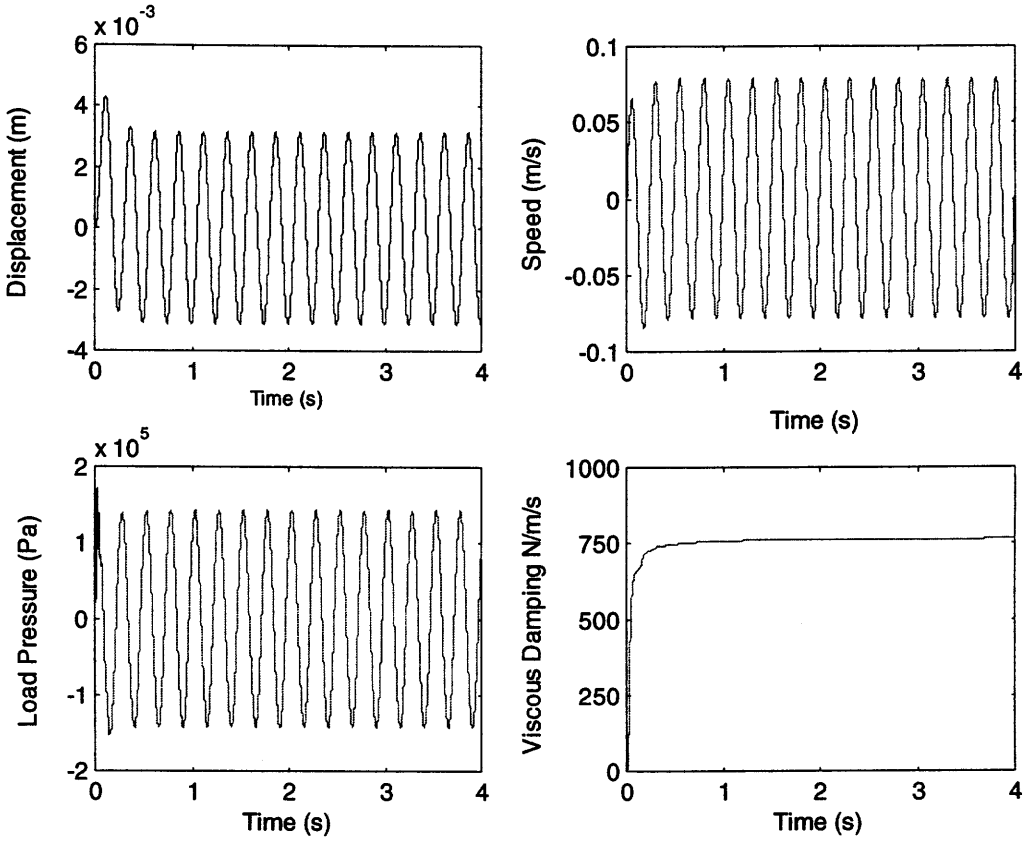

Figure 6.12: Estimating Viscous Damping Coefficient Using More Complex Model

The viscous damping coefficient was then increased from 760 Ns/m to a maximum value of 4000Ns/m (maximum estimation error of 0.3 %) and then reduced to a minimum value of 300 Ns/m (maximum estimation error of 2 %). The estimated parameters are depicted in Figure 6.13. The estimated states (displacement, velocity and load pressure) match the simulated ones very closely in each case. It was concluded that changes in viscous damping coefficient in the simulated model were detected and estimated to an error of 2%.

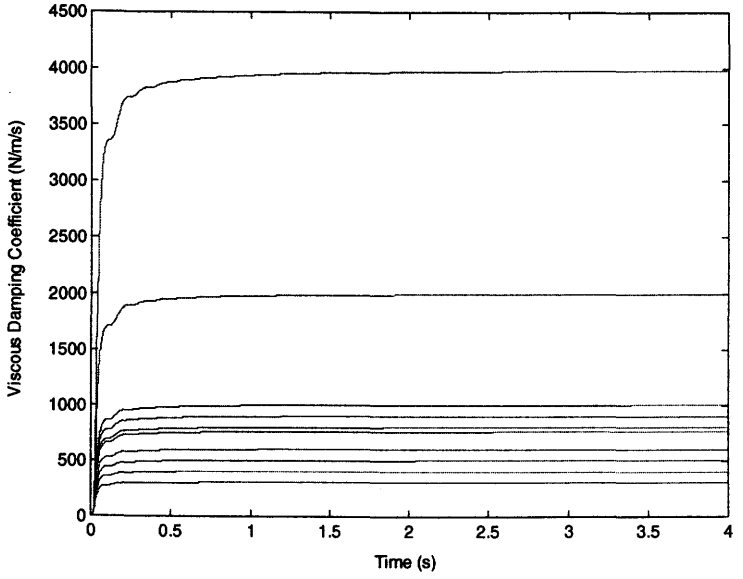

Figure 6.13: EKF Estimates New Viscous Damping Coefficients Successfully

The final value for the estimated viscous damping coefficient using the EKF was shown to be independent of the initial value of the parameter used in the EKF algorithm as illustrated in Figure 6.14.

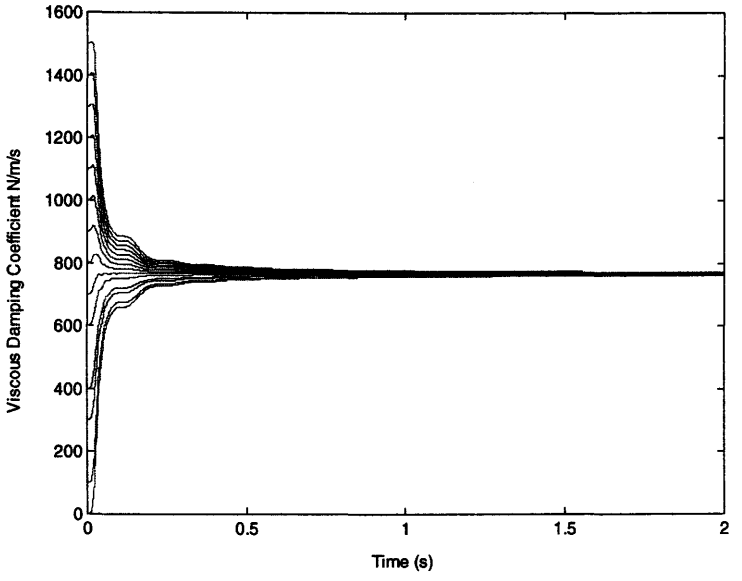

Figure 6.14: Initializing the EKF Algorithm Using Different Initial Values

It should be pointed out that using the model described in Equation (6.37), both the effective bulk modulus and viscous damping coefficient were also expressed as states and the three measurements, namely piston position, velocity and load pressure were used as measurements to estimate the two parameters simultaneously. However, it was found that the system was not observable with the rank of the observability matrix being equal to 4 and the length of the augmented state vector being 5.

6.7 Concluding Remarks

In this chapter, a simulation study was carried out to investigate the feasibility of using the Extended Kalman Filter (EKF) to estimate two important parameters for the Electrohydraulic Actuator (EHA), namely the effective bulk modulus and the viscous friction coefficient. This is an important contribution because it means that the two parameters in the EHA which are physically extremely difficult to measure directly can now be observed over an extended period of time.

It was seen that including all the parameters of interest as states and applying the EKF rendered the state space reformulation for the EHA unobservable. An improved methodology for this particular application, which took into account observability of the reconfigured state space model, involved first estimating the viscous friction coefficient and substituting that estimated value in the state space model needed to now estimate the effective bulk modulus. This strategy seemed more effective than estimating both parameters simultaneously.

It was also found that the observability condition was necessary for the Kalman filter to successfully estimate states. Using the examples of the mass damper and mass spring damper systems (Appendix B), it was found that using position as measurement for systems having "direct derivatives" such as velocity as the state, always made the system observable. As such, the Kalman Filter estimated the states successfully in the mechanical systems when the systems were observable. When the mass damper system (Type 1 system), was made unobservable by using velocity as the measurement, the estimated position showed a "bias" compared to the simulated position whereas the estimated velocity converged to the estimated velocity. This "bias" disappeared when

the initial position was known and state estimation was then successful for the unobservable mass damper system. This behavior was consistent with the EHA, also a type 1 system. The mass spring damper system (Type 0 system) remained observable in spite of using velocity as the only measurement. The Kalman filter was able to estimate the initial position using the velocity as measurement. The reason was believed to be because of the presence of the displacement term in the velocity equation.

It was interesting to note that the Kalman filter estimated states for the unobservable mass damper and EHA systems (when velocity was used as measurement). The estimated position showed a "bias" which disappeared when the initial position was known. The error covariance for the estimated position was found to be constant (same as the set initial error covariance value for position) when the two systems were unobservable. As such, the Kalman gain associated with the estimated position was very small. It was believed that the estimated position was due to the "prediction equation" of the Kalman filter which made use of the system model to predict the state. Therefore, it could be said that the position was not being "estimated" as such, but was being "predicted".

When the EKF was used to estimate a parameter in the mass damper and mass spring damper system, using observable systems (position as measurement), the single parameter was estimated accurately and changes in the parameter also estimated accurately. In the case of multiple parameter estimation, for the mass spring damper system (a type 0 system), when position was used as the only measurement, the system was not observable as a result of augmentation of the state vector to accommodate the parameters. But the EKF was able to accurately estimate 2 parameters and changes in the parameters when only 1 state variable was not observable. When velocity was used as measurement in the mass spring damper system, the EKF was not able to estimate the parameters accurately when the initial position was not known, but estimated them successfully when the initial position condition was known. Thus, for the mass spring damper system, parameter estimation was possible when the system failed the observability test due to an augmentation of the state matrix (1 unobserved state).

Parameter estimation was also only possible in the same system when velocity was used as measurement (resulting in 2 unobserved states) when the initial position was known.

In the case for the more complex EHA system, the Kalman filter showed similar behavior to the mass damper system. When the Kalman filter was used to estimate states using position as measurement, the system was fully observable and state estimation was successful. The use of velocity as measurement made the system unobservable and the estimated position was "biased".

The EKF, however showed a different behavior for the EHA as compared to the mass spring damper system when it was used for multiple parameter estimation in the EHA. The mass spring damper and the EHA examples were not observable when multiple parameter estimation were attempted, using position as measurement. The EKF showed difficulty to differentiate between changes in the parameters of the EHA (once the filter was tuned). In the mass spring damper example, the EKF was able to correctly estimate the parameters initially and estimated changes in the parameters accurately. This observation was not the same for the more complex EHA system where the parameters were estimated accurately initially but changes in parameters were not accurately estimated.

The final approach used for parameter estimation in the EHA was as follows. The two parameters of interest were estimated iteratively using two different models which ensured that observability condition was satisfied each time. In previous studies the same model was used to estimate all the parameters. It was believed that this strategy would render fault detection via parameter estimation using the EKF more effective in terms of accuracy of the parameter estimations and repeatability.

Following the extensive simulation study carried out in this chapter, it is believed that the EKF can estimate the damping coefficient and the effective bulk modulus for a real system. In Chapter 7, the two parameters will be estimated using measurements from the EHA prototype. The EKF algorithms of Chapter 7 are similar to the ones developed for the simulation study but measured data will be used instead of simulated data. The initial conditions of the filter as well as the input signals applied to the EHA prototype will be similar to the simulation studies.

Chapter 7

Experimental Results

Parameter Estimation in the EHA

In this Chapter the results obtained, when the measured responses from the Electrohydraulic Actuator prototype (EHA) were used to estimate viscous friction coefficient and effective bulk modulus by the Extended Kalman Filter (EKF), are reported. Following the simulation study carried out in Chapter 6, the EKF algorithm was applied to the EHA prototype. The system measurements were differential pressure, electric motor angular velocity, and actuator position. The methodology described in Chapter 6 was applied, in that the viscous friction coefficient was estimated first using a reduced model of the actuator and thus using the known value for that parameter, in effective bulk modulus estimation. The experimental estimations cannot be compared to "known" values of these parameters.

7.1 Procedures for Collecting Experimental Data

The experimental procedure was essentially an off-line approach where the sine wave (desired piston position) was used as input to the closed loop EHA prototype and measurements from the prototype were recorded (illustrated in Figure 7.1). The measured data (piston position, load pressure and pump angular velocity) were recorded using a computer. Subsequently, the data was used to estimate the parameters by the EKF. The state space formulation required by the EKF was similar to the model used for the simulation study reported in Chapter 6.

The computer code (EKF algorithm) used for the simulation study was also used for the experimental study. The same sampling time (1ms), input signals (4Hz, 0.01m sine wave and 25 Hz, 0.005m sine wave) and initial matrices (initial state vector, system and measurement noise covariance matrices and error covariance) for the EKF algorithm, as used in the simulation study were used to estimate the two parameters (viscous damping coefficient and the effective bulk modulus of the prototype).

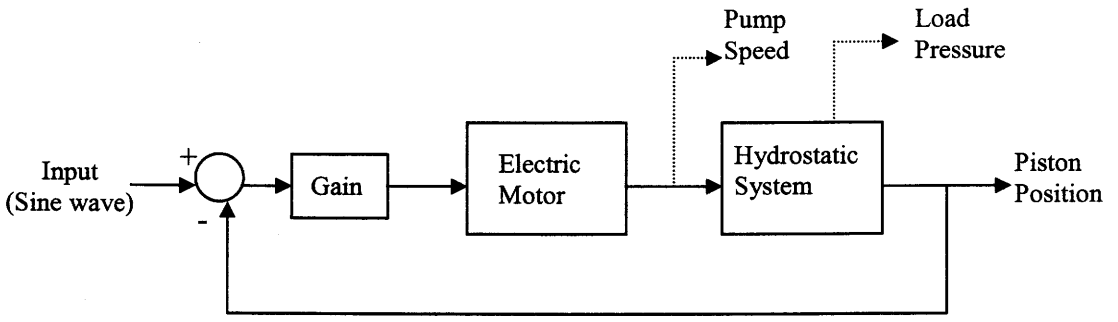

Figure 7.1: Measurements From the EHA Prototype Used by the EKF

The pump/electric motor angular velocity was measured by a "Speed monitor output", which has a sensitivity of ±8 V for ±14000 rpm (183rad/s/V), built in the "controller block" of the electric motor (which drives the bi-directional gear pump of the EHA). The 'controller block" has a "*series of racks of Pulse Width Modulation Servo Amplifiers that provide speed control for the electric motor...The amplifiers control directly the motor torque and speed by means of the information provided by a transmitter resolver sensor... Protections include the amplifier rated current overload, motor overtemperature, amplifier overtemperature*", [Operating Manual, Infranor Inc, 1999]. The voltage applied to the input control (maximum voltage was ±10 V DC) for the electric motor was proportional to the speed of the motor (The sensitivity was ±10 V for 4000rpm, i.e. 41.88rad/s/V) [Infranor, 1999].

An optical encoder (which replaced an LVDT at a later stage of the research) was used for actuator piston displacement measurements. The encoder has been described in Chapter 4. A differential pressure transducer, also introduced in Chapter 4, was used to measure the differential load pressure across the two chambers of the actuator. The safety crossover relief valve was pre-set to 250 psi. Calibration of the LVDT and of the pressure sensor was described in Chapter 4. These sensors (except for the optical encoder) produced voltages, which were directly proportional to the physical quantity they were measuring.

The signals from the sensors were recorded using a computer data acquisition system (12 bit A/D-D/A Data Acquisition Board; CIO-DAS 1602/12 I/O Card). The CIO-DAS1600 analog connector was a 37-pin connector accessible from the rear of the computer and wiring from the sensors and to the voltage control of the motor was done in the connector. "Real Time Windows Target" was used in the acquisition system and provided in the Matlab/Simulink® environment. The software was designed to operate the EHA in a closed-loop form, making use of the optical encoder. Software was used (C++) to "link" the optical encoder to "Real Time Workshop" such that "Real Time Workshop" was able to "read" measurements from the optical encoder. Through Real Time Workshop, the desired piston position (input signal for the closed-loop EHA system) was compared to the measured piston output and the error signal was amplified by a proportional controller (set to 585), which "fed" a voltage to the electric motor.

The experiments were always performed at a temperature of $24 \pm 1\,^{0}C$ (measured using thermocouples). The temperature was monitored and the experiments spaced in time to allow the oil to cool down and reach the same temperature before the next set of experiment was performed.

The actuator piston was always positioned at the "middle" to have approximately equal volumes in the two chambers of the actuator and to ensure that it did not hit the end of the stroke.

7.2 Viscous Damping Coefficient Estimation

The viscous damping coefficient was estimated by the EKF and the filter used the measured load pressure and actuator piston measurements from the EHA prototype. The input signal to the prototype (plant) was a desired position of 0.01 m, 4 Hz sine wave, of amplitude 0.01 m. The input signal (desired piston position) was applied to the closed loop EHA prototype. The measured pressure difference, as well as the measured piston position are shown in Figure 7.2. The measured pressure difference from the plant was the input to the EKF, and piston displacement was the measurement for the EKF. As shown in Figure 7.2, the EKF algorithm, as it progresses with each iteration, gives a prediction of displacement, piston velocity and the viscous damping coefficient.

The state space model embedded in the EKF was described in Chapter 6 and given as Equation (6.15). The sampling time used was 1ms.

The estimated piston displacement, $X_1(k)$, and the estimated velocity $X_2(k)$, match the measured states, as shown in the superimposed plots below and the viscous friction coefficient $X_3(k)$ converges to a value of 761 Ns/m. There is little differences between the estimated and measured states.

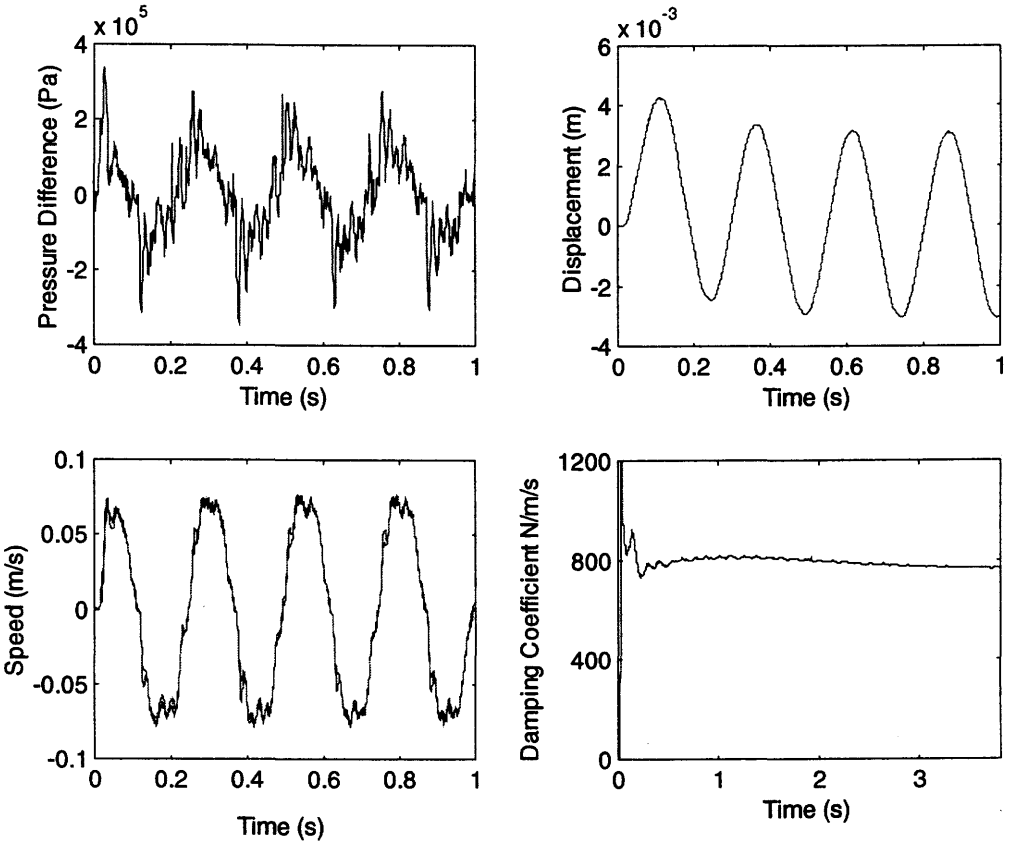

Figure 7.2: Estimation of Viscous Damping Coefficient in the EHA Prototype (Estimated and Measured States Superimposed)

In Chapter 6, it was shown that the state space model for the simple model was fully observable, (Rank of the observability matrix being equal to the length of the state matrix for each iteration). Only displacement was used as a measurement. Similar to the simulation study, the initial value used for the viscous friction coefficient in the EKF

code was changed and the results shown in Figure 7.3. In this figure, the time-scale is magnified to show the initial parameter values used in the EKF code to initialize the state vector. Previously, the estimation process illustrated by Figure 7.2 was initialized with a zero vector (no a priori information about the states).

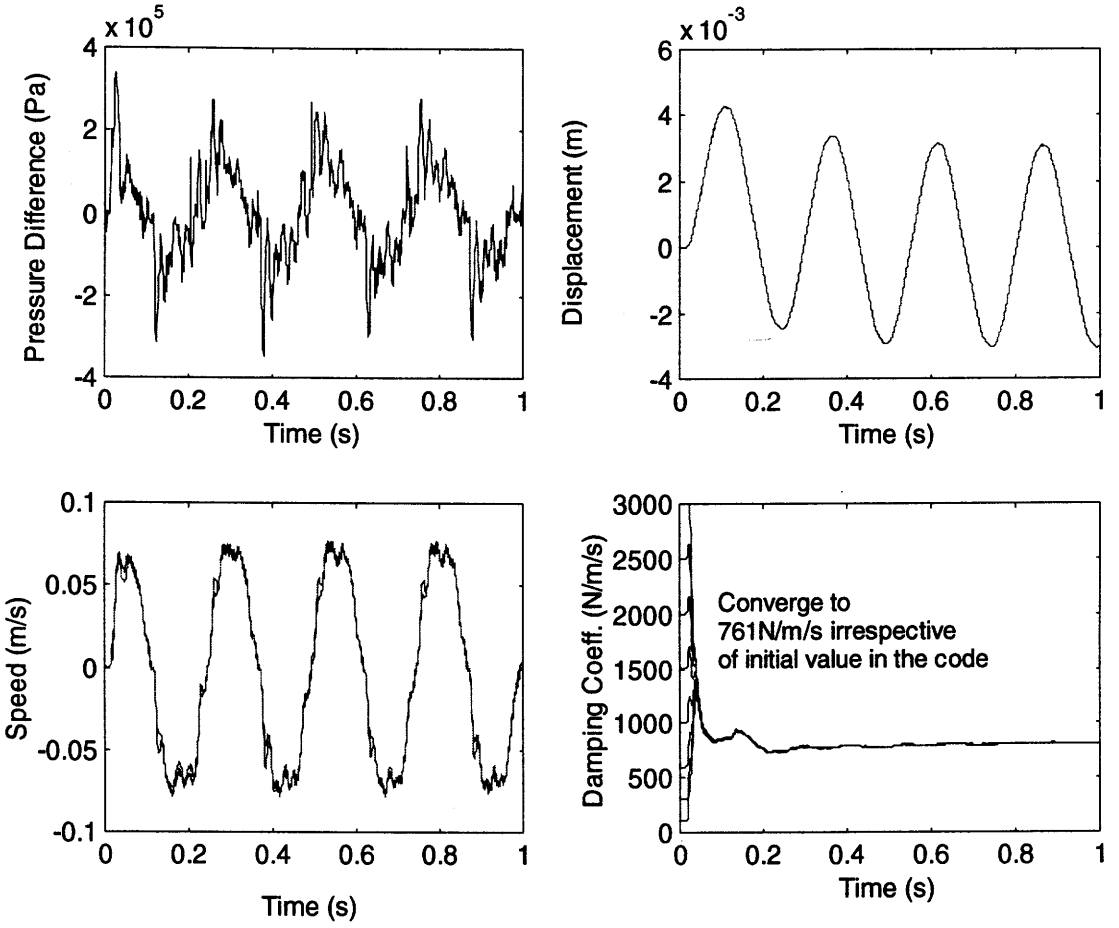

Figure 7.3: Estimation of Viscous Damping Coefficient (Independent of Initial Values)

The viscous friction coefficient estimate converges to the same value irrespective of the starting value in the code. This indicates that a global minimum was achieved by the EKF. Also, since the initial values used were the same as for the simulation study, it was believed that the prediction had more or less the same level of accuracy (less than 2% error). Moreover, since in simulation, changes in this parameter were detected and accurately predicted it was believed that changes in this important parameter in the EHA prototype would be detected accurately.

The experiment was repeated several times, on different occasions and the following table summarizes the results for estimation of viscous friction coefficient, using a 4 Hz sine wave as input. It is worth mentioning that all the tabulated results are for experiments which were carried out at an oil temperature of $24 \pm 1\,^{0}C$.

Table 7.1: Viscous Damping Coefficient Estimation at a Temperature of $24 \pm 1\,^{0}C$

Experiment Number	Number of iterations required for convergence	Estimated Viscous Friction Coefficient (Ns/m)
1	3500	761
2	3600	762
3	3800	770
4	3780	775
5	3598	755
6	3760	750
	Mean Value	762
	Standard deviation	8.43

In the literature, it was reported that the EKF often diverges if the reference point about which the linearization takes place is poor and therefore setting the initial matrix is important. If no a priori information about the true estimate is available, a large initial error covariance matrix is usually necessary. However, in estimating the damping coefficient in the EHA prototype, no priori information was assumed.

It is believed that the initial value, if required for a particular system, should only be used to determine how fast convergence is occurring. If the EKF converges only when the initial value is chosen very close to the true value, then the final solution may not be optimal and a situation referred to as "local-minima" might have been reached due to lack of observability in the EKF formulation. Therefore, it can be seen that the initial matrix is very important; if convergence occurs, when no a priori

knowledge is available, i.e. with a zero matrix as the initial state estimate, this is a strong indication that an optimal solution is reached.

Furthermore, the system noise and measurement covariance matrices in the EKF algorithm need to reflect the amount of uncertainty in the model and the noise of the actual measurements. A noisy signal would imply using a numerically larger measurement noise covariance matrix. In fact, before using an optical encoder to measure the position of the load, an LVDT was used, resulting in noisy position measurements. The noisy position measurements were also used to estimate the viscous friction coefficient, as illustrated by Figure 7.4. The initial matrices used in the EKF algorithm are given in Equation 7.2. It can be seen that the measurement noise was increased from an initial value of $R(k)=1\times10^{-9}$ (when the optical encoder measurements were used) to a value of $R(k)=1\times10^{-4}$ (when the LVDT was used).

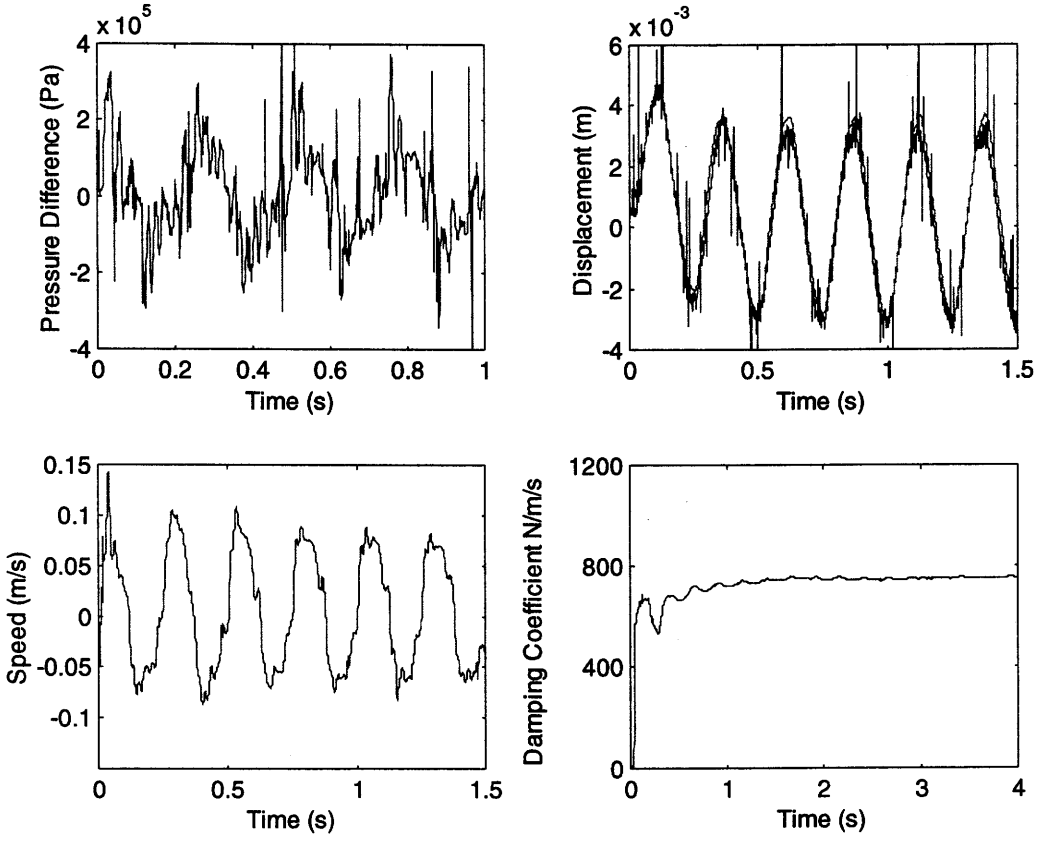

Figure 7.4: Estimation of the Viscous Damping Coefficient Using Noisy Measurements

This result is important because it shows that parameter estimation can be carried out using the EKF even with noisy signals (in applications where there are no optical encoders for example) since the EKF algorithm does include a measurement noise model.

The initial matrices used in the EKF algorithm were set as:

$$X(0)=[0 \quad 0 \quad 0]^T \quad , \; R(k)=1\times10^{-4} \tag{7.2}$$

$$P(0)=\begin{bmatrix} 1\times10^{2} & 0 & 0 \\ 0 & 1\times10^{2} & 0 \\ 0 & 0 & 1\times10^{7} \end{bmatrix} \; , \; Q(k)=\begin{bmatrix} 1\times10^{-9} & 0 & 0 \\ 0 & 1\times10^{-4} & 0 \\ 0 & 0 & 1\times10^{-4} \end{bmatrix}$$

From Figure 7.4, it is seen that the estimated displacement matches the measured displacement and an estimate for velocity is also shown. The EKF converges to a value of 760 Ns/m. It can also be pointed out that usually LVDT measurements can be less noisy in other applications, but for the EHA, the close proximity of the sensor to the electric motor caused noise emanating from electric motor coils to be picked up by the LVDT. This, together with the need for high precision measurements (the EHA has an accuracy of 1 micron) motivated the use for an optical encoder which, unlike the LVDT, produced a digital signal (as explained in Chapter 4).

7.3 Effective Bulk Modulus Estimation

A similar approach to that detailed in Chapter 6 was used to estimate the bulk modulus, but instead of using the simulated data (namely simulated electric motor angular velocity and the simulated actuator piston position), the actual measurements were used to estimate the effective bulk modulus of the prototype using the EKF algorithm. The state space formulation was described in Equation (6.19). A 25 Hz sine wave input (desired position) of 0.005 m, was applied to the EHA prototype; the measured electric motor speed was the input to the EKF and the piston position and velocity (obtained by differentiation) from the prototype were the measurements for the EKF. The EKF algorithm, as it progresses with each iteration, gives its prediction of estimated states (piston displacement, velocity and acceleration). The states and the

estimated effective bulk modulus are shown in Figure 7.5. It is seen that the estimated displacement and velocity match the measured displacement and velocity very closely, as illustrated by the superimposed plots in Figure 7.5. The estimated effective bulk modulus was 2.1×10^{8} Pa.

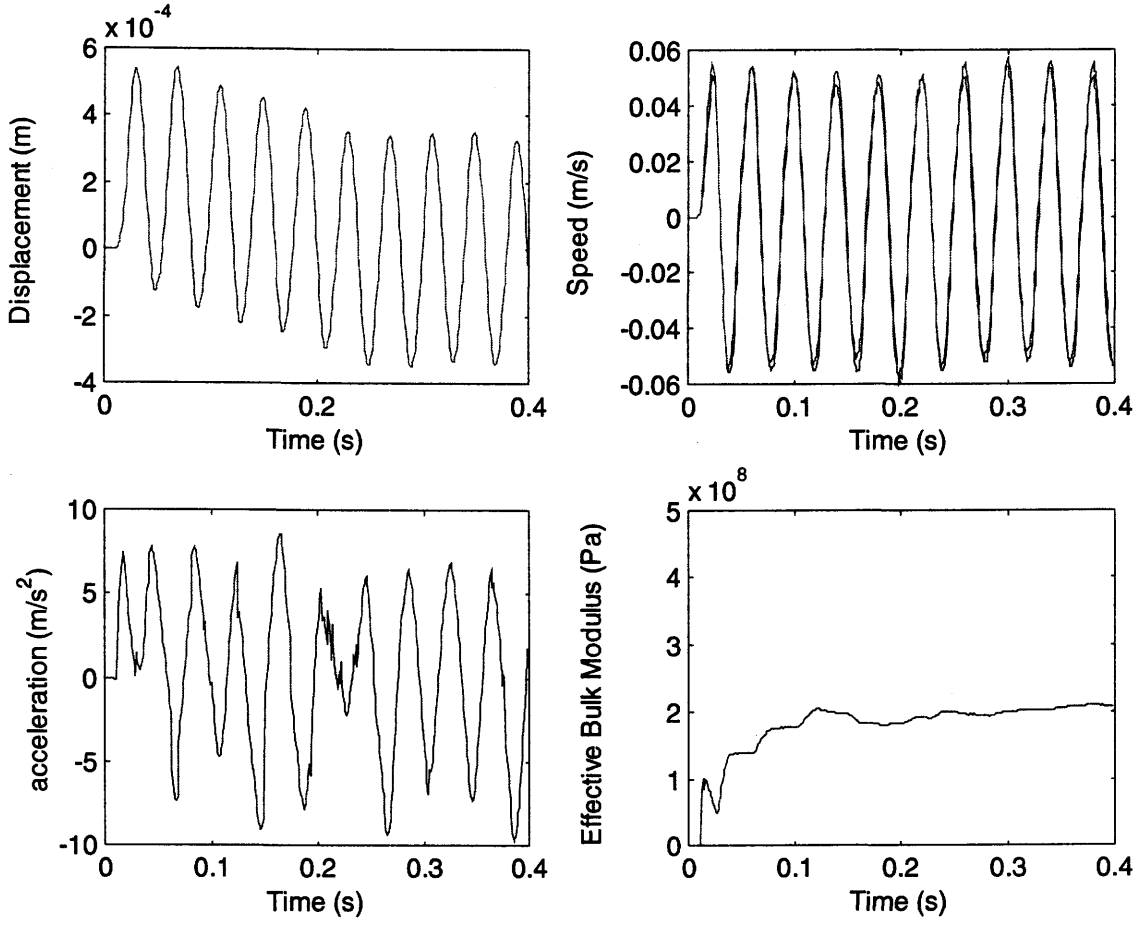

Figure 7.5: Estimating Effective Bulk Modulus in the EHA Prototype

The initial matrices used (identical to the matrices used for the simulation study) were set as follows:

$$X(0)=\begin{bmatrix}0 & 0 & 0 & 0\end{bmatrix}^{T} \qquad R(k)=\begin{bmatrix}1\times10^{-12} & 0\\ 0 & 1\times10^{-3}\end{bmatrix} \tag{7.3}$$

$$P(0) = \begin{bmatrix} 1\times10^{9} & 0 & 0 & 0 \\ 0 & 1\times10^{9} & 0 & 0 \\ 0 & 0 & 1\times10^{19} & 0 \\ 0 & 0 & 0 & 1\times10^{19} \end{bmatrix}$$

$$Q(k) = \begin{bmatrix} 1\times10^{-12} & 0 & 0 & 0 \\ 0 & 1\times10^{-3} & 0 & 0 \\ 0 & 0 & 1\times10^{-9} & 0 \\ 0 & 0 & 0 & 1\times10^{-8} \end{bmatrix}$$

The procedure was repeated several times and the results given in Table 7.2. Estimation for the effective bulk modulus estimation was repeatable as shown in Table 7.2.

Table 7.2: Effective Bulk Modulus Estimation at a Temperature of $24\pm1\,^{0}C$

Experiment Number	Number of iterations required for convergence	Estimated Effective Bulk Modulus (Pa)
1	150	2.1×10^{8}
2	200	2.19×10^{8}
3	230	2.09×10^{8}
4	180	2.15×10^{8}
5	174	2.11×10^{8}
6	260	2.1×10^{8}
	Mean Value	2.12×10^{8}
	Standard Deviation	3.54×10^{6}

Similarly to the simulation study, the initial value used in the EKF algorithm for the estimation of the effective bulk modulus was changed and the effect (if any) investigated. The estimated effective bulk modulus value in the prototype was independent of the initial value used, as illustrated in Figure 7.6, where the same set of data was used but with a different initial effective bulk modulus value in the EKF code.

The estimated effective bulk modulus is shown as a superimposed plot for different initial values in the EKF code. The estimated position and velocity were found to match the measured states every time. It should be noted that the estimated effective bulk modulus converges to the value 2.1×10^{8} Pa (approximately) after 350 iterations.

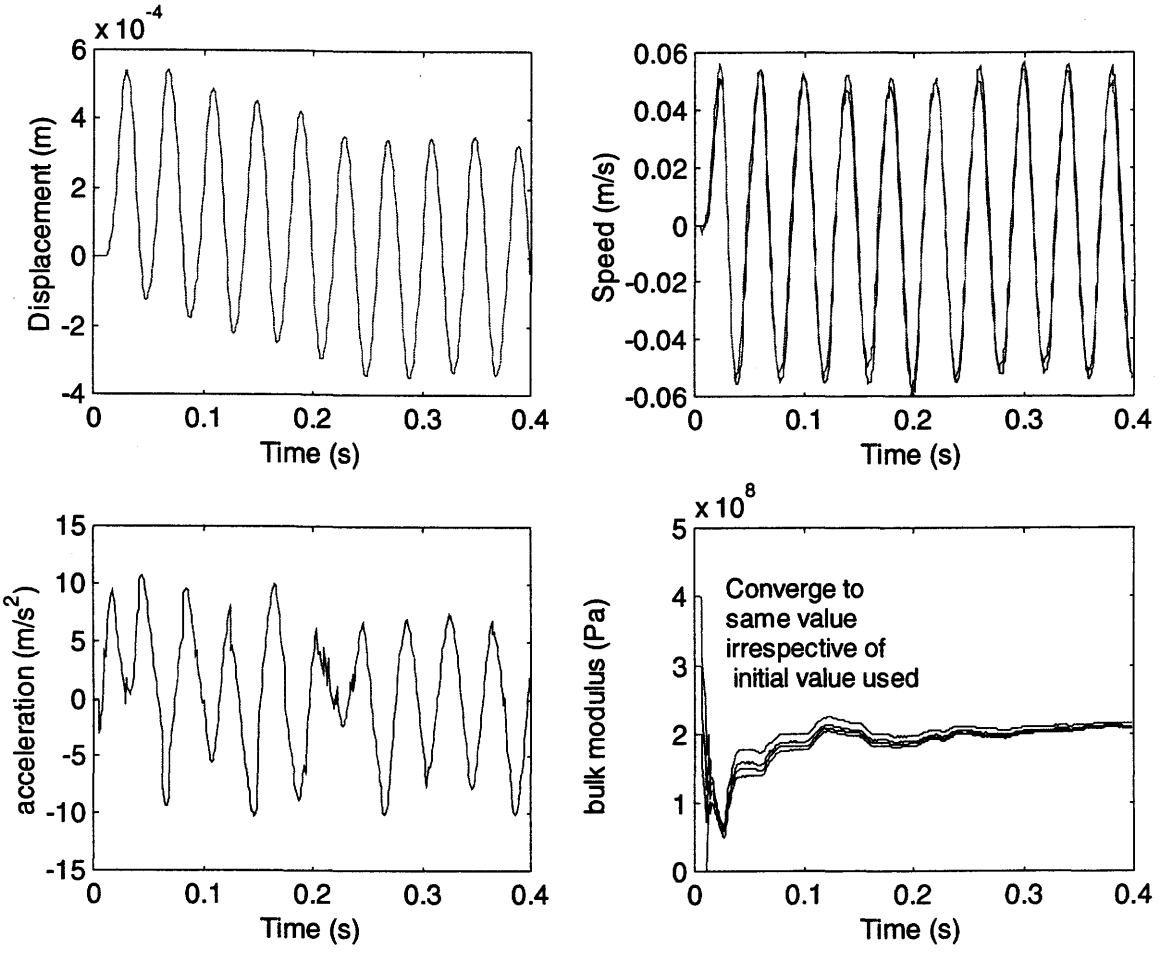

Figure 7.6: Estimation of the Effective Bulk Modulus in the Prototype by Setting the Initial Matrix in the EKF Code with Different Starting Values for the Parameter.

Similar to the case of the viscous damping coefficient estimation, experiments were also conducted using the LVDT (instead of the optical encoder) to measure the piston displacement in the prototype, in order to estimate the effective bulk modulus using the 25 Hz signal. The estimation process is illustrated in Figure 7.7. It can be seen

that the estimated position by the EKF agrees with the measurement position using the LVDT. The measured piston displacement is shown in Figure 7.7 and is seen to be very "noisy". The reason was, as in the previous case, the LVDT picked noise from the nearby electric motor.

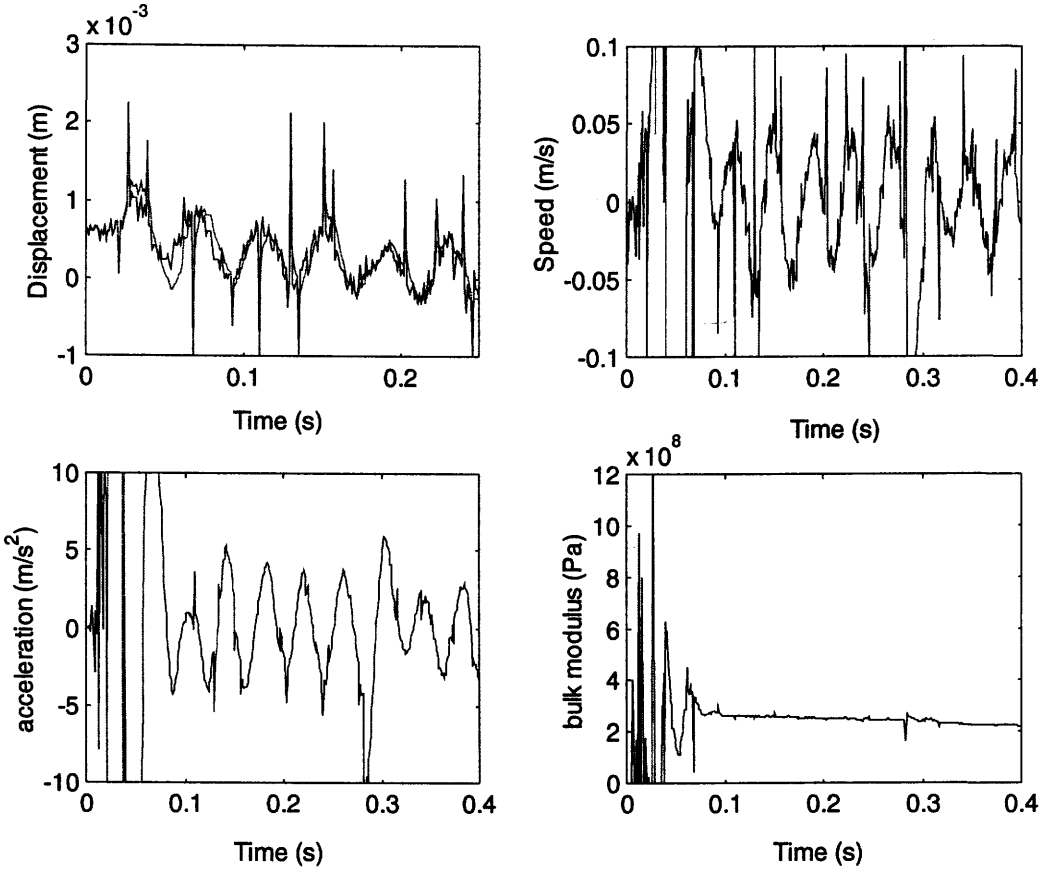

Figure 7.7: Estimation of the Effective Bulk Modulus Using Noisy Measurements

As seen in Figure 7.7, the EKF estimates velocity and acceleration (accuracy of the estimated states seems reasonable when compared to estimated states using the optical encoder) and the estimated effective bulk modulus was 2.16×10^{8} Pa. However, it should be reported that these results were not as repeatable as when the encoder was used to estimate this parameter. Variations of up to 10 % (i.e. $2.16\times10^{8}\pm10\%$) in the estimated value for the effective bulk modulus was recorded when the experiment was repeated. The reason was believed to be because of large amount of noise in the system,

which made the estimation of the effective bulk modulus more challenging. It should also be pointed out that the initial state vector was set to zero and the measurement noise covariance matrix was "larger" to reflect the level of noise in the physical system.

The initial matrices used (when piston displacement was measured by the use of the LVDT) were set as:

$$X(0) = [0 \quad 0 \quad 0 \quad 0]^T \qquad R(k) = \begin{bmatrix} 1\times10^{-2} & 0 \\ 0 & 1 \end{bmatrix} \tag{7.4}$$

$$P(0) = \begin{bmatrix} 1\times10^{1} & 0 & 0 & 0 \\ 0 & 1\times10^{2} & 0 & 0 \\ 0 & 0 & 1\times10^{2} & 0 \\ 0 & 0 & 0 & 1\times10^{19} \end{bmatrix}$$

$$Q(k) = \begin{bmatrix} 1\times10^{-3} & 0 & 0 & 0 \\ 0 & 1\times10^{-2} & 0 & 0 \\ 0 & 0 & 1\times10^{-4} & 0 \\ 0 & 0 & 0 & 1\times10^{-8} \end{bmatrix}$$

7.4 Estimating Viscous Friction Coefficient Using the Complex Model

Similar to the simulation study carried out in Section 6.5, the more complex model was used in the EKF to estimate the viscous friction coefficient for the EHA. In practice, this more complex method of estimating the viscous friction coefficient would not be used since the simpler method explained previously was found to be appropriate to estimate this parameter. However, in this section, the complex method is described for academic purposes and to show that using a different input and different measurements, a similar result can be obtained for the estimated viscous friction coefficient. The state space formulation assumed that the effective bulk modulus was known (iterative approach) and measurements from the physical system were piston position, piston velocity and load pressure. The input to the EKF algorithm was the measured pump/motor angular velocity and the other three mentioned measurements from the EHA prototype were used as measurements for the EKF. The EKF estimations are shown in Figure 7.8. The estimated states (position, velocity and load pressure)

show good agreement with the measured ones. The estimated viscous friction coefficient value was 750 Ns/m.

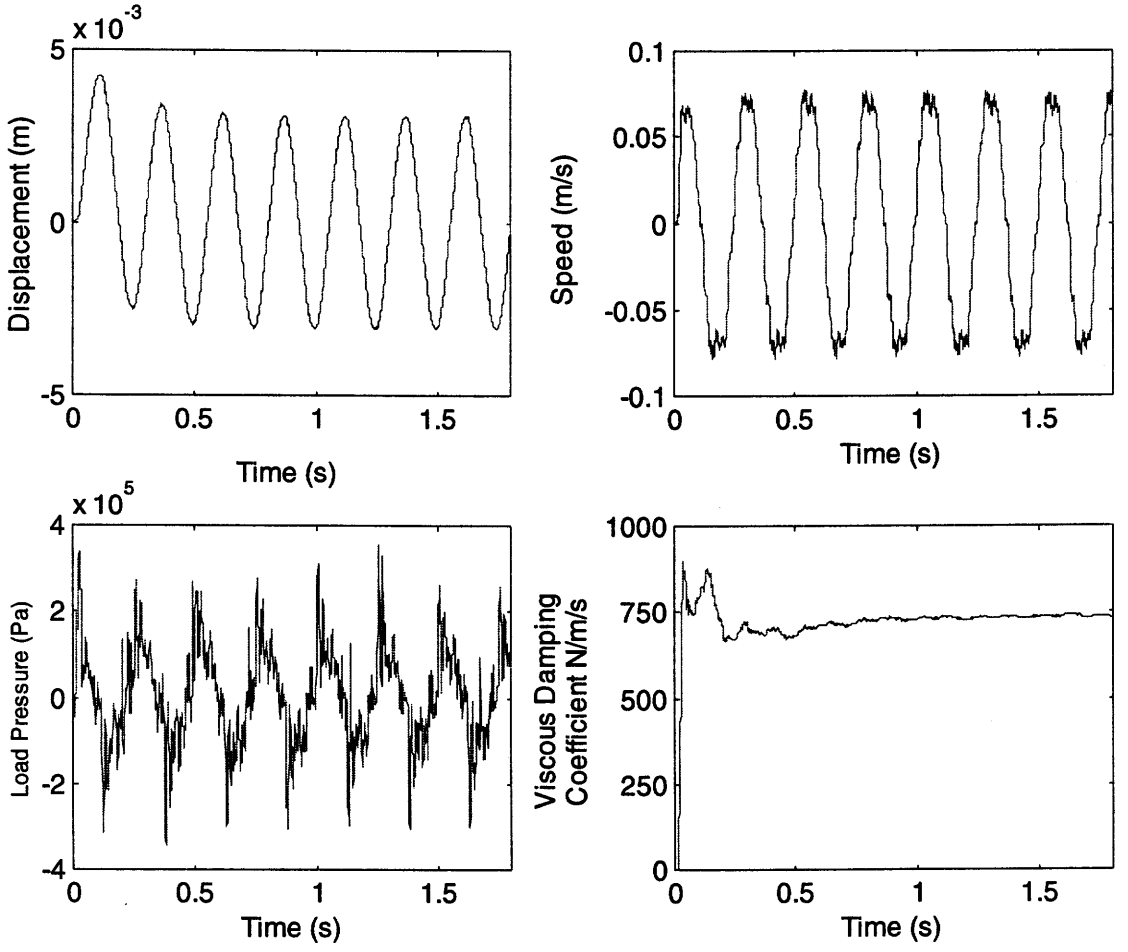

Figure 7.8: Estimating Viscous Friction Coefficient in EHA Prototype Using Complex Model Assuming Known Effective Bulk Modulus Value

The initial viscous damping coefficient value used in the EKF code was manually changed and the results are shown in Figure 7.9. From this Figure, it is seen that the estimated viscous friction coefficient in the EHA prototype always converges to the same value (750 Ns/m), irrespective of the starting value used to initialize the algorithm.

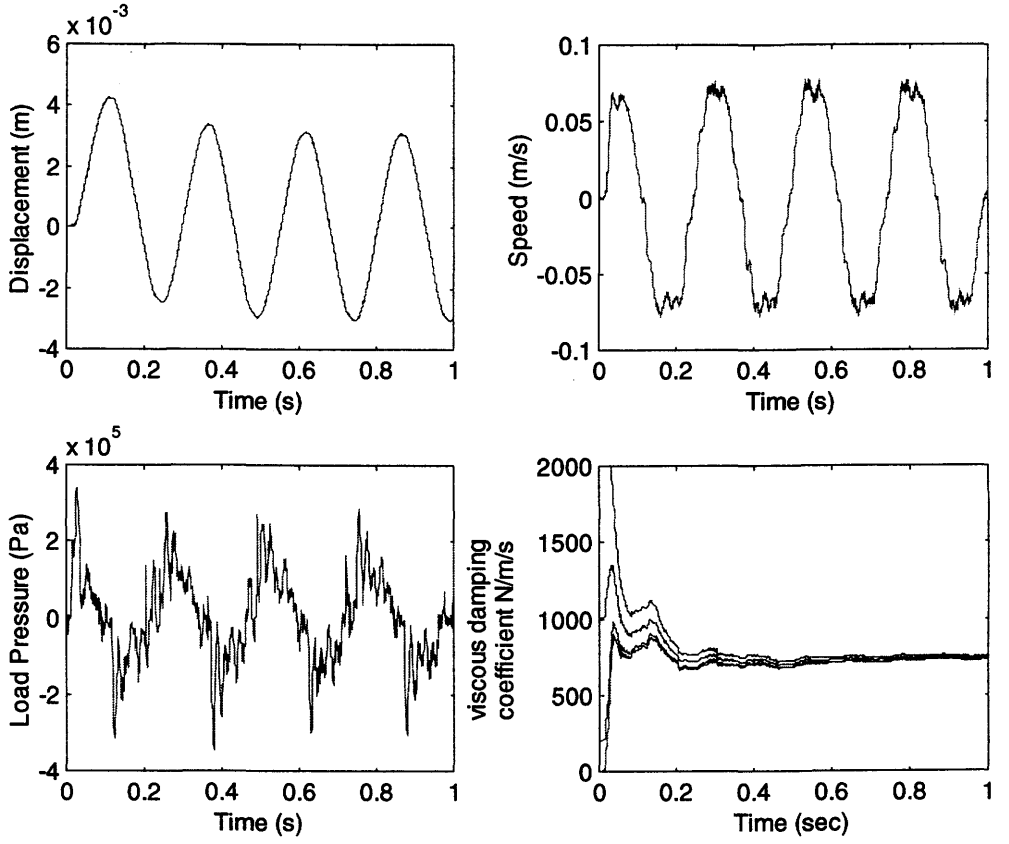

Figure 7.9: Viscous Damping Coefficient Independent of Initial Values Used in EKF

7.5 Estimation of Parameters Iteratively using Three EKFs

The iterative approach to estimate one parameter at a time was automated and a code, having three Extended Kalman Filters in series (a "bank" of EKFs) was implemented. The first parameter, viscous friction coefficient, was estimated using load pressure as the input, and piston position as measurement to the EKF. The input to the EHA prototype was the 4 Hz, 0.01 m signal. Next, using the estimated viscous friction coefficient (from the first EKF), the second EKF used pump angular speed as its input and piston position and piston velocity as measurements to estimate the effective bulk modulus. The input to the EHA prototype was in this case a 25 Hz, 0.005 m signal. Finally, using the known value for effective bulk modulus from the second EKF, the third EKF used pump angular velocity as its input and three measurements, namely

piston position, velocity and load pressure to estimate the viscous friction. The input to the EHA prototype was a 4 Hz, 0.01m signal. The estimation process for this "bank" of EKFs are shown in Figure 7.10.

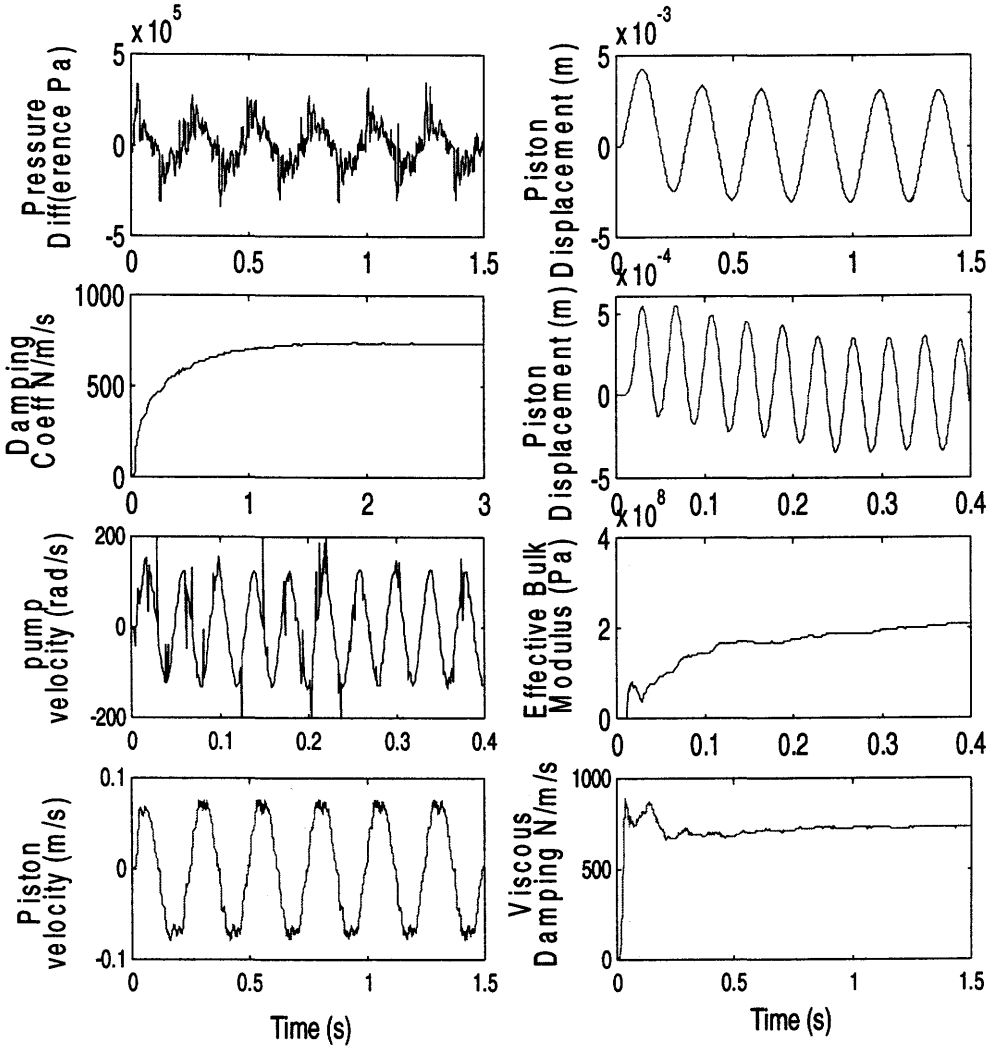

Figure 7.10: Estimating Two Parameters "Iteratively" in the EHA Prototype Using Three EKF Algorithms in Series and Two Sets of Data, i.e. A Sine Input of 4 Hz and 0.01 m for Viscous Damping Coefficient Estimation and A Sine Input of 25 Hz and 0.005 m for Effective Bulk Modulus Estimation

This iterative approach serves to verify the value for the viscous friction coefficient, estimated previously by using a simpler model in the first EKF. Negligible difference in the estimated values, less that 1% variation about the mean value were obtained making further iterations of the 3 EKFs in the form of a loop unnecessary. It should be pointed out that in this iterative approach, all three EKFs were using state space formulations which were observable at all times.

Furthermore, as demonstrated by the simulation study and experimental results, the EKF estimates are independent of the starting values. This is believed to help achieving "repeatability" of the results, an essential criteria for effective condition monitoring using parameter estimation approach.

7.6 Introducing Faults in the EHA Prototype

A major objective of this research is to use the EKF to detect faults in the EHA. As such, two faults were introduced in the system; increasing the viscous damping coefficient by attaching a damper to the symmetrical actuator and reducing the effective bulk modulus by connecting two, long flexible hoses filled with oil to the two chambers of the actuator in the EHA. It was believed that these circuit modifications would change the parameters of interest and that the EKF would be able to detect a change in the values of the parameters.

The procedure detailed in Section 7.2 to estimate the viscous damping coefficient was repeated but this time with a "damper" connected to the system. The "damper" consisted of a symmetrical actuator with a needle valve (bleed valve) connecting the two sides of the actuator. The inertial load of the EHA was connected to this second passive actuator, as shown in Figure 7.11. The friction characteristics of the custom made symmetrical actuator of the EHA was modified by adjusting the needle valve of the second, passive actuator. The measurements of interest were the load pressure and the actuator piston position, as shown in Figure 7.12. These data were stored in the computer and the EKF used the load pressure as its input, and the piston displacement as its measurement to estimate the viscous friction coefficient.

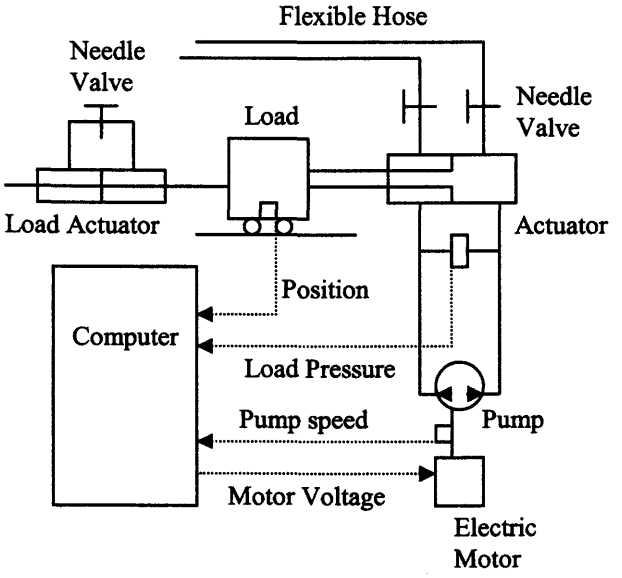

Figure 7.11: Simplified Schematic of the EHA and the "Faults" Introduced in the Experimental Rig

The measured load pressure and measured piston position when the damper was connected to the inertial load of the EHA, are shown in this Figure 7.12. Estimation of the viscous damping coefficient by the EKF, using measured data, is also illustrated in Figure 7.12 It is seen that although the measured piston position does not appear to change when compared to Figure 7.3 (scenario with no damper in the system), the measured load pressure increased. This was expected since a larger force was required to move the inertial load because of an increase in the opposing friction force (assumed to be due to increased viscous damping coefficient as a result of additional shearing of the fluid in the damper). The estimated viscous damping coefficient, illustrated in Figure 7.12, was 1970Ns/m, as compared to 761 Ns/m when no damper was used. This showed a significant increase in the estimated value for this parameter.

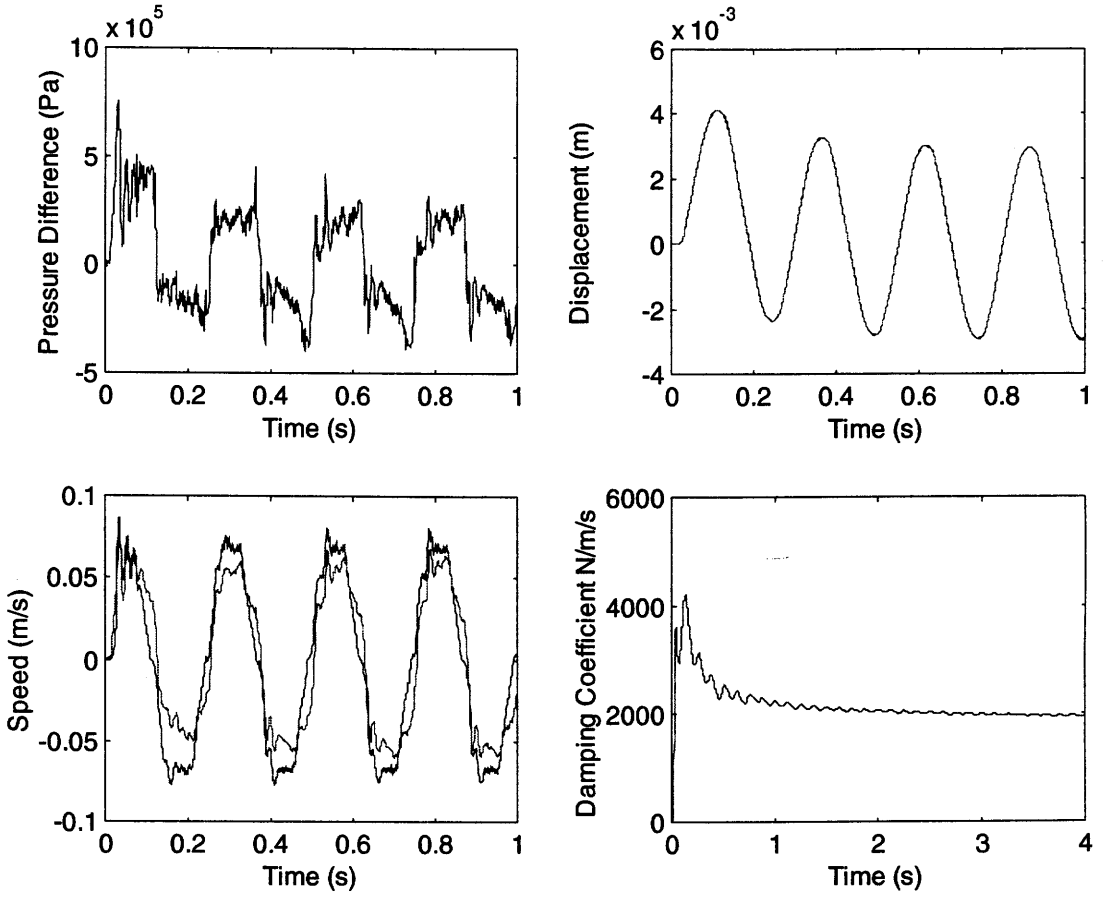

Figure 7.12: Estimated States and Parameter with a Damper Connected to EHA System

The experiment was repeated several times, with the same opening of the valve, and the results were found to be very repeatable (standard deviation was 9.2). These results are not presented here for brevity. The temperature of the oil was kept at $24 \pm 1\,^{0}C$ each time, by spacing the experiment in time to enable the oil to cool down. Also, it should be pointed out that the input signals lasted 4 seconds only and as such, temperature control was not difficult. Thermocouples were used to monitor the oil temperature both at the load actuator and at the EHA custom made actuator.

Next, by changing the opening of the valve (increasing), the damping coefficient was changed (reduced), as illustrated in Figure 7.13, where the estimated viscous damping coefficient was 1670Ns/m. Similarly, the experiment was performed several

times and the results were very repeatable (standard deviation was 8.7), provided that the temperature was constant.

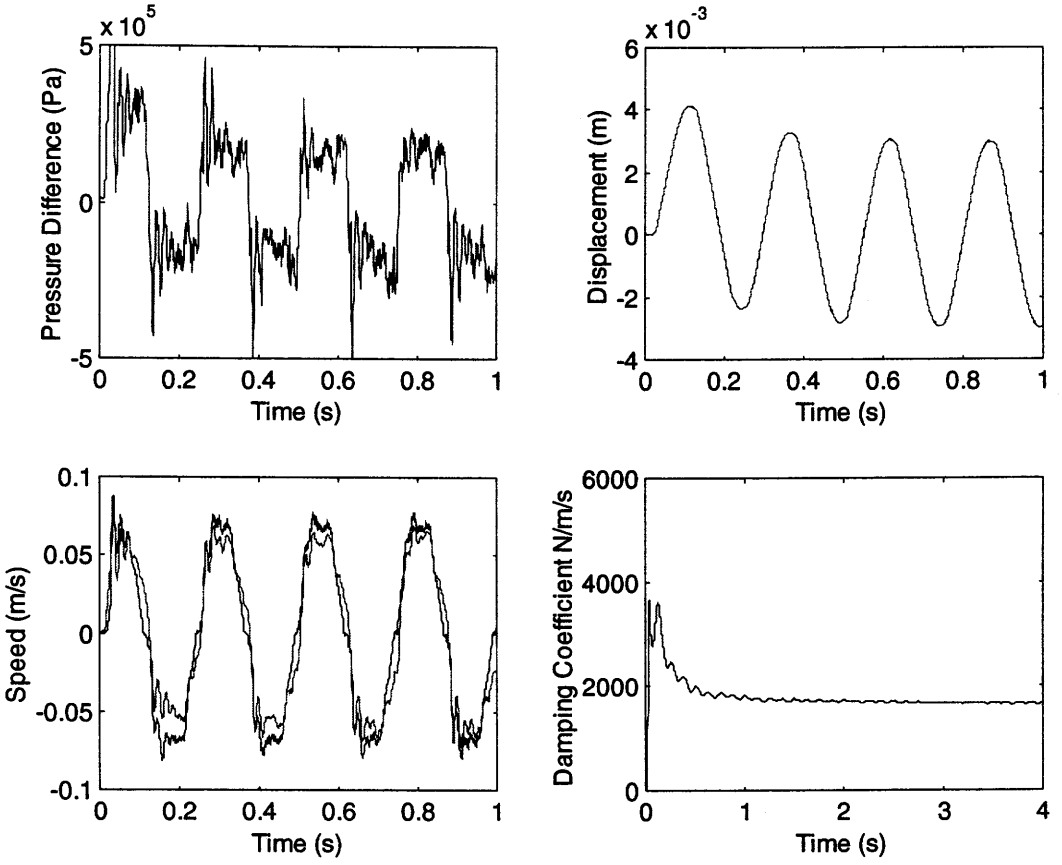

Figure 7.13: Estimated States and Parameter with a Damper Connected to EHA System and Reducing the Damping Coefficient by Opening the Valve

The second type of fault which was investigated was a reduction in the effective bulk modulus of the oil. This parameter was estimated in the EHA prototype, by first using the normal viscous damping coefficient value (760 Ns/m), i.e. with no damper in the system. As illustrated in the schematic of the experimental set up shown in Figure 7.11, this was achieved by connecting two flexible hoses filled with oil, one at each side of the actuator to mimic a reduction in the effective bulk modulus due to air entrapment. The EKF was used to estimate the effective bulk modulus for the modified system. The

estimation process for the effective bulk modulus with the hoses connected to the actuator is shown in Figure 7.14. It should be pointed out that the added volume of oil (in the hoses) was included in the EKF algorithm (to update the existing EHA model in the EKF algorithm).

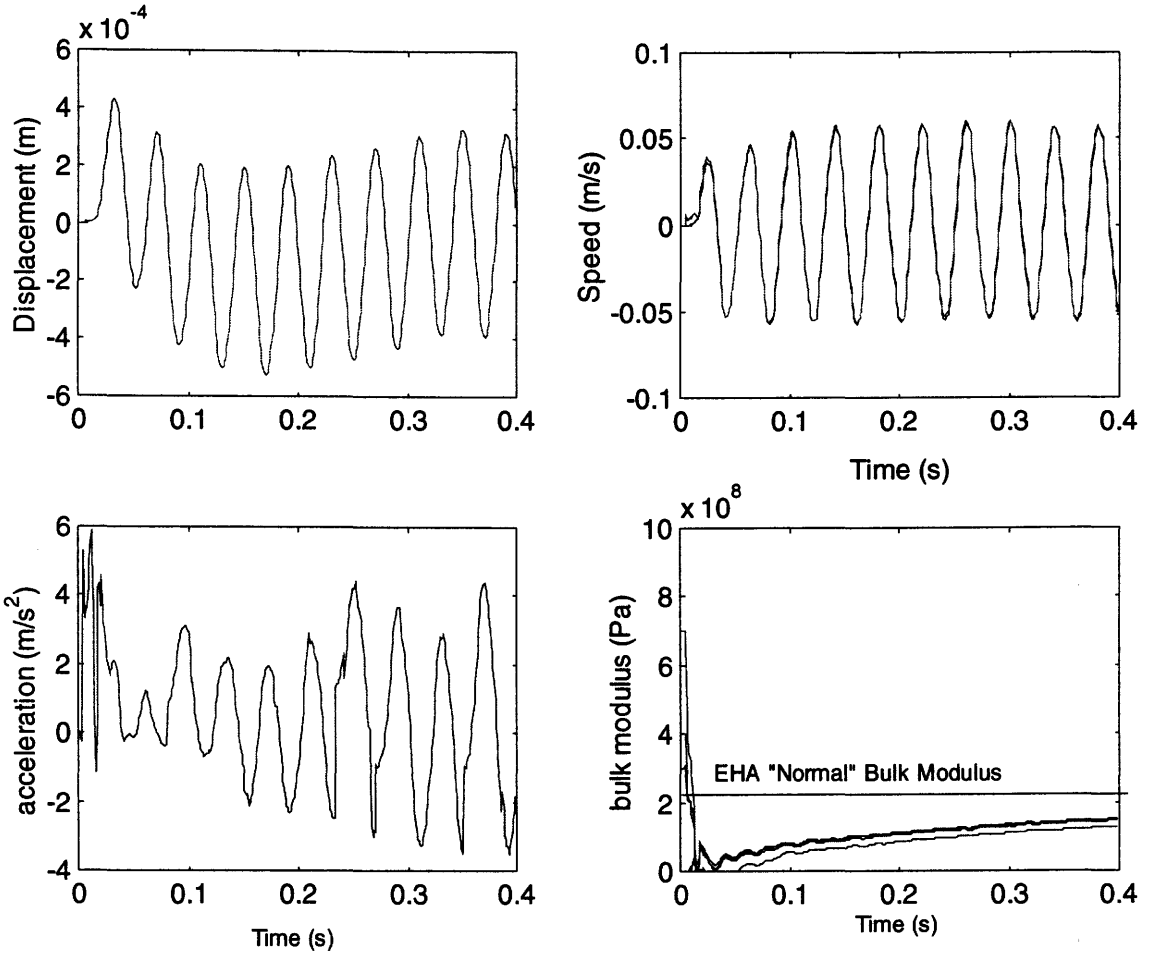

Figure 7.14: Estimated States and Parameter with Hoses Connected to the Actuator

From Figure 7.12, it can be seen that the measured position of the EHA was "different" from the measured response of a "healthy" EHA. This was due to a reduction in the natural frequency of the system as a result of a reduction of the effective bulk modulus. The measurements used from the EHA prototype were the pump angular velocity (used as the input to the EKF) and the piston position (used as

the measurement for the EKF). From Figure 7.14, the estimated effective bulk modulus was approximately 1.3×10^{8} Pa, irrespective of the initial value used for the effective bulk modulus in the EKF code. Previously, the estimated effective bulk modulus value was 2.1×10^{8} Pa. A reduction of the effective bulk modulus value was detected by the EKF and this reduction was due to the additional volume of entrained air in the oil in the hoses and because of the flexibility of the hoses. The experiment was repeated several times, without the damper in the system and results were found to be repeatable (standard deviation was 1.2×10^{7}). Results are not shown here for brevity. The temperature was kept at 24 ± 1^{0}C for all the tests.

Next, the effective bulk modulus was estimated in the EHA prototype with this time the damper connected (opening of valve kept constant) to the system, with hoses not connected. This was done to verify that the increase in damping coefficient did not affect the estimated effective bulk modulus of the EHA. Using the estimated damping coefficient of 1692 Ns/m (with the damper connected), the effective bulk modulus was found to show a slight change in its value (Mean was 2.24×10^{8} Pa and the standard deviation was 4.1×10^{6} when the experiment was repeated several times). The new damping coefficient value (1692 Ns/m) was used to update the model in the EKF.

In addition to the above scenario, the effective bulk modulus was also estimated in the EHA prototype with both the Damper connected (same opening of valve as previous case; viscous damping coefficient being 1692 Ns/m) to the system and with hoses connected (to reduce the effective bulk modulus in the prototype). The EKF detected a change in the effective bulk modulus and the results were similar to the case where no damper were connected but with hoses connected. The estimated effective bulk modulus was around 1.35×10^{8} Pa (the mean value) and had a standard deviation of 1.42×10^{7}.

Next, the viscous damping coefficient was estimated (with a reduced effective bulk modulus) with the EHA prototype by having the hoses connected to the system and with damper not connected. Using the simple model to estimate the viscous damping coefficient, the EKF estimated a value of 761 Ns/m repeatedly. The use of the complex

model to estimate the viscous damping coefficient (one which assumed a known value of effective bulk modulus) did not affect the estimated viscous damping coefficient.

7.7 Conclusions

In this chapter, the EKF has been applied to the EHA prototype to estimate two parameters, namely the viscous damping coefficient and the effective bulk modulus. The simulation study reported in Chapter 6, explained the methodology used and in this chapter, simulated data has been replaced by measured data.

The EKF estimated the two parameters using the same initial conditions as well as the same type of inputs used for the simulation study. It could be expected that the level of accuracy in the estimations of the parameters, for the prototype, was comparable to the accuracy level obtained from the simulation study. The EKF was also able to detect faults in the EHA prototype which were introduced by connecting a damper to the symmetrical actuator to mimic changes in viscous friction and by connecting two flexible hoses, one at each side of the actuator, to mimic a decrease in the effective bulk modulus. The experiments were repeated several times and the mean as well as the standard deviations in the results were reported in this chapter.

In the next chapter, the friction characteristics of the symmetrical actuator in the EHA would be investigated. This study on the symmetrical actuator of the EHA was motivated by experimental results which revealed the presence of a different friction model, other than the linear viscous friction model, which had been assumed so far in this thesis.

Chapter 8

Estimation of Nonlinear Friction Using EKF

The main focus of this chapter is to introduce a technique to estimate the nonlinear friction characteristics at the actuator for the Electrohydraulic actuator (EHA). In Chapter 3, a linearized model for the EHA was presented, where it was assumed that only viscous friction (a linear friction model) was present in the actuator. In so doing, a linearized load equation was obtained and the hydraulic model, after some mathematical manipulations, was approximated to a third order transfer function. However, as will be shown, experimental work has demonstrated the presence of nonlinear friction characteristics in the EHA prototype and in this chapter, a nonlinear friction model for the actuator is first measured and later, the coefficients of a proposed nonlinear friction model estimated. A novel quadratic model for the friction force is presented. The Extended Kalman Filter is subsequently used to estimate the coefficients for the quadratic function, taking into account observability conditions described earlier (that is estimation of the coefficients for the quadratic friction characteristics is done iteratively to ensure observability condition). Using the new friction characteristics, the effective bulk modulus is estimated using the procedure outlined in Chapter 6. Both simulation and experimental results are presented.

8.1 Friction Nonlinearities in Hydraulic Actuators

In hydraulic cylinders, movement of the piston (and of the fluid in the actuators) is subject to friction arising as a result of physical contact between moving and non moving parts and of shearing of the fluid between mating/moving parts. Static friction must be overcome before the piston can move. As the actuator piston starts to move, this friction force can decrease suddenly. These changes in friction can result in jerky actuator motion, commonly referred to as "stick-slip" friction. Stick-slip is a combination of static friction and a negative transition region and is found in the "Stribeck" region of the friction-velocity curve [Merrit, 1967].

Static friction is due to the overcoming of bonds (microscopic roughness) between two surfaces in contact and these bonds need to be sheared before motion starts. Viscous friction occurs as the fluid exerts resistance to shearing and it is directly proportional to the velocity. The viscous friction coefficient is proportional to the fluid viscosity, the area of contact and inversely proportional to the clearance or oil film thickness [Merrit, 1967].

In this study, a linear viscous friction model was assumed for the EHA. However, experimental results, as detailed in the next section, showed that friction characteristics in the EHA prototype, were nonlinear.

8.2 Nonlinear Friction Model For the Electrohydraulic Actuator

In this section, an attempt is made to generate an experimental friction-velocity curve. The experimental procedure consisted of keeping the piston velocity constant (zero acceleration) and measuring the pressure difference across the actuator. This approach has been successfully used by Burton to measure friction characteristics in an actuator as reported in [Burton, 1974].

For an ideal actuator with no slip stick, zero acceleration will imply that the force, required to move the piston at constant velocity, overcomes viscous friction and stick slip friction only as shown below:

$$(P_1 - P_2)A = M\ddot{x} + B\dot{x} + F_{static} + F_{transition} \tag{8.1}$$

Therefore, a series of triangular waves, which represented the desired piston position for the closed loop EHA system, was used as inputs to the EHA prototype and the pressure difference (load pressure) at each piston velocity was measured. The slope of the triangular input signal was in fact velocity. The procedure followed was to measure the point on the velocity-time trace in which the velocity was constant and then measure an average value of force. The magnitude of the actuation velocity was changed and the corresponding force recorded. The test was repeated many times at a constant temperature ($24 \pm 1\,^0$C) and the results shown in Figure 8.1. This Figure shows the measured forces required for overcoming friction and their corresponding constant piston velocities.

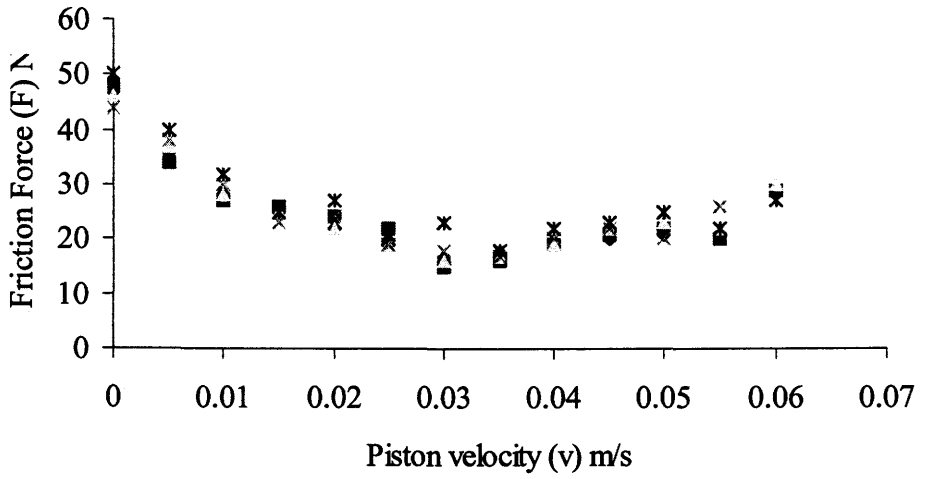

Figure 8.1: Measured Force Versus Measured Piston Velocity for the Actuator

8.2.1 Equivalent Viscous Friction

From Figure 8.1, it is observed that the force/velocity relationship is not linear (unlike the linear viscous friction model that was assumed so far in this thesis). Thus, a more realistic model for the friction should emulate the form shown in Figure 8.1 and in this study, a novel "quadratic" model is assumed. Also, the friction force measurement reveals that when the EKF was used to estimate the viscous friction coefficient in the prototype, as detailed in Chapter 7 (using a linear viscous friction model in the EKF), it was actually an "equivalent" viscous friction coefficient that was being estimated.

In this section, the "equivalent viscous friction coefficient is further investigated. Unlike in Chapter 7 where a sine wave of frequency of 4 Hz and amplitude of 0.01m was used as the input to the EHA prototype and resulting load pressure was the input to the EKF in order to estimate the viscous friction coefficient, in this section, a series of triangular waves are used as inputs to the closed loop EHA prototype and their resulting load pressures are used as inputs to the EKF. The slope of the triangular inputs translate into constant piston velocities. Thus, it was expected that as the piston velocities were changed, by changing the slopes of the triangular inputs, the value of the estimated viscous friction coefficient by the EKF would change as well, being larger at low piston velocities and lower at higher piston velocities. This is illustrated in Figure 8.2 where the triangular wave input translates into a piston velocity of 0.01 m/s in the EHA

prototype. The input to the EKF was the measured pressure difference; the measured piston displacement was used as the measurement for the EKF algorithm.

The estimated "equivalent" viscous friction coefficient value is 5051 Ns/m, which is much higher than the value estimated (760 Ns/m) in Chapter7 using a sine wave. It is also seen that the measured velocity is not "smooth", but instead tends to show "stick-slip" motion.

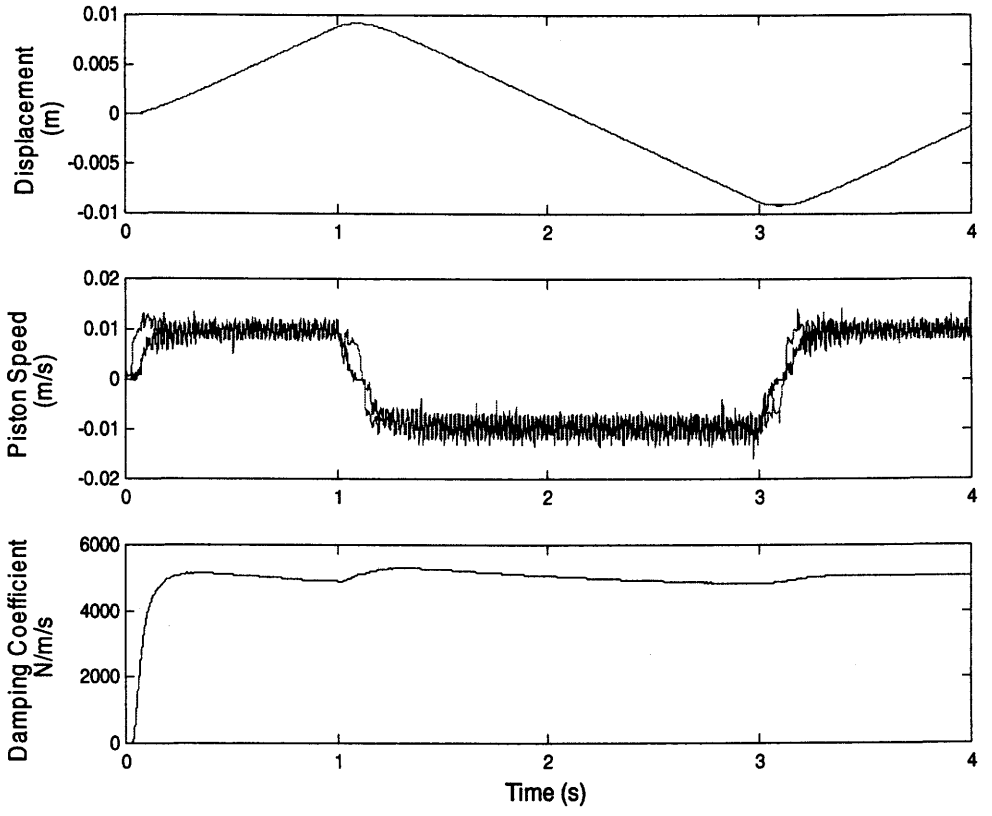

Figure 8.2: Estimating Viscous Damping Coefficient Using a Triangular Waveform.

The initial matrices used in the EKF were set as:

$$X(0) = [0 \quad 0 \quad 0]^T, \; R(k) = 1 \times 10^{-9} \tag{8.2}$$

$$Q(k) = \begin{bmatrix} 1\times10^{-9} & 0 & 0 \\ 0 & 1\times10^{-4} & 0 \\ 0 & 0 & 1\times10^{-4} \end{bmatrix},$$

$$P(0) = \begin{bmatrix} 1\times10^{2} & 0 & 0 \\ 0 & 1\times10^{2} & 0 \\ 0 & 0 & 1\times10^{7} \end{bmatrix}$$

The procedure was repeated at different piston velocities (using triangular inputs of different slopes) and "equivalent" viscous damping coefficients estimated each time. The estimated equivalent viscous friction coefficient at different piston velocities are summarized in Table 8.1.

Table 8.1: Estimated Viscous Damping Coefficient at Different Velocities

Measured Piston Velocity (m/s)	Estimated Equivalent Viscous Damping Coefficient (Ns/m)
0.01	5051
0.02	1904
0.03	1152
0.04	716
0.05	758
0.06	780
0.07	775

An illustration of the EKF algorithm estimation at a different velocity is shown in Figure 8.3. From the Figures 8.2 and 8.3 and from Table 8.1, it is evident that as the velocity is increased, the equivalent viscous friction coefficient converges to that found in Chapter 7 (760 Ns/m). From the estimations, it is seen that, at low piston velocities, the EKF estimates an equivalent viscous friction at a higher value than at higher velocities.

It should be mentioned here that the estimated "equivalent" viscous friction coefficient at each piston velocity was independent of the value used to initialize the parameter in the initial state matrix found in the EKF algorithm. This was consistent with the trends found in Chapters 6 and 7.

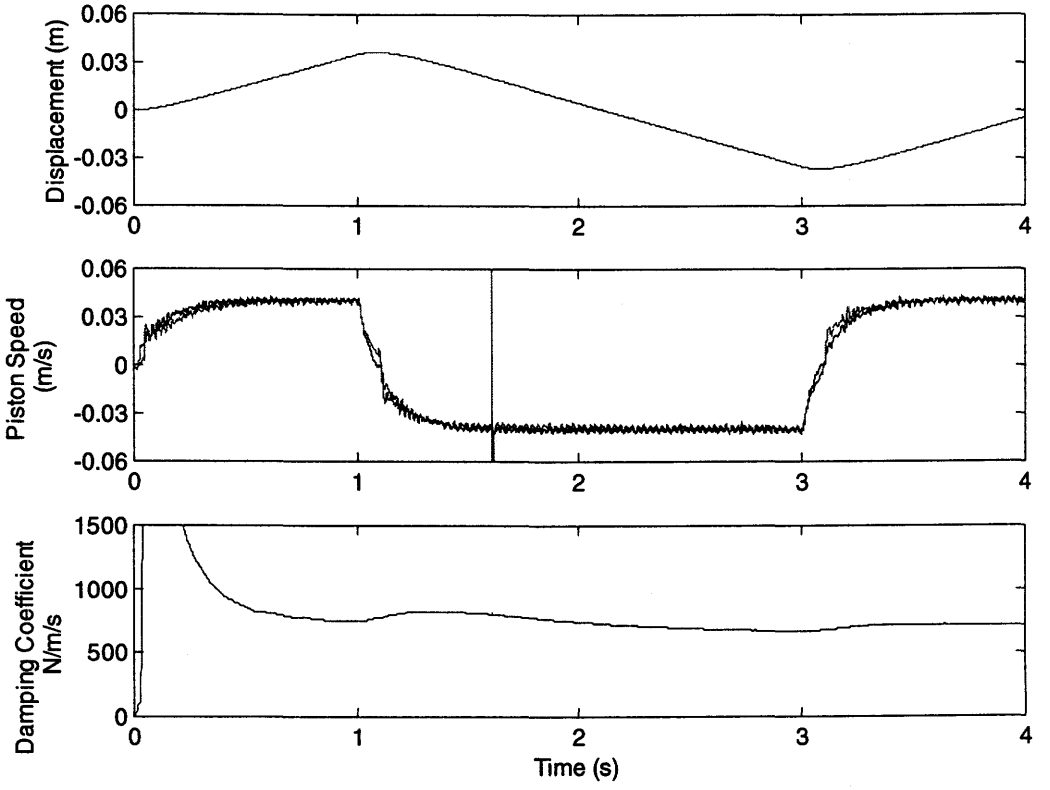

Figure 8.3: Estimating Viscous Damping Coefficient Using a Triangular Waveform at a Higher Piston Velocity (0.04 m/s)

From this section, it can be concluded that using a linear model for friction in the EKF to estimate the viscous friction coefficient in the prototype does result in an "effective" viscous friction coefficient being estimated by the filter. The use of a sine wave as the desired input to the prototype translates into a changing piston velocity profile for the actuator. The use of the load pressure as the input to the EKF and of the

piston displacement as the measurement for the EKF is sufficient to "characterize" the "equivalent" viscous friction coefficient. The load pressure, when the piston velocities are changing, is rich enough for the EKF to estimate the viscous friction coefficient repeatedly at constant temperature, as shown in Chapter 7.

8.2.2 Quadratic Friction Model

From the measured friction force/velocity characteristics for the actuator, a quadratic friction model was assumed for the Electrohydraulic Actuator friction characteristics. The actuator model can be expressed in the general form as given by Equation (8.3)

$$(P_1 - P_2)A = M\ddot{x} + a_1\dot{x}^2 + a_2\dot{x} + a_3 \tag{8.3}$$

where a_1, a_2, a_3 are the coefficients of the quadratic function. The coefficients of the quadratic are estimated using the Extended Kalman Filter, with the input to the filter being load pressure, $(P_1 - P_2)$ and with both piston velocity ($\dot{x}$) and piston position (x) being used as measurements. The coefficients of the quadratic expression are expressed as states in the model below with $X_3(k), X_4(k), X_5(k)$ assigned to a_1, a_2, a_3 respectively. (Note, the coefficients do change sign when velocity changes sign, i.e. when the piston extends and retracts and this is included in the EKF algorithm such that only the numerical value is of interest when the piston velocity is negative).

At this point it should be mentioned that with the increase in the number of states, the system is not observable. As will be demonstrated at a later stage in this Chapter, the EKF is made observable but first, the concept will be demonstrated with the unobservable system. The discrete state space model for Equation (8.3), (the coefficients of the quadratic expression are expressed as states in the model below with $X_3(k), X_4(k), X_5(k)$ assigned to a_1, a_2, a_3 respectively), can be expressed as follows:

$$X_1(k+1) = X_1(k) + T_s X_2(k) + T_s w_1(k)$$

$$X_2(k+1) = \frac{U(k)AT_s}{M} - \frac{X_3(k)T_s X_2(k)^2}{M} - \frac{X_4(k)X_2(k)T_s}{M} - \frac{X_5 T_s}{M} + X_2(k) + T_s w_2(k)$$

$$X_3(k+1) = X_3(k) + T_s w_3(k) \tag{8.4}$$

$$X_4(k+1) = X_4(k) + T_s w_4(k)$$

$$X_5(k+1) = X_5(k) + T_s w_5(k)$$

$$Z(k) = \begin{bmatrix} 1 & 0 & 0 & 0 & 0 \\ 0 & 1 & 0 & 0 & 0 \end{bmatrix} \begin{bmatrix} X_1(k) \\ X_2(k) \\ X_3(k) \\ X_4(k) \\ X_5(k) \end{bmatrix} + \begin{bmatrix} v_1(k) \\ v_2(k) \end{bmatrix}$$

$$\Phi(k) = \frac{\partial f(X(k))}{\partial X(k)} = \begin{bmatrix} \Phi_{11} & \Phi_{12} & \Phi_{13} & \Phi_{14} & \Phi_{15} \\ \Phi_{21} & \Phi_{22} & \Phi_{23} & \Phi_{24} & \Phi_{25} \\ \Phi_{31} & \Phi_{32} & \Phi_{33} & \Phi_{34} & \Phi_{35} \\ \Phi_{41} & \Phi_{42} & \Phi_{43} & \Phi_{44} & \Phi_{45} \\ \Phi_{51} & \Phi_{52} & \Phi_{53} & \Phi_{54} & \Phi_{55} \end{bmatrix}$$

$$\Phi_{11}(k) = 1, \Phi_{12}(k) = T_s, \Phi_{13}(k) = 0, \Phi_{14}(k) = 0, \ \Phi_{15}(k) = 0$$

$$\Phi_{21}(k) = 0, \Phi_{22}(k) = 1 - \frac{2X_3(k)X_2(k)T_s}{M} - \frac{X_4(k)T_s}{M}$$

$$\Phi_{23}(k) = -\frac{X_2(k)^2 T_s}{M}, \ \Phi_{24}(k) = -\frac{X_2(k)T_s}{M}, \Phi_{25}(k) = -\frac{X_5(k)T_s}{M}$$

$$\Phi_{31}(k) = 0, \ \Phi_{32}(k) = 0, \Phi_{33}(k) = 1, \Phi_{34}(k) = 0, \Phi_{35}(k) = 0$$

$$\Phi_{41}(k) = 0, \ \Phi_{42}(k) = 0, \Phi_{43}(k) = 0, \Phi_{44}(k) = 1, \Phi_{45}(k) = 0$$

$$\Phi_{51}(k) = 0, \ \Phi_{52}(k) = 0, \Phi_{53}(k) = 0, \Phi_{54}(k) = 0, \Phi_{55}(k) = 1$$

Preliminary simulation and experimental studies revealed that the triangular wave used to estimate the coefficients of the quadratic function was not a good waveform to use since only one velocity was available each time. There was not sufficient information available to the EKF to estimate the coefficients and therefore, a more reliable input was found to be one where the velocity was changing. Similar to Chapter 7, a sinusoid input (4 Hz, 0.01 m) was found to be more suitable (since it is richer in terms of range of velocity information) and some typical experimental results of the EKF algorithm in estimation of a_1, a_2, a_3 are shown in Figure 8.4. The temperature was kept constant at $24 \pm 1\,^0$C.

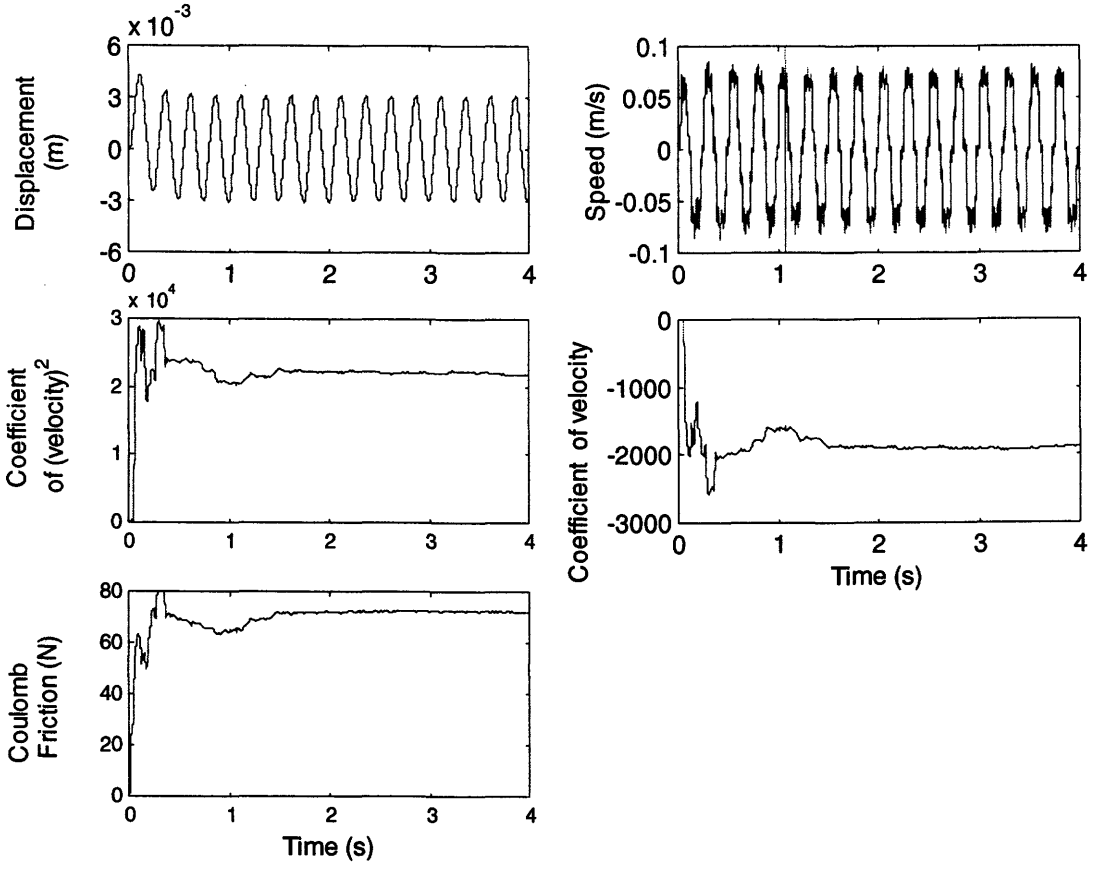

Figure 8.4: Estimation of the Coefficients of the Quadratic Friction Model in the EHA Prototype Using the EKF

The initial matrices used in the EKF were set as:

$$X(0) = [0 \quad 0 \quad 0 \quad 0 \quad 0]^T,$$

$$R(k) = \begin{bmatrix} 1\times10^{-10} & 0 \\ 0 & 1\times10^{-3} \end{bmatrix} \tag{8.5}$$

$$Q(k) = \begin{bmatrix} 1\times10^{-10} & 0 & 0 & 0 & 0 \\ 0 & 1\times10^{-7} & 0 & 0 & 0 \\ 0 & 0 & 1\times10^{-7} & 0 & 0 \\ 0 & 0 & 0 & 1\times10^{-4} & 0 \\ 0 & 0 & 0 & 0 & 1\times10^{-2} \end{bmatrix},$$

$$P(0) = \begin{bmatrix} 1\times10^9 & 0 & 0 & 0 & 0 \\ 0 & 1\times10^9 & 0 & 0 & 0 \\ 0 & 0 & 1\times10^9 & 0 & 0 \\ 0 & 0 & 0 & 1\times10^9 & 0 \\ 0 & 0 & 0 & 0 & 1\times10^9 \end{bmatrix}$$

From Figure 8.4, it can be seen that the estimated states (superimposed on measured states), displacement and velocity match the measured states closely. The EKF estimated the coefficients a_1, a_2, a_3 as 2.176×10^4, -1.885×10^3 and 73.2 respectively. A plot of the measured friction-velocity relationship of the prototype using the estimated coefficients is shown in Figure 8.5. The curve (solid line) is the estimated friction force-velocity relationship.

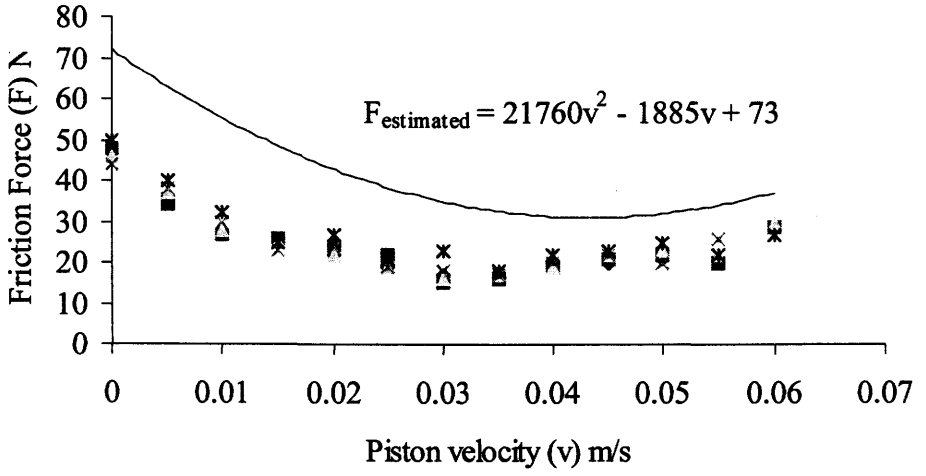

Figure 8.5: Estimated Friction Model Compared to Measured Friction Model

From Figure 8.5, the estimated friction model and measured friction characteristic differ. In addition, the estimation results were found not to be repeatable (± 12 % variation about the mean values). As mentioned earlier, Equation (8.4) was in fact not observable. Therefore, a somewhat unique methodology was used to estimate the coefficients for the quadratic in an iterative fashion in order to ensure that observability condition was met and in order to achieve a closer fit between the

estimated friction "curve" and the measured friction "curve". This was similar to the approach used to iteratively determine the equivalent viscous friction coefficient and effective bulk modulus as discussed in Chapter 6.

Using the same set of data as in the previous section, i.e using a sine wave of 4Hz in frequency and 0.01 m in amplitude as input to the EHA, the load pressure as input to the EKF and with the measurement for the EKF being the piston position, the Coulomb friction coefficient (a_3) was first estimated assuming that the other coefficients were zero. The equation now becomes that described in Equation (8.6).

$$\begin{aligned} &(P_1 - P_2)A = M\ddot{x} + a_3 \\ &a_3 > 0, \dot{x} > 0 \\ &a_3 < 0, \dot{x} < 0 \end{aligned} \tag{8.6}$$

The discrete state space formulation of Equation (8.6) is expressed as follows:

$$X_1(k+1) = X_1(k) + T_s X_2(k) + T_s w_1(k) \tag{8.7}$$

$$X_2(k+1) = \frac{U(k)AT_s}{M} - \frac{X_3(k)T_s}{M} + X_2(k) + T_s w_2(k)$$

$$X_3(k+1) = X_3(k) + T_s w_3(k)$$

$$Z(k) = X_1(k) + v(k)$$

where $X_1(k)$, $X_2(k)$, $X_3(k)$ are the displacement, velocity and Coulomb friction coefficient a_3 respectively, $w(k)$ is the system noise, $U(k) = (P_1 - P_2)$ is the pressure difference between the actuator chambers, $Z(k)$ is the measurement vector and $v(k)$ represents the measurement or sensor noise.

The linearized system matrix is:

$$\Phi(k) = \frac{\partial f(X(k))}{\partial X(k)} = \begin{bmatrix} \Phi_{11}(k) & \Phi_{12}(k) & \Phi_{12}(k) \\ \Phi_{21}(k) & \Phi_{22}(k) & \Phi_{23}(k) \\ \Phi_{31}(k) & \Phi_{32}(k) & \Phi_{33}(k) \end{bmatrix}, \tag{8.8}$$

where $\Phi_{11}(k) = 1, \Phi_{12}(k) = T_s, \Phi_{13}(k) = 0$

$$\Phi_{21}(k) = 0,\ \Phi_{22}(k) = 1,\ \Phi_{23}(k) = -\frac{T_s}{M},$$

$$\Phi_{31}(k) = 0,\ \Phi_{32}(k) = 0,\ \Phi_{33}(k) = 1$$

The results of the EKF estimations are shown in Figure 8.6 where a_3 converges to a value of 46 N.

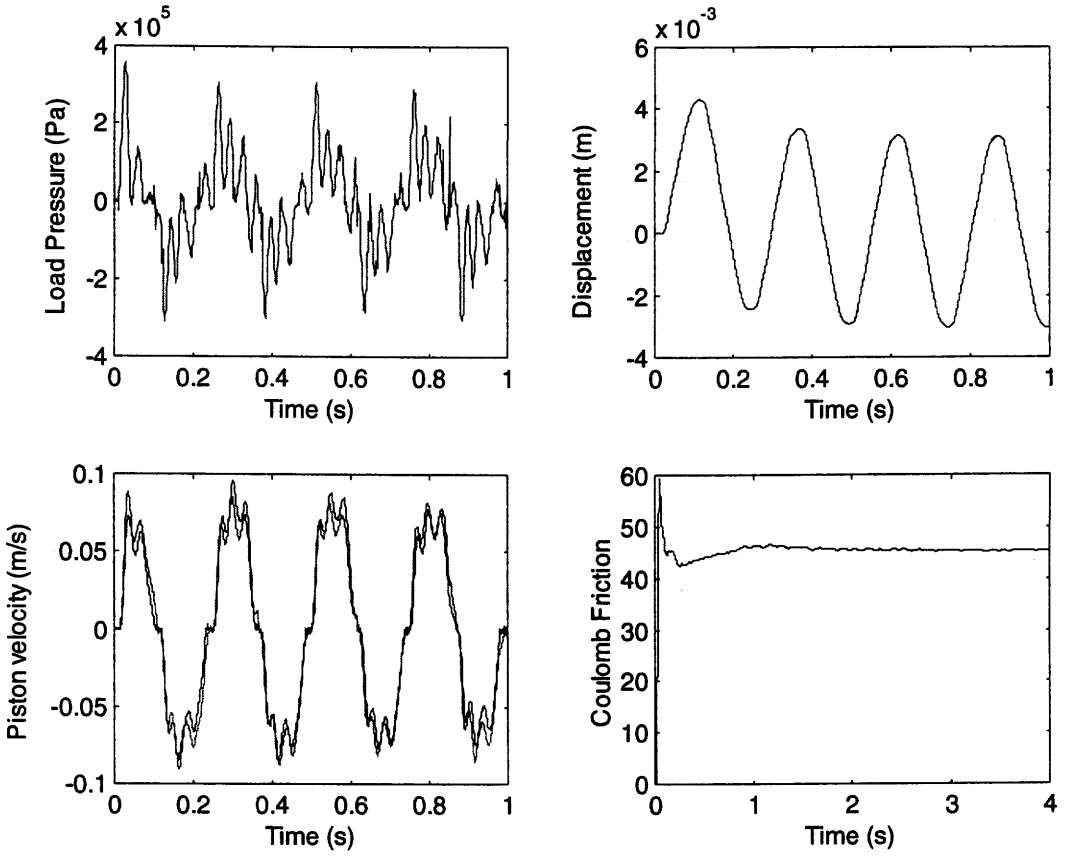

Figure 8.6: Estimating a_3 (Coulomb Friction) in the Quadratic Friction Model for the Electrohydraulic Actuator Prototype

The initial matrices used in the EKF were set as

$$X(0)=[0 \quad 0 \quad 0]^T \quad , \; R(k)=1\times10^{-9} \tag{8.9}$$

$$P(0)=\begin{bmatrix} 1\times10^{9} & 0 & 0 \\ 0 & 1\times10^{9} & 0 \\ 0 & 0 & 1\times10^{9} \end{bmatrix},$$

$$Q(k)=\begin{bmatrix} 1\times10^{-9} & 0 & 0 \\ 0 & 1\times10^{-12} & 0 \\ 0 & 0 & 1\times10^{-4} \end{bmatrix}$$

From Figure 8.6, it is seen that the estimated piston displacement and velocity match the measured displacement and velocity closely (shown as superimposed plots). The estimated Coulomb friction was 46 N. The estimated value was also very close to the measured value for friction, using the triangular waves as inputs, when the velocity was small. The system was observable (with the rank of the observability matrix and the state matrix length both being equal to 3 for all iterations), It was also verified that the estimated Coulomb friction in the EHA prototype was independent of its initial value used to initialize the state matrix in the EKF algorithm, as illustrated in Figure 8.7.

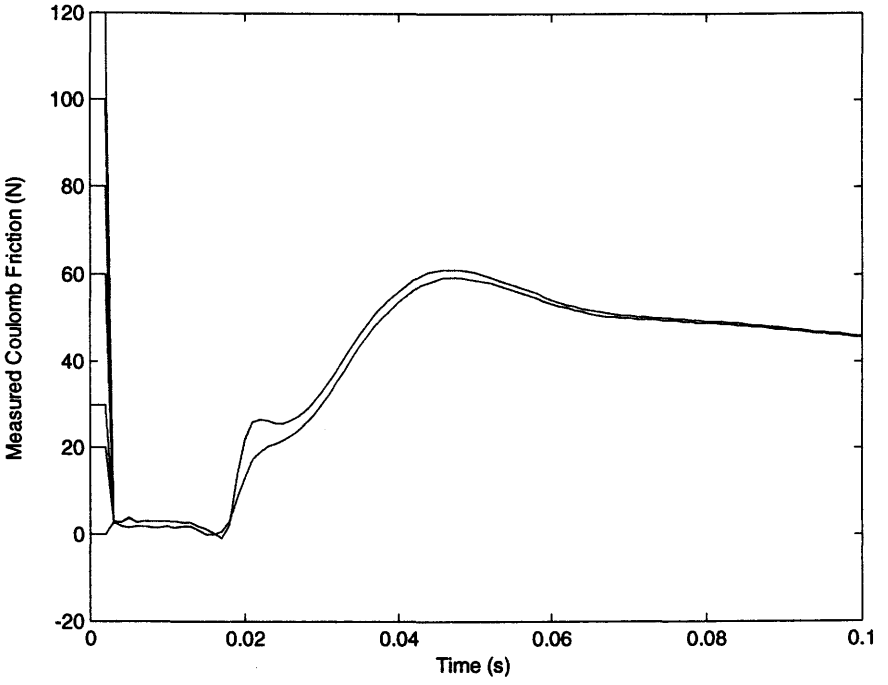

Figure 8.7: Estimation of Coulomb Friction in the Prototype when Different Starting Values are Used to Initialize the EKF Algorithm

In the study carried out by [Zavarehi, 1997], it was reported that the "*Coulomb Friction estimation was inaccurate and had a bias due to lack of observalibity*". In this study, a simpler and observable spate space model was embedded in the EKF and then used to estimate Coulomb friction. It is worth mentioning that the system was

observable even though only the piston displacement was used as the only measurement. No improvement was found (in this particular case) in the estimation process when both piston position and velocity were used as measurements.

Using the known estimated Coulomb friction coefficient (a_3), the other two coefficients of the quadratic friction model, a_1 and a_2, were then estimated together by using the EKF technique. In this case, both piston position and velocity were used to make the state space model observable. The discrete state space system is given in Equation (8.10).

$$X_1(k+1) = X_1(k) + T_s X_2(k) + T_s w_1(k) \tag{8.10}$$

$$X_2(k+1) = \frac{U(k)AT_s}{M} - \frac{X_3(k)T_s X_2(k)^2}{M} - \frac{X_4(k)X_2(k)T_s}{M} - \frac{a_3 T_s}{M} + X_2(k) + T_s w_2(k)$$

$$X_3(k+1) = X_3(k) + T_s w_3(k)$$

$$X_4(k+1) = X_4(k) + T_s w_4(k)$$

$$Z(k) = \begin{bmatrix} 1 & 0 & 0 & 0 & 0 \\ 0 & 1 & 0 & 0 & 0 \end{bmatrix} \begin{bmatrix} X_1(k) \\ X_2(k) \\ X_3(k) \\ X_4(k) \end{bmatrix} + \begin{bmatrix} v_1(k) \\ v_2(k) \end{bmatrix}$$

$$\Phi(k) = \frac{\partial f(X(k))}{\partial X(k)} = \begin{bmatrix} \Phi_{11}(k) & \Phi_{12}(k) & \Phi_{13}(k) & \Phi_{15}(k) \\ \Phi_{21}(k) & \Phi_{22}(k) & \Phi_{23}(k) & \Phi_{24}(k) \\ \Phi_{31}(k) & \Phi_{32}(k) & \Phi_{33}(k) & \Phi_{34}(k) \\ \Phi_{41}(k) & \Phi_{42}(k) & \Phi_{43}(k) & \Phi_{44}(k) \end{bmatrix}$$

$$\Phi_{11}(k) = 1, \Phi_{12}(k) = T_s, \Phi_{13}(k) = 0, \Phi_{14}(k) = 0, \Phi_{21}(k) = 0$$

$$\Phi_{22}(k) = 1 - \frac{2X_3(k)X_2(k)T_s}{M} - \frac{X_4(k)T_s}{M} \quad \Phi_{23}(k) = -\frac{X_2(k)^2 T_s}{M}, \quad \Phi_{24}(k) = -\frac{X_2(k)T_s}{M},$$

$$\Phi_{31}(k) = 0, \ \Phi_{32}(k) = 0, \Phi_{33}(k) = 1, \Phi_{34}(k) = 0,$$

$$\Phi_{41}(k) = 0, \Phi_{42}(k) = 0, \Phi_{43}(k) = 0, \Phi_{44}(k) = 1.$$

Estimation of the coefficient of the quadratic friction model is illustrated in Figure 8.8. The estimated position and velocity match the measured states very closely and the estimated coefficients were $a_1 = 2.1 \times 10^4$ and $a_2 = -1450$.

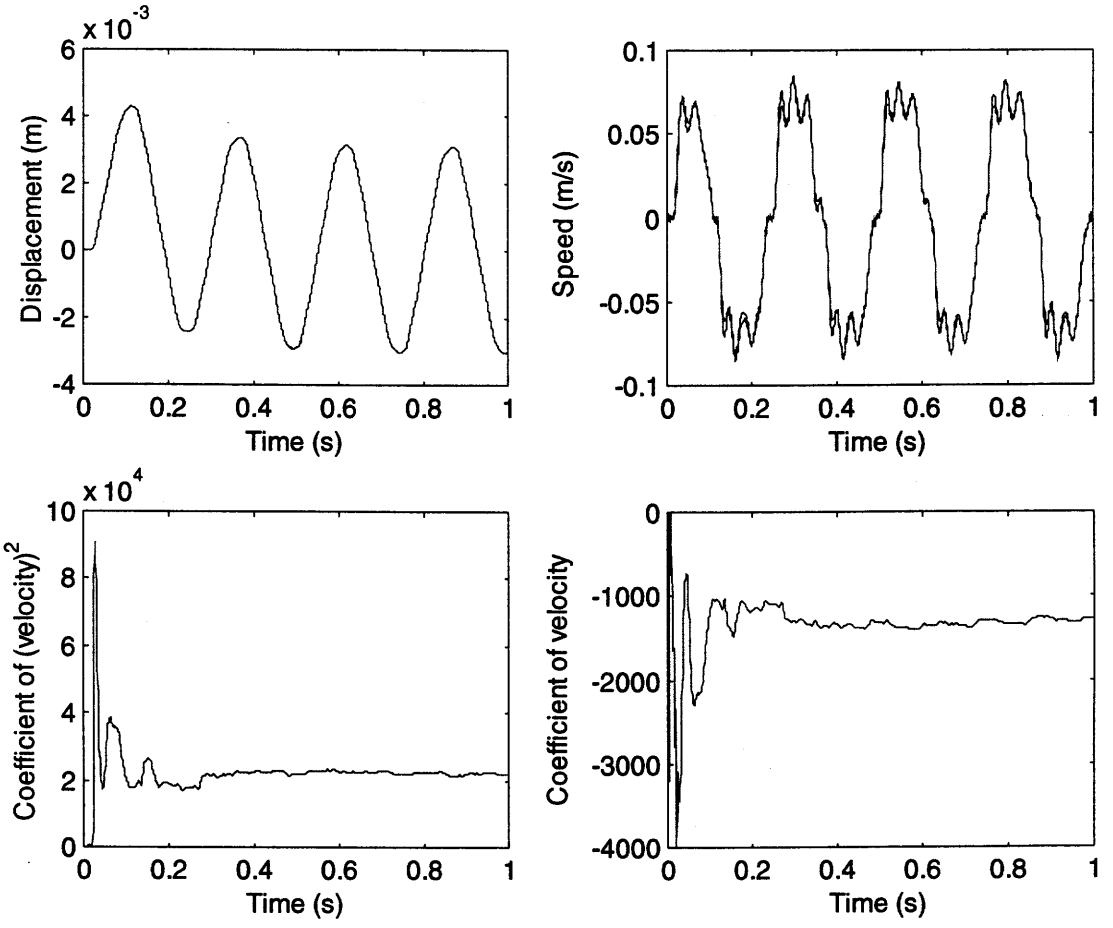

Figure 8.8: Estimation of Coefficients for Quadratic Friction Model

Furthermore, similar to previous sections in this thesis, the initial values used for the coefficients a_1 and a_2 of the quadratic friction model were changed in the EKF algorithm and as illustrated in Figure 8.9, it was verified that the estimated values were independent of the initial matrix used.

The initial matrices used for the EKF were set as:

$$X(0)=[0 \quad 0 \quad 0 \quad 0]^T \quad , R(k)=\begin{bmatrix} 1\times10^{-12} & 0 \\ 0 & 1\times10^{-3} \end{bmatrix} \tag{8.11}$$

$$P(0)=\begin{bmatrix} 1\times10^{9} & 0 & 0 & 0 \\ 0 & 1\times10^{9} & 0 & 0 \\ 0 & 0 & 1\times10^{10} & 0 \\ 0 & 0 & 0 & 1\times10^{9} \end{bmatrix}$$

$$Q(k)=\begin{bmatrix} 1\times10^{-12} & 0 & 0 & 0 \\ 0 & 1\times10^{-7} & 0 & 0 \\ 0 & 0 & 1\times10^{-7} & 0 \\ 0 & 0 & 0 & 1\times10^{-4} \end{bmatrix}$$

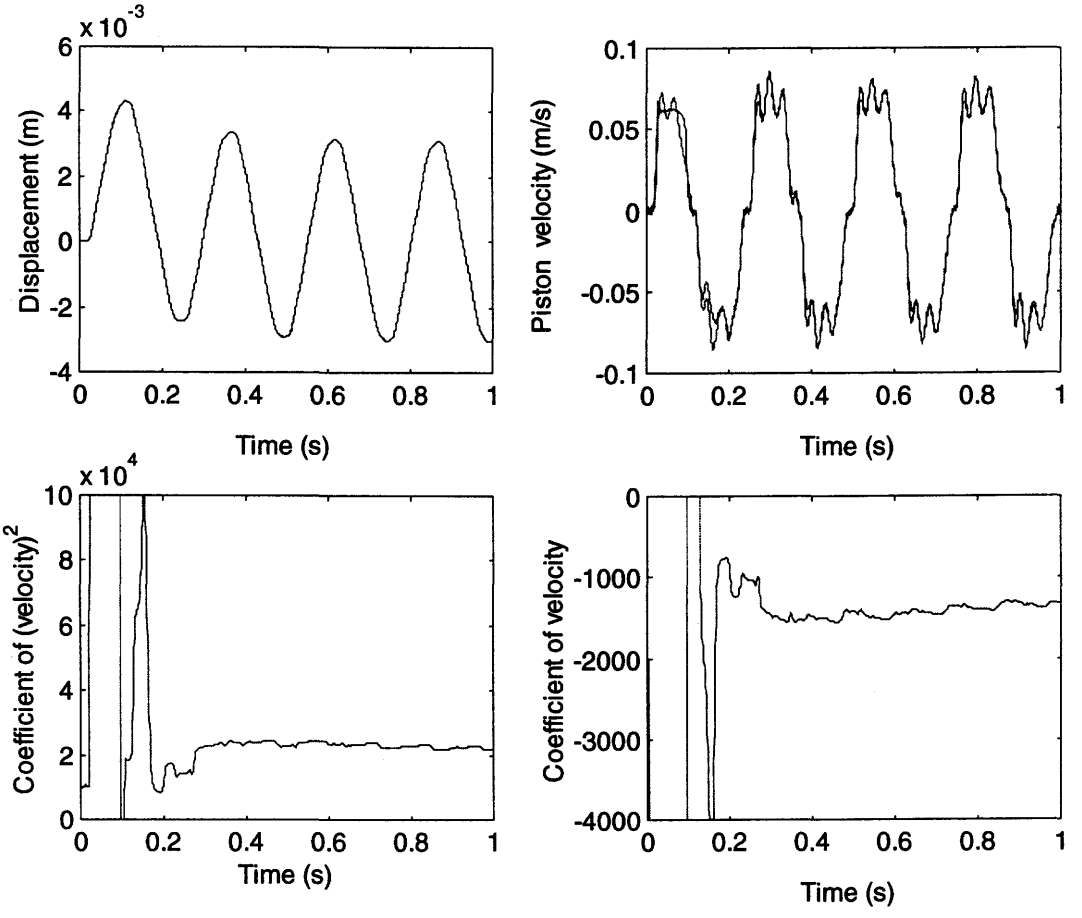

Figure 8.9: Estimation of Coefficients for Quadratic Friction Model Using Different Starting Values in the EKF for the Coefficients of the Model

Thus, the estimated friction model can be summarized as follows:

$(P_1 - P_2)A = M\ddot{x} + 2.1\times10^4\dot{x}^2 - 1450\dot{x} + 46$, when $\dot{x}>0$ (illustrated in Figure 8.10)

$(P_1 - P_2)A = M\ddot{x} - 2.1\times10^4\dot{x}^2 - 1450\dot{x} - 46$ when $\dot{x}<0$. (illustrated in Figure 8.11)

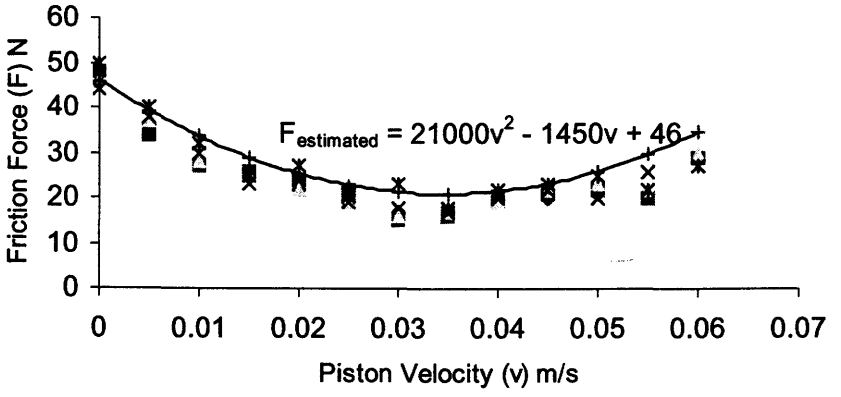

Figure 8.10: Quadratic Friction Model for Positive Piston Velocities

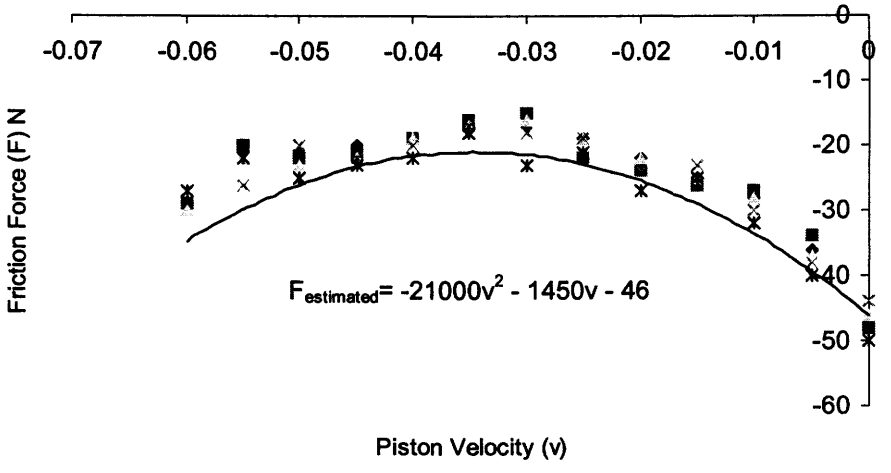

Figure 8.11: Quadratic Friction Model for Negative Piston Velocities

An LVDT (position transducer) was also used in the EHA prototype to estimate the quadratic friction characteristics under noisy signal conditions. A velocity transducer measured the piston velocity. The noisy position measurement was used to estimate the coefficient a_3 of the quadratic friction model. The Coulomb friction estimation is shown in Figure 8.12. Load pressure was used as the input to the EKF.

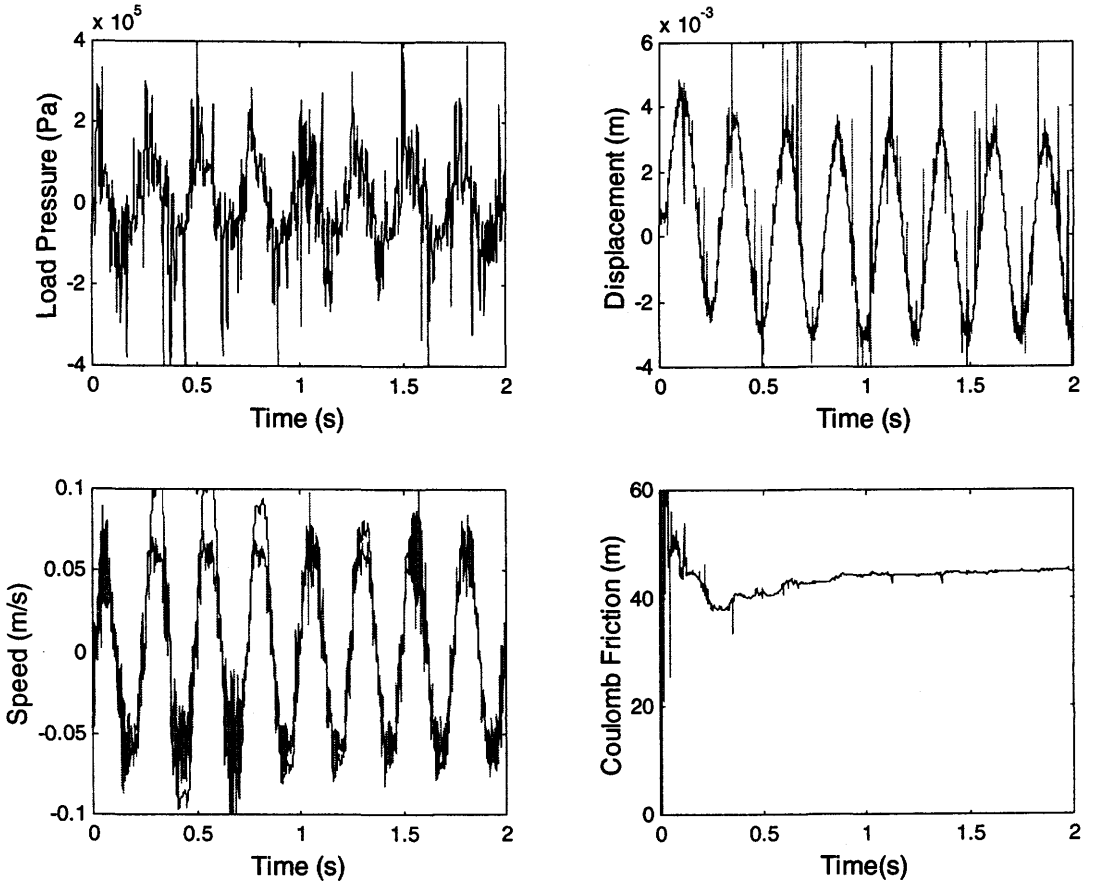

Figure 8.12: Estimation of Coulomb Friction in the EHA Prototype Using Noisy Measurements and Equation (8.10).

The estimated Coulomb friction was 46 N. The estimated displacement (which is shown as a superimposed plot) "follows" the noisy measurements. Using $a_3 = 46$, the EKF was used to estimate a_1 and a_2, as shown in Figure 8.13. The estimated values

were $a_1 = 2.26 \times 10^4$ and $a_2 = -1448$ as compared to $a_1 = 2.1 \times 10^4$ and $a_2 = -1450$ for the previous test.

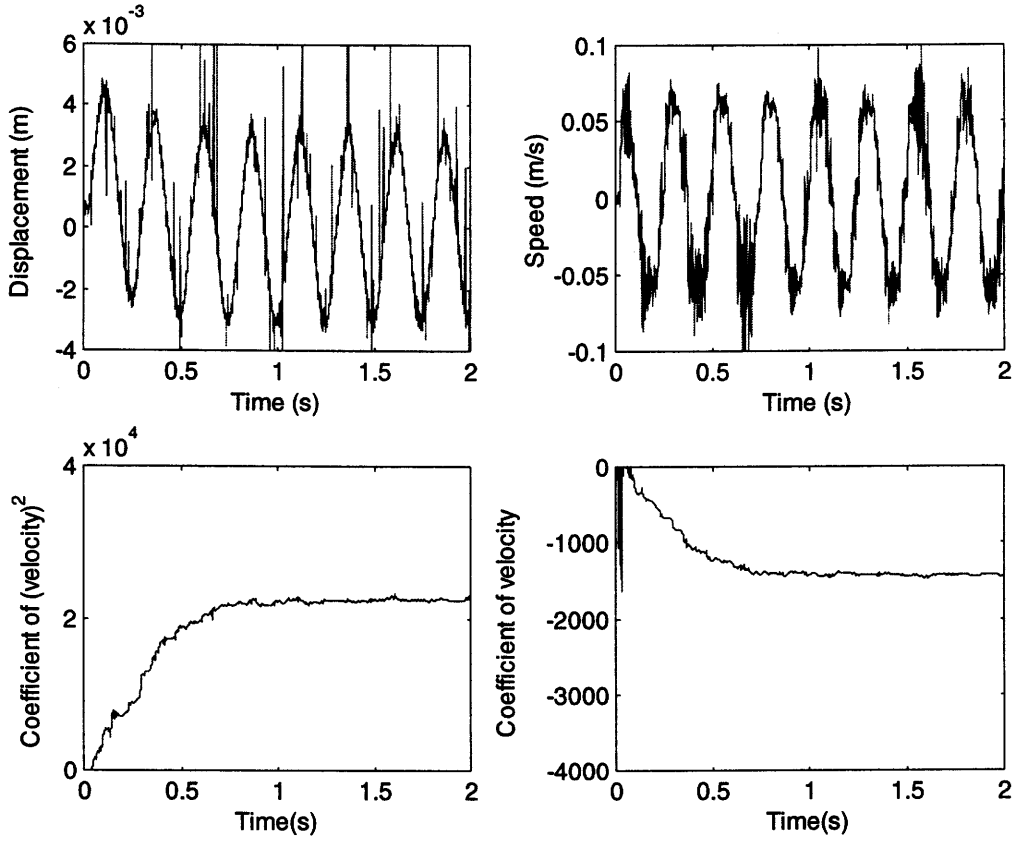

Figure 8.13: Estimation of the Coefficients of the Quadratic Friction Model Using Noisy Measurements from the LVDT

It must be mentioned that the initial matrices used in the EKF algorithm, when noisy data were used as measurement, were different from the matrices used when "clean" data were used.

8.2.3 Summary

From the experiments conducted to measure the friction characteristics and from the EKF estimations using the optical encoder, a quadratic non-linear friction model was considered and based on experimental results, the resulting form was:

$(P_1 - P_2)A = M\ddot{x} + 2.1\times10^4\dot{x}^2 - 1450\dot{x} + 46$, when $\dot{x}>0$ (Illustrated in Figure 8.10)

$(P_1 - P_2)A = M\ddot{x} - 2.1\times10^4\dot{x}^2 - 1450\dot{x} - 46$ when $\dot{x}<0$. (Illustrated in Figure 8.11)

Also, it was found that using the iterative approach to maintain observability of the EKFs, the estimated coefficients were more repeatable and were closer to the measured friction "curve". However it should be pointed out that repeatability of results was dependent on doing the test at the same temperature. Therefore, using the above friction model (which has been experimentally determined), a more accurate simulation of the EHA model was possible, as explained in the next section.

8.3 Simulation Study Using the Quadratic Friction Model

In this section, an "improved" EHA model is used to conduct an extensive simulation study first involving (for completeness and to be consistent with previous chapters) the estimations of the coefficients of the quadratic function for a normal simulated system using the EKF and then estimations of changes in the simulated friction characteristics. This is done to verify that the EKF can, in fact, estimate changes in the known coefficients values and to know the level of accuracy in the predictions. Also, similar to previous chapters, the initial values used in the EKF (to initialize the state matrix) are changed.

An additional simulation is done whereby the simulated EHA model (plant) having a quadratic friction characteristic at the actuator is used with the EKF to estimate the equivalent viscous friction value where the EKF has a linear friction model embedded in it. This study is similar to that carried out on the experimental system with nonlinear friction and the EKF with a viscous friction only model. The simulated load pressures (for both the linear friction scenario and the quadratic friction scenario) are compared to measured load pressures from the EHA prototype and a visual comparison made. Finally the improved EHA simulated model is used to estimate the effective bulk modulus but with a nonlinear friction model embedded in the EKF.

The friction model given in Equations (8.9) and (8.10) was used in the nonlinear Matlab/Simulink® EHA model (plant) and the EKF was used to estimate the coefficients of the quadratic function iteratively once again to maintain observability.

Only the Coulomb friction was estimated by assuming that a_1 and a_2 were initially zero. The state space formulation was described in Equation 8.9 and the initial matrices used given in Equation 8.10. From Figure 8.14, it is seen that the estimated coulomb friction value is 45.2N, showing an estimation error of 1.7 %.

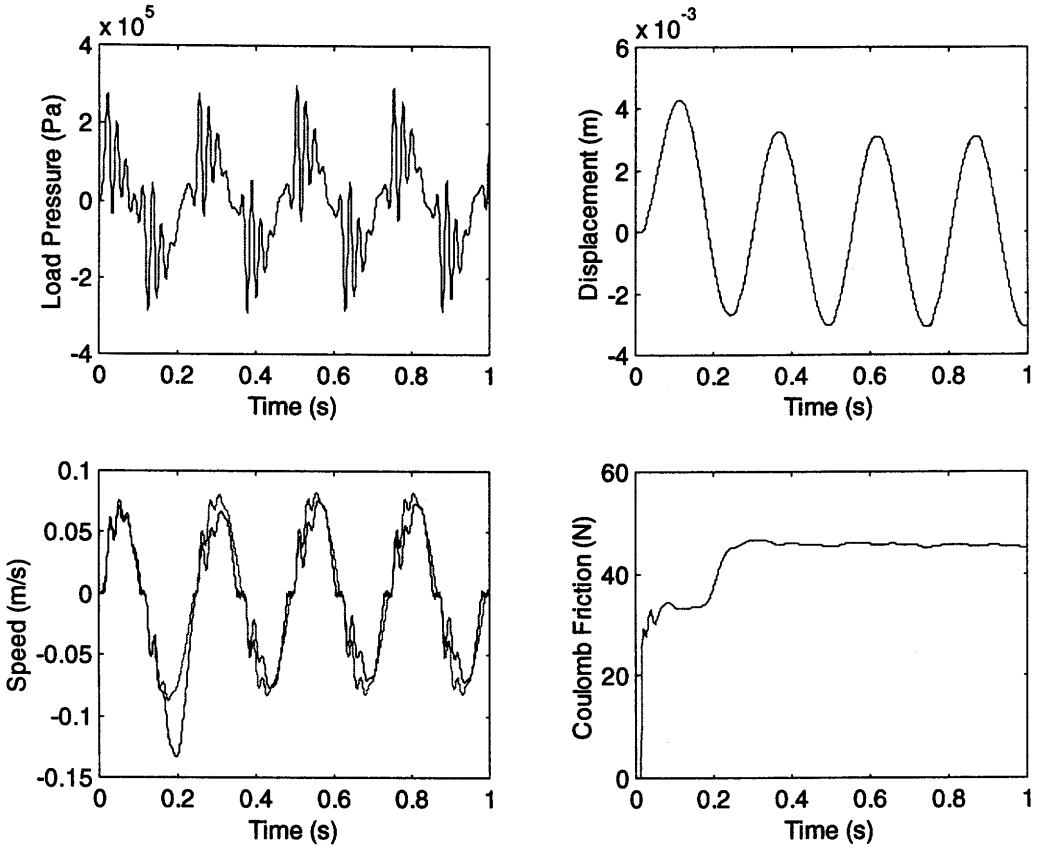

Figure 8.14: Estimated Coulomb Friction in Simulation using Quadratic Friction Model

In addition, the initial value used in the EKF algorithm to estimate the simulated Coulomb friction was changed (increased and decreased) and the results are shown in Figure 8.15. It is seen that the estimated Coulomb friction is independent of the initial value used.

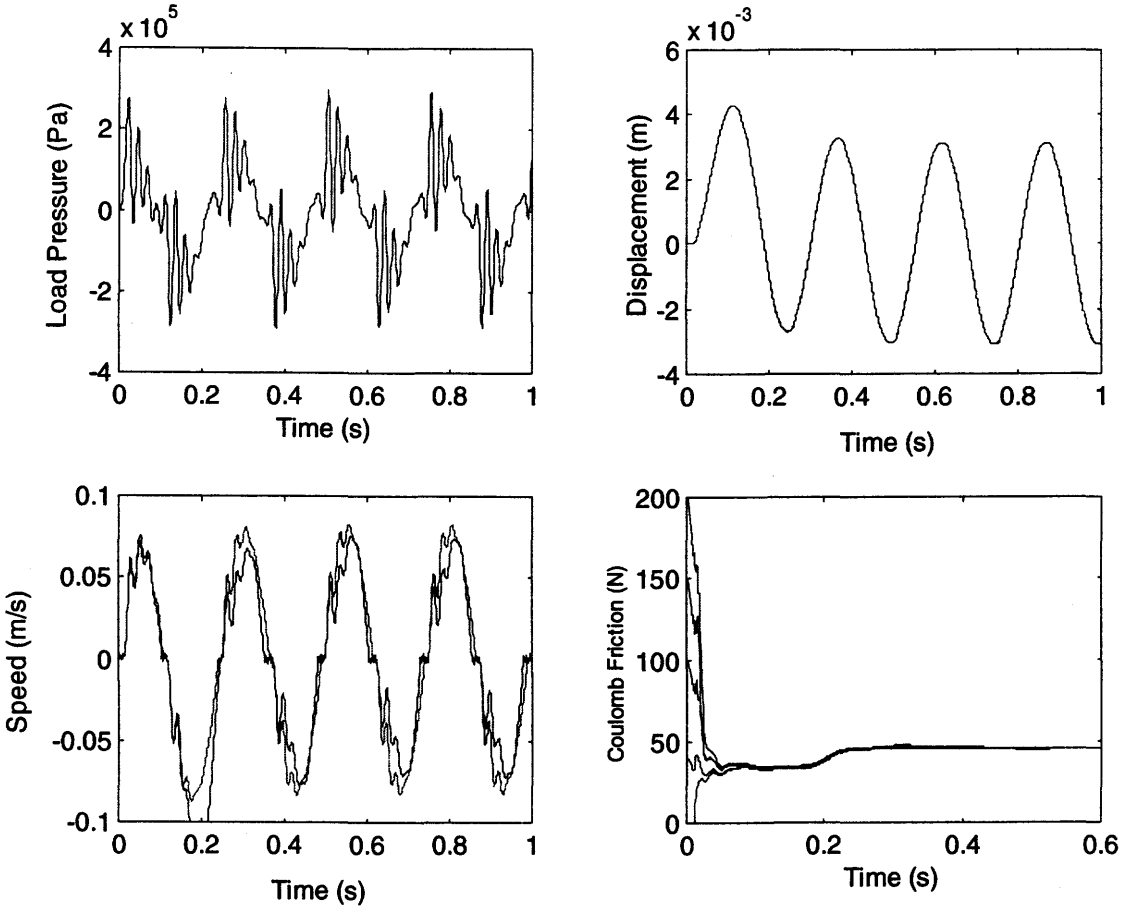

Figure 8.15: Estimating Coulomb Friction in the Simulated Model of the EHA Having the Quadratic Friction Model.

For condition monitoring purposes, changes in the Coulomb friction have to be detected. Therefore, in the simulated EHA model (plant), the Coulomb friction was both increased and decreased and the EKF used in each case to estimate the corresponding values. These results are illustrated by means of Figure 8.16. The EKF estimated the parameter to within 3% error each time (the results are not tabulated for brevity).

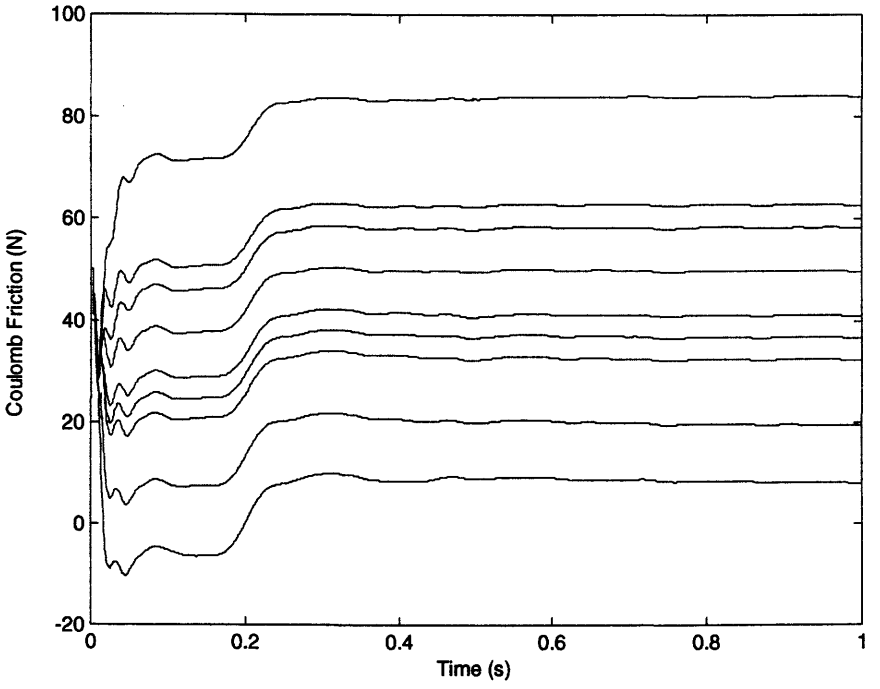

Figure 8.16: Estimating Changes in Coulomb Friction in Simulation

The next step was to use the estimated value for Coulomb friction in the EKF model and estimate the remaining coefficients of the quadratic function. The state space formulation and initial matrices used were given in Equation (8.10) and the estimated coefficients of the quadratic friction model are shown in Figure 8.17. The simulated position and velocity are very close to the estimated states and the estimated parameters are $a_1 = 2.1195 \times 10^4$ (1% error) and $a_2 = -1456$ (0.4 % error). Also, for the observability condition to be satisfied, both piston position and velocity must be used in the estimation process. The initial state matrix (in the EKF algorithm) is also changed and, as illustrated by Figure 8.18, the estimated values are independent of the initial values used.

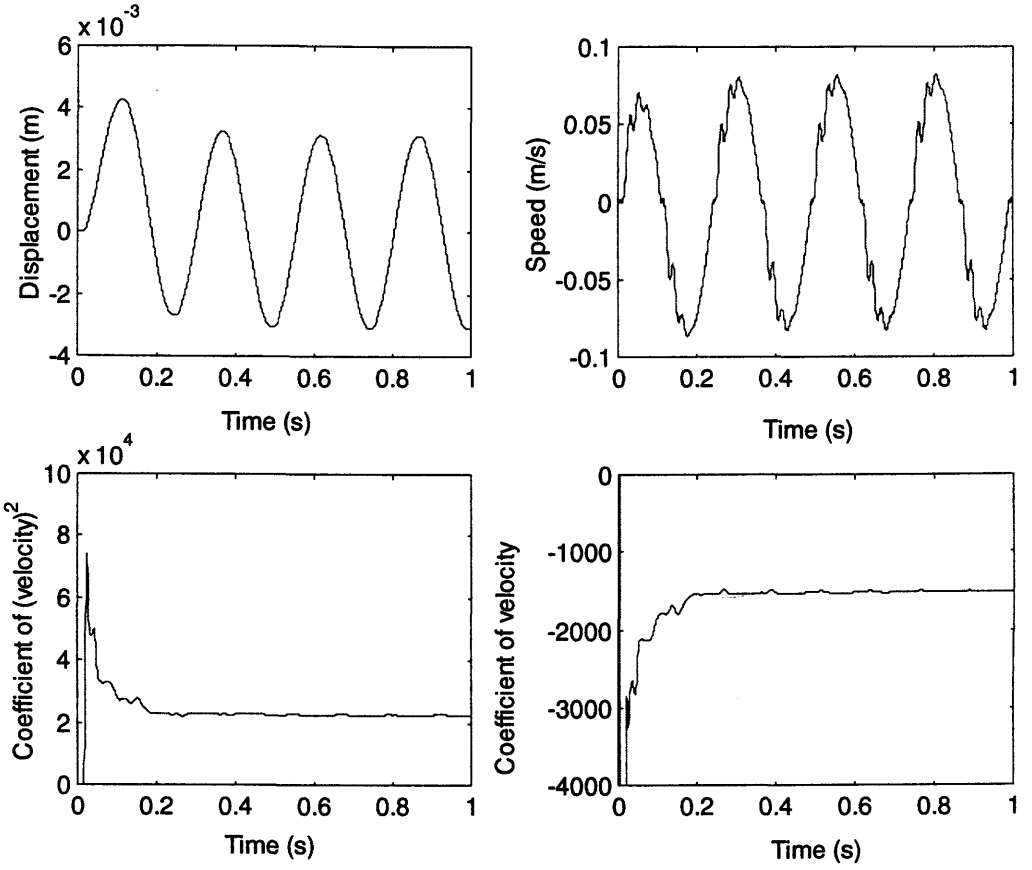

Figure 8.17: Estimation of the Coefficients of the Quadratic Friction Model in Simulation Using the EKF

The parameters (a_1, a_2, a_3) were changed in the simulated EHA system (i.e the friction characteristic for the actuator in the simulated EHA (plant) was changed) and the EKF was used to estimate their values. Changes in the coefficients of the quadratic friction model were detected and estimated with estimation errors being less than 5%. When plotting the simulated and estimated friction characteristics, the simulated friction quadratic profile and its estimated counterpart were very close as illustrated in Figures 8.19(a) to 8.19(f), where both the simulated and estimated quadratic models are plotted on the same axes. Since changes in the coefficients of the simulated quadratic friction model were detected, it was believed that changes in the coefficients in the actual prototype would be detected as well.

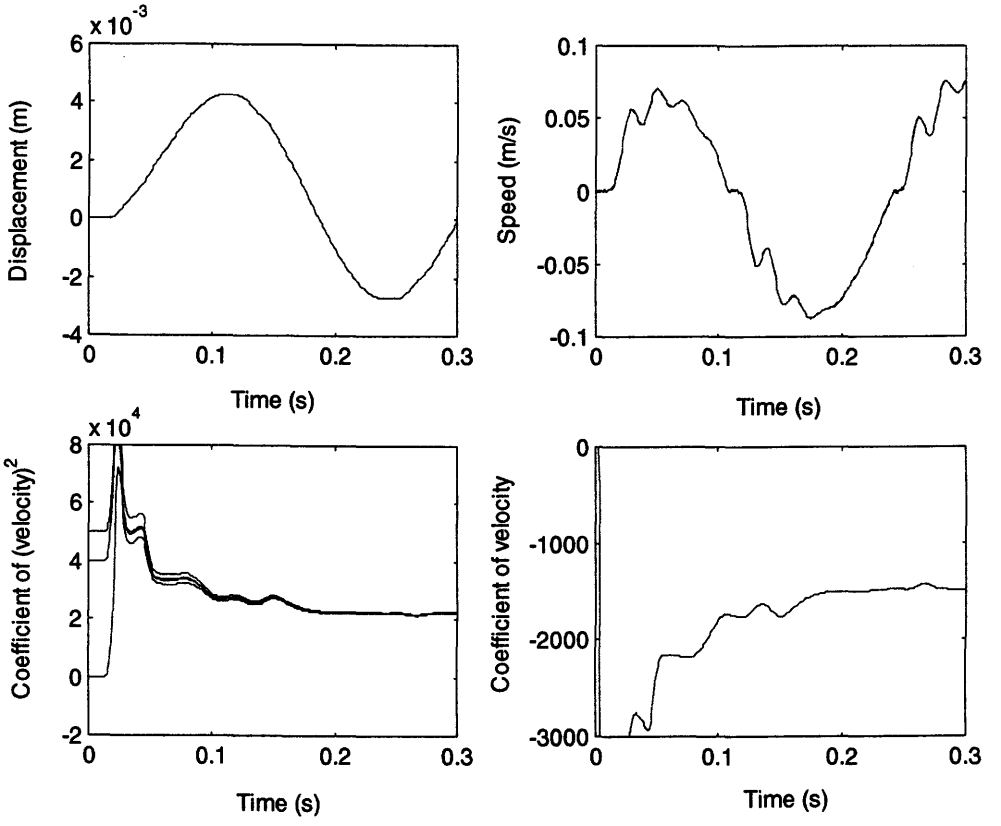

Figure 8.18: Estimating the Coefficients of the Quadratic Friction Model in Simulation Using Different Initial Values in the EKF Algorithm

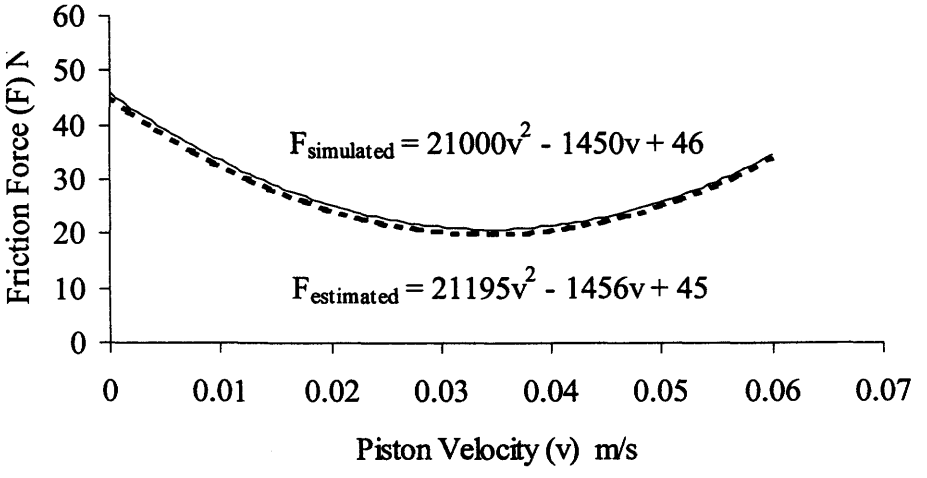

Figure 8.19 (a): Simulated (solid curve) and Estimated Friction Force

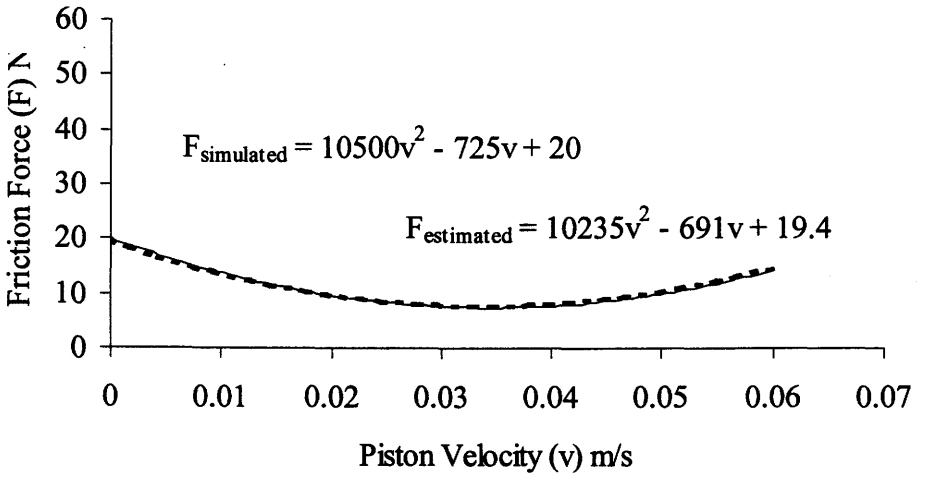

Figure 8.19(b): Simulated (solid curve) and Estimated Friction Model

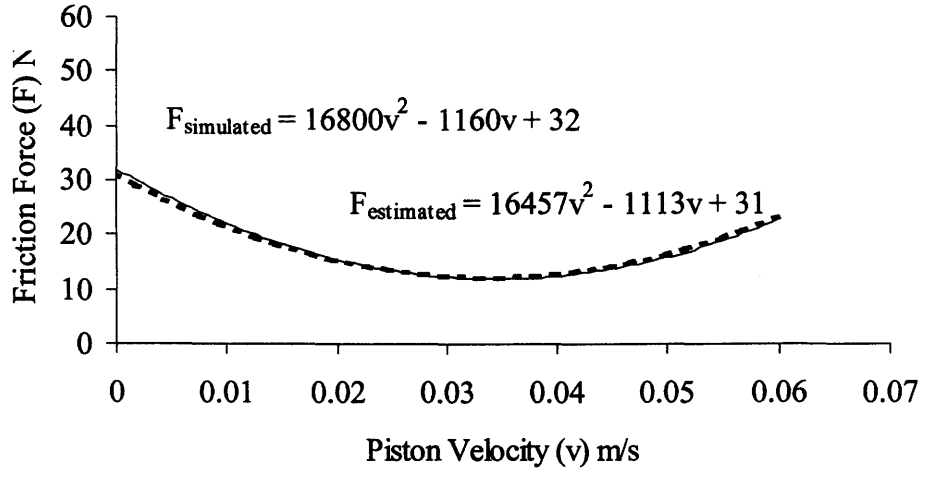

Figure 8.19 (c) Simulated (solid curve) and Estimated Friction Model

It should also be pointed out that similar to the experimental study, the simulated coefficients were estimated iteratively.

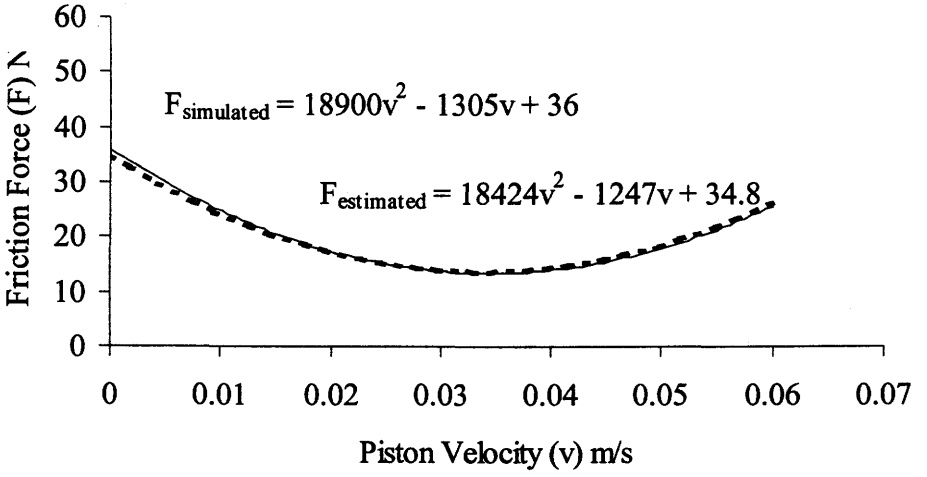

Figure 8.19 (d) Simulated (solid curve) and Estimated Friction Model

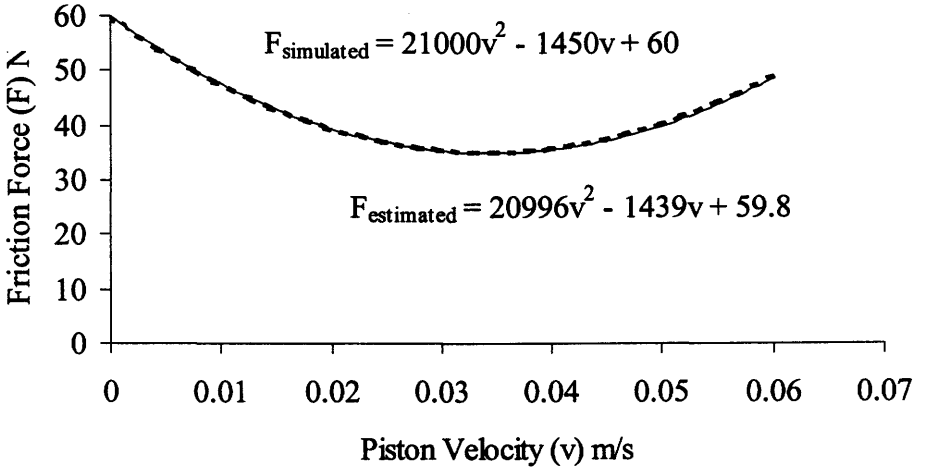

Figure 8.19 (e) Simulated and Estimated Friction Model

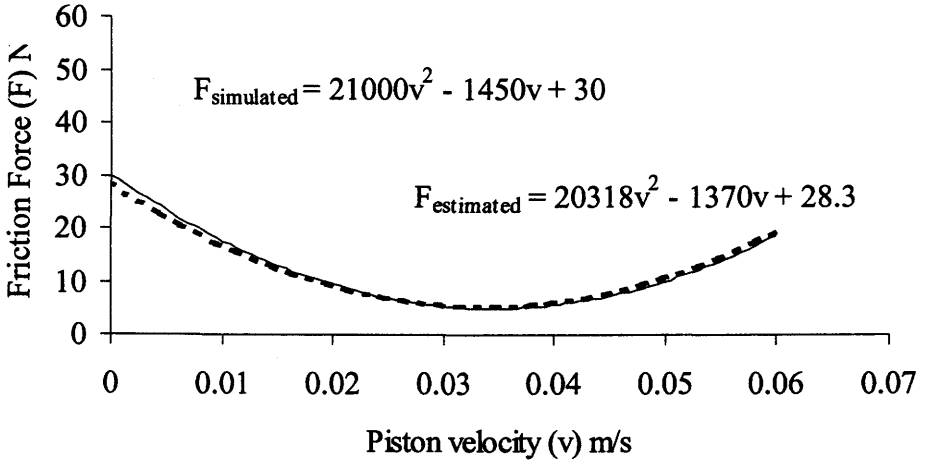

Figure 8.19 (f) Simulated (solid curve) and Estimated Friction Model

From the simulation study, it could be concluded that changes in the friction model were detected and estimated accurately (within 5% estimation error). Thus the proposed methodology of estimating the coefficients of the quadratic function iteratively was verified in simulation and was expected to work equally well in the experimental EHA system.

Next, in simulation, using a linear friction model for the EKF (instead of the quadratic model) and still using the quadratic friction model in the simulated EHA (plant), an equivalent viscous friction coefficient is estimated. The estimation process is illustrated in Figure 8.20. The estimated equivalent viscous friction coefficient converges to a value of 731 Ns/m, as compared to a value of 760 Ns/m using measurements from the EHA prototype (showing a 4 % difference). This exercise shows that the simulated friction model is an equivalent or average value of the actual friction model in the prototype.

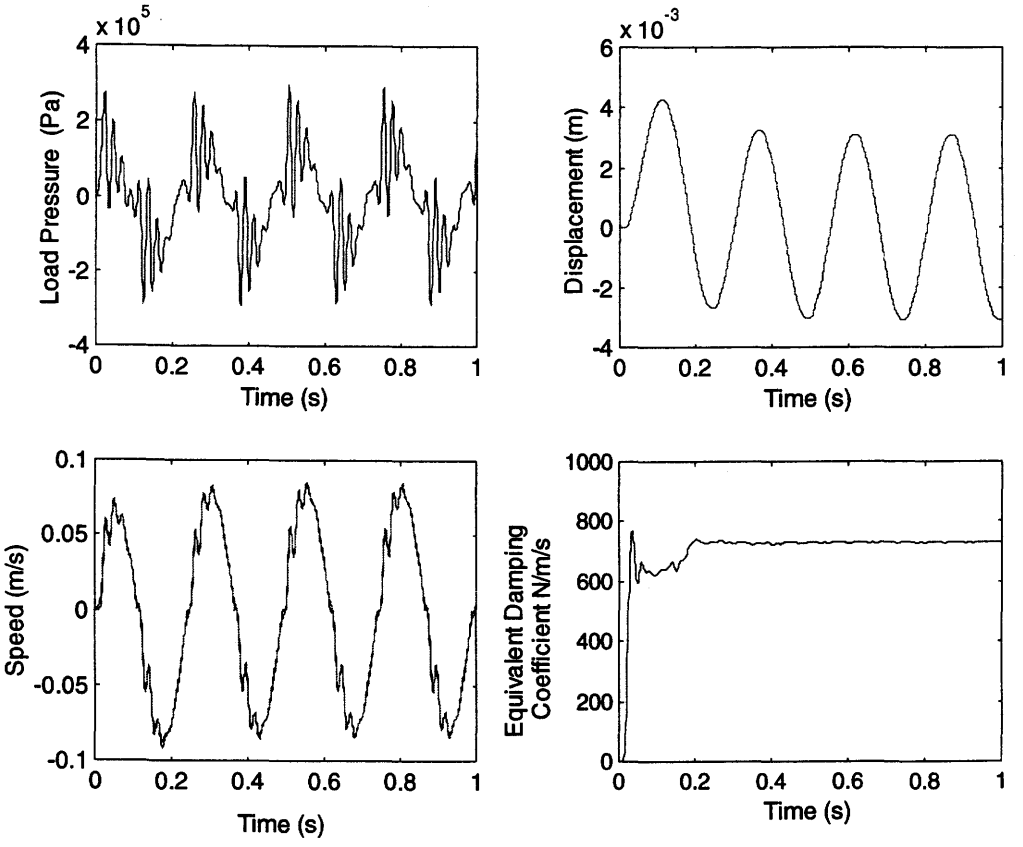

Figure 8.20: Estimating Equivalent Viscous Friction in Simulation

When the simulated pressure difference (with the nonlinear friction model being used in the simulated EHA model), is compared to the measured pressure difference from the EHA prototype, it is seen that the two pressure profiles (Figure 8.21) match very closely. The "spikes" in the differential pressure difference profiles are a result of a nonlinear friction characteristic, as compared to the simulated pressure profile (Figure 8.22) when a linearized friction model is used for the simulated EHA model, which does not reflect any slip stick pattern.

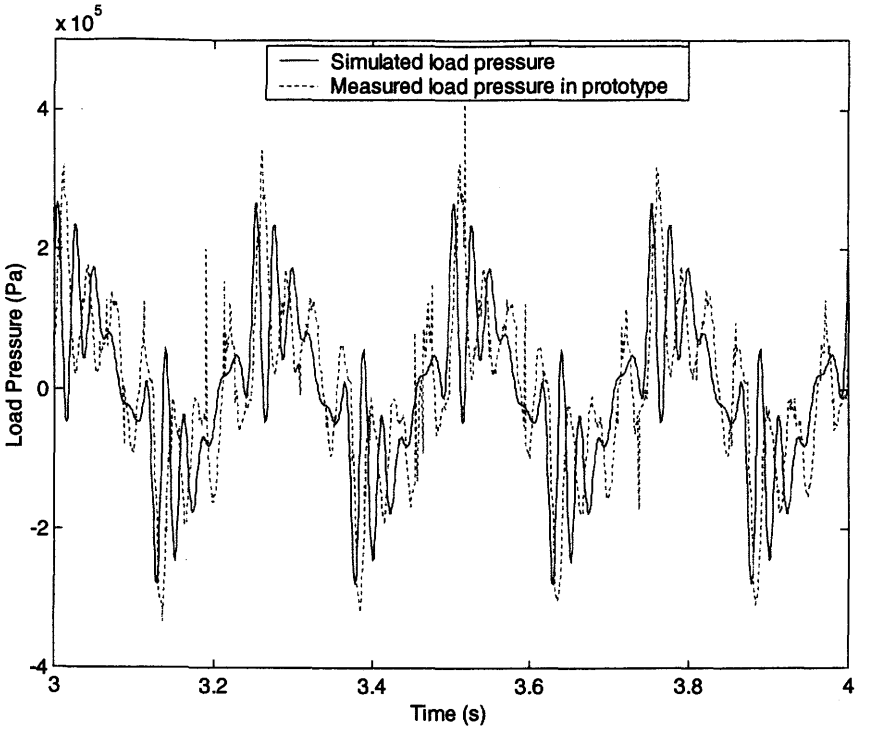

Figure 8.21: Measured and Simulated Pressure Difference (Quadratic Friction Model)

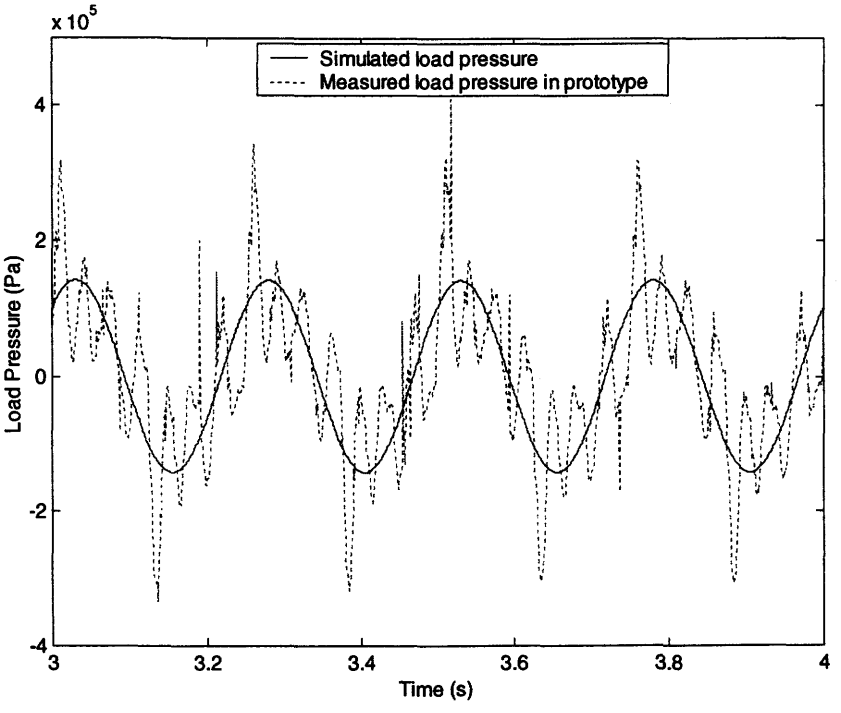

Figure 8.22: Measured and Simulated Pressure Difference (Linear Friction Model)

Figures 8.19 (a) to (f) showed that changes in the quadratic friction model (the shape of the friction force versus piston velocity profile in the simulated EHA model) could be detected and estimated quite accurately. Using a linear friction model in the EKF, the "equivalent" viscous friction was estimated when the simulated quadratic friction characteristics in the EHA Simulink model was changed (similar to Figures 8.19(a) to (f)). As expected, changes in the friction profiles were detected by the EKF although the filter was using a linear friction model. The corresponding equivalent viscous damping coefficients for the various quadratic friction models are shown in Figure 8.23.

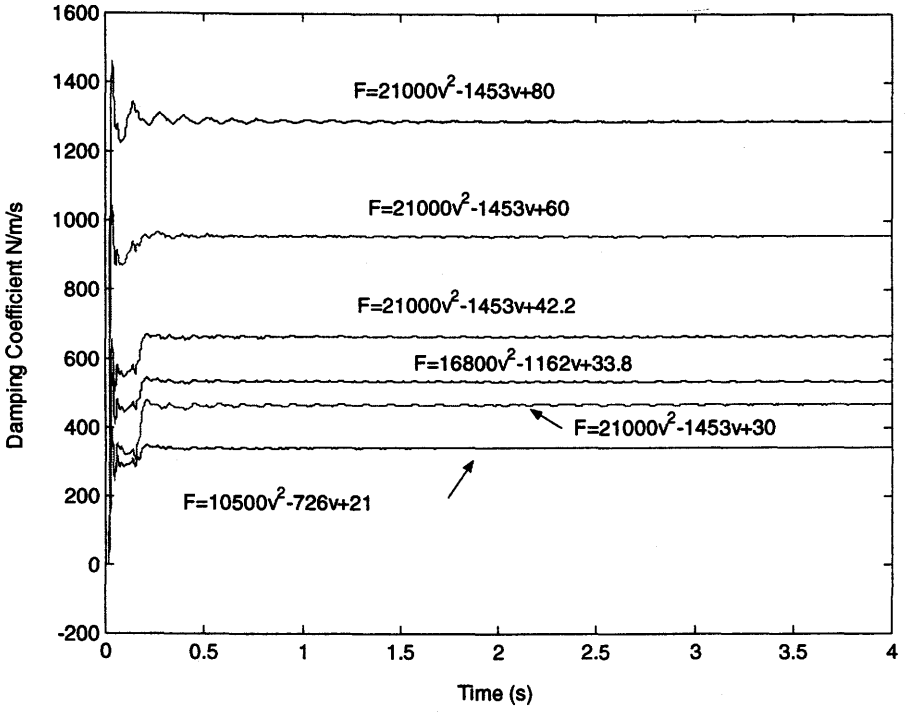

Figure 8.23: Estimation of Changes in Equivalent Viscous Damping Coefficient in Simulation Using Quadratic friction Model for the EHA and Linear Model for EKF.

It could be concluded that the EKF, when using a linear friction model, estimated an equivalent friction value, which was dependent on the quadratic friction model used. This was important since it showed that the EKF, even when it used a

simplified friction model, could detect, in simulation, a change in the quadratic friction characteristics.

Also, the effective bulk modulus was changed in simulation and its effect on the estimation of the coefficient of the quadratic friction function, as well as on the equivalent viscous coefficient investigated. It was found that the changes in the effective bulk modulus did not affect the estimations for coefficients of the quadratic friction term or for the equivalent viscous friction coefficient. This could be attributed to the relatively low frequency being used as input (4 Hz sine wave) of the simulated EHA Simulink model and to the EKF being observable (with load pressure being its input and piston position/and velocity being the measurement(s) to the filter).

8.4 Estimation of the Effective Bulk Modulus in Simulation Using the Quadratic Friction Model of the EHA in the EKF

From the previous sections, it was seen that the measured friction force in the EHA was nonlinear and as such could be approximated using a quadratic function. Using this more "accurate" friction model (as compared to the linear viscous friction model assumed in Chapter 6), in this section, the effective bulk modulus is estimated using this quadratic friction model in the EKF model. The effective bulk modulus is estimated iteratively, using the known values for the coefficients of the estimated friction model. This is done to maintain the observability condition.

From Equations (6.12), (6.13) and (6.14), the following approximations and load pressure equation can be written as:

$$\frac{dP_L}{dt} = \left[2D_p\omega_p - 2\xi P_L - LP_L - 2A\dot{x}\right]\frac{\beta_e}{V_t} \tag{8.12}$$

$$P_L A = M\ddot{x} + (a_1\dot{x}^2 + a_2\dot{x} + a_3)$$

where $P_L = P_1 - P_2$ and $V_t = V_0 + Ax = V_0 - Ax$

The state space model can be expressed as:

$$\dot{X}_1 = X_2 + w_1$$

$$\dot{X}_2 = \frac{X_3 A}{M} - \frac{(a_1 X_2^2 + a_2 X_2 + a_3)}{M} + w_2$$

$$\dot{X}_3 = \left[2D_p \omega_p - 2\xi X_3 - LX_3 - 2AX_2\right]\frac{X_4}{V_t} + w_3$$

$$\dot{X}_4 = w_4$$

$$Z = \begin{bmatrix} 1 & 0 & 0 & 0 \\ 0 & 1 & 0 & 0 \end{bmatrix}\begin{bmatrix} X_1 \\ X_2 \end{bmatrix} + \begin{bmatrix} v_1 \\ v_2 \end{bmatrix} \tag{8.13}$$

where X_1 is the state variable x, X_2 is the state variable $\dot{x}$, X_3 is the state variable P_L, X_4 is β_e, the effective bulk modulus and w_1, w_2, w_3 , w_4 are the system noise, v_1, v_2 are the measurement noise.

Using the forward difference approximation and applying it to the continuous state space model, the discrete state space model of the EHA is as follows:

$$X_1(k+1) = X_1(k) + T_s X_2(k) + T_s w_1(k)$$

$$X_2(k+1) = X_2(k) + \frac{T_s X_3(k) A}{M} - \frac{(a_1 X_2(k)^2 + a_1 X_2(k) + a_3) T_s}{M} + T_s w_2(k)$$

$$X_3(k+1) = \left[2D_p \omega_p(k) - 2\xi X_3(k) - LX_3(k) - 2AX_2(k)\right]\frac{X_4(k) T_s}{V_t} + X_3(k) + T_s w_3(k)$$

$$X_4(k+1) = X_4(k) + T_s w_4(k) \tag{8.14}$$

The linearized system matrix becomes:

$$\Phi(k) = \frac{\partial f(X(k))}{\partial X(k)} = \begin{bmatrix} \Phi_{11}(k) & \Phi_{12}(k) & \Phi_{13}(k) & \Phi_{14}(k) \\ \Phi_{21}(k) & \Phi_{22}(k) & \Phi_{23}(k) & \Phi_{24}(k) \\ \Phi_{31}(k) & \Phi_{32}(k) & \Phi_{33}(k) & \Phi_{34}(k) \\ \Phi_{41}(k) & \Phi_{42}(k) & \Phi_{43}(k) & \Phi_{44}(k) \end{bmatrix} \tag{8.15}$$

where

$\Phi_{11}(k) = 1$, $\Phi_{12}(k) = T_s$, $\Phi_{13}(k) = 0$, $\Phi_{14}(k) = 0$.

$\Phi_{21}(k) = 0$, $\Phi_{22}(k) = 1 - \frac{(2a_1 X_2(k) + a_2) T_s}{M}$, $\Phi_{23}(k) = \frac{T_s A}{M}$, $\Phi_{24}(k) = 0$.

$\Phi_{31}(k) = 0$, $\Phi_{32}(k) = \frac{-2AT_s X_4(k)}{V_t}$, $\Phi_{33}(k) = 1 - \left(\frac{2\xi + L}{V_t}\right) X_4(k) T_s$,

$$\Phi_{34}(k) = (2D_p\omega_p(k) - 2\xi X_3(k) - LX_3(k) - 2AX_2(k))\frac{T_s}{V_t}$$

$$\Phi_{41}(k) = 0,\ \Phi_{42}(k) = 0,\ \Phi_{43}(k) = 0,\ \Phi_{44}(k) = 1.$$

8.4.1 Simulation Studies: Effective Bulk modulus Estimation

The effective bulk modulus was estimated using a simulated EHA model (plant) using the previously estimated quadratic friction model in both the EHA and the EKF. A similar input as used previously to estimate the effective bulk modulus was used (25 Hz, 0.005 m sine wave). The measurements were the simulated piston position and velocity and the input was pump/electric motor angular velocity. The results for the EKF estimations are shown in Figure 8.24. The estimated displacement, position and load pressure match the simulated states closely. The EKF converges to a value of 2×10^8 Pa, showing an estimation error of 4.8 %, which is comparable to the estimation error when using the linearized friction model The known value for the effective bulk modulus was 2.1×10^8 Pa.

The initial state vector and the error, system noise, and measurement noise covariance matrices used in the EKF were set as:

$$X(0) = [0 \quad 0 \quad 0 \quad 0]^T \quad , R(k) = \begin{bmatrix} 1\times10^{-12} & 0 \\ 0 & 1\times10^{-4} \end{bmatrix} \tag{8.16}$$

$$P(0) = \begin{bmatrix} 1\times10^{19} & 0 & 0 & 0 \\ 0 & 1\times10^{19} & 0 & 0 \\ 0 & 0 & 1\times10^{19} & 0 \\ 0 & 0 & 0 & 1\times10^{20} \end{bmatrix}$$

$$Q(k) = \begin{bmatrix} 1\times10^{-12} & 0 & 0 & 0 \\ 0 & 1\times10^{-4} & 0 & 0 \\ 0 & 0 & 1\times10^{10} & 0 \\ 0 & 0 & 0 & 1\times10^{-4} \end{bmatrix}$$

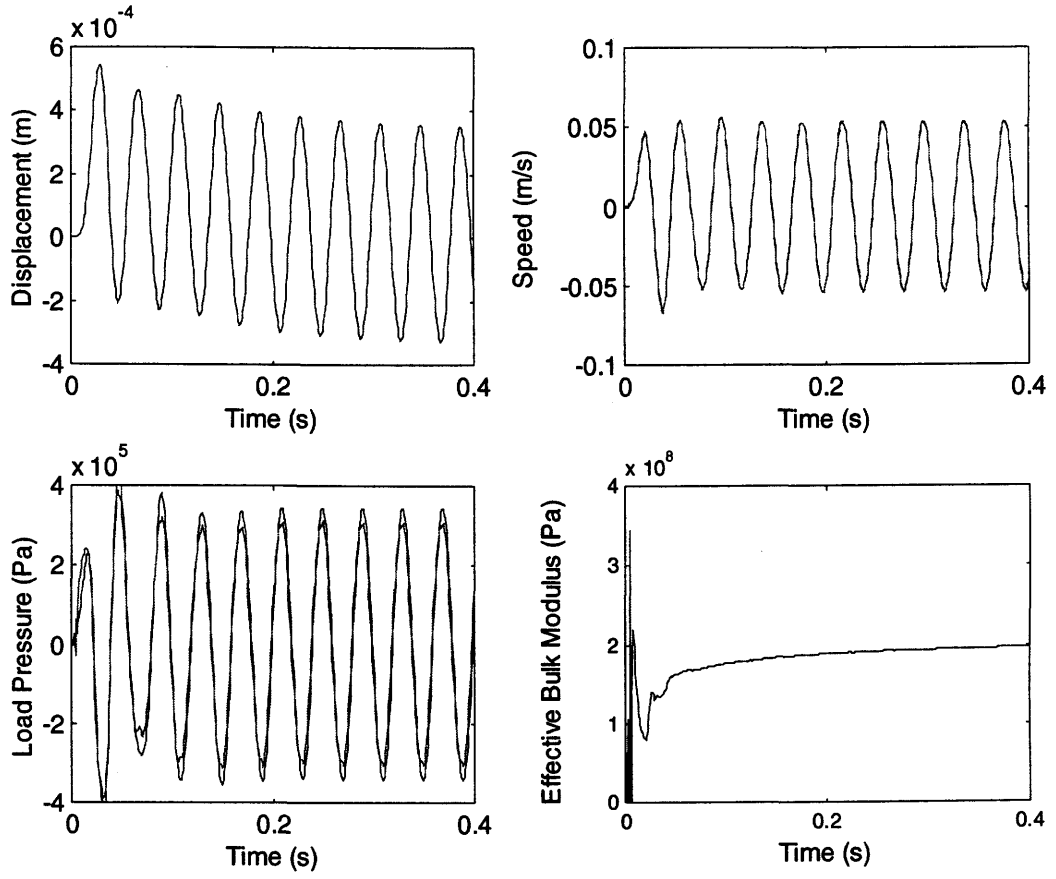

Figure 8.24: Estimating Effective Bulk Modulus in Simulation Using the Quadratic Friction Model

The value used for the effective bulk modulus to initialize the EKF was changed and the results shown in Figure 8.25. It is seen that the EKF converges to the same value for the estimated effective bulk modulus, regardless of the initial value used in the algorithm. This is consistent with all studies in which the observability condition was satisfied.

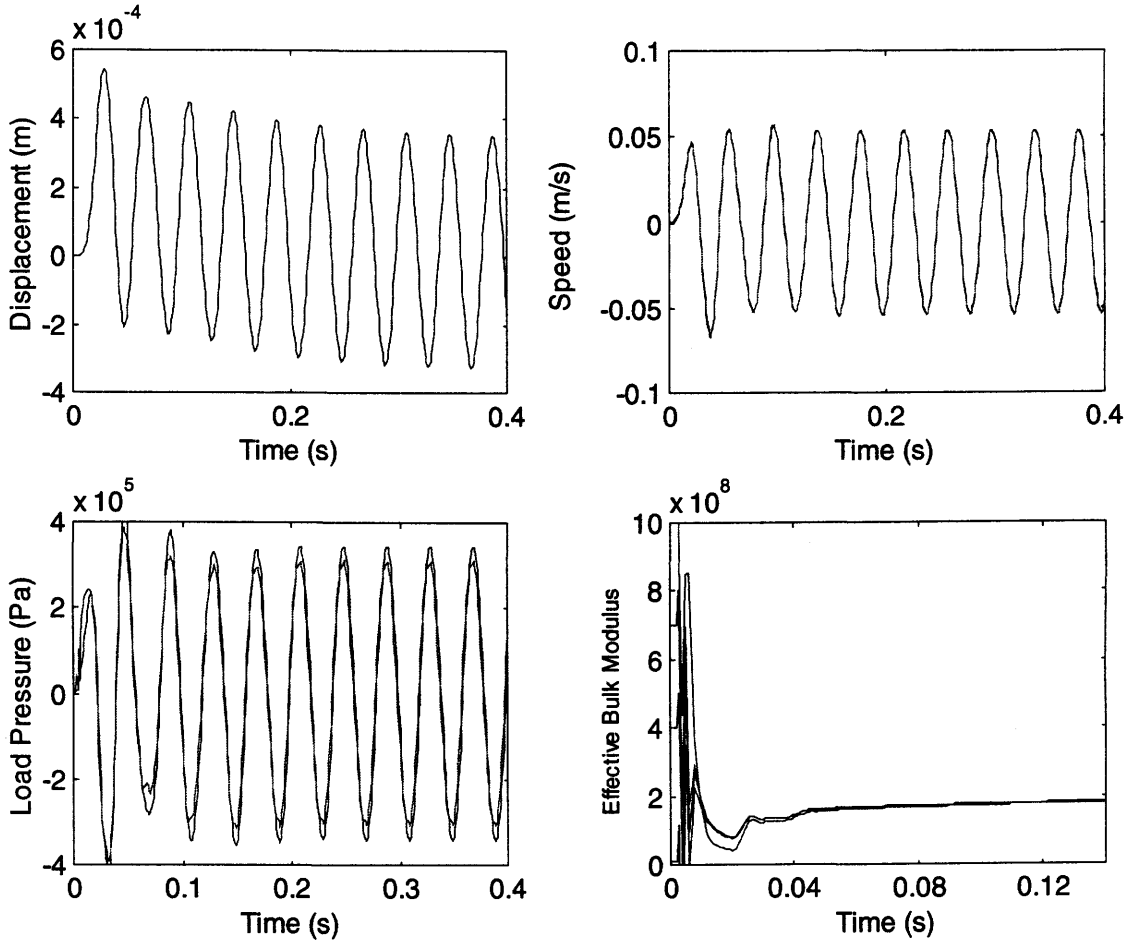

Figure 8.25: Estimating Effective Bulk Modulus in Simulation Using the Quadratic Friction Model and Using Different Parameter Values to Initialize the EKF Algorithm

Changes in the effective bulk modulus were also detected in simulation when a quadratic friction model was embedded in the EKF model and used to estimate the simulated effective bulk modulus value. Estimation errors were less than 5 % in each case. Therefore, the next step was to estimate the effective bulk modulus for the EHA prototype with the EKF using the quadratic friction model.

8.4.2 Experimental Studies: Estimating the Effective Bulk Modulus Using the Quadratic Friction Model in the EKF

Using the same initial matrices as used in the simulation study, the effective bulk modulus for the EHA prototype was estimated, with the nonlinear friction model embedded in the EKF. The results are shown in Figure 8.26. It is seen that the estimated bulk modulus is 2.08×10^8 Pa. The estimated states and the measured states match, as shown in the superimposed plots in Figure 8.26.

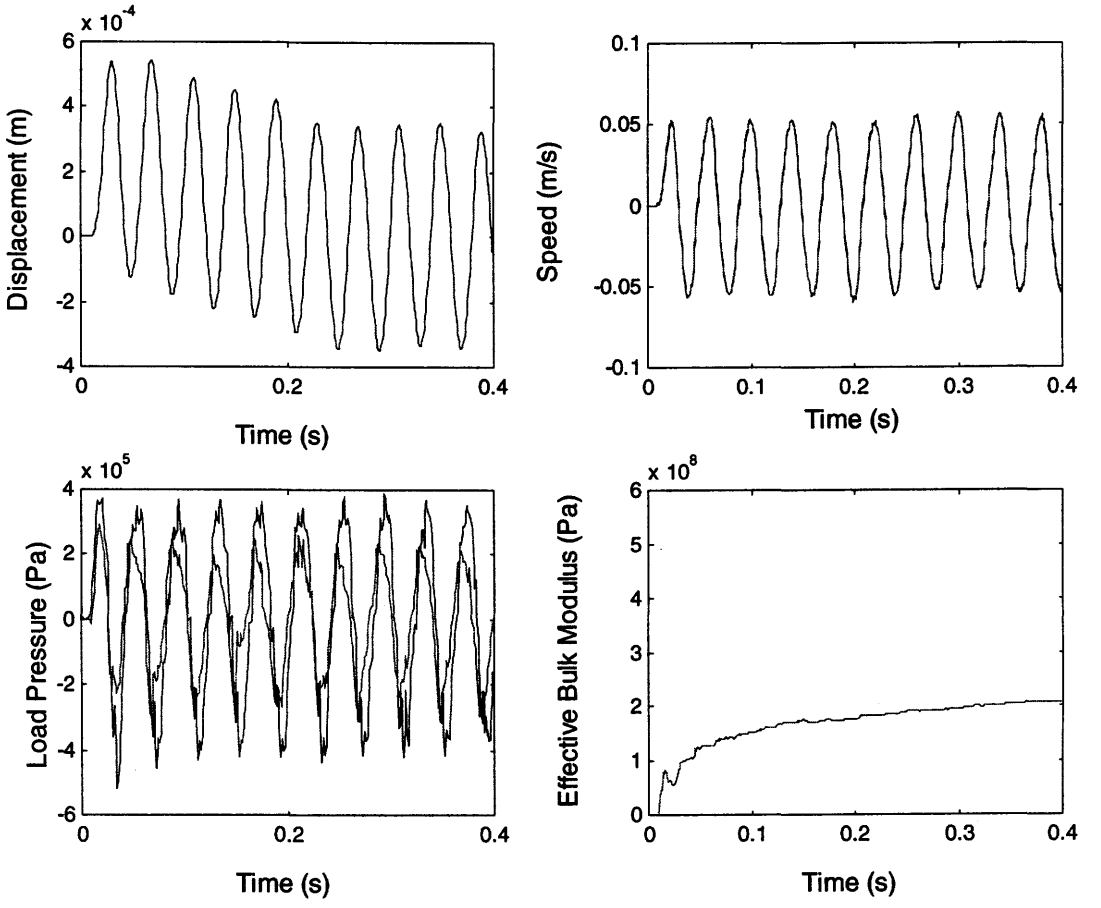

Figure 8.26: Estimating Effective Bulk Modulus in EHA Prototype Using the Quadratic Friction Model

As illustrated in Figure 8.27, it was verified that the estimated effective bulk modulus value of the EHA prototype (using system measurements), was independent (with very

slight variations in the estimated value) of the value used to initialize the EKF algorithm.

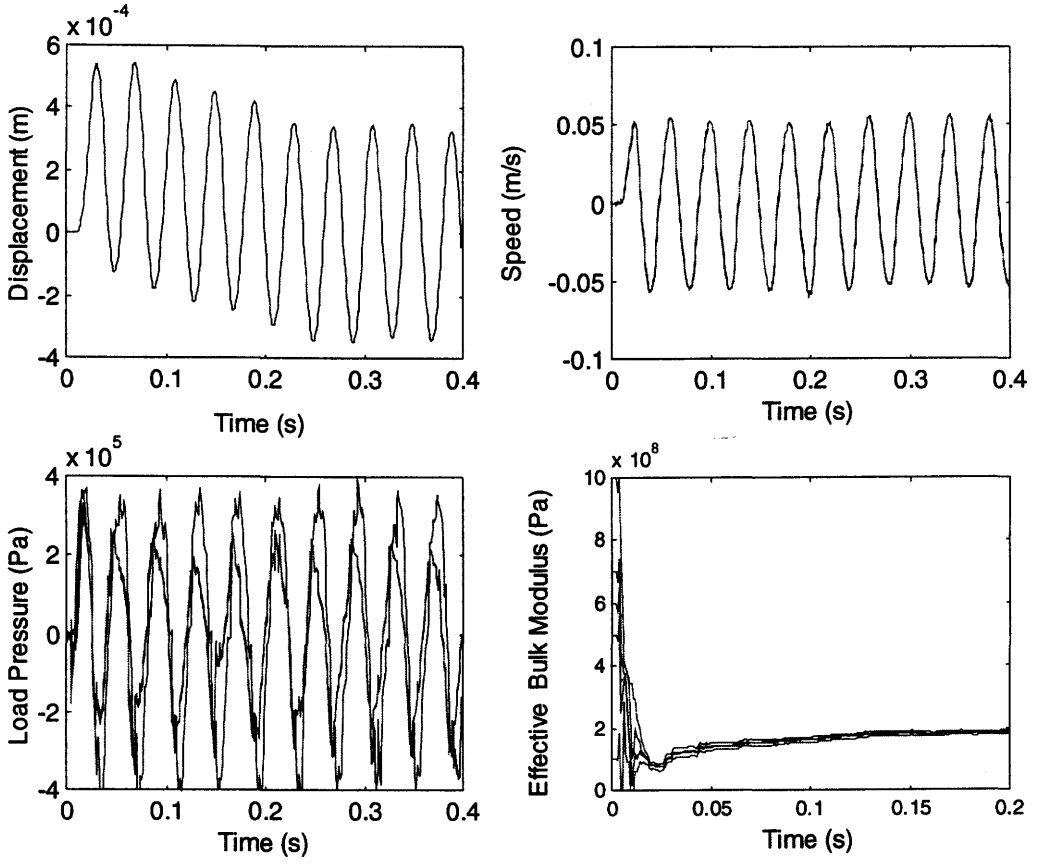

Figure 8.27: Estimating Effective Bulk Modulus in EHA Prototype Using the Quadratic Friction Model and Changing the Initial Value Used for the Parameter in the EKF Code

8.5 Conclusions

In this chapter, a novel approach to modeling friction in the Electrohydraulic Actuator was presented. The methodology consisted of approximating the friction versus velocity profile using a quadratic function. In the previous studies done on the EHA, the actuator friction model had been assumed to be linear (that is consisting of viscous friction only) but in this research, measurements carried out on the prototype revealed the presence of a nonlinear friction characteristic.

The Extended Kalman Filter approach was used to estimate the coefficients of the quadratic friction model, a nonlinear function. This approach had not been encountered in the literature. The EKF estimated successfully the coefficients as shown in the simulation studies described in this chapter. This was remarkable since although the EKF needed to linearize the nonlinear quadratic function, the EKF was still able to estimate the coefficients of the quadratic function accurately. Changes in the coefficients, which resulted in changes in the friction-velocity profile, were also detected, as shown in the simulation study.

Another interesting point was the ability for the EKF to estimate Coulomb friction (both in simulation and using measurements from the EHA prototype) and to detect changes when this parameter was varied in simulation. In the study carried out by [Zavarehi, 1997], the author reported difficulties in estimating Coulomb friction and the estimations were "*biased*". In this study, by maintaining the observability condition, Coulomb friction was estimated quite successfully both in simulation and when using measurements from the EHA prototype. This was achieved by estimating the coefficients for the quadratic function iteratively, first by estimating the Coulomb friction and then using the known value to estimate the remaining coefficients of the quadratic function. This was verified both in simulation and when using measurements from the actual system.

A thorough investigation of using different starting values to initialize the EKF was provided in this chapter. It was seen that if the system was observable, the parameter value to which the EKF converged was independent of the initial value used in the EKF algorithm, once the filter was tuned. This was considered to be important since it showed that the solution was an optimal one and had higher repeatability, which was vital for any condition monitoring strategy.

Using the quadratic friction model both in simulation and from experimental results, it was demonstrated that a linear viscous friction coefficient estimated by the EKF in the actual system, was in fact an "equivalent" viscous friction. Also included in this chapter were plots of simulated load pressure, which were compared to measured load pressure. It was seen that the quadratic friction model developed resulted in a

simulated load pressure, which was "closer" to the measured load pressure and was believed to be a more accurate representation of the actual system.

Estimation of the effective bulk modulus for the EHA, using a nonlinear friction model was also described in this chapter. A different state space formulation of the problem (in the EKF) from the one described in Chapter 6 was described. The states were piston position, velocity and load pressure. This study was carried out to investigate the effect of estimating the effective bulk modulus in the EHA using a more accurate system model (one which included nonlinear friction). The state space formulation was presented and the nonlinear friction model was assumed to be known when estimating the effective bulk modulus (an iterative approach was used because of observability). Simulation and experimental results were presented and it was found that no apparent improvement in the estimation of the effective bulk modulus was seen. Therefore, it was believed that the linearized transfer function model for the hydraulic subsystem (presented in Chapter 3) was accurate enough to estimate effective bulk modulus in the EHA, as described in the simulation study shown in Chapter 6, followed by experimental results in Chapter 7. Also, the "equivalent" viscous friction model could therefore be used in the linearized transfer function to estimate the effective bulk modulus value.

Chapter 9

Conclusions and Recommendations

9.1 Summary

The objective of this thesis was to devise an effective and practical condition monitoring strategy for a high performance hydrostatic actuation system, referred to as the Electrohydraulic Actuator (EHA) system. The EHA has potential applications for flight surface actuation in aircrafts and as such, safety is a major concern. The different condition monitoring strategies available were discussed and for the reasons enumerated in Chapter 2, the Extended Kalman Filter (EKF) was chosen for fault detection in the actuator.

The EKF was used to estimate two parameters of interest in the EHA, namely the viscous damping coefficient and the effective bulk modulus, which could be directly linked to potential faults in the EHA system. Changes in the viscous damping coefficient can indicate wearing of the actuator seals or deterioration of the lubricating properties of the oil. Changes in the estimated effective bulk modulus can indicate air entrapment in the system (occurring during maintenance actions and while refilling of the hydrostatic system with oil). Both parameters are extremely difficult to measure "on" or "off" line.

A state space model for the EHA was proposed and the feasibility of this approach for fault detection was investigated in simulation using Simulink/ Matlab®. The accuracy of the estimations (estimated parameters compared to the simulated known values of the parameters), as well as the ability for the EKF to estimate changes in the parameters, were investigated.

The use of the EKF for fault detection in a hydraulic system was not new since previous research (some carried out at the University of Saskatchewan) used the same methodology (with some accuracy problem). In this particular application, the use of the EKF for multiple parameter estimation revealed some unexpected difficulties. It was

believed that these difficulties were linked to an "observability" problem, an important aspect which previous research had overlooked. Indeed, in previous research, the EKF was made to work by setting the initial states, of the augmented state vector for the EKF, close to the desired states. This was not desirable in this study since such an approach would tend to reveal that the EKF could be in a local minima situation and not achieving an optimal solution for the states.

In this study, by using a new iterative methodology, this observability problem was overcome and for the first time, no a priori knowledge of the states was required for the EKF to successfully estimate parameters in a hydraulic system. Also, it was found that "tuning' of the filter (setting of the noise and error covariance matrices) was less tedious, hence making the use of the EKF more appealing.

Concepts like detectability (which is the ability for the EKF to detect a change in a parameter) and differentiability (which is the ability for the EKF to differentiate between changes in two, or more, parameters when these parameters are estimated simultaneously) were investigated in this work. It was found that the system did not have to be observable for it to be detectable but that the converse was true. Differentiability was also found to be linked (although no explicit mathematical equations were presented) to system observability.

The EKF was applied successfully to the EHA prototype and faults in the systems (producing changes in the effective bulk modulus and viscous damping coefficient) were detected.

9.2 Outcomes

The results of this study, in which the proposed preventive maintenance approach for the EHA involved monitoring the system by estimating parameters of interest, led to the following outcomes:

1. The mathematical model for the EHA, using measured parameters, was accurate enough for condition monitoring purposes. A mathematical model for the EHA has been proposed in earlier studies but this research revealed some inaccuracies in terms of the values of the parameters used.

2. Simulation studies verified the feasibility of using the Extended Kalman Filter (EKF) to estimate the effective bulk modulus and the viscous damping coefficient in the Electrohydraulic Actuator (EHA). The simulation involving the EHA, as well as the EKF algorithm was implemented using Matlab/Simulink®.
3. The simulation studies established the level of accuracy in the estimations of the parameters by the EKF and also verified that changes in the parameters was both detected and accurately estimated.
4. The importance of observability for the Kalman Filter and the Extended Kalman Filter was investigated and this concept was used to predict the performance of the filter in successfully estimating states and parameters. Difficulties in estimating both the effective bulk modulus and the viscous friction coefficient at the same time could be traced to the EHA system not being observable when both parameters were expressed as states and included in the augmented state vector. However, changes in the parameters were detected. Observability condition was used to improve the performance of the EKF in terms of accuracy and repeatability of results. Also, this concept was used to ensure "decoupling" of parameters by estimating the parameters iteratively. The concept of "detectability" was investigated.
5. The EKF was initialized without any a-priori knowledge rather than using some initial parameter values close to the known values.
6. A sensitivity analysis was performed to select the input signal to use in the parameter estimation process. It was found that the type of input, especially the frequency used, affected the ability of the EKF to successfully estimate parameters or at least estimate changes in the parameters.
7. The EKF was applied successfully to the EHA prototype. The effective bulk modulus and the viscous damping coefficient in the prototype were estimated successfully using an iterative approach which ensured the use of observable state space models in the EKF. The estimations were very repeatable and independent of the initial matrices used in the EKF.
8. The EKF was used to successfully estimate parameters in the EHA prototype using both "noisy" and "clean" data. The noisy piston measurements were obtained when

using an LVDT and a clean signal was obtained when an optical encoder was used. This showed the flexibility and practicality of using the EKF for parameter estimation in hydraulic systems in general.

9. The friction characteristic of the actuator in the EHA was investigated and an improved model for friction at the actuator was proposed.
10. The EKF was used to estimate the coefficients of the quadratic friction model which was proposed and to estimate changes in the friction model as a result of faults.

9.3 Conclusions

From the outcomes of this research, it was concluded that the Extended Kalman Filter was an effective strategy for fault detection in the hydrostatic actuation system. The effective bulk modulus and the viscous damping coefficient were estimated accurately in simulation and repeatably in the actual system. Changes in the parameters were detected both in simulation and in the actual prototype.

It was also concluded that the iterative approach used to estimate the two parameters, in order to maintain system observability, ensured that the estimated parameters were not biased and were independent of initial values used in the EKF algorithm. The expected level of accuracy when the parameters were estimated using measurements from the actual prototype was determined in simulation by using identical input, measurements and initialization matrices for the EKF in simulation and while doing the experiments.

It was also concluded that the EKF was a viable tool for fault detection using both clean measurements (using the optical encoder) and in the presence of noise, as shown when noisy LVDT measurements (instead of the "clean" optical encoder measurements) were used to estimate parameters in the actual prototype.

Finally, it was concluded that the friction model proposed in this study appeared to represent the actual friction in the system more accurately than the linear viscous friction model which was assumed in previous studies involving the EHA. The EKF had demonstrated a remarkable ability to estimate the coefficients of the nonlinear friction function accurately in simulation. Experimental results also tend to support the use of

the EKF for estimating the friction characteristics. The concept of maintaining system observability by estimating the coefficients of the friction function was applied successfully when the coefficients of the friction function were estimated iteratively.

9.4 Important Contributions

A number of major contributions have been made to the field of hydrostatic actuation systems and fault detection in such systems, and they are as follows:

- The feasibility of using the Extended Kalman Filter (EKF) to estimate parameters in a hydrostatic system was shown in this thesis. In the past, the EKF was applied to different hydraulic components, never to a hydrostatic system. This research thus paves the way for an effective method of detecting faults in hydrostatic systems.
- In this research, the effective bulk modulus, a very difficult parameter to measure, was estimated using system measurements by the EKF. The effective bulk modulus is a parameter that depends on the amount of air entrapped in the fluid (air which is dissolved in the fluid does not affect the effective bulk modulus). The amount of entrapped air cannot be possibly known at any point of time and this study provides an effective method of estimating this important parameter. The effective bulk modulus affects the natural frequency of hydraulic systems and in closed loop systems changes in the natural frequency can result in the system going unstable.
- The existing mathematical model for the Electrohydraulic Actuator (EHA) was derived and updated with realistic, measured leakage coefficients (for the pump and actuator) and with a more accurate viscous friction coefficient.
- An iterative method for estimating the viscous friction coefficient and the effective bulk modulus was proposed. This method ensured that the systems were observable for parameter estimation using the EKF and changes in the parameters were both detected and accurately estimated. This was done in simulation and verified using measurements from the EHA prototype.

- The reliance of the EKF on the initial state vector for the EKF disappeared when observable systems were used for parameter estimations. Suboptimal performance of the filter was believed to be achieved when the EKF needed to be initialized with parameter values close to the desired ones, for the estimation process to be successful. In this study, the EKF converged to the same value irrespective of the initial value of the state vector. This was considered to be a good test for a "global minimum" situation where an optimal performance of the filter was achieved. This made the initialization process of the EKF less tedious. "Tuning" of the filter for observable system was found to be relatively easy in contrast to what has been reported in many studies.
- The friction characteristics of the custom made symmetrical linear actuator was investigated and a novel empirical quadratic friction model was proposed. This model was found to be a more accurate representation of the friction characteristics in the actuator for the prototype than the classical Coulomb and viscous friction model usually used for linear hydraulic actuators.
- The EKF was then used to estimate the coefficients of the quadratic friction model for the first time. The simulation study showed the feasibility of the approach. The EKF successfully estimated the coefficients of the friction function in simulation and changes in the friction function. The EKF was then used to estimate the coefficients of the quadratic function in the EHA prototype. The ability of the EKF to successfully estimate the coefficients and changes in the coefficients, in spite of the function being nonlinear was quite remarkable.

9.5 Future Research Recommendations

Recommendations for future work include:

- Investigate the effect of the accumulator on the dynamics of the system. In this research, it was assumed that the dynamics of the accumulator were negligible. This has to be verified by a detailed simulation study of the accumulator and by experiments.
- Augment the fault detection scheme for the EHA by using a combination of several methods. Leakage faults for example can be easily detected by monitoring the accumulator pressure but the location of the fault is more challenging. Wearing of the gears in the bi-directional gear pump can be detected by spectral analysis of the pressure ripples in the lines. Temperature monitoring of the oil is another method that can be used for detection of faults since it can imply, for instance, that excessive load pressure is causing the cross-over relief valve to short the lines and therefore the oil temperature to increase.
- Increase the load in the prototype and investigate its effects on the estimated parameters. The effective bulk modulus is known to increase with pressure. The low effective bulk modulus estimated in this thesis was partly due to the low system pressure. The effect of a small amount of entrapped air is greater at low load pressures than at higher load pressures where the air is forced to dissolve in the fluid and not exist as air pockets.
- Increase the temperature of the oil and investigate its effect on the estimated viscous friction coefficient (Viscous friction decreases as oil viscosity decreases).
- Use Neural Networks or Expert Systems for the decision part of the fault detection strategy proposed in this research.

List of References

Atkinson A., "A Neural Network Approach to Fault Diagnosis in Electro-Hydraulic Systems", Proceedings of the Comadem 96 Conference on Condition Monitoring and Diagnostic Engineering Management, University of Sheffield, UK, 1996.

Ansarian A., "Parameter Estimation of a Solenoid Hydraulic Proportional Valve, using the OLS and ML Techniques", M.Sc. Thesis, University of Saskatchewan, Canada, 2001.

Ansarian A., Schoenau G. and Burton R., "Utilization of Statistical Techniques in a Two Step Parameter Estimation For a hydraulic valve", SAE, 2002-01-1395, 2002.

Backe W. and Winner, D., "Investigation of the contamination sensitivity of hydraulic pumps", IMech E Conference Publications 1984, Contamination Control in hydraulic systems, University of Bath, 1984.

Bryson A. and Kortum W., "Estimation of the Local Attitude of Orbiting Spacecraft", Automatica Vol. 7, pp163-180, 1971.

Brown R. and Hwang P., Introduction to Random Signals and Applied Kalman Filtering, 3rd Edition, John Wiley &Sons, 1997.

Burton R.T. and Sargent M., "Some Experiences with Expert Systems for the Design, Monitoring and Maintenance of Hydraulic Circuits", SAE Transactions, pp532-540, 1990.

Burton R. T. "Indirect Measurement of Operational Bulk Modulus", M.Sc. Thesis, University of Saskatchewan, 1971.

Burton R., "Analytic and Experimental Prediction of Limit Cycle Oscillations in an Inertially Loaded Hydraulic Control Valve", Ph.D. Thesis, University of Saskatchewan, Canada, 1974.

Cao H., "Parameter Estimation Using Extended Kalman Filter For the Swash Plate Assembly and Control Piston in a Load Sensing Pump," M.Sc. Thesis, University of Saskatchewan, Canada, Spring 2001.

Chen C.K., Kalman Filtering with Real Time Applications, Spriger Verlag New York, 1987.

Chinniah Y., Habibi S. and Burton R., "Feasibility Study for the Estimation of Effective Bulk Modulus and Viscous Damping in a Hydrostatic System", Proceedings of the 19th Canadian Congress of Applied Mechanics, Calgary, Jun. 01- 05, 2003.

Chinniah Y., Burton R. and Habibi S., "Modeling of a Hydrostatic System using Measured Parameters", Proceedings of the 19th Canadian Congress of Applied Mechanics, Calgary, Jun. 01-05, 2003.

Chinniah Y., Burton R. and Habibi S., "Parameter Estimation in a Hydrostatic System Using Extended Kalman Filter", Proceedings of ASME International Mechanical Engineering Congress, FPST-Vol., New York, Nov. 10-15, pp125-136, 2001.

Chinniah Y., Habibi S. and Burton R., "Simulation of a Nonlinear model of a new High Performance Electrohydraulic Actuator", Proceedings of the 18th Canadian Congress of Applied Mechanics, Newfoundland, June 01-05, 2001.

Coreless., Devonport. and Dockyard., " Contamination control during the repair of hydraulic machinery", I Mech E Conference Publications 1984, Contamination Control in hydraulic systems, University of Bath, 1984.

Cox H., "On the Estimation of State Variables and Parameters for Noisy Dynamic Systems", IEEE Transactions on Automatic Control, Vol. AC-9, pp5-12 , Feb. 1964.

Crowther W., Edge K. and Burrows C., "Fault Diagnosis of Hydraulic Actuator Circuit Using Neural Networks- A State Space Classification Approach", University of Bath, UK, 1996

Dean G., "An Introduction to Kalman Filters", Measurement and Control, Vol.19, pp69-73, 1986.

Esposito A., Fluid Power with Applications, Fifth Edition, Prentice Hall Inc, 2000.

Franklin G., Powell D., and Workman M., Digital Control of Dynamic Systems, Addison Wesley Publishing, 1990.

Grewal M. and Andrews A., Kalman Filtering, Theory and Practice, Prentice Hall, 1993.

Guo Q., Burton R.T., Schoenau G. J. and Sargent C.M., "Self-Diagnosis of Hydraulic Circuits Using Expert Systems", JHPS, International Symposium on Fluid Power, Tokyo, pp309-315, Mar. 1989.

Gupta M., Introduction to Theory and Applications of Neural and Fuzzy-Neural Systems, University of Saskatchewan, Graduate Class, ME 885.3, 2001.

Habibi S.R. and Goldenberg A., "Design and Analysis of a New Symmetrical Linear Actuator For Hydraulic and Pneumatic Systems", Transactions of the CSME, Vol. 23, No 3&4, pp377-397, 1999.

Habibi S. R., "Comparison of Hydrostatic and Servovalve Controlled Hydraulic Actuation Systems in Robotics", SAE Transactions, Journal of Commercial Vehicles, Section 2, pp231-243, 2000.

Habibi S.R and Goldenberg A., "Design and Analysis of a New High Performance ElectroHydraulic Actuator", Proceedings of ASME-IMECE, Vol.6. pp9-15, 1999.

Habibi S.R. and Goldenberg A., "A Mechatronics Approach for the Design of a New High Performance Electrohydraulic Actuator", SAE Transactions, Journal of Commercial Vehicles, Section 2, pp353-361, 1999.

Habibi S.R. and Singh G., "Derivation of Design Requirements For Optimization of a High Performance Hydrostatic Actuation System", International Journal of Fluid Power 1, No2 pp11-27, 2000.

Habibi S.R. and Goldenberg A., "Design of a New High-Performance ElectroHydraulic Actuator", IEEE/ASME Transactions on Mechatronics, Vol.5, No.2, pp158-164, June 2000.

Habibi S.R., Pastrakuljic V. and Goldenberg A., "Experimental Analysis of a High Performance Hydrostatic Actuation System", SAE Transactions, Journal of Commercial Vehicles, Section 2, Vol. 109, pp367-377, 2001.

Habibi S.R., Pastrakuljic V. and Goldenberg A., "Model Identification and Analysis of a High Performance Hydrostatic Actuation System", Proceedings of SAE International Off-Highway & Powerplant Congress & Exhibition, Milwaukee, WI, Sep. 11-13, 2000.

Heney P., "F-35 Fighter incorporates EHA", Hydraulics & Pneumatic. The International Magazine of Fluid Power and Motion Control Systems, Penton Publication, USA, Vol. 55, No. 12, pp16, Dec.2002.

Hindman J., "Condition Monitoring of Valves and Actuators in a Mobile Hydraulic System Using an Artificial Neural Network and Expert Data", M.Sc. Thesis, University of Saskatchewan, Canada, 2002

Hindman J., Burton R., and Schoenau G., "Condition Monitoring of Fluid Power Systems: A survey", Hydraulic Fluids, Systems and Components, SAE international SP 1708-2002, pp1-7, 2002.

Hogan P.A., "Automated Fault Tree Analysis for Hydraulic Systems", Transactions of the ASME, Vol. 118, pp278-282, June 1996.

Horton M.P., "Real-time identification of missile aerodynamics using a linearized Kalman filter aided by an artificial neural network", IEE Proc. Control Theory Application, Vol. 144, No 4, July 1997.

Hunt T.M., "A Review of Condition Monitoring Techniques Applicable to Fluid Power Systems", Proceedings of the 7th Int. Fluid Power Symposium, University of Bath, pp285-295, Sep.1986.

Isermann R., "Process Fault Detection Based on Modeling and Estimation Methods-A survey", Automatica, Vol. 20, No. 4, pp387-404, 1984.

Isermann R., "Fault Diagnosis of Machines via Parameter Estimation and Knowledge Processing- Tutorial Paper", Automatica, Vol.29, No. 4, pp815-835, 1993.

Isermann R. and Freyermuth B., "Process Fault Diagnosis Based on Process Model Knowledge", Journal of Dynamic Systems, Measurement and Control, Vol. 113, pp627- 633, Dec. 1991.

Kamen E.W., and Su J.K., Introduction to Optimal Estimation, Springer-Verlag London Limited 1999.

Konrad R., Gunter S, Yaz and Unbehausen R., "Stochastic Stability of the Discrete Time Extended Kalman Filter", (Web). Author's email address: konrad.reif@mailexcite.com.

Ljung L., "Asymptotic Behavior of the Extended Kalman Filter as a Parameter Estimator For Linear Systems", IEEE Transactions on Automatic Control, Vol. AC-24, No1, Feb. 1979.

Merrit H.E., Hydraulic Control Systems, John Wiley & Sons, Inc, New York 1967.

Ogata, K., Modern Control Engineering, Fourth Ed. Prentice Hall, 2002.

Rosa A., "Estimating Parameters of a Proportional Solenoid Valve Using Neural Networks", M.Sc. Thesis, University of Saskatchewan, Canada, 2001.

Sasaki A. and Dunthorne O.M., "Electrostatic liquid cleaning of hydraulic fluid", ImechE Conference Publications 1984, Contamination Control in hydraulic systems, University of Bath, 1984.

Schoenau G., Stecki J. and Burton R., "Utilization of Artificial Neural Networks in the Control, Identification and Condition Monitoring of Hydraulic Systems-An overview", SAE Transactions, Journal of Commercial Vehicles, 2000.

Sorsa T. and Koivo H., "Application of Artificial Neural Networks in Process Fault Diagnosis", Automatica, Vol. 29, pp843-849, 1993.

Southall B., Buxton B., and Marchant A., "Controllability and Observability: Tools for Kalman Filter Design", Dept. of Computer Science, University College London, UK (Web). Author's email address: B.Southall@cs.ucl.ac.uk.

Stecki J., Schoenau G., "Application of Simulation and Knowledge Processing in Contamination Control", SAE Transactions, Journal of Commercial Vehicles, 2000.

Stecki J. and Andrzey G., Hydraulic Control System- Design and Analysis, Fluid Power Net Publications, Melbourne, 2000.

Welch G. and Bishop G., "An Introduction to the Kalman Filter", Department of Computer Science, University of North Carolina at Chapel Hill, US 1999.

Willsky, A., "A Survey of Design Methods for Failure Detection in Dynamic Systems", Automatica, Vol. 12, pp601-611, 1976.

Wright G., "Parameter Estimation of a Hydraulic Proportional Valve using Extended Kalman Filtering," M.Sc. Thesis, University of Saskatchewan, Canada, 2001.

Zarchan P., "Tactical and Strategic Missile Guidance" 3rd Edition , Progress in Astronautics, Vol. 176, American Institute of Aeronautics and Astronautics Inc, pp373-380, 1997.

Zavarehi M., "On-line Condition Monitoring and Fault Diagnosis in Hydraulic System components using Parameter Estimation and Pattern Classification", Ph.D. Thesis, University of British Columbia, 1997.

Zavarehi M., Sassani F., and Lawrence P., "Condition Monitoring of a Hydraulic Valve Through On-Line Estimation of the Valve Orifice Area Profile", SAE Transactions, Journal of Commercial Vehicles, Vol. 109, pp224-251, 2000.

Appendix A

Statistical Review of Random (Stochastic) Signals

"Random signals cannot be described with explicit mathematical functions like sine waves or step functions" [Brown, 1997]. Their description needs to be put in probabilistic terms. A random signal always has some element of chance associated with it. While considering the Kalman filter, noise is treated as a random signal. The system noise and the measurement noise are assumed to be random processes.

A.1 Expectation (Average)

In the study of random variables, the conceptual average for an infinite number of trials is considered. This hypothetical average is called the expected value $E(X)$, which represents the expected value of the random variable X. It can be expressed as[Brown,1997]:

$$E(X) = \overline{X} = \sum_{i=1}^{n} X_i P_i \tag{A.1}$$

where

X is the random variable, n is the number of allowable values of X, X_i being the i^{th} value of X and, P_i is the probability that X_i occurs.

A.2 Variance

The variance of X is the second moment of X about the mean. It is a measure of the dispersion of X about its mean. The variance is expressed as [Brown, 1997],

$$Var(X) = E(X^2) - [E(X)]^2 \tag{A.2}$$

A.3 Normal or Gaussian Random Variables

The random variable X is called normal or Gaussian if its probability density function is given by [Brown,1997]:

$$f_X(X) = \frac{1}{\sqrt{2\pi}\sigma} \exp\left[-\frac{1}{2\sigma^2}\left(X - \overline{X}\right)\right] \tag{A.3}$$

where $f_X(X)$ is the probability density function, σ is the standard deviation of X, and $\overline{X}$ represents the mean of X.

The shorthand notation for a normal random variable with mean $\overline{X}$ and variance σ^2 is $X \approx N(\overline{X}, \sigma^2)$. The normal density function is symmetric and peaks about its mean value. The mean is seen as the most likely value with values on either side of the mean gradually becoming less likely as the distance from the mean becomes larger. Many natural random phenomena seem to very nearly exhibit this central tendency. Variance is a measure of dispersion about the mean. Thus a small σ corresponds to a sharp peaked density curve whereas a large σ will yield a curve with a flat peak.

A.4 Covariance

The covariance of two random processes X and Y having mean as $\overline{X}$ and $\overline{Y}$ respectively is given by [Brown, 1997],

$$Cov(X,Y) = E[(X_i - \overline{X})(Y_i - \overline{Y})] \tag{A.4}$$

The covariance represents the dispersion extent of the two random variables. Furthermore, if the two random variables are the same, then their covariance is the variance of the variable. The covariance is also an indication of the correlation between the two functions. If $Cov(X,Y) = 1$, X and Y are highly correlated and if $Cov(X,Y) = 0$, they are completely uncorrelated.

Appendix B

Importance of Observability Condition to the Kalman Filter

B.1 Observability Condition and Formula

Suppose that an N dimension system is represented by:

$$X(k+1) = AX(k) \tag{B.1}$$

$$Z(k) = HX(k) \tag{B.2}$$

The system (A,H) is observable if for any $X(0)$, there is a finite N such that $X(0)$ can be computed from observation of $Z(0), Z(1), Z(2) \ldots Z(N-1)$ [Franklin et al., 1990].

The successive outputs from $k = 0$ to $k = N-1$ are:

$$Z(0) = HX(0) \tag{B.3}$$

$$Z(1) = HX(1) = HAX(0)$$

$$Z(2) = HX(2) = HAX(1) = HA^2X(0)$$

$$Z(N-1) = HA^{N-1}X(0)$$

In a matrix form, Equation (B.3) can be written as:

$$\begin{bmatrix} Z(0) \\ Z(1) \\ Z(2) \\ \\ Z(N-1) \end{bmatrix} = \begin{bmatrix} H \\ HA \\ HA^2 \\ \\ HA^{N-1} \end{bmatrix} X(0) = O_N \times X(0), \text{ where } O_N = \begin{bmatrix} H \\ HA \\ HA^2 \\ \\ HA^{N-1} \end{bmatrix} \tag{B.4}$$

The above equation can be solved for $X(0)$ if and only if the observability matrix O_N, has rank N [Kamen, 1990]. Thus, the system is observable when the rank of the observability matrix O_N, equals the system length.

B.2. Mass -Damper System

In order investigate the importance of observability to the Kalman Filter and to the Extended Kalman Filter, a simple Mass-Damper system was considered. The Kalman

Filter was applied to the linear system to estimate the two states, namely position and velocity. The mechanical system is described by Equation B.5.

$$M\ddot{X}(t) + B\dot{X}(t) = u(t) + w(t) \tag{B.5}$$

where $X(t)$ is the displacement (m), $\dot{X}(t)$ the velocity (m/s), $u(t)$ the driving force (N), $w(t)$ the additive white noise (N), B viscous damping coefficient (Ns/m) and M the mass (kg). The state space model for the Mass-Damper system is described by Equation (B.6).

$$\dot{X}_1(t) = X_2(t) + w_1(t) \tag{B.6}$$

$$\dot{X}_2(t) = \frac{(u(t) - BX_2(t))}{M} + w_2(t)$$

Using the "forward difference" approximation, with T_s being the sampling time, the following expression is written:

$$\dot{X}(t) \approx \frac{X(k+1) - X(k)}{T_s} \tag{B.7}$$

The discrete state space model for the mechanical system can be expressed as:

$$X_1(k+1) = X_1(k) + T_s X_2(k) + T_s w_1(k) \tag{B.8}$$

$$X_2(k+1) = (u(k) - BX_2(k))\frac{T_s}{M} + X_2(k) + T_s w_2(k)$$

$$Z(k) = X_1(k) + v(k)$$

The Mass-Damper system was simulated in Simulink/Matlab®. The input $u(k)$ was a sinusoid with amplitude of 0.1N and a frequency of 1 Hz. A mass of 1Kg and damping coefficient of 2 Ns/m were used as system parameters. The simulated input and position were inputs to the Kalman Filter algorithm (written using Matlab) and the estimated states (displacement and velocity) are depicted in Figure B.1. The general representation of the Mass-Damper system used was determined to be:

$$\begin{bmatrix} X_1(k+1) \\ X_2(k+1) \end{bmatrix} = A\begin{bmatrix} X_1(k) \\ X_2(k) \end{bmatrix} + B[u(k)] + w(k) \tag{B.9}$$

$$Z(k) = H\begin{bmatrix} X_1(k) \\ X_2(k) \end{bmatrix} + v(k)$$

$$\text{where } H = \begin{bmatrix} 1 & 0 \end{bmatrix} \text{ and } A = \begin{bmatrix} 1 & T_s \\ 0 & 1 - \frac{BT_s}{M} \end{bmatrix} = \begin{bmatrix} 1 & 0.001 \\ 0 & 0.998 \end{bmatrix}$$

The observability matrix was written as follows:

$$Observability\ Matrix = \begin{bmatrix} H \\ HA \end{bmatrix} = \begin{bmatrix} 1 & 0 \\ 1 & 0.001 \end{bmatrix} \tag{B.10}$$

The rank of the observability matrix in this case was 2, which was equal to the length of the system matrix. Therefore, the system was considered to be observable. The estimated states converged to the simulated position and velocity (there was no visible difference between the simulated and estimated state), as illustrated in Figure B.1.

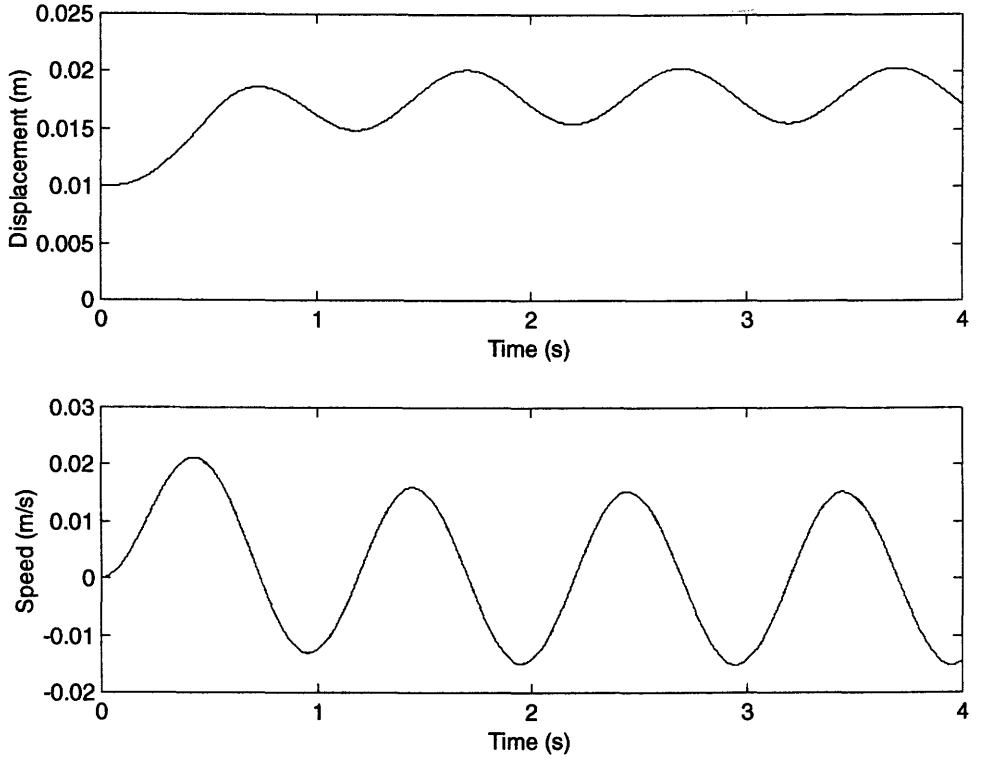

Figure B.1: Estimated States for the Observable Mass-Damper System Using Position as the only Measurement

The initial state matrix and the initializing matrices for the EKF code were set to:

$$X(0) = \begin{bmatrix} 0 & 0 \end{bmatrix},\ P(0) = \begin{bmatrix} 1\times10^2 & 0 \\ 0 & 1\times10^2 \end{bmatrix} \tag{B.11}$$

$$Q(k) = \begin{bmatrix} 1\times10^{-9} & 0 \\ 0 & 1\times10^{-12} \end{bmatrix},$$

$$R(k) = 1\times10^{-12}$$

Next, the Mass-Damper system was used with velocity as measurement. The simulated input and velocity were the two inputs to the Kalman Filter. Therefore, in this case, the observability matrix was found as follows:

$$Observability\ Matrix = \begin{bmatrix} H \\ HA \end{bmatrix} = \begin{bmatrix} 0 & 1 \\ 0 & 0.998 \end{bmatrix} \tag{B.12}$$

The rank of the observability matrix given by Equation (B.12) is 1, which is less than the length of the system matrix and the system was not considered to be observable. The Kalman Filter was applied to the system and used to estimate the position and velocity. The estimated position did not match the simulated position, as shown in Figure B.2.

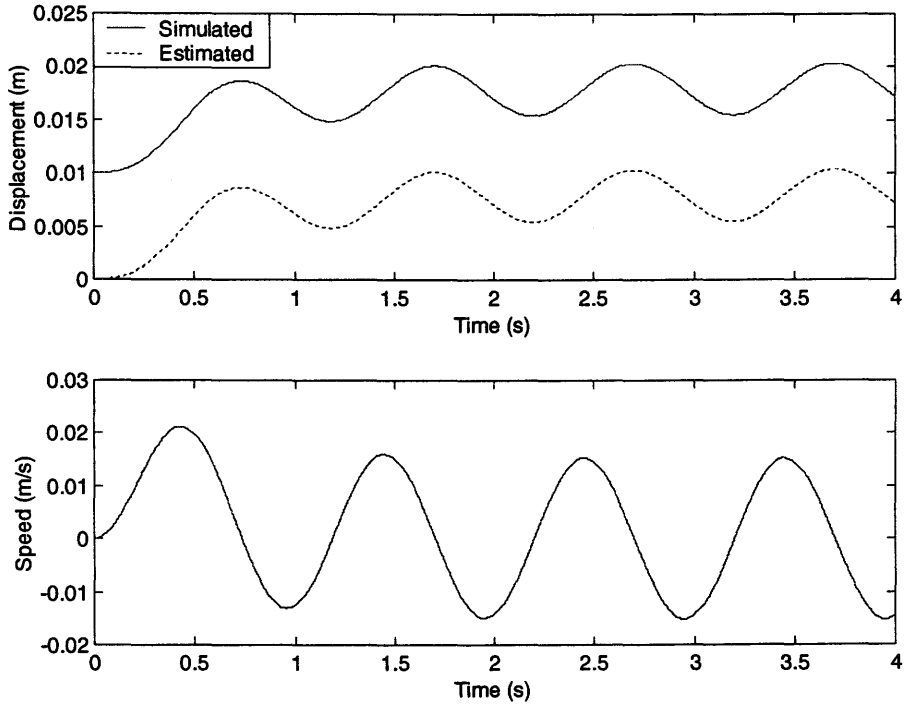

Figure B.2: Estimated States for the Unobservable Mass-Damper System

From Figure B.2, it is observed that the estimated position is "biased". The shift in the estimated position is equal in magnitude to the initial condition of position used in the simulation (0.01 m). In simulation, it was found that using velocity as the only measurement was insufficient to estimate the initial condition of the position, but was sufficient to estimate the change in position.

In summary, for the Mass-Damper system, position as a measurement was sufficient for the system to be observable and for the Kalman Filter to estimate velocity (a derivative of position). The observability test in that case showed that all initial conditions (position and velocity) could be traced back by using the measurements. The observability condition failed when velocity was used as measurement and it was showed that the initial conditions could not be traced back. As such, from the Mass-Damper system, it could be deduced that the Kalman filter successfully estimated states for observable systems.

From Equation (B.6), it can be seen that for the Mass-Damper system, if the position is a measurement (i.e. known), velocity can be obtained (estimated). However, the converse is not true since the position term is not present in the velocity equation. Therefore, it can be deduced that using position as the measurement, information about both states (position and velocity) can be obtained, but when velocity is used as the measurement, information about position is not obtained (system is not observable). It was surprising to observe that the Kalman filter, even in such adverse conditions, was able to estimate the position when velocity was the measurement, although failing to estimate the initial position. Next, using the same unobservable Mass-Damper system, it was assumed that the initial position was known and the two states were once again estimated. The "bias" disappeared and the Kalman Filter was seen to estimate both states successfully, in spite of the system being unobservable.

Next, the effect of using both the position and velocity was also investigated in simulation. In this particular scenario, the rank of the observability matrix was 2 and therefore the system was fully observable, as shown below.

$$\textit{Observability Matrix} = \begin{bmatrix} H \\ HA \end{bmatrix}, \text{ where } H = \begin{bmatrix} 1 & 0 \\ 0 & 1 \end{bmatrix}, A = \begin{bmatrix} 1 & T_s \\ 0 & 1 - \frac{BT_s}{M} \end{bmatrix} = \begin{bmatrix} 1 & 0.001 \\ 0 & 0.998 \end{bmatrix}$$

$$Observability\ Matrix = \begin{bmatrix} H \\ HA \end{bmatrix} = \begin{bmatrix} 1 & 0 \\ 0 & 1 \\ 1 & 0.001 \\ 0 & 0.998 \end{bmatrix} \tag{B.13}$$

The Kalman filter successfully estimated the states as illustrated in Figure B.3.

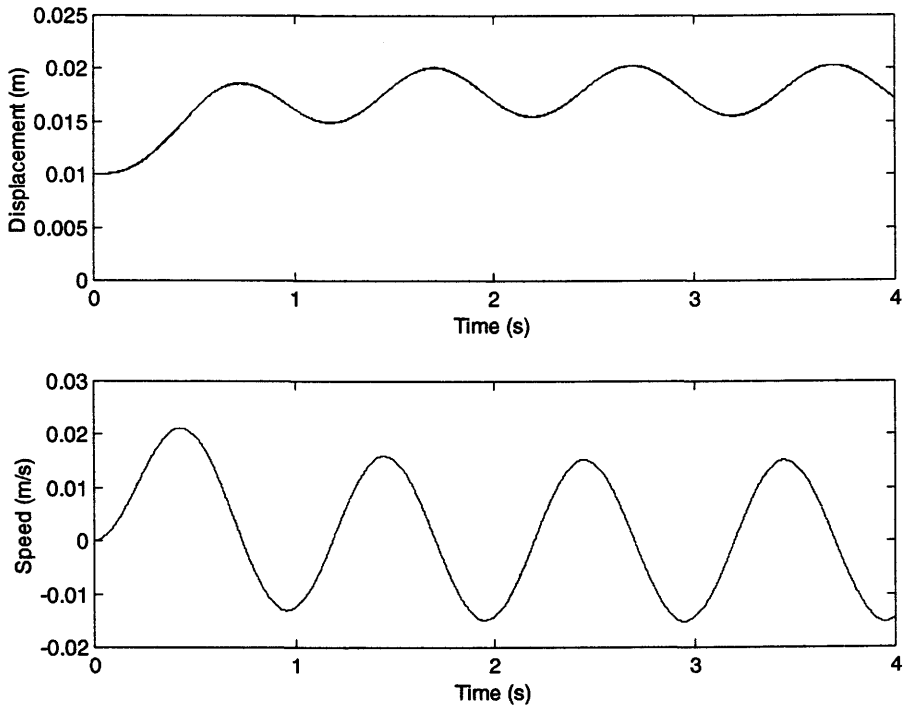

Figure B.3: Estimated States for System made Observable by Using both Position and Velocity as Measurements.

The initial state matrix and the initializing matrices for the EKF code for this scenario were set to:

$$X(0) = [0 \quad 0], \qquad P(0) = \begin{bmatrix} 1\times10^{2} & 0 \\ 0 & 1\times10^{4} \end{bmatrix} \tag{B.14}$$

$$Q(k) = \begin{bmatrix} 1\times10^{-4} & 0 \\ 0 & 1\times10^{-3} \end{bmatrix}, \quad R(k) = \begin{bmatrix} 1\times10^{-4} & 0 \\ 0 & 1\times10^{-2} \end{bmatrix}$$

In this simulation study, consistent with what has been reported in the literature, the Kalman filter estimated correctly the states for observable systems only. When the

system was made unobservable by using velocity instead of position as the measurement, the Kalman filter estimated velocity successfully but revealed the presence of a "bias" equal to the initial position used for the estimated position. The knowledge of the initial condition enabled the Kalman filter to estimate position successfully in spite of the system not being observable. In the following section, the Mass-Damper system is used to illustrate the importance of observability in order to estimate states (position, velocity and viscous damping) using the Extended Kalman Filter. This time, since two states and one parameter were estimated, the resulting state space model was nonlinear and hence, the Extended Kalman Filter was used.

B.3 Application of Extended Kalman Filter to the Mass-Damper System

In this study, the Extended Kalman Filter is used as a technique for parameter estimation and the parameters are described as coefficients of the state equations. Simultaneous estimation of the states and the parameters, via a state vector augmentation, results in a nonlinear problem [Ljung, 1979]. In order to estimate the parameters, the EKF requires a state model that includes all parameters or coefficients as state variables in the state vector. Thus, an extended state vector is as follows:

$$X'(t) = [X(t), \theta(t)]^T \tag{B.15}$$

where $\theta(t)$ represents the system parameter vector, $X'(t)$ the extended state vector, and $X(t)$ the state vector. The EKF technique is then used to obtain a real-time estimate of the extended state vector, $X'(t)$, which includes the required parameters or coefficients.

Using the Mass-Damper system, the Extended Kalman Filter was used to estimate the damping coefficient in simulation and the state space model used was as follows:

$$\dot{X}_1(t) = X_2(t) + w_1(t) \tag{B.16}$$

$$\dot{X}_2(t) = \frac{(u(t) - X_3(t)X_2(t))}{M} + w_2(t)$$

$$\dot{X}_3(t) = w_3(t)$$

where $X_1(t)$ is the displacement, (m), $X_2(t)$ the velocity, (m/s), $X_3(t)$ the damping coefficient, (Ns/m) and w_1, w_2 and w_3 the system noise.

Using the "forward difference" approximation, with T_s being the sampling time, the discrete state space model for the mechanical system was expressed as

$$X_1(k+1) = X_1(k) + T_s X_2(k) + T_s w_1(k)$$

$$X_2(k+1) = (u(k) - X_3(k)X_2(k))\frac{T_s}{M} + X_2(k) + T_s w_2(k)$$

$$X_3(k+1) = X_3(k) + T_s w_3(k)$$

$$Z(k) = X_1(k) + v(k) \qquad \text{(B.17)}$$

where the sampling time, T_s, was 0.001s for this example.

Equations (5.34) and (5.35) (presented in Chapter 5) are the general nonlinear discrete state space model and are shown below:

$$X(k+1) = f(X(k), U(k)) + W(k) \qquad (5.34)$$

$$Z(k) = h(X(k)) + V(k) \qquad (5.35)$$

Using Equations (5.40) and (5.41) also repeated below, the linearized system for the Mass-Damper example becomes:

$$X(k+1) = \Phi(k)X(k) + U_1(k) + W(k) \qquad (5.40)$$

$$Y(k) = H(k)X(k) + V(k) \qquad (5.41)$$

The linearized state matrix for the Mass-Damper system was expressed as:

$$\text{where } \Phi(k) = \frac{\partial f(X(k))}{\partial X(k)} = \begin{bmatrix} \Phi_{11}(k) & \Phi_{12}(k) & \Phi_{13}(k) \\ \Phi_{21}(k) & \Phi_{22}(k) & \Phi_{23}(k) \\ \Phi_{31}(k) & \Phi_{32}(k) & \Phi_{33}(k) \end{bmatrix}$$

$$\Phi_{11}(k) = 1,\ \Phi_{12}(k) = T_s, \Phi_{13}(k) = 0$$

$$\Phi_{21}(k) = 0,\ \Phi_{22}(k) = 1 - \frac{X_3(k)T_s}{M},\ \Phi_{23}(k) = \frac{-X_2(k)T_s}{M}, \qquad \text{(B.18)}$$

$$\Phi_{31}(k) = 0,\ \Phi_{32}(k) = 0, \Phi_{33}(k) = 1.$$

Using the linearized state matrix, the observability matrix for this system was:

$$Observability\ Matrix = \begin{bmatrix} H \\ H\Phi \\ H(\Phi)^2 \end{bmatrix}, \text{ where } H = \begin{bmatrix} 1 & 0 & 0 \end{bmatrix}. \tag{B.19}$$

It should be noted that only X_1 was a measurement. The observability matrix was calculated at each iteration and the results are shown in Figure B.4. It was seen that the rank of the observability matrix was 3 at each iteration and it was equal to the length of the augmented state matrix (length is 3). Therefore, based on the results of the previous simulation, it was expected that the EKF should be able to estimate the states and parameters successfully and accurately.

The EKF code (consisting of the Kalman Filter equations and of the linearized state matrix) was written in "Matlab". The sinusoidal input and the output (displacement) were both fed to the EKF. Figure B.4 depicts the plots for the estimated states (displacement and velocity) and for the estimated damping coefficient.

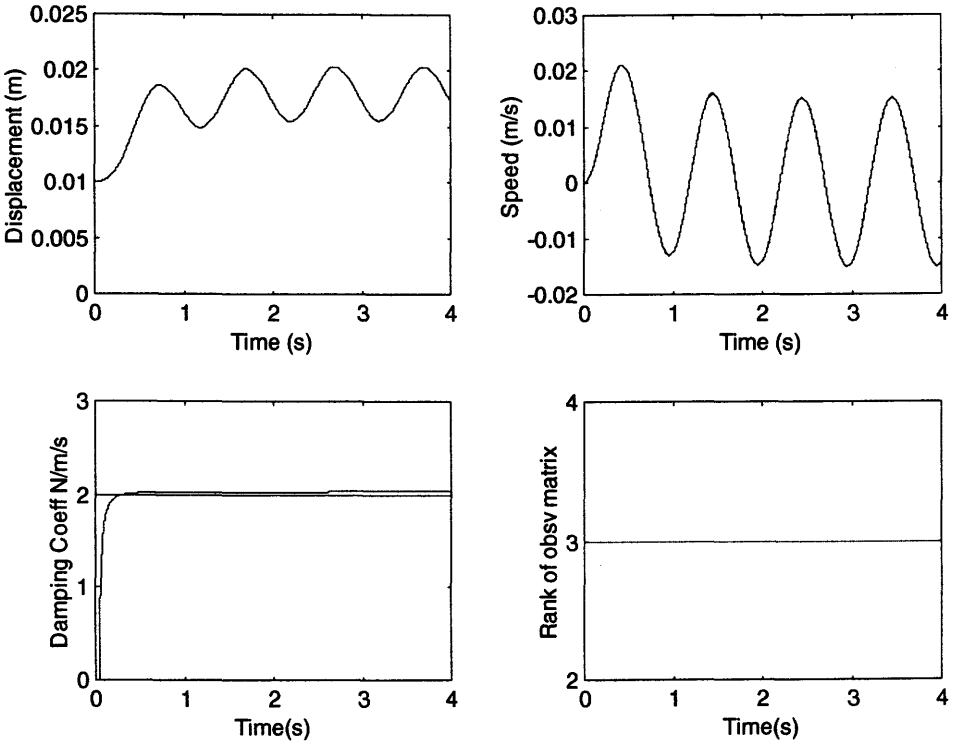

Figure B.4: Applying the EKF to the Observable Mass-Damper System

The known value for the parameter is also shown in this Figure. The estimated states match the simulated states very closely as shown in Figure B.4. The estimated viscous damping coefficient is 2.035 Ns/m (1.75 % estimation error). The results are consistent with the previous case.

The initial state matrix and the initializing matrices used for the EKF code were:

$$X(0) = [0 \quad 0 \quad 0]^T \qquad R(k) = 1\times10^{-9} \tag{B.20}$$

$$P(0) = \begin{bmatrix} 1\times10^{2} & 0 & 0 \\ 0 & 1\times10^{2} & 0 \\ 0 & 0 & 1\times10^{12} \end{bmatrix} \qquad Q(k) = \begin{bmatrix} 0 & 0 & 0 \\ 0 & 1\times10^{-3} & 0 \\ 0 & 0 & 1\times10^{-4} \end{bmatrix}$$

Since the objective of any condition-monitoring scheme is to detect changes in parameters, the damping coefficient was changed in the simulated model and the EKF used to estimate its corresponding value. The results are shown in Table B.1 and it can be concluded that for the observable system, the EKF estimates the changes in the parameter within 2% with the accuracy improving as the damping coefficient increased.

Table B.1: EKF was Used to Estimate Changes in the Damping Coefficient for the Observable System (Simple Mass-Damper System)

Simulated Damping Coefficient Ns/m	**Estimated Damping Coefficient Ns/m**	**Estimation Error (% error)**
2	2.0348	1.74
3	3.036	1.2
1	1.031	3.1
5	5.037	0.74
10	10.038	0.38
30	30.039	0.13
100	100.04	0.04
300	300.04	0.013
1000	999.59	0.041

Next, the same system was used and velocity was used as a measurement instead of position. This was done to render the system unobservable. This was verified by carrying the observability test at each time step, as shown in Figure B.5. The rank of the observability matrix was 2 as compared to the length of the augmented state matrix which was 3. Therefore it was concluded that the system was not observable.

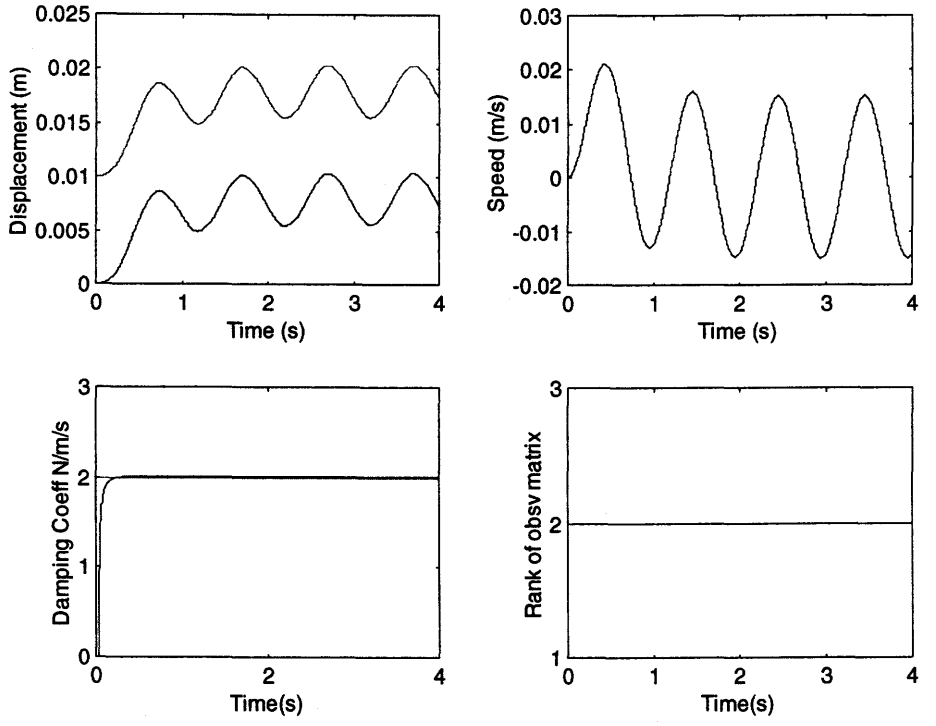

Figure B.5: Using the EKF to Estimate States and Parameters for Unobservable System

The EKF was used to estimate the position, velocity and damping coefficient for this system. From Figure B.5, it is seen that the estimated and the simulated position do not match (reveals the presence of a bias equal to the initial condition of position). The estimated and simulated velocity match. The estimated parameter is shown in Figure B.5 and is seen to be close to the known value of the parameter. The initial matrixes used were similar to the ones used previously and was given in Equation (B.20). When the initial position was known, the "bias" disappeared. It can be concluded that the EKF estimated the parameter successfully in spite of the system not being observable.

Examination of Equation (B.16) reveals that, if velocity is known (measured), damping coefficient will be estimated by the Kalman Filter. The unobservable system was next made observable by using both position and velocity. As shown in Figure B.6, the rank of the observability matrix was equal to the length of the augmented state; the EKF output showed good agreement between the simulated states and estimated stated as well as between the estimated parameter and the known parameter used in the simulation study.

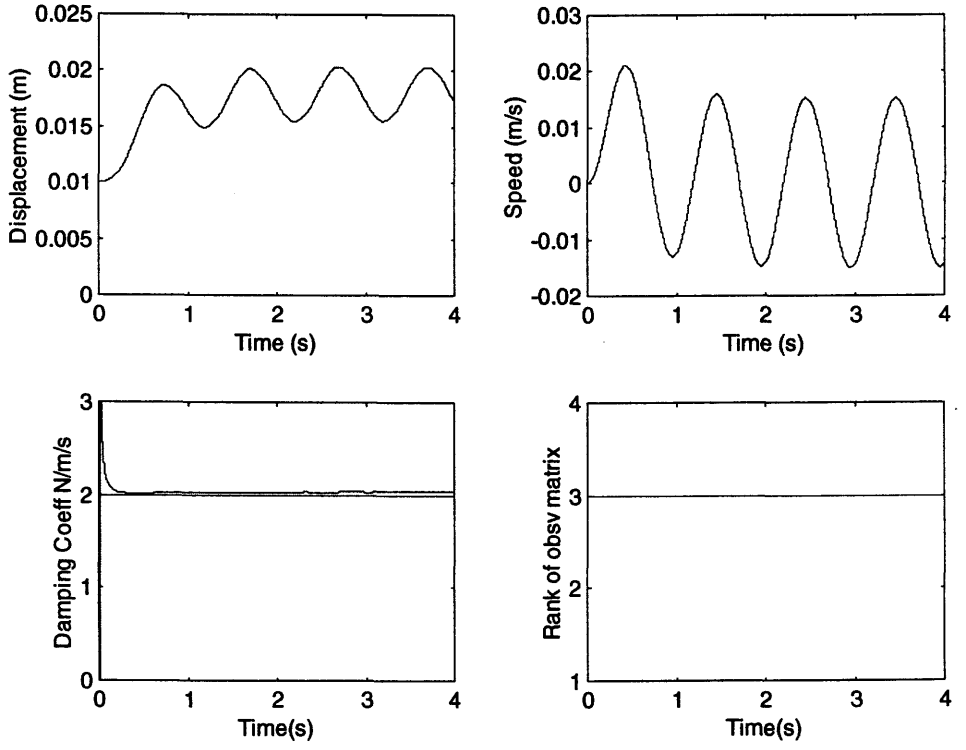

Figure B.6: EKF Applied to the Unobservable Mass-Damper System Rendered Observable by Using More Measurements

The initial state matrix and the initializing matrices for the EKF were set to:

$$X(0) = [0 \quad 0 \quad 0], \qquad P(0) = \begin{bmatrix} 1\times10^{2} & 0 & 0 \\ 0 & 1\times10^{2} & 0 \\ 0 & 0 & 1\times10^{12} \end{bmatrix} \tag{B.21}$$

$$Q(k)=\begin{bmatrix}0 & 0 & 0\\ 0 & 1\times10^{-3} & 0\\ 0 & 0 & 1\times10^{-4}\end{bmatrix},\ R(k)=\begin{bmatrix}1\times10^{-9} & 0\\ 0 & 1\times10^{-4}\end{bmatrix}$$

The estimated states matched the simulated states and the estimated damping coefficient was 2.034Ns/m (1.7 % estimation error).

From this section, it was concluded that observability condition was important for the Kalman Filter to successfully estimate states in the Mass-Damper system. The Extended Kalman Filter successfully estimated a parameter even when the observability test failed (when using velocity as the only measurement). However, the use of velocity as measurement produced one unobserved state which was position and estimation of the viscous damping coefficient did not depend on position, as shown by equation B.16. The estimated position was biased when velocity was the measurement. The magnitude of the state estimation, however, was accurate and if the initial position was known and used in the EKF code, the estimated position matched the simulated position very accurately. It was also seen that when the number of measurements was increased (using both position and velocity) and the system was made observable (for the Mass-Damper system), the output of the Kalman filter and the EKF showed good agreement between the estimated states/parameters and the simulated ones. In the next section, the order of the state matrix was increased by including a spring in the Mass-Damper system.

B.4 Mass-Spring-Damper System

The Kalman Filter and the Extended Kalman Filter were applied to a simple second order, underdamped mechanical system (Mass-Spring-Damper system) which is described by Equation (B.22).

$$M\ddot{X}(t)+B\dot{X}(t)+KX(t)=u(t)+w(t) \tag{B.22}$$

where $X(t)$ is the displacement (m), $\dot{X}(t)$ the velocity (m/s), $u(t)$ the driving force (N), $w(t)$ the additive white noise (N), B the viscous damping coefficient, K the spring constant and M was the mass. This example, is the same that had been used in [Grewal et al, 1993]. Grewal used the Mass-Spring-Damper system to demonstrate the methodology used when the Kalman and the Extended Kalman Filter were applied to the

system in order to estimate states and the damping ratio $\{\varsigma = \frac{B}{2(\sqrt{MK})}\}$. Two states were estimated successfully using the EKF (position and velocity) and the estimated damping ratio agreed with its simulated value when only position was used as measurement. An analysis of the observability matrix showed that when the state matrix was augmented to accommodate the damping ratio, the system was observable.

An extension of the example has been reported in [Zavarehi, 1997] and [Cao, 2001] where the EKF technique was applied to a Mass-Spring-Damper system and the EKF was used to estimate two parameters, namely the viscous damping coefficient and the spring constant coefficient. The equations describing the Mass-Spring-Damper system were simulated. The input $u(k)$ was a sinusoid with amplitude of 0.1N and a frequency of 1 Hz. A mass of 1 kg, a damping coefficient of 2 Ns/m and a spring constant of 25 N/m were used as the simulation parameters.

In the first instance, the Kalman Filter was applied to the linear system which was fully observable for position measurement only. The state space model for the Mass-Spring-Damper system is described by Equation (B.23).

$$\dot{X}_1(t) = X_2(t) + w_1(t) \tag{B.23}$$

$$\dot{X}_2(t) = \frac{(u(t) - BX_2(t) - KX_1(t))}{M} + w_2(t)$$

Using the "forward difference" approximation, with T_s being the sampling time, discrete state space model for the mechanical system can be expressed as:

$$X_1(k+1) = X_1(k) + T_s X_2(k) + T_s w_1(k) \tag{B.24}$$

$$X_2(k+1) = (u(k) - BX_2(k) - KX_1(k))\frac{T_s}{M} + X_2(k) + T_s w_2(k)$$

$$Z(k) = X_1(k) + v(k)$$

The estimated states (displacement and velocity) are shown in Figure B.7. The sinusoidal input and the output (displacement) were used to estimate the position and velocity. No visible difference in the estimated and simulated states was observed, as shown in Figure B.7

The initial matrices in the EKF algorithm used for this scenario were set as:

$$X(0)=\begin{bmatrix}0 & 0\end{bmatrix}, \qquad P(0)=\begin{bmatrix}1\times10^{2} & 0\\ 0 & 1\times10^{2}\end{bmatrix} \tag{B.25}$$

$$Q(k)=\begin{bmatrix}1\times10^{-4} & 0\\ 0 & 1\times10^{-5}\end{bmatrix},\ R(k)=1\times10^{-9}$$

The observability matrix was written as:

$$Observability\ Matrix=\begin{bmatrix}H\\ HA\end{bmatrix}, \tag{B.26}$$

$$\text{where } H=\begin{bmatrix}1 & 0\end{bmatrix} \text{ and } A=\begin{bmatrix}1 & T_s\\ \frac{-KT_s}{M} & 1-\frac{BT_s}{M}\end{bmatrix}=\begin{bmatrix}1 & 0.001\\ -0.025 & 0.998\end{bmatrix}$$

$$Observability\ Matrix=\begin{bmatrix}H\\ HA\end{bmatrix}=\begin{bmatrix}1 & 0\\ 1 & 0.001\end{bmatrix}$$

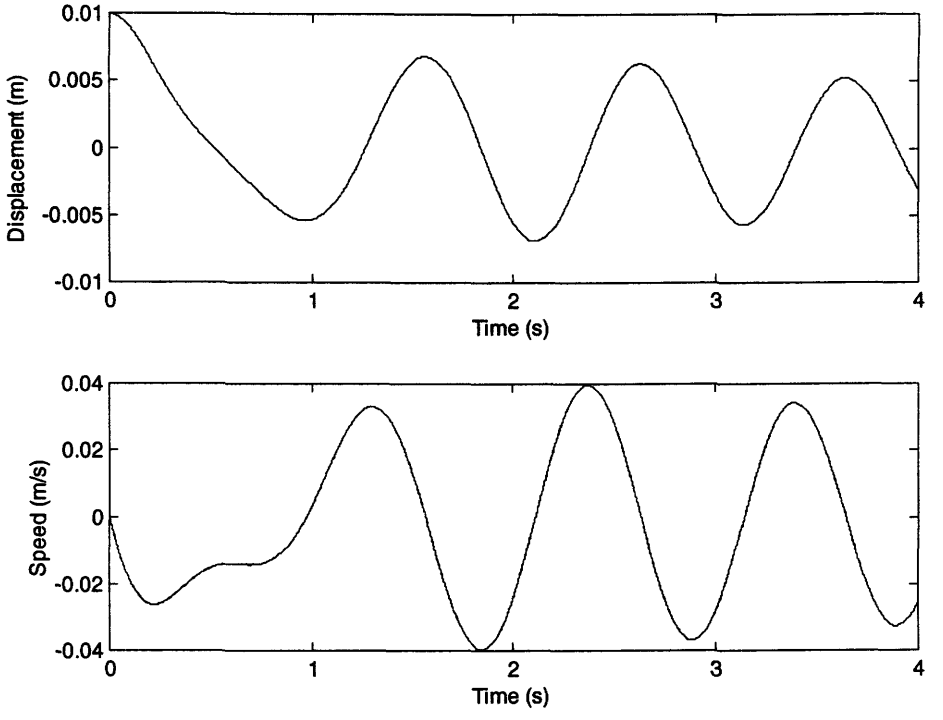

Figure B.7: Estimated States by the Kalman Filter for the Observable Mass-Spring-Damper System

From Equation (B.26), the rank of the observability matrix was 2, which was equal to the length of the state matrix and thus it was confirmed that the system was fully observable. As was done with the Mass-Damper system, an attempt was made to make the system unobservable by using a different set of measurements i.e. by using velocity only. However, it was observed that the system remained observable as shown by the following equations:

$$Observability\ Matrix = \begin{bmatrix} H \\ HA \end{bmatrix} = \begin{bmatrix} 0 & 1 \\ -0.025 & 0.998 \end{bmatrix} \tag{B.27}$$

The rank of the observability matrix remained 2 and thus the system was observable. The Kalman Filter was next applied to the system and as expected, the estimated states showed good agreement with the simulated ones as illustrated in Figure B.8.

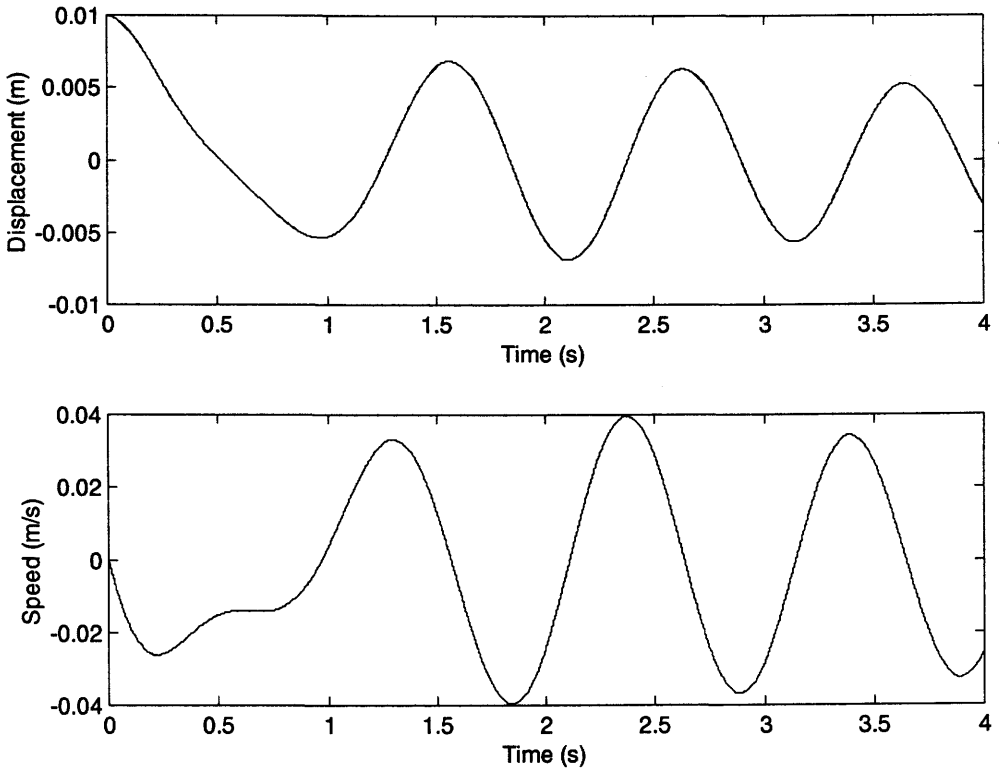

Figure B.8: Estimated States Match the Simulated ones when Kalman Filter is Applied to the Observable Mass Spring Damper System, with Velocity as Measurement

In this scenario, the velocity was dependent on force exerted by the spring. The system remained observable although velocity alone was used as measurement. It was interesting to note that unlike the Mass-Damper example (Type 1 system), the Mass-Spring-Damper scenario (Type 0 system) had the displacement term in the velocity equation given by Equation (B.24), which accounted for the Kalman filter being able to use velocity measurements to trace back the initial condition for position. Also, it was verified in simulation that using different initial positions always made the estimated position by the Kalman filter to agree with the simulated position. In this example, observability condition was not obvious but could be deduced mathematically. Consistent with previous cases, the Kalman filter estimated the states accurately when the system was observable.

B.5 Using the EKF to Estimate Parameters (and states) for the Mass-Spring-Damper System

In this section, one parameter, namely the viscous damping is estimated using the Extended Kalman Filter technique. In the first instance, for the Mass-Spring-Damper system, it was assumed that the spring constant value was known. The importance of this particular study lies in reducing the number of states (three states only, similar to the work reported in [Grewal, et al, 1993]), and ensuring that the observability condition was satisfied. The state space model for the Mass-Spring-Damper system described by Equation B.23 can be written as follows:

$$\dot{X}_1(t) = X_2(t) + w_1(t)$$

$$\dot{X}_2(t) = \frac{(u(t) - X_3(t)X_2(t) - KX_1(t))}{M} + w_2(t)$$

$$\dot{X}_3(t) = w_3(t) \qquad \text{(B.28)}$$

where $X_1(t)$ is the displacement, (m), $X_2(t)$ the velocity, (m/s), $X_3(t)$ the damping coefficient, (Ns/m) , w_1, w_2 and w_3 the system noise.

Using the "forward difference" approximation, with T_s being the sampling time, the discrete state space model for the mechanical system can be written as:

$$X_1(k+1) = X_1(k) + T_s X_2(k) + T_s w_1(k) \tag{B.29}$$

$$X_2(k+1) = (u(k) - X_3(k)X_2(k) - KX_1(k))\frac{T_s}{M} + X_2(k) + T_s w_2(k)$$

$$X_3(k+1) = X_3(k) + T_s w_3(k)$$

$$Z(k) = X_1(k) + v(k)$$

The linearized system for the Mass-Spring-Damper system is described as follows:

$$X(k+1) = \Phi(k)X(k) + U_1(k) + W(k) \tag{B.30}$$

$$\text{where } \Phi(k) = \frac{\partial f(X(k))}{\partial X(k)} = \begin{bmatrix} \Phi_{11}(k) & \Phi_{12}(k) & \Phi_{13}(k) \\ \Phi_{21}(k) & \Phi_{22}(k) & \Phi_{23}(k) \\ \Phi_{31}(k) & \Phi_{32}(k) & \Phi_{33}(k) \end{bmatrix}$$

$$\Phi_{11}(k) = 1,\ \Phi_{12}(k) = T_s, \Phi_{13}(k) = 0$$

$$\Phi_{21}(k) = \frac{-KT_s}{M},\ \Phi_{22}(k) = 1 - \frac{X_3(k)T_s}{M},\ \Phi_{23}(k) = \frac{-X_2(k)T_s}{M},$$

$$\Phi_{31}(k) = 0,\ \Phi_{32}(k) = 0, \Phi_{33}(k) = 1.$$

The EKF code (consisting of the Kalman Filter equations and of the linearized state matrix) was written in "Matlab". Figure B.9 depicts the plots for the estimated states (displacement and velocity), and for the damping coefficient .The sinusoidal input and the output (displacement) were both fed to the EKF. Results showed good agreement between the estimated and the simulated states. The estimated parameter agreed with the known simulated parameter value. The estimated viscous damping coefficient was 2.037 Ns/m, showing an estimation error of 1.85%. As mentioned previously, the rank of the observability matrix and the length of the state matrix were equal.

The initial state matrix and the initializing matrices for the EKF code were set as:

$$X(0) = [0 \quad 0 \quad 0]^T \qquad R(k) = 1\times10^{-9} \tag{B.31}$$

$$P(0) = \begin{bmatrix} 1\times10^{2} & 0 & 0 \\ 0 & 1\times10^{2} & 0 \\ 0 & 0 & 1\times10^{12} \end{bmatrix} \quad Q(k) = \begin{bmatrix} 0 & 0 & 0 \\ 0 & 1\times10^{-3} & 0 \\ 0 & 0 & 1\times10^{-4} \end{bmatrix}$$

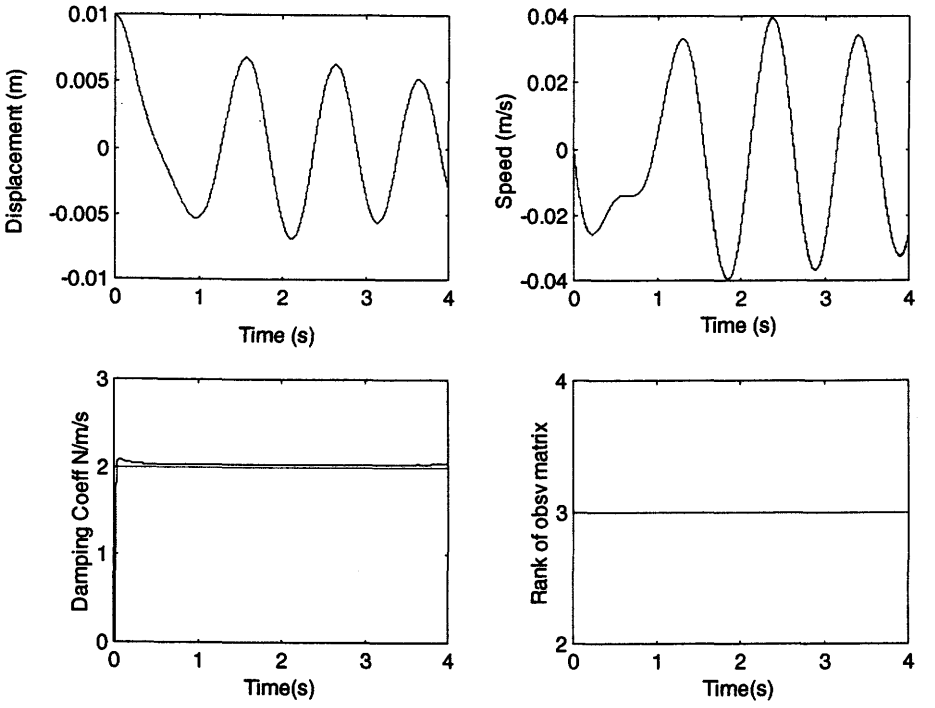

Figure B.9: Plots for Estimated States and Viscous Damping Coefficient for the Observable Mass-Spring-Damper System.

The viscous damping coefficient value was then changed in the simulated model and the EKF used to estimate its value and the results are shown in Table B.2. This was done to verify that the EKF detected the changes and estimated them accurately.

From Table B.2, it was concluded that the EKF estimated the viscous damping coefficient within 2.5% error at all the values used for the spring constant coefficient. The estimation error decreased with increased damping. Also, as mentioned earlier, the system used in the simulation study was completely observable. As was found in Section B.2, for an observable Mass-Spring-Damper system, the EKF was able to estimate the targeted parameter as well as changes in the parameter in simulation to within 2% for the conditions estimated.

Next, the effect of using velocity as measurement and using the EKF to estimate position, velocity and damping coefficient in the Mass-Spring-Damper system was investigated. Using the linearized state matrix, the observability matrix for this particular scenario has been determined to be:

$$Observability\ Matrix = \begin{bmatrix} H \\ H\Phi \\ H(\Phi)^2 \end{bmatrix}, \text{ where } H = [0 \quad 1 \quad 0]. \tag{B.32}$$

The rank of the observability matrix was calculated at each iteration and the results are shown in Figure B.10. As seen in Figure B.10, the rank for the observability matrix is always equal to 2 (the length of the augmented state matrix, which has a length of 3). In this case, the estimated position does not match the simulated position, as shown in Figure B.10. The estimated damping coefficient does not converge to the known damping coefficient value used in the simulation, in spite of tuning the filter extensively.

Table B.2: Estimated Viscous Damping Coefficient in the Mass-Spring-Damper System

Simulated Spring Constant, K (N/m)	**Simulated Viscous Damping, (Ns/m)**	**Estimated Viscous Damping (Ns/m)**	**Estimation Error (%)**
25	2	2.037	1.85
25	4	4.038	0.95
25	10	10.04	0.4
25	20	20.04	0.2
25	40	40.04	0.1
25	100	100.3	0.3
25	200	200.4	0.2
25	300	300.04	0.013
25	500	500.01	0.002
25	1000	999.6	0.04
10	2	2.036	1.8
5	2	2.036	1.8
30	2	2.038	1.9
100	2	2.046	2.3
100	20	20.04	0.2
100	500	500.01	0.002
300	20	20.04	0.2

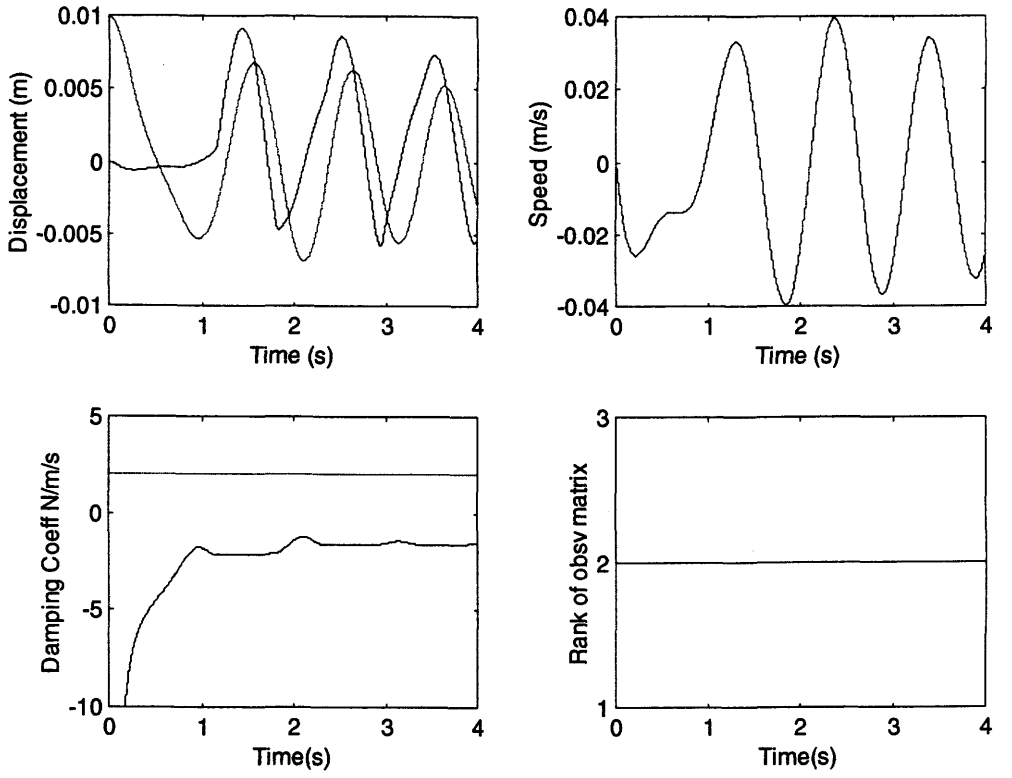

Figure B.10: Applying the EKF to the Unobservable Mass-Spring-Damper System (Velocity as Measurement)

In this scenario, the damping coefficient depends on the position, as shown in Equation (B.28) and position is not known. For state estimation, the Kalman Filter was able to obtain position using the velocity measurements but not the EKF which has two unknowns, namely position and viscous damping coefficient.

Next, for the same Mass-Spring-Damper system, the spring constant was estimated using the EKF. The state space formulation, with $X_3(k)$ being the estimated spring constant is written as follows

$$X_1(k+1) = X_1(k) + T_s X_2(k) + T_s w_1(k) \tag{B.33}$$

$$X_2(k+1) = (u(k) - BX_2(k) - X_3(k)X_1(k))\frac{T_s}{M} + X_2(k) + T_s w_2(k)$$

$$X_3(k+1) = X_3(k) + T_s w_3(k)$$

$$Z(k) = X_1(k) + v(k)$$

The linearized system for the Mass-Spring-Damper system is described as follows:

$$X(k+1) = \Phi(k)X(k) + U_1(k) + W(k) \tag{B.34}$$

$$\text{where } \Phi(k) = \frac{\partial f(X(k))}{\partial X(k)} = \begin{bmatrix} \Phi_{11}(k) & \Phi_{12}(k) & \Phi_{13}(k) \\ \Phi_{21}(k) & \Phi_{22}(k) & \Phi_{23}(k) \\ \Phi_{31}(k) & \Phi_{32}(k) & \Phi_{33}(k) \end{bmatrix}$$

$$\Phi_{11}(k) = 1,\ \Phi_{12}(k) = T_s, \Phi_{13}(k) = 0$$

$$\Phi_{21}(k) = \frac{-X_3(k)T_s}{M},\ \Phi_{22}(k) = 1 - \frac{BT_s}{M},\ \Phi_{23}(k) = \frac{-X_1(k)T_s}{M},$$

$$\Phi_{31}(k) = 0,\ \Phi_{32}(k) = 0, \Phi_{33}(k) = 1.$$

Figure B.11 depicts the plots for the estimated states (displacement and velocity), and for the estimated spring constant using the EKF when position is used as an input to the filter.

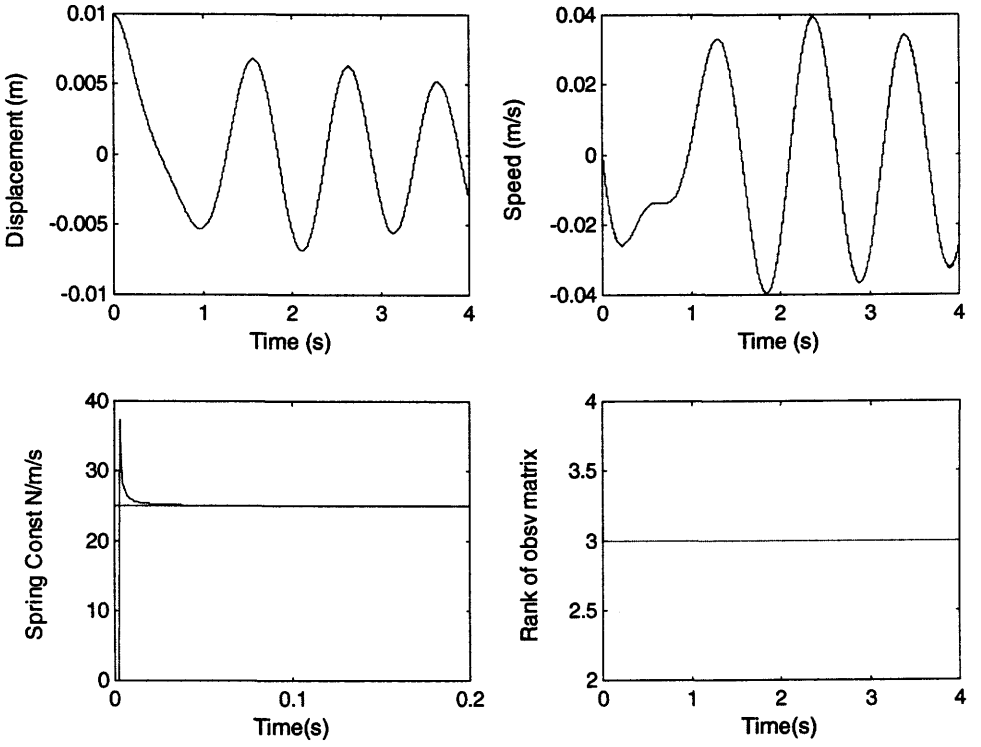

Figure B.11: Applying the EKF to the Observable Mass-Spring-Damper System to Estimate Spring Constant

The observability test was carried out at each iteration and the system was found to be fully observable (Rank of the observability matrix was equal to the length of the augmented state matrix, both being 3). The estimated and the simulated states agreed with each other and the estimated parameter converged to the known simulated parameter value. The estimated spring constant was 25.01 N/m, showing an estimation error of 0.05 %. The initial state matrix and the initializing matrices for the EKF code were set as:

$$X(0) = \begin{bmatrix} 0 & 0 & 0 \end{bmatrix}^T \qquad R(k) = 1\times10^{-9} \tag{B.35}$$

$$P(0) = \begin{bmatrix} 1\times10^{2} & 0 & 0 \\ 0 & 1\times10^{2} & 0 \\ 0 & 0 & 1\times10^{12} \end{bmatrix} \quad Q(k) = \begin{bmatrix} 0 & 0 & 0 \\ 0 & 1\times10^{-3} & 0 \\ 0 & 0 & 1\times10^{-4} \end{bmatrix}$$

Next, the spring constant value was then changed and the EKF was used to estimate the new values for this parameter. The value of the viscous damping coefficient was assumed to be known. The estimated spring constant and the corresponding estimation errors, are shown in Table B.3.

It was confirmed that the estimated states and parameter by the EKF showed good agreement with the simulated states and parameter when the system was observable. Next the system was made unobservable by using velocity as measurement and the EKF was used to estimate the position, velocity and the spring constant. The observability test was done at each iteration and it was confirmed that the system was not observable (Rank of the observability matrix was 2 and the length of the state matrix was 3). The estimated states and parameter are shown in Figure B.12.

From Figure B.12, it is observed that the estimated states and parameter do not match when the Mass-Spring-Damper system was not observable. This was consistent with the previous case where the same unobservable system was used to estimate viscous damping coefficient. However, the estimated position was better than the previous case where the damping coefficient was unknown and was estimated. Knowledge of the damping coefficient appeared to improve the estimated position. The bias disappeared if initial position is assumed to be known. It was interesting to note that in this example,

the EKF behaved differently when compared to the Mass-Damper system, where the filter estimated a parameter successfully even when the system was not observable.

Table B.3: Estimated Spring Constant in the Mass-Spring-Damper system

Simulated Viscous Damping (Ns/m)	Simulated Spring Constant (N/m)	Estimated Spring Constant (N/m)	Estimation Error (%)
2	25	25.01	0.04
2	50	49.99	0.02
2	75	74.9	0.13
2	100	99.82	0.18
2	200	199.6	0.20
2	500	498.9	0.22
2	1000	997.4	0.26
2	20	20.01	0.05
2	10	10.01	0.1
2	5	5.005	0.1
10	25	24.99	0.04
10	100	99.6	0.4
30	10	9.998	0.02
30	5	5.003	0.06
100	20	19.997	0.015

In summary, the importance of observability in terms of the EKF is not clear at this point although some observations can be made already. It is known that the two systems were different, one being of Type 1 (Mass-Damper) and the other of Type 0 (Mass-Spring-Damper). As such, the use of position as measurement (either as the only measurement or as one of the measurements) made the systems observable. State estimation (as well as the estimation of a single parameter) was successful for both examples. The contribution of velocity as a measurement differed for the systems. In the

Mass-Damper system, the use of velocity as measurement affected the estimated position only by introducing a "bias" in the estimation. The system was not observable. The estimated damping coefficient converged to its known value accurately. In the Mass-Spring-Damper system, the use of velocity as measurement proved to be insufficient to estimate either position or the viscous damping coefficient. The position term was present in the velocity equation and not knowing the position was sufficient not to make the estimated viscous damping coefficient converge to its known value.

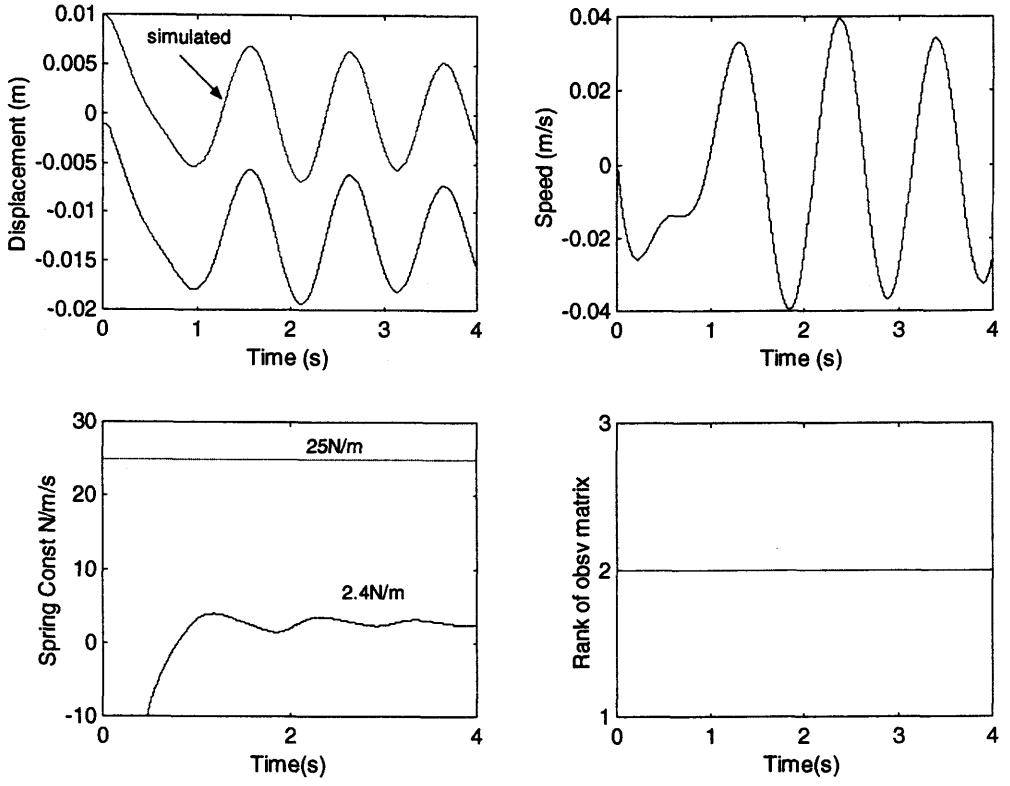

Figure B.12: Estimated States and Spring Constant using an Unobservable Mass-Spring-Damper System

B.6 Estimating Two Parameters in Mass-Spring-Damper system

Using the Mass-Spring-Damper system example, two parameters (namely the viscous damping coefficient and the spring constant) were estimated simultaneously

using position as the only measurement. This approach was similar to the one used in [Zavarehi, 1997] and [Cao, 2001]. The observablity test showed that augmenting the state matrix when using the two parameters resulted in the system failing the observability condition (Rank of observability matrix, 3 and the length of the augmented state matrix, 4). But since in the work done previously by the two authors showed that the EKF estimated the two parameters successfully, (in spite of the observability condition for their systems not being met), their work is repeated here for completeness.

Using equation (B.36), the state space model for the system can be expressed as follows:

$$\dot{X}_1(t) = X_2(t) + w_1(t) \tag{B.36}$$

$$\dot{X}_2(t) = \frac{(u(k) - X_3(t)X_2(t) - X_4(t)X_1(t))}{M} + w_2(t)$$

$$\dot{X}_3(t) = w_3(t)$$

$$\dot{X}_4(t) = w_4(t)$$

where $X_1(t)$ is the displacement, (m), $X_2(t)$ the velocity, (m/s), $X_3(t)$ the damping coefficient, (Ns/m), $X_4(t)$ the spring constant coefficient, (N/m), w_1, w_2, w_3 and w_4 the system noise.

The discrete state space model for the mechanical system can be expressed as

$$X_1(k+1) = X_1(k) + T_s X_2(k) + T_s w_1(k) \tag{B.37}$$

$$X_2(k+1) = (u(k) - X_3(k)X_2(k) - X_4(k)X_1(k))\frac{T_s}{M} + X_2(k) + T_s w_2(k)$$

$$X_3(k+1) = X_3(k) + T_s w_3(k)$$

$$X_4(k+1) = X_4(k) + T_s w_4(k)$$

$$Z(k) = X_1(k) + v(k)$$

where the sampling time, T_s was 0.001s for this example.

Using the nonlinear state space model of the mechanical system described by Equation (B.34), Equation (B.35) can be written as:

$$f(X(k),U(k)) = \begin{bmatrix} X_1(k) + T_s X_2(k) \\ X_2(k) - T_s X_3(k) X_2(k) - T_s X_1(k) X_4(k) + T_s u(k) \\ X_3(k) \\ X_4(k) \end{bmatrix}$$

$$W(k) = \begin{bmatrix} T_s w_1(k) \\ T_s w_2(k) \\ T_s w_3(k) \\ T_s w_4(k) \end{bmatrix}, \quad h(X(k)) = \begin{bmatrix} X_1(k) \\ 0 \\ 0 \\ 0 \end{bmatrix} \tag{B.38}$$

The linearized system can be described as follows:

$$\text{where } \Phi(k) = \frac{\partial f(X(k))}{\partial X(k)} = \begin{bmatrix} \Phi_{11}(k) & \Phi_{12}(k) & \Phi_{13}(k) & \Phi_{14}(k) \\ \Phi_{21}(k) & \Phi_{22}(k) & \Phi_{23}(k) & \Phi_{24}(k) \\ \Phi_{31}(k) & \Phi_{32}(k) & \Phi_{33}(k) & \Phi_{34}(k) \\ \Phi_{41}(k) & \Phi_{42}(k) & \Phi_{43}(k) & \Phi_{44}(k) \end{bmatrix} \tag{B.39}$$

$$\Phi_{11}(k) = 1,\ \Phi_{12}(k) = T_s, \Phi_{13}(k) = 0, \Phi_{14}(k) = 0$$

$$\Phi_{21}(k) = \frac{-X_4(k)T_s}{M},\ \Phi_{22}(k) = 1 - \frac{X_3(k)T_s}{M},\ \Phi_{23}(k) = \frac{-X_2(k)T_s}{M},\ \Phi_{24}(k) = \frac{-X_1(k)T_s}{M},$$

$$\Phi_{31}(k) = 0,\ \Phi_{32}(k) = 0, \Phi_{33}(k) = 1,\ \Phi_{34}(k) = 0$$

$$\Phi_{41}(k) = 0,\ \Phi_{42}(k) = 0, \Phi_{43}(k) = 0, \Phi_{44}(k) = 1$$

The EKF code (consisting of the Kalman Filter equations and of the linearized state matrix) was written in "Matlab". Figure B.13 depicts the plots for the estimated states (displacement and velocity), and the estimated parameters (damping coefficient and spring constant). The sinusoidal input and the output (displacement) were both fed to the EKF. The known values for the parameters are shown in Figure B.13. The estimated parameters converged to their known values. The estimated states matched the simulated states very closely as shown by their superimposed plots in Figure B.13.

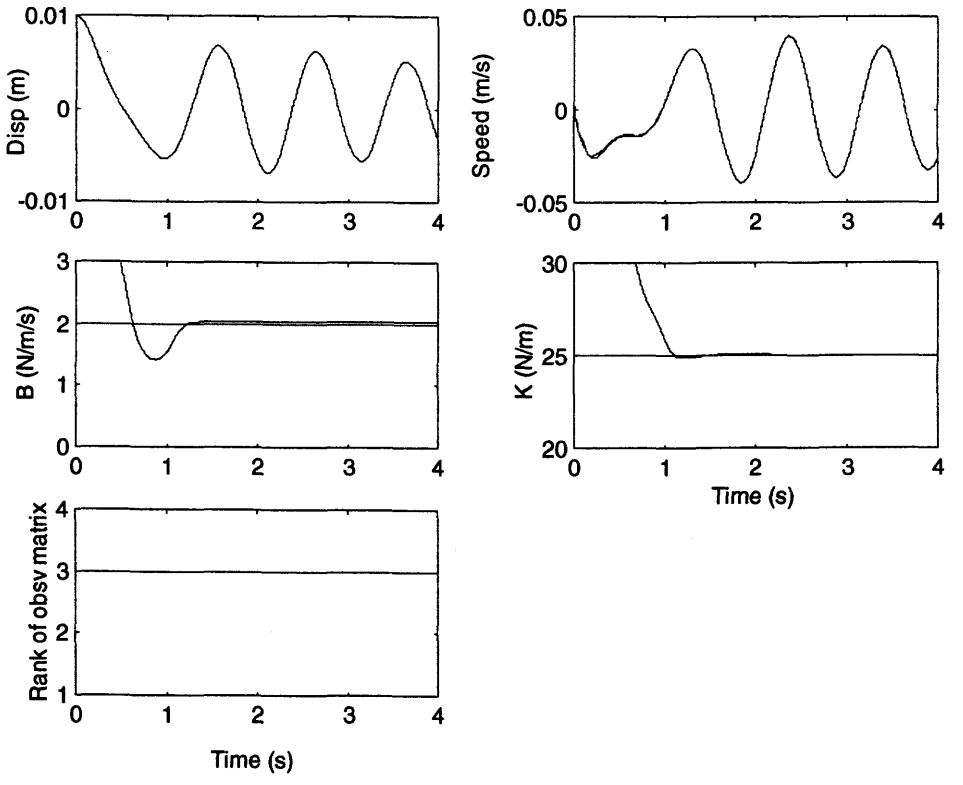

Figure B.13 Plots for the Estimated States and Parameters for the Mass-Spring-Damper System Using Position as Measurement.

Quite unexpectedly, in spite of the system not being completely observable, the estimated states and parameters by the EKF did match the simulated states and parameters. The estimated viscous damping coefficient was 2.04 Ns/m (2% error) and the estimated spring constant, 25.04 N/m (0.16% error).

The initial state matrix and the initializing matrices for the EKF code were:

$$X(0) = [0 \quad 0 \quad 0 \quad 0]^T \qquad R(k) = 1\times10^{-9}$$

$$P(0) = \begin{bmatrix} 1\times10^{2} & 0 & 0 & 0 \\ 0 & 1\times10^{2} & 0 & 0 \\ 0 & 0 & 1\times10^{22} & 0 \\ 0 & 0 & 0 & 1\times10^{22} \end{bmatrix}, \quad Q(k) = \begin{bmatrix} 0 & 0 & 0 & 0 \\ 0 & 0 & 0 & 0 \\ 0 & 0 & 1\times10^{-4} & 0 \\ 0 & 0 & 0 & 1\times10^{-3} \end{bmatrix} \tag{B.40}$$

It must be mentioned that in this example, the rank of the observability matrix was 3 and the length of the augmented state vector was 4 (position, velocity, damping coefficient and spring constant being the states/parameters to be estimated). As such there seems to be one unobserved state. It is not clear at this point what is the nature of that unobserved state since all the states are accurately estimated. By inspection of the state space model for this scenario, it can be deduced that when position is used as a measurement (known), velocity can be estimated and knowledge of both velocity and position is sufficient to estimate the two parameters which are damping coefficient (associated with velocity) and spring constant (associated with position).

Next, the parameters were changed, one at a time at first, followed by changing both of them and the EKF was applied to the simulated system and used to estimate the two states and two parameters. The results are given in Table B.4

It can be observed that the EKF detected changes and estimated the "new" values for the parameters successfully when the parameters were changed and position was used as measurement. The new parameter values seen in [Cao, 2001] were used and it was found that, indeed, the EKF estimated the parameters within a maximum error of 1.5%.

To summarize, the EKF was applied to a simple Mass-Spring -Damper system and its ability to detect changes in the parameters of interest, investigated. It was seen that when only one parameter was estimated using position as the only measurement, the resulting state space model was observable and the estimated states/parameter converged to their simulated values. This was true when position was used, not when velocity was used as the only measurement (system was then made unobservable). However, augmenting the state space model further by including a second parameter (spring constant) rendered the state space model unobservable, although position was used. It was expected that the estimated states and parameter by EKF would not show good agreement but instead, the EKF estimated the states and parameters successfully. It appears that given position as the measurement, state augmentation using parameters did not matter to the EKF, although the observability test showed the system not being observable.

Table B.4: Estimated Parameters for Mass-Spring-Damper System Using Position as Only Measurement.

Simulated Spring Constant, N/m	Simulated Viscous Damping Coefficient N/m/s	Estimated Spring Constant N/m	Estimation Error (%) Spring Constant	Estimated Viscous Damping Coefficient N/m/s	Estimation Error (%) Viscous Damping Coefficient
25	2	25.04	0.16	2.04	2
15	3	15.06	0.4	3.04	1.3
30	4	30.08	0.25	4.04	1
20	5	20.1	0.51	5.04	0.8
25	4	25.08	0.32	4.04	1
25	10	25.2	0.8	10.006	0.06
25	20	25.36	1.44	20.05	0.25
25	40	25.10	0.4	40.04	0.1
25	100	25.22	0.88	100.1	0.1
25	200	25.2	0.8	200.2	0.1
25	300	25.1	0.4	299.5	0.17
25	500	24.99	0.04	499.7	0.06
25	1000	25.01	0.04	999	0.1
10	2	10.037	0.37	2.04	2
5	2	5.04	0.8	2.04	2
30	2	30.04	0.13	2.04	2
100	2	102	2	1.986	0.7
200	2	200.2	0.1	2.02	1
100	20	100.4	0.4	20.04	0.2
100	300	99.25	0.75	297	1
100	500	99.7	0.3	498.3	0.34
300	20	303.5	1.17	20.04	0.2

The state space model however reveals that if position is known, velocity can be estimated and knowing the two states, the two parameters which are associated with the two states can be estimated. The system still behaved as an observable system since all the states were estimated from measurements in spite of failing the observability test. The issue here is whether the observability test can be extended to the EKF or not.

As a next step, the Mass-Spring-Damper system was made unobservable by using velocity as the measurement. The observability equation becomes:

$$Observability\ Matrix = \begin{bmatrix} H \\ H\Phi \\ H(\Phi)^2 \\ H(\Phi)^3 \end{bmatrix}, \text{ where } H = \begin{bmatrix} 0 & 1 & 0 & 0 \end{bmatrix}. \tag{B.41}$$

The rank for the observability matrix was calculated for each time step and it was found to be 2, as shown in Figure B.14. The length of the augmented state matrix was 4. This resulted in 2 unobservable states as compared to 1 unobservable state when position was used as measurement. The EKF was then applied to the unobservable system as illustrated in Figure B.14. It was observed that the EKF output was erratic and the estimated parameters did not match the known simulated parameters. Actually, the two estimated parameters did not settle down to constant values. However the estimated velocity matched the simulated velocity. The estimated position did not match the simulated position and actually showed a large bias in its estimation. Therefore, for this scenario, the estimated states and parameters did not show good agreement with their simulated counterparts when two states were not observable, as illustrated in Figure B.14. However, when the initial condition was known, parameter estimation was successful and the estimated parameters converged to their known values. It seemed that for this particular scenario, the absence of knowledge about the initial position was sufficient to confuse the EKF.

To summarize, all the results are shown in Tables 6.1 to Table 6.5, in Chapter 6. For brevity, these results are not repeated here. From these tables, it could be deduced that the observability condition was important for the Kalman Filter to successfully estimate states. The EKF successfully estimated states and parameters for all cases when the system was observable (or was made observable using more measurements). But in

some cases, the estimated states and parameters showed good agreement with their simulated counterparts even though the system was not observable. However, it was also seen that when the system was not observable as a result of insufficient measurements, rather than as a result of state augmentation using parameters, the EKF had difficulty in successfully estimating states and parameters. In parameter estimation, a judicious choice is therefore a problem formulation that is observable.

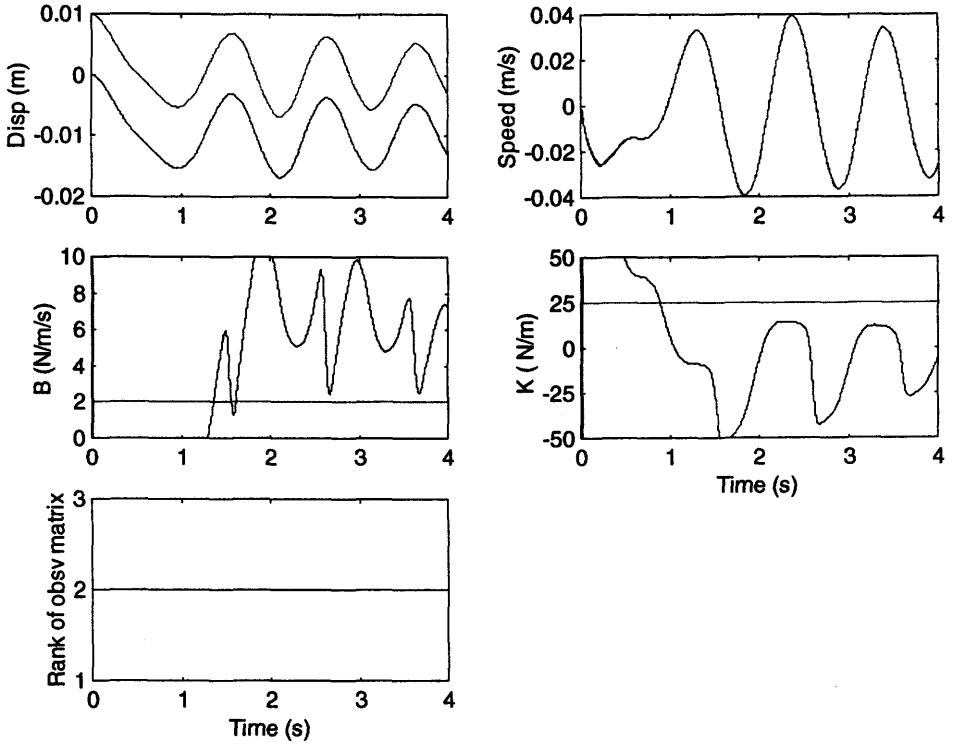

Figure B.14: Applying the EKF to the Unobservable Mass-Spring Damper System with Velocity being Used as Measurement